DESIGN AND SIMULATION OF AN INTEGRATED ACTIVE YAW CONTROL
SYSTEM FOR ROAD VEHICLES

A THESIS SUBMITTED TO
THE GRADUATE SCHOOL OF NATURAL AND APPLIED SCIENCES
OF
MIDDLE EAST TECHNICAL UNIVERSITY

BY

GÖKHAN TEKİN

IN PARTIAL FULFILLMENT OF THE REQUIREMENTS
FOR
THE DEGREE OF MASTER OF SCIENCE
IN
MECHANICAL ENGINEERING

FEBRUARY 2008

I hereby declare that all information in this document has been obtained and presented in accordance with academic rules and ethical conduct. I also declare that, as required by these rules and conduct, I have fully cited and referenced all material and results that are not original to this work.

Name, Last name: Gökhan Tekin

Signature:

ABSTRACT

DESIGN AND SIMULATION OF AN INTEGRATED ACTIVE YAW CONTROL SYSTEM FOR ROAD VEHICLES

Tekin, Gökhan

M.S., Department of Mechanical Engineering

Supervisor: Prof. Dr. Y. Samim Ünlüsoy

February 2008, 159 pages

Active vehicle safety systems for road vehicles play an important role in accident prevention. In recent years, rapid developments have been observed in this area with advancing technology and electronic control systems. Active yaw control is one of these subjects, which aims to control the vehicle in case of any impending spinning or plowing during rapid and/or sharp maneuver. In addition to the development of these systems, integration and cooperation of these independent control mechanisms constitutes the current trend in active vehicle safety systems design.

In this thesis, design methodology and simulation results of an active yaw control system for two axle road vehicles have been presented. Main objective of the yaw control system is to estimate the desired yaw behavior of the vehicle according to the demand of the driver and track this desired behavior accurately.

The design procedure follows a progressive method, which first aims to design the yaw control scheme without regarding any other stability parameters, followed by the development of the designed control scheme via taking other stability parameters

such vehicle sideslip angle into consideration. A two degree of freedom vehicle model (commonly known as "Bicycle Model") is employed to model the desired vehicle behavior. The design of the controller is based on Fuzzy Logic Control, which has proved itself useful for complex nonlinear design problems. Afterwards, the proposed yaw controller has been modified in order to limit the vehicle sideslip angle as well.

Integration of the designed active yaw control system with other safety systems such as Anti-Lock Braking System (ABS) and Traction Control System (TCS) is another subject of this study. A fuzzy logic based wheel slip controller has also been included in the study in order to integrate two different independent active systems to each other, which, in fact, is a general design approach for real life applications. This integration actually aims to initiate and develop the integration procedure of the active yaw control system with the (ABS). An eight degree of freedom detailed vehicle model with nonlinear tire model is utilized to represent the real vehicle in order to ensure the validity of the results. The simulation is held in MATLAB/Simulink environment, which has provided versatile design and simulation capabilities for this study. Wide-ranging simulations include various maneuvers with different road conditions have been performed in order to demonstrate the performance of the proposed controller.

Keywords: Active yaw control (AYC), Integrated Vehicle Safety Systems, Fuzzy Logic Control (FLC), Wheel Slip Control, Vehicle sideslip angle limitation

ÖZ

YOL ARAÇLARI İÇİN TÜMLEŞİK AKTİF DÖNÜŞ DENETİM SİSTEMİ TASARIMI VE SİMÜLASYONU

Tekin, Gökhan

Yüksek Lisans, Makine Mühendisliği Bölümü

Tez Yöneticisi: Prof. Dr. Y. Samim Ünlüsoy

Şubat 2008, 159 sayfa

Araç aktif güvenlik sistemleri trafik kazalarını engellemede büyük rol oynamaktadır. Son yıllarda elektronik denetleyicilerin gelişimi ve diğer teknolojik gelişmeler ışığında bu alanda hızlı değişiklikler göze çarpmaktadır. Yol araçlarında keskin manevralar sırasında sıkça görülen önden veya arkadan kayma hareketlerini denetlemeyi amaçlayan aktif dönüş denetleyici tasarımları da bunlardan biridir. Bu alandaki gelişimlere paralel olarak, bağımsız araç aktif güvenlik sistemlerinin tümleşik ve uyumlu tasarımı ve çalıştırılması da son zamanlardaki uygulamalardan birisidir.

Bu tez çalışmasında, iki akslı yol araçları için aktif dönüş denetleyici tasarımı ve detaylı benzetim sonuçları sunulmuştur. Tasarlanan denetleyici sisteminde, temel olarak sürücünün istediği davranışının kestirimini yapmak ve bu davranışı hassas biçimde takip etmek amaçlanmıştır. Tasarımda sürekli ilerleyen/değişen bir yaklaşım izlenmiştir. Öncelikle, dönüş denetimi için gereken yapı herhangi bir araç davranış parametresi düşünülmeden ortaya çıkartılmış, sonrasında tasarlanan denetim mekanizması araç yüzme açısı gibi diğer parametreler de göz önünde bulundurularak

geliştirilmiştir. İki serbestlik dereceli araç modeli (bisiklet modeli) sürücünün istediği araç davranışını kestirmek üzere kullanılmıştır. Denetleyici tasarımında daha çok doğrusal olmayan tasarım problemlerinde kullanılan Bulanık Mantık Denetim metodu kullanılmıştır. Daha sonra, tasarlanan denetleyici, araç yüzme açısını da sınırlayacak biçimde geliştirilmiştir.

Tasarlanan ve geliştirilen aktif dönüş denetim sisteminin diğer aktif güvenlik sistemleriyle tümleşik hale getirilmesi de bu çalışmanın hedeflerindendir. Bulanık mantık temelli teker kayma denetleyici tasarımı, uygulamadaki genel yaklaşım olan ortak çalışma prensibine uygun olarak, iki farklı bağımsız aktif güvenlik sisteminin tümleşik hale getirilmesi için bu çalışmada sunulmuştur. Bu uygulama, aktif dönüş denetimini ve ABS olarak bilinen tekerlek kilitlenmesini önleme sisteminin uygulamada tümleştirilmesinin adımlarını atmayı ve bu işlem için gerekli ön tasarım yordamını sunmayı amaçlamaktadır. Doğrusal olmayan bir lastik modeliyle sekiz serbestlik dereceli ayrıntılı bir araç modeli gerçek bir aracın benzetimini yapmakta ve yapılan tasarımın performansını denemekte kullanılmıştır. Benzetim çalışması MATLAB/Simulink ortamında yapılmıştır, bu sayede yazılımın çok yönlü tasarım ve benzetim becerilerinden yararlanılmıştır. Ayrıca, yapılan nihai denetleyici tasarımlarının başarımlarını görmek için değişik yol koşulları ve manevralar içeren geniş ölçekli benzetimlere yer verilmiştir.

Anahtar Kelimeler: Aktif Yalpa Denetimi, Tümleşik Araç Güvenlik Sistemi, Bulanık Mantık Denetimi, Tekerlek Kayma Denetimi, Araç Yüzme Açısı Denetimi

Dedicated to My Family, who have always shown unconditional love and support at every single moment in my life…

ACKNOWLEDGEMENTS

First, I would like to express my special thanks to my supervisor Prof. Dr. Y. Samim Ünlüsoy, who has guided me to this topic, endlessly supported and encouraged while saving me with practical solutions during his supervision of this study.

I would like to state my appreciation to Murat Şahin for his patient support and pleasant friendship, Emir Kutluay for his useful advises and company at every part of the study, Görkem Oktay and Hakan Temizsoy for their abundantly helpful and enjoyable attitude throughout this thesis. After all these years, I have got quite a bunch of friends in the department, which I cannot stop without stating my appreciation to all of them. Also, financial support of TÜBİTAK is also gratefully acknowledged.

My endless thankfulness goes to my friend Zeynep Erdoğan, who has stimulated and supported me with patience and wisdom. Without her, this study would never finish.

My last, but not the least, thanks go to my valuable family. They have endlessly supported, guided and protected me in all stages of my life. I can never imagine a life without their love and dedication.

TABLE OF CONTENTS

LIST OF TABLES

TABLES

LIST OF FIGURES

LIST OF SYMBOLS

a	Distance of center of gravity of the vehicle from the front axle
a_p	Tire contact patch length
a_{p0}	Tire contact patch length at design conditions
A_i	Experimental tire parameters for stiffness characteristics
a_x	Vehicle longitudinal acceleration
a_y	Vehicle lateral acceleration
α	Tire slip angle
b	Distance of center of gravity of the vehicle from the rear axle
B_i	Experimental tire parameters for friction characteristics
$C_{\phi i}$	Roll damping
C_f	Front wheel cornering stiffness for bicycle model
C_r	Rear wheel cornering stiffness for bicycle model
C_i	Experimental tire parameters for saturation function
Cs/Fz	Experimental coefficient for tire model
δ	Steer angle
F_x	Longitudinal tire force
F_y	Lateral tire force
F_z	Normal tire load
F_{ZT}	Tire design load
g	Gravitational acceleration
h	Height of the sprung mass center of gravity
h_s	Distance of sprung mass center of gravity from roll axis
I_w	Rotational inertia of the tire
I_{zz}	Vehicle inertia about z axis
I_{xx}	Sprung mass inertia about x axis
K_a	Coefficient for tire patch elongation
k_c	Longitudinal stiffness coefficient
$k_c{}'$	Transition stiffness coefficient
ks	Lateral stiffness coefficient

kμ	Friction transition coefficient
K_R	Front roll stiffness ratio
$K_{\Phi f}$	Front Roll stiffness coefficient
$K_{\Phi r}$	Rear Roll stiffness coefficient
M	Total vehicle mass
M_b	Wheel brake moment
M_s	Sprung mass
μ	Longitudinal coefficient of friction
μ_0	Peak tire/road friction coefficient
ω	Wheel angular velocity
φ	Roll angle
R	Wheel radius
r	Yaw rate
σ	Composite slip
s	Longitudinal wheel slip ratio
S_r	Steering wheel ratio
T	Track length
T_w	Tire width
T_p	Tire pressure
t	Simulation time step
u	Longitudinal vehicle velocity
v	Lateral vehicle velocity
v_w	Vehicle velocity in the plane of the wheel
W	Weight of the total vehicle

LIST OF ABBREVIATIONS

4WD	4 Wheel Drive
ABS	Anti-Lock Braking Systems
AWD	All Wheel Drive
AYC	Active Yaw Control
CAN	Control Area Network
DYC	Dynamic Yaw Control
EBD	Electronic Brake Distribution
ECU	Electronic Control Unit
ESP	Electronic Stability Program
FLC	Fuzzy Logic Control
FWS	Front Wheel Steering
HIL	Hardware-in-the-Loop
HILS	Hardware-in-the-Loop Simulations
ICE	Internal Combustion Engine
LQR	Linear Quadratic Controller
PWM	Pulse Width Modulation
RWD	Rear Wheel Drive
RWS	Rear Wheel Steering
SISO	Single input, Single output
SMC	Sliding Mode Control
TCS	Traction Control System
VSC	Vehicle Stability Control

CHAPTER 1

INTRODUCTION

The goal of this thesis study is to design and simulate an integrated active yaw controller for road vehicles. The integration will include and coordinate independent active safety systems such as Anti-lock Braking System (ABS), Traction Control System (TCS), and Active Yaw Control (AYC) systems. Thus, an introduction to active safety systems in general and the basic elements and functions of AYC will be given.

1.1   INTRODUCTION TO ACTIVE SAFETY SYSTEMS

Safety systems applied to road vehicles can be classified into two categories as active and passive safety systems. Passive safety systems are designed to prevent or lessen the damage to the passengers, pedestrians and the vehicle(s) involved after the accident has occurred. Typical applications for passive systems are seat belts, air bags, door shock absorber bars, etc.

Contrary to their passive conjugates, active safety systems aim to prevent accidents by detecting any jeopardy of instability and take partial or full control of the vehicle to take appropriate measures necessary for prevention of the accident.

During the last century, with growing research on safety applications, several independent active safety applications have been developed. The eldest, most known and successful example is ABS (Antilock Brake System), which prevents locking of wheels during braking. ABS aims to fulfill its goal by keeping the tire

slip at or around the value, which provides the highest brake force and at the same time makes it possible to generate the lateral tire forces required for adequate directional control and stability. The main aim of ABS is, contrary to general opinion, to maintain stability and controllability during braking rather than shortening the braking distance. After the astonishing success of ABS, several other independent active safety systems have been developed. Some examples are ASR (Anti Slip Regulation), TCS (Traction Control System) both of which are based on ABS sensor system but manipulating the acceleration period rather than braking. Other systems include EBD (Electronic Brake Distribution) system which controls the distribution of the front and rear brake forces, EDL (Electronic Differential Lock) system for better traction on surfaces with non-uniform friction characteristics and AYC (Active Yaw Control), which intend to prevent out-of-boundary yaw motion (drifting, spinning etc.) by controlling the individual brakes and engine management system, and creating a contra-yaw moment. Although this system seems similar to ABS in terms of sensor and control phases, the cases for activation and the decision mechanism is quite different. The dynamics of yaw motion are subject to numerous nonlinearities stemming from tire force dependencies on lateral slip, longitudinal slip, loading condition, surface condition, and even track temperature.

1.2   INTRODUCTION TO ACTIVE YAW CONTROL SYSTEMS

Active yaw control systems are becoming essential safety systems for road vehicles as the number of electronic controllers involved in road vehicles increases. The main aim of the yaw controller is to regulate the yaw motion of the vehicle according to the driver's inputs (steer, longitudinal acceleration etc.). A simplified vehicle model is utilized for predicting the driver's intention and independent brakes for wheels and/or drive torques are made use of creating yaw moments to track the yaw motion of the simplified model. However, this tracking is not realized at all costs, since the vehicle sideslip angle is another important parameter in vehicle dynamics. The yaw controller tracks the desired yaw rate as long as the vehicle sideslip angle is in a limited range. As the vehicle sideslip angle reaches or

surpasses a limit value, which is about 12 degrees for high surface friction coefficients, e.g., the vehicle may become unresponsive to steer inputs. For these cases, the controller should make a compromise between tracking the yaw rate and limiting the vehicle side slip angle.

There are various cases in which a vehicle may go unstable considering the yaw motion. First case is the steady state cornering. Here, the vehicle may not track the desired trajectory by getting out of the track displaying the so-called understeering or oversteering behavior. Understeering occurs when the vehicle does not 'yaw' enough to turn through cornering so that the vehicle turns a larger diameter curve than intended. Oversteering case is the contrary, as the vehicle turns round a smaller diameter curve. Fig.1.1 illustrates these behaviors and the ideal behavior. In part a, the desired behavior is shown as the solid line and the trajectory of the understeering vehicle is shown in dashes. As observed, the vehicle tends to follow a straighter path and leaves the track. In part b, however, the vehicle tends to turn excessively and the driver loses longitudinal control.
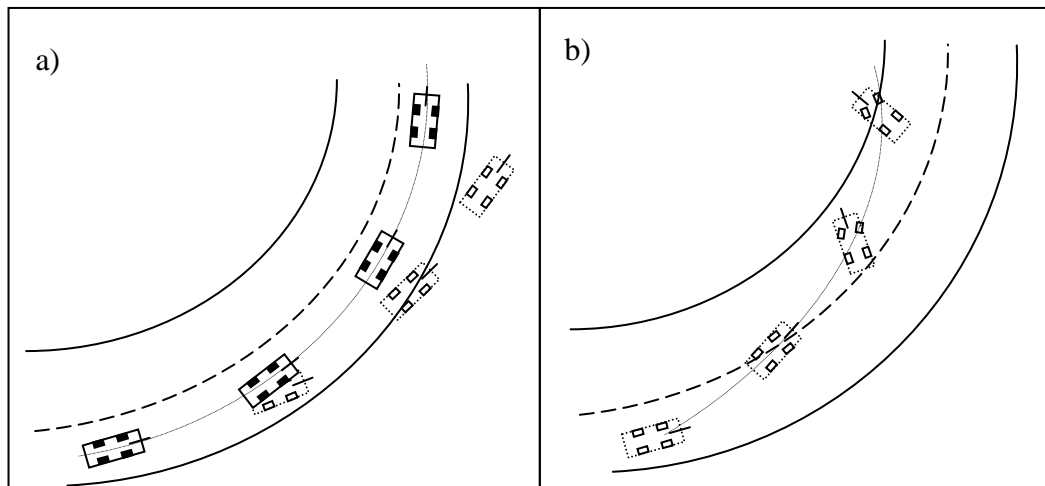
Fig.1.1 Vehicle behaviors in steady state cornering-
a) Neutral and understeering b) Oversteering

Another important case for yaw control systems is the lane change (or Moose Test) maneuver (Fig.1.2). This maneuver generally occurs on a sudden obstacle on the road (such as wild animals, a dropped box from another vehicle etc.) when the driver is too late to avoid it. In such a case, changing the lane without colliding with the obstacle is possible with braking and evasive steer manipulation. Without active yaw control, the initial steering input will cause the yaw rate and the sideslip angle increase excessively such that the vehicle becomes unresponsive to the driver's intervention. Driver's aim to avoid the foreign object is limited by the high drift angle, and the collision occurs. With active yaw control, however, the vehicle can be steered accordingly so that the oscillation is 'damped' by applying pro- and contra yaw moments to the vehicle. This results in a more stable and more responsive vehicle (Fig.1.2.c).
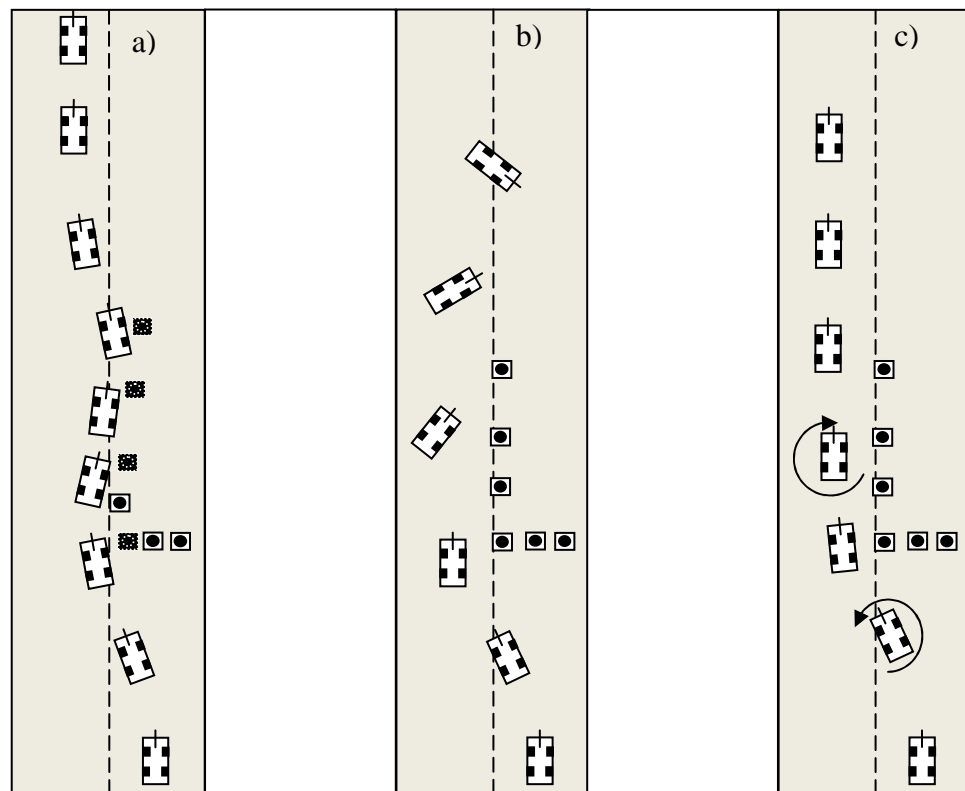
Fig. 1.2 Vehicle Behavior in Lane Change maneuver

a) An instability example for double lane change maneuver without AYC

4

b) An instability example for double lane change maneuver without AYC (excessive oversteer behavior)

c) Stabilized vehicle for double lane change maneuver with AYC

1.3   ACTIVE YAW CONTROL SYSTEM ELEMENTS

An active yaw control system consists of different hardware such as electronic control units, sensors, communication networks, and the software [1]. For the functioning of active yaw control system, the following sensors are required:

—   Yaw rate sensor

—   Lateral and longitudinal acceleration sensors

—   Wheel rotational speed sensors

—   Steering angle sensor

—   Brake pressure sensors

These sensors are used for determining the driver demand and the vehicle's actual response. Some parameters such as surface friction coefficient, vehicle sideslip angle, etc., cannot be measured directly, so these parameters should also be estimated via the existing sensor information. The general configuration of the sensors and other equipment is shown in Fig. 1.3.
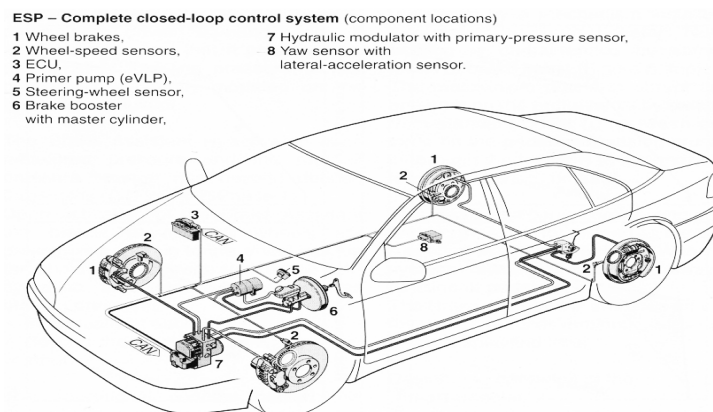
Fig.1.3 Basic components of an integrated control system and their locations on the vehicle [1]

The descriptions of the components are as follows:

—   Wheel Brakes: These components are the end actuators of the integrated stability system on the vehicle. Their primary task is to apply decelerating torque to the wheels to create longitudinal tire forces. These generated forces are to be used to slow down or to create yaw moments.

—   Wheel Speed Sensors: These sensors provide wheel rotational speeds as frequencies to the electronic control unit. This information is used for determining the vehicle speed and calculating the independent longitudinal tire slips.

—   Electronic Control Unit (ECU): This unit is responsible for receiving, amplifying, filtering, and processing the signals coming from the sensors to estimate the vehicle velocity, vehicle sideslip angle, etc., and set thresholds for the stability parameters. The ECU should create necessary signals for the actuators to produce tire slips required for longitudinal and lateral stability. In a vehicle with integrated active safety systems, these tasks may be distributed among different ECUs via Control Area Network (CAN).

—   Primer Pump: This component is used for rapid pressure generation on the brake fluid for compensating the brake delay on cold weather during active braking.

—   Steering wheel sensor: This unit provides the angle of the steering wheel so that the electronic control unit can estimate the driver's intention of vehicle trajectory and motion.

—   Brake Booster and Master cylinder: This integrated unit is used for amplifying the brake pressure coming from the brake pedal. The amplified pressure is then supplied to the hydraulic modulator. One main objective is to generate necessary pressure rapidly during 'panic braking'.

—   Hydraulic Modulator: The primary function of the hydraulic modulator is to implement the commands coming from ECU via regulating the brake pressure in the chamber. The regulation is done using solenoid valves.

—   Yaw and lateral acceleration sensor: This sensor is the most important sensor for the active yaw control system. Its primary function is to measure the yaw rate and the lateral acceleration of the vehicle. It is generally placed at or very near to the centre of gravity of the vehicle.

A schematic view of the active yaw control is given in Fig. 1.4. Here, the driver demand (throttle and steer inputs) are fed to both the plant (e.g. the vehicle) and the controller. The desired behavior is estimated via a linearized vehicle model and compared with the actual vehicle motion. Then, according to the error signals, the controller produce differential signals to activate the independent wheel brakes in order to create yaw moments. The most important design part here is the controller, since it should handle different situations such as excessive yaw motion, different surface conditions, sideslip angle limitations, etc. Thus, the controller should have various different capabilities in order to complete these tasks.
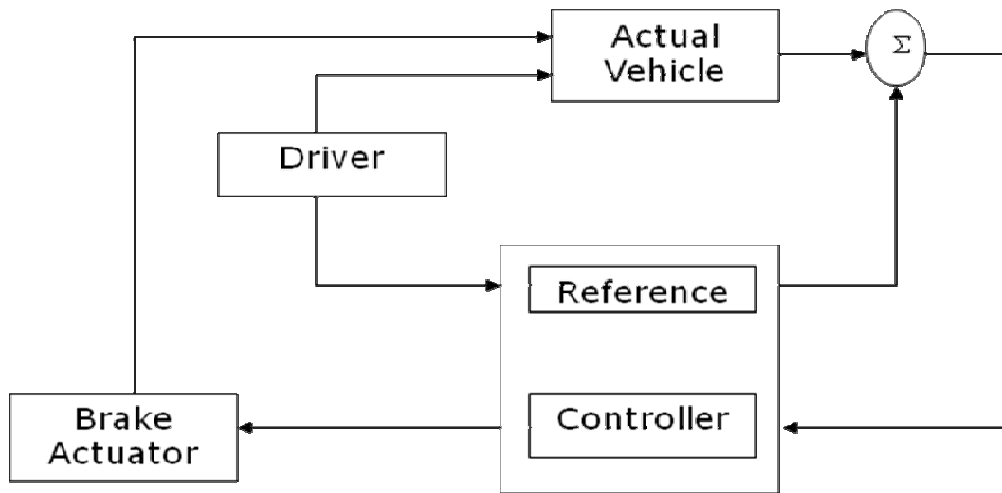
Fig. 1.4. Basic Schematic View of Yaw controller

Generally, active safety systems work independent from each other on road vehicles. However, the activities of these independent systems may interfere with each other while operating in difficult situations. One example can be given as the action of high steering angles on ice while braking. In this situation, the ABS and the yaw controller may intervene with the brake actuation and the vehicle may display an undesired behavior. To eliminate this possibility, a hierarchical controller should be designed The upper level controller should evaluate the conditions/responses of the vehicle and the error levels with respect to the desired

motion. Afterwards, it should create signals necessary to sublevel controllers such as ABS for braking, TCS for engine management, etc. Maximizing brake force, hence, the yaw moment and the prevention of the threat of intervention can be done in this hierarchical structure. An example I/O diagram for the hi-level controller and its connections to other components such as sensors, sublevel controllers, etc. are shown in Fig. 1.5.

It should be noted that the yaw moment actuation in this study is done via using differential braking, which has drawn most attention from the researchers and the companies. Other methods are also available, such as active torque distribution and active steering (front and/or rear). Generally, the active torque distribution is used in electric vehicles and vehicles with active differential systems. Active differential systems can distribute the available shaft torque to wheels independently so that uneven tractive forces may generate yaw moments. Active steering systems, however, create yaw moments by manipulating the steer angles and generate lateral forces, which result in yaw moment differences. The steering manipulation is done by first measuring the steering wheel angle and then computing the additional steering angle to the wheels so that the corrective yaw moments is generated.

```
HI-LEVEL CONTROLLER

        Monitors
        measured
    variables from the
        vehicle

Calculates the setpoint          Calculates the
for yaw rate and                 estimated variables
sideslip angle                   such as sideslip
                                 angle

        Calculates the necessary yaw
        moment and corresponding
        brake pressures

        Calculates the brake locking
        torque and necessary
        adjustments
```

```
LOW-LEVEL CONTROLLER          VEHICLE (PLANT)
(ABS, TCS etc.)               Monitored variables such as;
                              -Yaw rate
Hydraulic Modulation or       -Wheel speeds
other actions are calculated  -Lateral acceleration
and realized.                 -Steering wheel angle
```

Fig.1.5 Basic input-output relation of the high and low level controllers of an integrated active yaw control system.

9

1.4 OUTLINE

In chapter 2, literature survey related to this study is introduced. The literature work can be divided into three groups; namely, yaw control algorithms, estimation methodologies, and integration studies. The latter two subjects are generally introduced for reasons of practical application.

In chapter 3, mathematical modeling of a nonlinear tire model, a nonlinear eight degree of freedom vehicle model, and a linear two degree of freedom vehicle model are introduced. The sign convention, tire force generation, and an overview of the vehicle models together with the designed controller are also given in this chapter.

In chapter 4, active yaw controller design procedure and details of the designed fuzzy logic controller are given. The design procedure contains two main controllers as active yaw controller, and active yaw controller with sideslip angle limitation. The differences between these two controllers are explained while a low level wheel slip controller design is also presented.

In chapter 5, the performance of the designed controller is introduced with simulation test results. The simulation tests are segregated into two main groups according to the maneuver types, namely, J-turn maneuver and double lane change maneuver. Each of these two tests is simulated with three different road conditions resembling real life conditions, such as dry, wet, and icy road surfaces. Simulation results are given for active yaw controller and the same controller extended to limit the vehicle sideslip angle. Results are discussed for each simulation tests.

In chapter 6, discussion, conclusion, and possible future work of the study are given.

Appendix A contains the vehicle and tire data used in the simulations while Appendix B contains a new set of simulations for decelerating vehicle in a J-turn maneuver, and double lane change.

CHAPTER 2

LITERATURE SURVEY

2.1 INTRODUCTION

The AYC systems are one of the most developing research subjects of vehicle dynamics. Numerous articles, theses and books have been published during last thirty years. These papers and other publications propose solutions to various parts of the design. To classify these papers according to their subjects, their relevance to the current study should be given. To sub issues of the study can be listed as follows:

— Active yaw controller design
— State estimation
— Vehicle and tire modeling

Active yaw controller design issue contains the selection of the design methodology of the controller, determination of required input/output parameters and application to mathematical vehicle model, real vehicle or Hardware-in-the-Loop simulation (HILS).

State estimation issue is concentrated on filtering noisy measurements and calculating indirect (not practically measurable) variables. These variables are generally used in prediction of the vehicle's general state of control, steerability etc. Besides, the manipulation of the vehicle via designed controller may depend on these estimated variables.

Vehicle and tire modeling is the last main issue. There are two different vehicle modeling purposes. First, a simple yet accurate model may be utilized to predict the

driver's intention. In other words, it may serve as a reference model. This modeling may consist of from a single equation to a large, nonlinear bunch of equations. The general approach is to include only related degree of freedoms as variables and keep the model simple as possible. Second purpose is the simulation and evaluation of the designed controller. This time, the constructed vehicle model is far more detailed than the former reference vehicle model. This detailed model should include controlled degree of freedoms and related degree of freedoms affecting these controlled variables in a strong manner. The tire modeling is also related with the real vehicle replacement with a mathematical model. There exist several tire models in the literature, some of them depend on empirical tire data while others have a more abstract approach.

2.2 LITERATURE SURVEY

The slip angle estimation plays an important role during controller phase of the ESP system, since the new yaw moment control systems need accurate slip-angle information. Fukada [3] has described a strategy of vehicle slip angle estimation. The difficulty in slip angle estimation is due to nonlinear characteristics of tires and influence of relative slant of the road surface. To solve this difficulty, a combined method of model observer and direct integration method is proposed. In this method, two kinds of values of the side forces of the wheels were provided, i.e., direct detected values by the G-sensor and values from a tire model. Then those values were combined appropriately which results in the combination of model observer and direct integration. A feedback algorithm, redesigned to suppress the influence of tire model error, is applied in the observer. Considering interference of road surface and its avoidance, road slant angle is estimated and consequently vehicle model was corrected. The estimated value of the road friction coefficient is given by the acceleration, and an adequate bias, depending on yaw-deviation, is added. An improved reference yaw velocity is also proposed in order to avoid interference of road slant and variation of dynamic characteristic of vehicle. This reference yaw velocity may be used for the prediction of reference yaw rate according to the driver's intention.

Hac and Simpson [4] have proposed an algorithm for estimation of vehicle yaw rate and sideslip angle using steering wheel angle, wheel speed, and lateral acceleration sensors. This algorithm uses two initial estimates of yaw rate from wheel speeds and lateral acceleration sensors. A weighed estimate was the realized using these two estimates. The results have come out to be accurate even in harsh conditions. This paper, in general, has presented a very efficient and applicable methodology to determine these parameters which can be used in the controller design. The main benefit of the method presented here is the reduction of yaw sensor need and accurate estimation of vehicle sideslip angle.

Kin, Yano and Urabe [5] have proposed methods to estimate vehicle dynamic parameters such as vehicle side slip angle, road friction coefficient, and tire side forces precisely in real time. Oversteer and understeer behavior is judged from the estimated 4 wheel tire forces. The yaw moment and side slip angle are then corrected with optimal 4 wheel slip control. Briefly speaking, there are 3 main aims introduced in this paper as

— Vehicle sideslip angle and tire sideslip angle estimation,
— Tire and road surface friction coefficient estimation, and
— Tire side force estimation.

For all these aims, optimal control, stability and steerability algorithms were proposed. These estimations may be utilized for accurate controlling for the current study since, as will be mentioned in the following chapters, sideslip angle and road surface friction coefficient estimation plays a crucial role in the designed control system.

Tire parameters are also needed online during system design and run period. Hewson [6] has proposed a simple mathematical tire model that estimates tire cornering stiffness. The model is derived by considering the tire to be a combination of two independent systems. The sidewalls were assumed to be negligibly stiff in the lateral

direction, and hence their influence on the lateral dynamics of the tire will be ignored. The belt and thread area of the tire have been considered to be a homogeneous uniform band, and its stiffness has been estimated with reference to measured tire data. The resulting model is estimated to yield cornering stiffness values within about 30 per cent of the actual measured values. This paper's work can be utilized to estimate simple tire characteristics for hardware in the loop tests, which is a future work for this study.

Takano, Nagai, Taniguchi, and Hatano [7] have employed a three-degree-of-freedom model for computer simulation to determine the relationship between the planar and roll motions of a large-size vehicle, so that the roll motion could be eventually predicted to prevent the vehicle from going dynamically unstable. Factors such as the varying center of gravity height and roll steer are also taken into consideration. This study may be helpful whenever the roll stability is to be introduced to DYC program of the vehicle.

Nguyen, in his M.Sc. Thesis [8], has derived vehicle handling and stability analysis using a state vector approach. The very basic vehicle models have been evolved to more complex models including roll effects, load transfer effects, tire nonlinearities etc. An improved method for vehicle handling assessment has also been proposed for these nonlinear models. These assessment results may be used for evaluating the vehicle performance with and without control systems.

Babala, Kempen and Zatyko [9] have studied the practical side of the topic and introduced several sets of sensors that can be used in Vehicle Stability Control systems. The sensor characteristics affect the performance of the VSC systems drastically; therefore appropriate selection considering size, weight, cost, etc. is necessary. This study presents several tables of comparison and short description of desired sensor properties. Also, a simple example of how to use these table-matrices in the design of VSC sensor systems is given. The selection of sensor sets and evaluation of their performance is of future work for this study, however may give an insight view about real life application.

Noomwongs, Yoshida, Nagai, Kobayashi and Yokoi [10] have worked on the development and application of a tire hardware-in-the-loop simulator (HILS) for evaluating vehicle dynamics. Tire HILS is a combination of a simulation (vehicle model) and an experimental (tires) part. In this paper, suspension and steering system models are introduced which, together with the steering model, have sufficient complexity to provide a response of the vehicle simulated on Tire HILS significantly closer to that of a real vehicle, as compared to simulation by an off-line linear tire model. This hardware in the loop simulation study is a transient test procedure before application of the designed control system to real vehicle, hence details of this procedure should be taken into account.

Tseng, Ashrafi, Madau, Brown, and Recker [11] have addressed realistic subjects encountered in the challenge of achieving technology improvement in a vehicle stability control system. They have included driver intent recognition, vehicle status measurement and estimation, control target generation, system actuation efficiency and smoothness, road bank angle detection, system development and evaluation, and fault detection. The steering wheel angle estimation is also introduced in detail in this paper. This comprehensive study points many possible problems which can be encountered during all stages of design, test, and application stages. Thus, as a profound source, general information about this paper is given in the current study.

Up to this point, no emphasis is given for the design of control system issue. The main work and aim for this study is the design of a control system for yaw rate control and simulation of the designed controller in the computer environment. The evaluation of the study may be done via comparing the performances of the present studies in the yaw control subject. The upcoming papers are related with the design and simulation/application results of the designed controllers.

Hahn, Hur, Yi, Kang, and Lee [12] have suggested a disturbance observer-based nonlinear vehicle stability controller. The disturbances acting on the yaw rate dynamics coming from tire forces, vehicle parameters and hydraulic actuators have

15

been estimated using a disturbance observer. This estimated disturbance is used then to stabilize the lateral dynamics of the vehicle. The model reduction technique is involved to incorporate the dynamics of the hydraulic actuator in the vehicle stability controller. Simulation results have indicated that the proposed disturbance observer-based vehicle stability controller can achieve the desired reference tracking performance as well as sufficient level of robustness.

Boada, and Díaz [13] have studied fuzzy logic methods for developing a new yaw moment control to improve vehicle handling and stability. They have emphasized that the advantages of fuzzy methods are their simplicity and their good performance in controlling non-linear systems. The developed controller has generated a suitable yaw moment which is obtained from the difference of the brake forces between the front wheels so that the vehicle follows the target values of the yaw rate and the sideslip angle. For testing the algorithm, a 8 DOF vehicle model with Dugoff tire model is introduced and the vehicle is subjected to different cornering steering maneuvers such as lane change and J-turn under different driving conditions (dry road and snow-covered). The vehicle model and testing maneuvers presented in this article have led to compare and improve the performance of the designed controller in the current work.

Park and Kim [14] have proposed a new scheme to enhance vehicle lateral stability with a traction control system during cornering and lane changes. This scheme has controlled wheel slip during cornering by varying the slip ratio as a function of the slip angle. It is assumed that a traction control system with the engine throttle angle is used. The scheme is dynamically simulated with a model of front-wheel-driven passenger vehicles. Simulation results have shown that the proposed scheme is robust and superior to a conventional one, which is based upon fixed slip ratios, during cornering and lane changes. The main emphasis of this study is the traction control integration for the control of the vehicle. Although not presented in the current study, the traction control integration into the proposed controller for future work.

Drakunov, Ashrafi, and Rosiglioni [15] have developed a yaw control algorithm to give an additional measure of vehicle stability control during adverse driving maneuvers over a variety of road conditions. The control law is based on optimum search for minimum yaw rate via sliding mode control. By measurements *of* vehicle states, the control algorithm has been determining the level of vehicle stability and intervenes in any jeopardy of instability through individual wheel braking to provide added stability and handling predictability.

Güvenç, Acarman, and Güvenç [16] have suggested a combined strategy for creating counter yaw moments which include additional steering angles and individual wheel braking. First, independent use of strategies is presented. Several combination and coordination strategies are then tested. For this purpose, a model regulator is used as the main controller which utilizes coordinated steering and wheel braking. The possible contribution of this study is the given principles of combining steer manipulation with the control via brake.

Güvenç, Güvenç, Öztürk, and Yiğit [17] have built a model regulator based yaw stability control system previously implemented and tested successfully as a steering controller; adapted to work as an individual wheel braking controller in the study. A two track nonlinear vehicle model is used to test the individual wheel braking actuated model regulator developed here. Simulation results are used to demonstrate the achievement of good yaw disturbance moment rejection by the proposed controller.

Zhou and Wang [18] have proposed a new model for 4WD vehicles including fuzzy controls for yaw stability during evasive maneuvers. Driver gives the front steer angle command while the controller commands rear steer angle and individual braking if necessary. Here, the suspension control (the distribution of normal forces to each tire thus affecting the lateral forces) is explained briefly. The fuzzy logic diagram is introduced and simulation results are given. Instead of braking, this paper presents an alternative way of the control output for the designed control system, namely rear steer manipulation.

Esmailzadeh, Goodarzi, and Vossoughi [19] have developed a new optimal control law for direct yaw moment control, to improve the vehicle handling. Although, this can be considered as part of a multi-layer system, for the traction control of a motorized wheels electric vehicle, the results are quite general and can be applied to other types of vehicles. The dynamic model of the vehicle system is initially developed and, using the well-known optimal control theory, an optimal controller is designed. Two different versions of control laws are considered here and the performance of each version of the control law is compared with each other. The differences between electric powered and ICE vehicles are described in a few words and traction or brake based VDC systems are applied to corresponding vehicle type. The numerical simulation of the vehicle handling with and without the use of the optimal yaw moment controller, using a comprehensive non-linear vehicle dynamic model, has been carried out. This paper presents comparable results with the current study, thus a good source for performance evaluation.

The modeling of physical systems also plays a crucial role in determining the ESP Yaw Control strategy. Kuang, Fodor, and Hrovat [20] have described the derivation of a hydraulic brake system model using the bond graph technique, and the design of a feedback control system with an adaptive gain schedule PD controller. In addition, simulation and experimental results are presented to illustrate the model validation and the controller performance. A detailed ABS schematic figure is included in the paper.

Mokhiamar and Abe [21] have presented a comparison study of the effect of model response on the performance of the model following type combined lateral force and yaw moment control. The combined controls have aimed to maximize stability limit as well as vehicle responsiveness. In order to realize this aim, two types of model responses are proposed to introduce the required lateral force and yaw moment control. The model responses (a) are the side-slip angle and yaw rate vehicle response of the two degree of freedom vehicle motion (bicycle model). The model responses (b) is an intentional modification of the model responses from (a) to the side slip angle converging to zero and first order yaw rate. Three different cases of

combining lateral force and yaw moment control have been investigated using the two types of model responses. The effect of model responses is examined by computer simulations of the vehicle response to a single sine wave steering input with braking for the combined control methods proposed. It has been found that the influence of the model response has a significant effect on the combined control performance. This paper have a similar vehicle configuration and similar maneuvers with the current study, thus it is available for performance comparison.

Youa, Hahnb, Choa, and Leea [22] have dealt with the feedback control of a hydraulic unit for direct yaw moment control, which actively maintains the dynamic stability of an automobile. The uncertain parameters and complex structure naturally call for empirical modeling of the hydraulic unit, which leads to a high-fidelity input/output model. The identified model is cross-validated against experimental data under various conditions, which helps to establish a stringent model uncertainty. Then, the H-∞ optimization technique was employed to synthesize a controller with guaranteed robust stability and performance against the model uncertainty. The performance of the synthesized controller is experimentally verified and the results have shown the viability of the proposed approach for real-world applications. This paper is utilized for realistic brake torque rate estimation.

Mokhiamar and Abe [23] have investigated the effectiveness of weighting coefficients adaptation in simultaneous optimum distribution of lateral and longitudinal tire forces for improvement of vehicle handling and stability. Three different cases of weighting coefficients adaptation are considered in this study. Similar weighting coefficients for rear and front wheels are adopted in case 1. In case 2, the weighting coefficients of front wheels are greater than the corresponding value of rear wheels. Finally for case 3, the weighting coefficients of rear wheels are adopted to be greater than the values of front wheels. The yaw rate response is simplified to first order lag, meaning neutral steer characteristics. The block diagrams are given for optimum force distribution technique and DYC+FWS+RWS combined control. It is concluded that weighting coefficients adaptation can exert a large influence on the vehicle handling performance. Besides, a general comparison

19

is held between, DYC only systems and integrated DYC together with front and rear wheel steer systems. From this point, the information given in this paper has led an insight view to control output selection for the design stage of the yaw controller.

Shim and Margolis [24] have introduced a differential braking control strategy using yaw rate feedback, coupled with μ feedforward for a vehicle cornering on different roads. A nonlinear 4-wheel car model is developed for this study. A desired yaw rate was calculated from the reference model based on the driver steering input. The feedforward action of friction coefficient has turned out to offer significant improvement of the vehicle desired trajectory over that of a yaw rate controller alone. Uncertainties and time delay in estimating μ were shown to yield a system that is still superior to that using no μ information at all. This result may be utilized in future work of the current study, since μ estimation consists an inevitable problem.

Choi and Cho [25] have offered more practical knowledge on building an Active Yaw Control system. In this study, a longitudinal four-wheel vehicle model with brake actuator is described and a sliding mode controller with pulse width modulation (PWM) method has been developed for passenger vehicles. Further, actuator dynamics are introduced in the system equations and an equivalent control input is derived theoretically. The proposed method includes using the PWM method to compensate for the discrete nature of actuator dynamics by duty control. Stability of the PWM controller for sliding mode control (SMC) is theoretically checked. The information given here is generally of practical value, since application issues such as pulse width modulation of brake signals have also been considered.

BuckHoltz [26] has introduced a fuzzy logic algorithm to minimize yaw rate error while the vehicle sideslip angle is also controlled in a range. The yaw rate error control has satisfactory results but the deterioration from tracking performance occurs while the controller tries to compensate a significant vehicle sideslip angle. Therefore the controller has been designed to handle both parameters. This analysis has shown how tire force characteristics can differ while still being able to track the

reference yaw rate. This paper has also presented similar maneuvers and vehicle parameters with the current study, so that comparison of performances is possible.

Sorniotti and Velardocchia [27] have published a study on Hardware-in-the-Loop (HIL) brake testing. They have introduced a HIL testing bench. Then, a description of all the necessary basic tests to characterize an ESP unit has been given in detail. These basic tests include step response of each valve, measurement of pressure limiter valves calibration, step response of motor pump unit, etc. The frequency responses of ESP valves are given using Pulse Width Modulation. Finally, an open loop actuation strategy for ESP is presented to obtain, in each condition, the desired wheels pressure levels without any pressure sensor in the hydraulic unit. An ESP control strategy (complete diagnostic algorithm) is added to actuation logic described before and tested.

Mitsubishi [28] has developed a different active yaw control system that utilizes a torque transfer differential which is controlled by various sensors and an electronic control unit (ECU) to enable a difference in torque to reach each of the rear wheels. The system works by increasing the level of torque to the left rear wheel and reducing the torque level to the right wheel, thus changing the yaw movement of the vehicle. This in turn will cause the vehicle to steer inwards and reduce the amount of slip on the front tires, thus resulting in reduced under-steer. It also works if over-steer occurs.

Osborn and Shim [29] have introduced an All-Wheel-Drive independent torque distribution control algorithm, which is essentially beneficial under acceleration close to the limit of stability. Besides, by applying yaw rate feedback to control front-rear torque and lateral acceleration to control left-right torque distribution together with a proportional-integral control strategy, the controlled vehicle has demonstrated a good performance under aggressive cornering acceleration conditions.

Gordon, Howell, and Brandao [30] have carried out a more general study on the integrated control methodologies and systems. The paper presents the architecture and layers of control systems, how they interact, and development of subsystem control strategies, etc. An example study is also presented at the end of the paper, which demonstrates a handling dynamics problem and some results with integrated control systems.

Burgio and Zegelaar [31] have developed an integrated vehicle control using state feedback linearization technique and demonstrated some results accordingly. They have first used a SISO controller utilizing steer control. Then, due to some deficiencies of the first controller design, they have used brake control as well as active steering.

A control strategy for future in wheel motored electric drive systems is proposed by Tahami, Farhangi, and Kazemi [32]. The paper mainly focuses on Fuzzy logic driver assist stability system for all-wheel-drive electric vehicles. The controller involves a yaw reference based dynamic yaw control. For this yaw rate reference, a feed-forward neural network is employed. The vehicle speed is estimated by a multi-sensor data fusion method and embedded accelerometer, whereas a Fuzzy logic system decides the comparative reliability. Vehicle speed is properly found, and a Fuzzy based yaw rate controller manipulates independent wheel torques to eliminate the instability.

Zheng, Tang, Han, Zhang [33] have developed an 8 DOF vehicle model and a Vehicle Dynamics Control system to track a desired vehicle behavior. The designed controller has built-in cascaded components such as yaw moment major controller and wheel slip minor controller, as it is an integrated vehicle stability system. For yaw controller design, LQR methodology is exploited and for wheel slip controller, sliding mode is applied.

CHAPTER 3

MATHEMATICAL VEHICLE MODELS

3.1 INTRODUCTION

To simulate the performance of the designed controller and make a throughout analysis, there is need for a real test vehicle or a detailed mathematical model of a vehicle. Real world testing has its own advantages, since, if the application is carefully done, the errors coming from simplifications in mathematical models are avoided. Furthermore, during the implementation of the designed controller and analysis of the performance, new problems which are not foreseen before can be detected. However, the real vehicle application lacks the flexibility and easiness of modifying the configuration. Besides, the cost of implementation is usually excessive compared with the modeling procedure in a computer environment. A detailed mathematical model of a real vehicle is another solution for these problems. The trouble-free application of the modifications and availability of numerous simulations within acceptable times, makes the mathematical modeling of a vehicle feasible against real vehicle application.

In this study, two vehicle models will be used for simulation and control purposes. The detailed 8 degree of freedom model will be utilized to simulate the actual vehicle behavior, thus imitating a real vehicle. A simpler 2 degree of freedom bicycle model will be used to predict the driver's intention and apply necessary control outputs to stabilize the vehicle.

3.2 VEHICLE MODEL

For the simulation of vehicle together with the designed yaw controller, an accurate but simple enough vehicle model is required. Several models are available in the literature for this purpose, containing different degree of freedoms. Hence, a decision making process should be done judging the complexity coming with added degree of freedoms and loss-of-accuracy with neglected degree of freedoms. Added degrees of freedoms generally result in increased computing time while the accuracy of the vehicle model slightly increases. On the other hand, some essential degree of freedoms should not be neglected to represent the vehicle behavior similar to the real vehicle behavior.

Considering the motions of interest and other motions strongly related to these,, the non-linear vehicle model considered in this study for simulation has 8 degree of freedoms (DOFs). These degrees of freedoms are namely the longitudinal and lateral motions, yaw, roll, and 4 wheel rotations. The pitch motion, suspension motions, suspension geometry, and body bounce motions are neglected since this study is generally about controlling the handling behavior of vehicles. Contrary to the aim of the study, these degree of freedoms have generally importance on ride comfort studies, and relatively unimportant in handling studies. Assuming that the tires are connected rigidly to the vehicle body and perpendicular to the road surface, a minute accuracy for vehicle response is lost. The local coordinate system is attached to the center of gravity of the vehicle and all equations are derived accordingly. The sprung and unsprung masses are considered separately so that the suspension stiffness/damping effects and roll motion can be investigated more accurately. The roll axis is defined as the line connecting the roll centers of the front and rear axles and assumed to be stationary throughout the vehicle length. The tilting and restoring moments due to the roll motion is taken into account while deriving the equations.

The steering angle is generally assumed to be equal for front right and front left tires and the vehicle is assumed to be FWS. The pitch motion and coupled motions arising from this is not considered during the derivation of the equations of motion; but the

load transfer due to pitch motion is taken into account. The torque inputs to the wheels resulting from driver commands are applied independently to each wheel. The degrees of freedoms are shown in Fig.3.1.
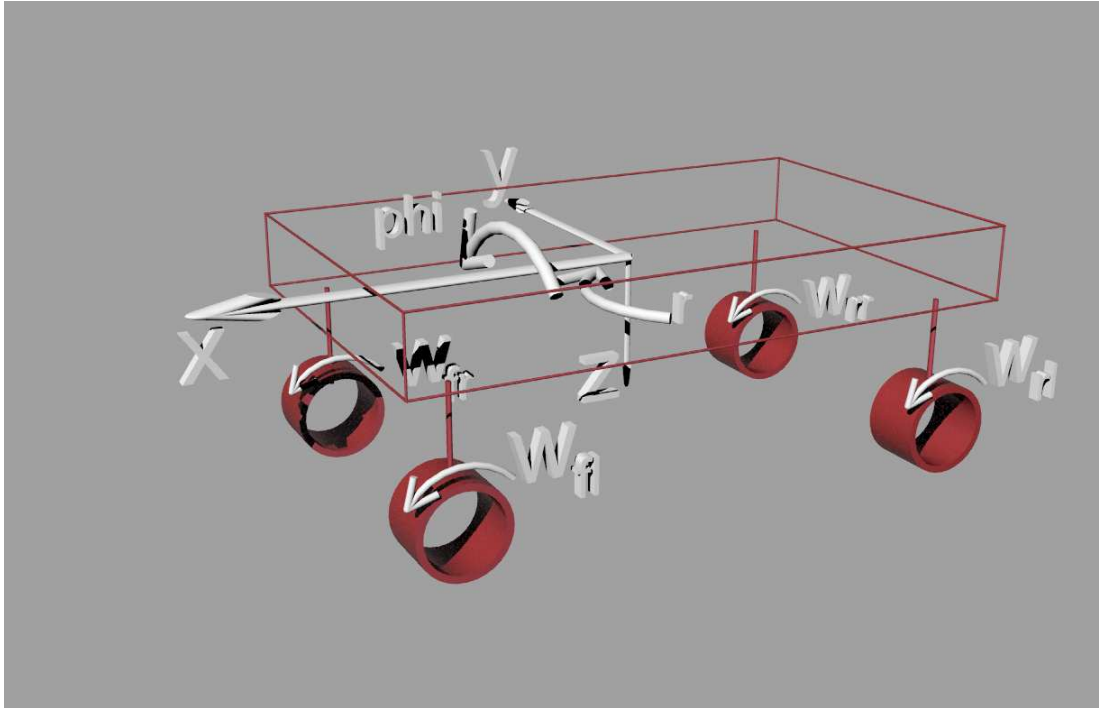
Fig.3.1 8 DOF Vehicle Model showing each DOF with arrows

As for the roll motion, the roll centers of the front and rear axles are assumed to be fixed during the motion of the vehicle. Furthermore, the rotational stiffness and damping constants for the roll motion are assumed to be fixed for the period of the roll motion. The forces derived from external sources such as air drag in x and y directions, unbalanced loading of the car, road gradients, etc. are neglected while deriving the equations of motion.

3.2.1 EQUATIONS OF MOTION AND THEIR REPRESENTATION

The Newtonian method is used to derive the equations of motion. The Newtonian equations of motion can be expressed simply as

F=m*a   (3.1)

The general free body diagram for the 8 DOF nonlinear vehicle model is shown in Fig.3.2 The roll motion's effects are shown using the free body diagram shown in Fig. 3.3.
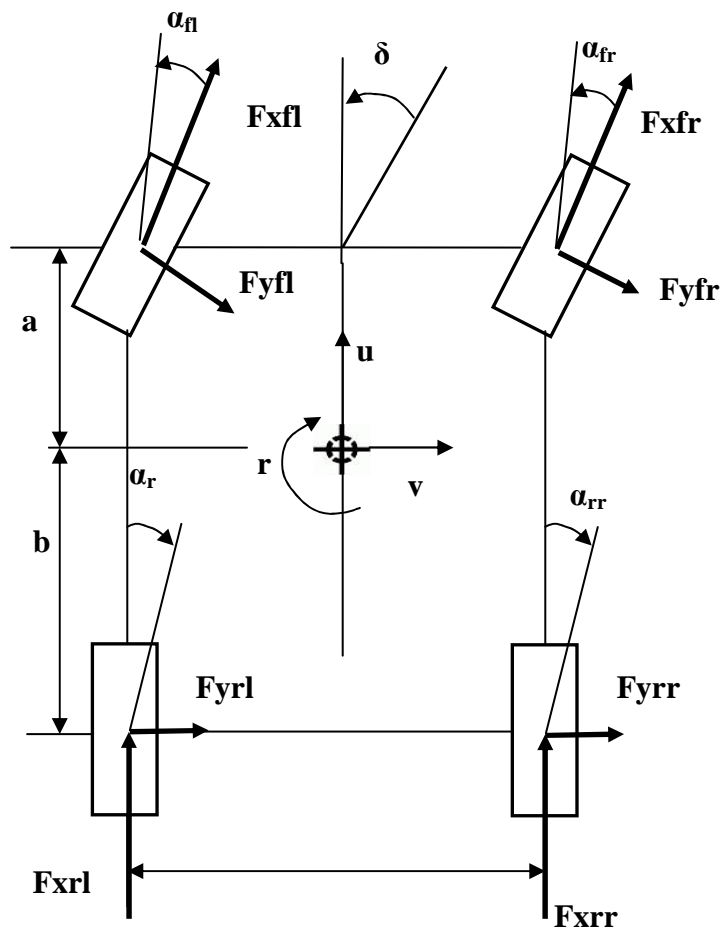
Fig. 3.2 Vehicle Model- Planar motion and forces (xy plane)
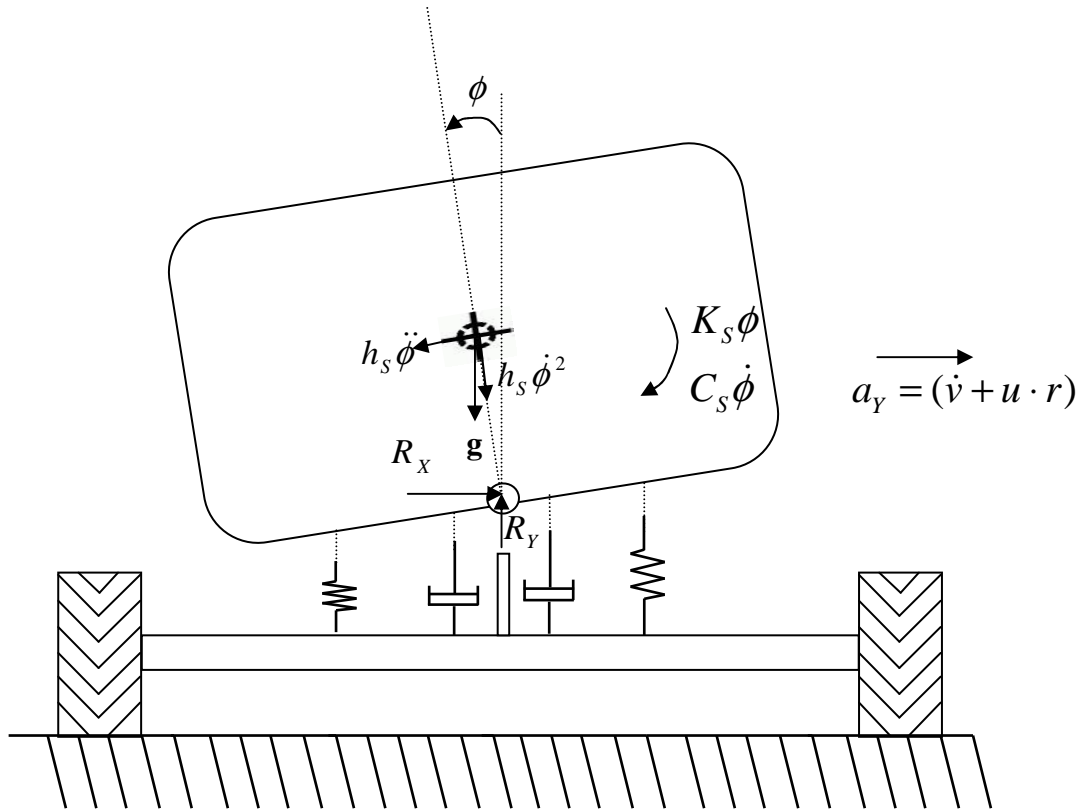
Fig. 3.3 Vehicle Model- Roll motion and forces (yz plane)

3.2.1.1 LONGITUDINAL MOTION (X-DIRECTION)

General force equilibrium for the vehicle body in x-direction is as follows:

$$M(\dot{u} - vr) + M_s h_s r\dot{\phi} = \sum F_x \qquad (3.2)$$

and

$$\sum F_x = \sum F_{vehicle} + \sum F_{other} \qquad (3.3)$$

while F_{other} represents forces such as air drag, forces coming from road gradients etc and $F_{vehicle}$ represent forces coming from tires. $F_{vehicle}$ can be defined as follows:

$$\sum F_{vehicle} = F_{xfl} \cos \delta_{fl} + F_{xfr} \cos \delta_{fr} + F_{xrl}$$
$$+ F_{xrr} - F_{yfl} \sin \delta_{fl} - F_{yfr} \sin \delta_{fr} \tag{3.4}$$

Assuming other forces (such as aerodynamic and rolling resistances) as negligible, the overall force acting on the longitudinal motion of the vehicle can be assumed as $F_{vehicle}$. Here, the longitudinal acceleration of the vehicle a_x is considered as $a_x = (\dot{u} - v \cdot r)$. Hence, the derivative of the velocity of the vehicle in x direction is

$$\dot{u} = \frac{1}{M}(F_{xfl} \cos \delta_{fl} + F_{xfr} \cos \delta_{fr} + F_{xrl} + F_{xrr} - F_{yfl} \sin \delta_{fl} - F_{yfr} \sin \delta_{fr})$$
$$- h_s r \dot{\phi} + v \cdot r \tag{3.5}$$

3.2.1.2 LATERAL MOTION (Y-DIRECTION)

General force equilibrium for the vehicle body in y-direction is as follows:
$$M(\dot{v} + u \cdot r) + M_s h_s \ddot{\phi} \cdot \cos(\phi) - M_s h_s \dot{\phi}^2 \cdot \sin(\phi) = \sum F_Y \tag{3.6}$$

while F_Y is the resultant of the tire forces:

$$\sum F_Y = F_{yfl} \cos \delta_{fl} + F_{yfr} \cos \delta_{fr} + F_{yrl}$$
$$+ F_{yrr} + F_{xfl} \sin \delta_{fl} + F_{xfr} \sin \delta_{fr} \tag{3.7}$$

The third term in the former equation is not taken into account in the model since the square of the roll rate is considerably small compared to other terms. Also, here the lateral acceleration of the vehicle a_Y is considered as $a_Y = (\dot{v} + u \cdot \gamma)$. Hence, the derivative of the velocity of the vehicle in x direction is

$$\dot{v} = \frac{1}{M}(F_{yfl} \cos \delta_{fl} + F_{yfr} \cos \delta_{fr} + F_{yrl} + F_{yrr} + F_{xfl} \sin \delta_{fl} + F_{xfr} \sin \delta_{fr})$$
$$- h_s \ddot{\phi} \cdot \cos(\phi) - u \cdot r \tag{3.8}$$

28

3.2.1.3 YAW AND ROLL MOTIONS

The equations for yaw and roll motion are coupled and these equations should be uncoupled before continuing.

$$I_{ZZ} \cdot \dot{r} - I_{XZ} \cdot \dot{p} = \sum M_Z \tag{3.8}$$

$$I_{XX} \cdot \dot{p} - I_{XZ} \cdot \dot{r} = \sum M_X \tag{3.9}$$

where $\dot{r}$ represents yaw acceleration and $\dot{p}$ represents the second derivative of the roll angle. When the necessary elimination is done, the equations for the yaw and roll motion can be expressed as;

$$\dot{r} = \frac{M_Z \cdot I_{XX} + M_X \cdot I_{XZ}}{I_{XX} \cdot I_{ZZ} - I_{XZ}^2} \tag{3.10}$$

and

$$\dot{p} = \frac{M_Z \cdot I_{XZ} + M_X \cdot I_{ZZ}}{I_{XX} \cdot I_{ZZ} - I_{XZ}^2} \tag{3.11}$$

where M_Z and M_X can be delineated as

$$
\begin{aligned}
M_Z = {}& a \cdot (F_{xfl} \sin \delta_{fl} + F_{xfr} \sin \delta_{fr} + F_{yfl} \cos \delta_{fl} + F_{yfr} \cos \delta_{fr}) \\
& + b(-F_{yrl} - F_{yrr}) + \frac{t_r}{2}(F_{xrl} - F_{xrr}) \\
& + \frac{t_f}{2}(F_{yfl} \sin \delta_{fl} - F_{yfr} \sin \delta_{fr} - F_{xfl} \cos \delta_{fl} + F_{xfr} \cos \delta_{fr})
\end{aligned} \tag{3.12}
$$

$$M_X = m_s \cdot h_s \cdot (\dot{v} + u \cdot r) + m_s \cdot h_s \cdot g \cdot \phi + M_{\phi f} + M_{\phi r} \tag{3.13}$$

The term $m_S h_S \dot{\phi}^2$ has been neglected due the relatively small magnitude of $\dot{\phi}^2$. Here, $M_{\phi f}$ and $M_{\phi r}$ are combination of roll stiffness and damping forces for front and rear axles and formulated as follows:

$$M_{\phi f} = -K_{\phi f} \cdot \phi - C_{\phi f} \cdot \dot{\phi} \qquad (3.14)$$

$$M_{\phi r} = -K_{\phi r} \cdot \phi - C_{\phi r} \cdot \dot{\phi} \qquad (3.15)$$

Here, if mass symmetry of the real vehicles with respect to x and z axis is taken into account, the I_{xz} term can be seen to have an especially low value relative to I_{xx} and I_{zz} in real vehicle data. Therefore, the terms with I_{xz} may be neglected in order to have the following equation of motions.

$$\dot{r} = \frac{1}{I_{zz}} \big[a \cdot (F_{xfl} \sin \delta_{fl} + F_{xfr} \sin \delta_{fr} + F_{yfl} \cos \delta_{fl} + F_{yfr} \cos \delta_{fr})$$

$$+ b(-F_{yrl} - F_{yrr}) + \frac{t_r}{2}(F_{xrl} - F_{xrr}) \qquad (3.16)$$

$$+ \frac{t_f}{2}(F_{yfl} \sin \delta_{fl} - F_{yfr} \sin \delta_{fr} - F_{xfl} \cos \delta_{fl} + F_{xfr} \cos \delta_{fr}) \big]$$

$$\dot{p} = \frac{1}{I_{xx}} m_S \cdot h_S \cdot (\dot{v} + u \cdot r) + m_S \cdot h_S \cdot g \cdot \phi - K_{\phi f} \cdot \phi - C_{\phi f} \cdot \dot{\phi}$$

$$- K_{\phi r} \cdot \phi - C_{\phi r} \cdot \dot{\phi} \qquad (3.17)$$

Up to this point, the motion of the vehicle is defined in terms of longitudinal and lateral acceleration, yaw rate and roll angular acceleration. However, the normal load distribution changes due to longitudinal and lateral accelerations and yaw and roll motions should be also taken into account.

3.2.2 NORMAL LOAD DISTRIBUTION

The normal load distribution can be expressed in terms of four different variants. These variants are static load, load transfer due to the longitudinal acceleration, load transfer due to the lateral acceleration, and load transfer due to the roll moment

transfer created by tilting motion of the sprung mass. Note that, for the lateral and longitudinal load transfer, $\dot{v}$ and $\dot{u}$ terms are not used, instead, a_x and a_y terms are preferred since yaw terms affect the longitudinal and lateral acceleration definitions. (See "Longitudinal and lateral motions" section).

$$F_{ZFL} = \frac{m \cdot g \cdot b}{2 \cdot (a+b)} - \frac{m \cdot a_x \cdot h}{2 \cdot (a+b)} - \frac{m \cdot a_y \cdot b \cdot h}{2 \cdot (a+b) \cdot t_f} + \frac{M_{\phi f}}{t_f} \tag{3.18}$$

$$F_{ZFR} = \frac{m \cdot g \cdot b}{2 \cdot (a+b)} - \frac{m \cdot a_x \cdot h}{2 \cdot (a+b)} + \frac{m \cdot a_y \cdot b \cdot h}{2 \cdot (a+b) \cdot t_f} - \frac{M_{\phi f}}{t_f} \tag{3.19}$$

$$F_{ZRL} = \frac{m \cdot g \cdot a}{2 \cdot (a+b)} + \frac{m \cdot a_x \cdot h}{2 \cdot (a+b)} - \frac{m \cdot a_y \cdot a \cdot h}{2 \cdot (a+b) \cdot t_r} + \frac{M_{\phi r}}{tr} \tag{3.20}$$

$$F_{ZRR} = \frac{m \cdot g \cdot a}{2 \cdot (a+b)} + \frac{m \cdot a_x \cdot h}{2 \cdot (a+b)} + \frac{m \cdot a_y \cdot a \cdot h}{2 \cdot (a+b) \cdot t_r} - \frac{M_{\phi r}}{tr} \tag{3.21}$$

3.2.3 WHEEL DYNAMICS

The equations of motion for the vehicle wheels include the brake/traction torque applied and the moment created by the force generated with the road-tire interaction. The self aligning torque is neglected since the effects of this torque to vehicle handling behavior are not significant. The rotational equations of motion are as follows:

$$\dot{\omega}_{fl} = \frac{1}{I_\omega} (-F_{xfl} \cdot R - M_{\omega fl}) \tag{3.22}$$

$$\dot{\omega}_{fr} = \frac{1}{I_\omega} (-F_{xfr} \cdot R - M_{\omega fr}) \tag{3.23}$$

$$\dot{\omega}_{rl} = \frac{1}{I_\omega} (-F_{xrl} \cdot R - M_{\omega rl}) \tag{3.24}$$

$$\dot{\omega}_{rr} = \frac{1}{I_\omega} (-F_{xrr} \cdot R - M_{\omega rr}) \tag{3.25}$$

Besides rotational motion, the lateral slip angles and the longitudinal slip values are also essential for tire force generation calculations. Lateral slip angle can be defined as the angle between the plane of the wheel rotation (not steering rotation) and the direction of motion. The derived equations for lateral slip angles are as follows:

$$\alpha_{fl} = \delta_{fl} - \tan^{-1}\left(\frac{v + a \cdot r}{u + \dfrac{t_f}{2} \cdot r}\right) \tag{3.26}$$

$$\alpha_{fr} = \delta_{fr} - \tan^{-1}\left(\frac{v + a \cdot r}{u - \dfrac{t_f}{2} \cdot r}\right) \tag{3.27}$$

$$\alpha_{rl} = \tan^{-1}\left(\frac{v - b \cdot r}{u + \dfrac{t_r}{2} \cdot r}\right) - \delta_{rl} \tag{3.28}$$

$$\alpha_{rr} = \tan^{-1}\left(\frac{v - b \cdot r}{u - \dfrac{t_r}{2} \cdot r}\right) - \delta_{rr} \tag{3.29}$$

For longitudinal slip calculations, the velocity component in the wheel plane direction should also be calculated. The related equations are as follows:

$$v_{\omega fl} = \sqrt{\left(u + \frac{t_f}{2} \cdot r\right)^2 + (v + a \cdot r)^2} \cdot \cos(\alpha_{fl}) \tag{3.30}$$

$$v_{\omega fr} = \sqrt{\left(u - \frac{t_f}{2} \cdot r\right)^2 + (v + a \cdot r)^2} \cdot \cos(\alpha_{fr}) \tag{3.31}$$

$$v_{\omega rl} = \sqrt{\left(u + \frac{t_r}{2} \cdot r\right)^2 + (v - b \cdot r)^2} \cdot \cos(\alpha_{rl}) \tag{3.32}$$

$$v_{\omega rr} = \sqrt{\left(u - \frac{t_r}{2} \cdot r\right)^2 + (v - b \cdot r)^2} \cdot \cos(\alpha_{rr}) \tag{3.33}$$

There exist two different longitudinal slip definitions for braking and traction conditions. Here, in this study, the attention mainly focuses on the braking situation, which is very likely to occur in emergency cases. However, the model is also capable of detecting the driver's intention of braking or acceleration and modifies the slip calculation accordingly. The corresponding longitudinal slip equations of braking and tractive effort for each wheel can be expressed as follows:

Braking Conditions:

$$S_{fl} = \frac{v_{\omega fl} - \omega_{fl} \cdot R}{v_{\omega fl}} \tag{3.34}$$

$$S_{fr} = \frac{v_{\omega fr} - \omega_{fr} \cdot R}{v_{\omega fr}} \tag{3.35}$$

$$S_{rl} = \frac{v_{\omega rl} - \omega_{rl} \cdot R}{v_{\omega rl}} \tag{3.36}$$

$$S_{rr} = \frac{v_{\omega rr} - \omega_{rr} \cdot R}{v_{\omega rr}} \tag{3.37}$$

Traction Conditions

$$S_{fl} = \frac{\omega_{fl} \cdot R - v_{\omega fl}}{\omega_{fl} \cdot R} \tag{3.38}$$

$$S_{fr} = \frac{\omega_{fr} \cdot R - v_{\omega fr}}{\omega_{fr} \cdot R} \tag{3.39}$$

$$S_{rl} = \frac{\omega_{fr} \cdot R - v_{\omega fr}}{\omega_{fr} \cdot R} \tag{3.40}$$

$$S_{rr} = \frac{\omega_{fr} \cdot R - v_{\omega fr}}{\omega_{fr} \cdot R} \qquad (3.41)$$

The overall equations needed for vehicle handling simulation excluding the tire dynamics and road-tire interaction are defined so far. The tire model is going to be presented in the next section.

3.3 TIRE MODEL

In order to simulate the vehicle behavior accurately, tire forces resulting from the normal load and other conditions should be calculated in a precise manner. The operating conditions may vary in a wide range, thus the model should be capable of simulating the tire behavior under different conditions. The challenging point in this simulation arises from the highly nonlinear behavior of the tires. There exist several models associated with this nonlinear behavior in the literature. In this study, tire model developed by Allen et. al. [34] is selected to simulate the tire behavior.

Allen tire model is a nonlinear tire model capable of calculating lateral and longitudinal forces by taking many parameters into account. The tire parameters are obtained experimentally. The operation range for the simulation lies between pure adhesion (no slip condition) to pure sliding (spinning). A more complex or simpler model may be used, but the complexity and the accuracy levels of this model are appropriate for the aim of this study.

Before starting to introduce the equations, zero camber angle is assumed so that self aligning moment is neglected. This assumption arises from the assumptions of the derivation of the Allen tire model. The input parameters for calculations are longitudinal wheel slip angle [Z], tire lateral slip angle [α], nominal road surface/tire friction coefficient [μ] and tire rotational velocity [ω]. The longitudinal and lateral tire forces are calculated using the following equations. There, F(σ) is the force saturation function whereas σ denotes composite slip function and C_i's are experimental coefficients. (i=1,2,3,4)

$$F(\sigma) = \frac{C_1\sigma^3 + C_2\sigma^2 + \frac{\pi}{4}\sigma}{C_1\sigma^3 + C_3\sigma^2 + C_4\sigma + 1}$$ (3.42)

whereas

$$\sigma = \frac{\pi \cdot a_p^{\,2}}{8 \cdot \mu_0 \cdot F_z} \cdot \left[k_s^{\,2} \cdot \tan^2\alpha + k_c^{\,2} \cdot \left(\frac{S}{1-S}\right)^2 \right]^{\frac{1}{2}}$$ (3.43)

Here, k_s and k_c denote the lateral stiffness coefficients and corrected longitudinal stiffness coefficients, respectively while a_p denotes the tire contact patch length. The necessary formulations for all these parameters are given below.

$$k_s = \frac{2 \cdot \left(A_0 + A_1 \cdot F_z - \frac{A_1}{A_2} \cdot F_z^{\,2} \right)}{a_{po}^{\,2}}$$ **(3.44)**

$$k_c = \frac{2 \cdot F_z \cdot \frac{CS}{F_z}}{a_{po}^{\,2}}$$ (3.45)

$$a_p = a_{po} \cdot \left(1 - k_a \cdot \frac{F_x}{F_z} \right)$$ (3.46) where $a_{p0} = \frac{0.0768 \cdot \sqrt{F_z \cdot F_{zt}}}{T_w \cdot \left(T_p + 5 \right)}$ (3.47)

In these equations, several experimental parameters are used. These are initial tire contact patch length, a_{p0}, tire contact patch coefficient, k_a, designed tire load, F_{zt}, thread width, T_w and the tire inflation pressure, T_p.

The given corrected longitudinal stiffness coefficient should converge to a common sliding friction coefficient at high slips. Moreover, the initial tire road friction

35

coefficient transforms into a sliding friction coefficient. For this purpose, a nonlinear modification parameter, so called k_μ, is used. Modified versions of this longitudinal stiffness coefficient and road surface friction coefficients are introduced as follows:

$$k_c' = k_c + (k_s - k_c) \cdot \sqrt{\sin^2(\alpha) + S^2 \cdot \cos^2(\alpha)} \tag{3.48}$$

and

$$\mu = \mu_0 \cdot \sqrt{1 - k_\mu \cdot \left(\sin^2(\alpha) + S^2 \cdot \cos^2(\alpha)\right)} \quad (3.49) \quad \text{where} \quad k_\mu = \frac{1}{11} \cdot \sqrt[4]{v_w} \tag{3.50}$$

While v_ω denotes the wheel speed in-wheel-plane and μ_0, denotes the peak tire-road friction coefficient, which can be expressed as

$$\mu_0 = 1.176 \cdot \mu_{nom} \cdot \left(B_1 F_z + B_3 + B_4 F_z^2\right) \tag{3.51}$$

The overall steps for calculating the longitudinal and lateral tire forces are covered so far. The normalized tire forces with respect to normal load on the wheel can be calculated as follows.

$$\frac{F_x}{\mu \cdot F_z} = \frac{-F(\sigma) \cdot k_c' \cdot S}{\sqrt{k_s^2 \cdot \tan^2 \alpha + k_c'^2 \cdot S^2}} \tag{3.52}$$

$$\frac{F_y}{\mu \cdot F_z} = \frac{F(\sigma) \cdot k_s \cdot \tan \alpha}{\sqrt{k_s^2 \cdot \tan^2 \alpha + k_c'^2 \cdot S^2}} \tag{3.53}$$

Figure 3.4 and figure 3.5 demonstrate the tire force behavior. The former figure represents the longitudinal tire brake force versus longitudinal slip ratio while the latter figure represents the lateral tire cornering force versus lateral slip angle of the wheel.

Normalized Braking Force F_x/F_z vs. Longitudinal Slip ratio S
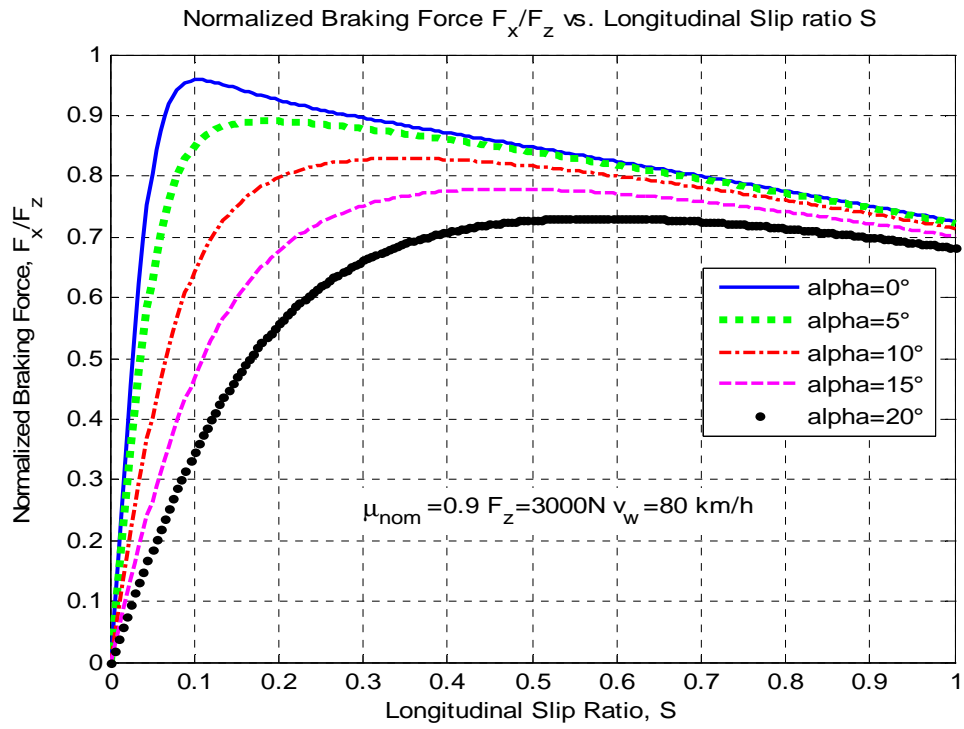
Fig. 3.4 Normalized Braking Force versus Longitudinal Slip Ratio

Normalized Cornering Force F_y/F_z vs. Lateral Slip Angle α [deg]
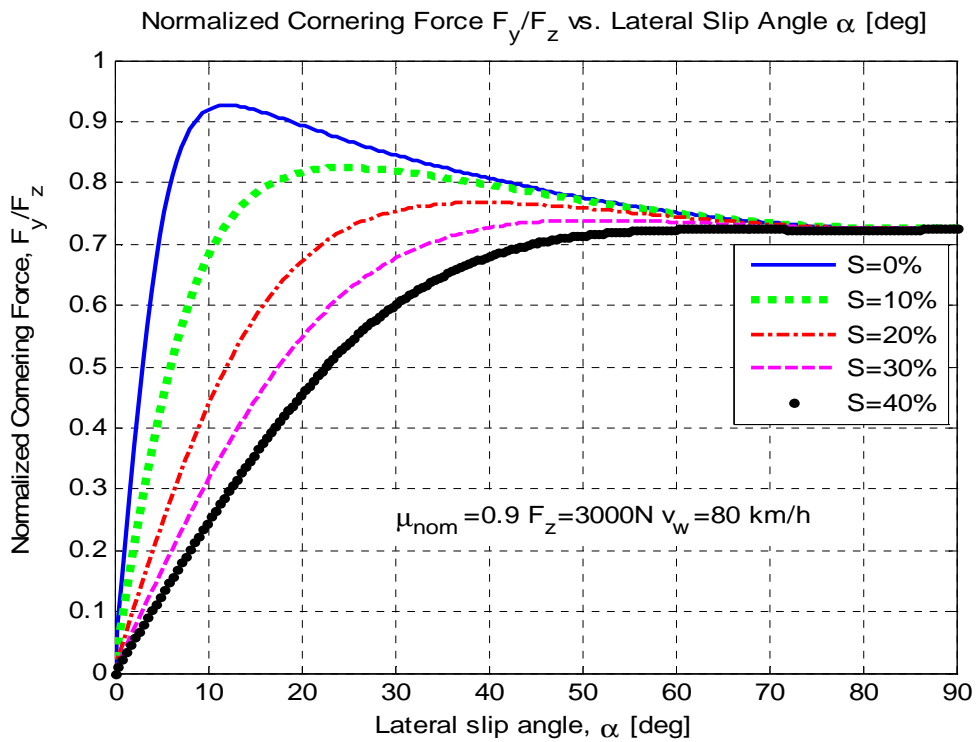
Fig. 3.5 Normalized Cornering Force versus Lateral Slip angle

Normalized Braking and Cornering Forces, F_x/F_z and F_y/F_z vs. Longitudinal Slip ratio S
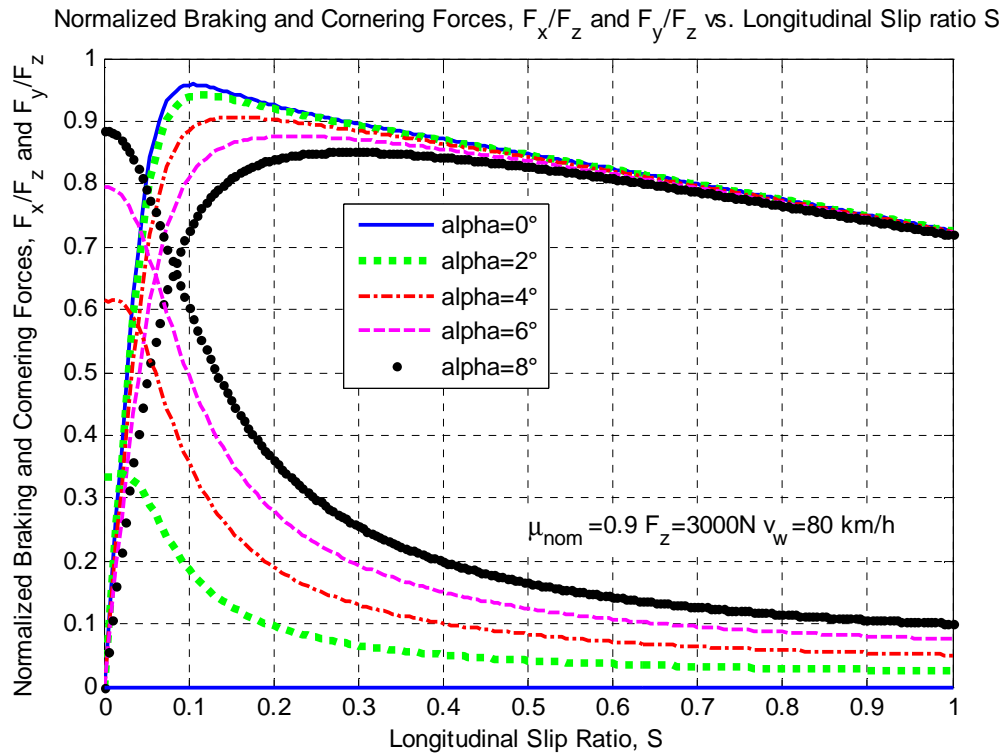
Fig. 3.6 Normalized Braking and Cornering Forces versus Longitudinal Slip Ratio

Normalized Cornering Force F_y/F_z vs. Normalized Braking Force, F_x/F_z
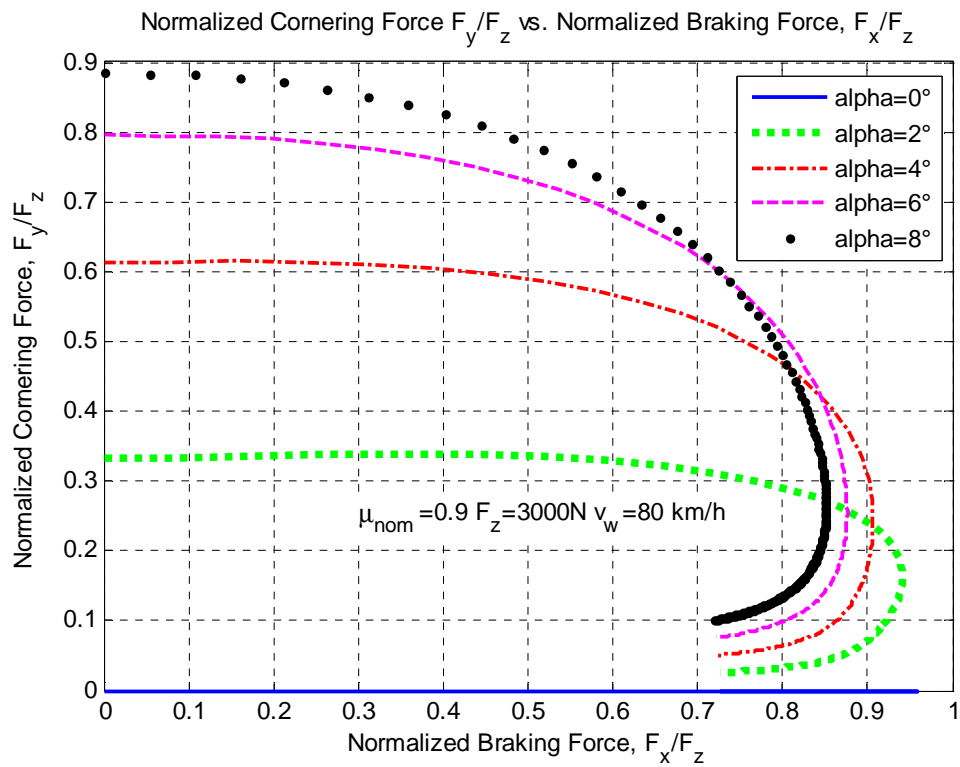
Fig. 3.7 Normalized Cornering Forces versus Normalized Braking Force

38

3.4 TWO DEGREE OF FREEDOM VEHICLE MODEL –BICYCLE MODEL

The main aim of the active yaw controller in this study is to interpret and track the driver's intention. For this purpose, there exist several ways to understand the driver's objective. These ways may vary from a single equation for the reference yaw rate derivation, which has an arbitrary constant for manipulating the reference vehicle behavior; to nonlinear set of equations, including all controlled/affected degree of freedoms [21],[33],[42]. The general idea here is, there should be an assigned vehicle behavior tendency which may be referred as under-/oversteering. This tendency should be presented by the reference equations, so that the drivers' manipulation is predicted as intended. For this purpose, building a simple vehicle model which is capable of presenting main behavior deducted by the input signals created by the driver is utilized. The input signals may include acceleration or brake demand, steering input, etc. In this study, a 2 degree of freedom model (commonly known as bicycle model) is built and used to interpret the driver's intention. The two degree of freedom vehicle model is obtained by lumping two wheels on the same axle to a single virtual wheel, which is aligned to the centerline of the vehicle. It is generally capable of demonstrating essential handling behavior of a vehicle for low lateral acceleration.

The two degree of freedom model presented here is a linearized model which accepts the vehicle longitudinal velocity and the steering angle as inputs. These inputs are measured variables and can be supplied directly. One crucial point is, the vehicle longitudinal velocity is not always measured, instead complex estimation algorithms are used while heavy braking conditions apply [32],[35]. The outputs of the model are lateral velocity and vehicle sideslip angle. The tire forces are estimated using a linearized model where the cornering force increases linearly with sideslip angle and the braking force increases linearly with the longitudinal slip. Figure 3.6 shows the forces applied on the vehicle model and the variables used in the model.
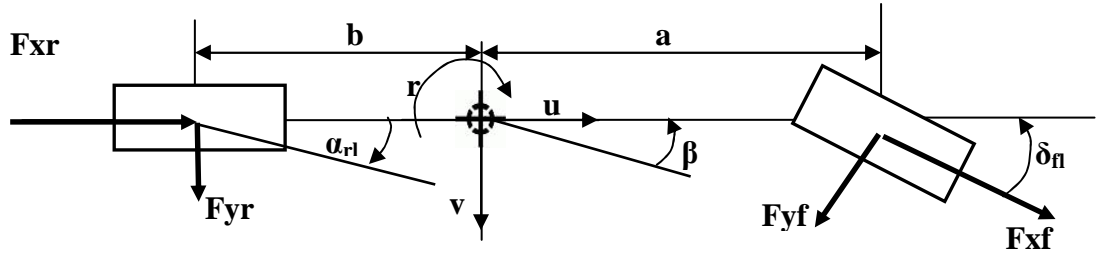
Fig. 3.8 Two degree of freedom model

In this model, the tire forces are lumped into one virtual wheel for every axle (e.g. $F_{xr} = F_{xrl} + F_{xrr}$). With this information, the equations of motion can be paraphrased as follows:

Longitudinal Motion:

$$m \cdot (\dot{u} - v \cdot r) = F_{xf} \cdot \cos(\delta) + F_{xr} - F_{yf} \cdot \sin(|\delta|) \tag{3.54}$$

Lateral Motion:

$$m \cdot (\dot{v} + u \cdot r) = F_{yf} \cdot \cos(\delta) + F_{yr} + F_{xf} \cdot \sin(|\delta|) \tag{3.55}$$

Rotational Motion:

$$J \cdot \dot{r} = \left(a \cdot F_{yf} \cdot \cos(\delta) - b \cdot F_{yr} \right) \cdot \mathrm{sgn}(\delta) + a \cdot F_{xf} \cdot \sin(\delta) \tag{3.56}$$

Note that the steer angle is measured as positive in the clockwise direction. Also, the sign functions for steering angle are necessary for left hand turns, since the equations change drastically. In the following simple form of the model, however, they will be neglected to articulate the state representation, although they are used in the predictor model. To simplify the model and linearize it in order to have a fast predictor for driver intention estimation, there should be some intuitive assumptions. First, the cornering tire forces are linearized for small tire slip angles as,

$$F_{yf} = C_f \cdot \alpha_f \tag{3.57}$$

40

and

$$F_{yr} = C_r \cdot \alpha_r \tag{3.58}$$

whereas the tire slip angles are defined as

$$\alpha_f = -\delta + \left(\frac{v + a \cdot r}{U} \right) \tag{3.59}$$

$$\alpha_r = \left(\frac{v - b \cdot r}{U} \right) \tag{3.60}$$

After this, the term (v*r) is dropped since it is considerably small in the linear operating range of the vehicle considering the longitudinal velocity, U. hence equation(3.54) can be replaced as

$$m \cdot \dot{U} = F_{xf} \cdot \cos(\delta) + F_{xr} - F_{yf} \cdot \sin(|\delta|) \tag{3.61}$$

Moreover, the vehicle longitudinal velocity can be kept as a constant parameter, thus reducing the input variables to two. Within the scope of the study, the vehicle longitudinal velocity is constantly supplied to the model but accepted as a parameter. Therefore, the degree of freedom of the vehicle model is reduced to two, expressed by equations (3.55) and (3.56). Also, small angle assumptions are made for steering wheel input, resulting in $\cos(\delta) \approx 1$ and $\sin(\delta) \approx 0$. These assumptions trim down the governing equations to the following form:

$$m \cdot (\dot{v} + U \cdot r) = F_{yf} + F_{yr} \tag{3.62}$$

$$J \cdot \dot{r} = a \cdot F_{yf} - b \cdot F_{yr} \tag{3.63}$$

Replacing these side forces with equations (3.57) and (3.58) with sideslip angle definitions given in (3.59) and (3.60), with a little housekeeping,

$$m \cdot \dot{v} = (C_f + C_r) \cdot \frac{v}{U} + (a \cdot C_f - b \cdot C_r - m \cdot U^2) \cdot \frac{r}{U} - C_f \cdot \delta \tag{3.64}$$

41

$$J \cdot \dot{r} = (a \cdot C_f - b \cdot C_r) \cdot \frac{v}{U} + (a^2 \cdot C_f + b^2 \cdot C_r) \cdot \frac{r}{U} - a \cdot C_f \cdot \delta \qquad (3.65)$$

which, in turn, can be expressed as in matrix form as,

$$\begin{bmatrix} m & 0 \\ 0 & J \end{bmatrix} \cdot \begin{Bmatrix} \dot{v} \\ \dot{r} \end{Bmatrix} = \begin{bmatrix} \dfrac{(C_f + C_r)}{U} & \dfrac{(a \cdot C_f - b \cdot C_r - m \cdot U^2)}{U} \\ \dfrac{(a \cdot C_f - b \cdot C_r)}{U} & \dfrac{(a^2 \cdot C_f + b^2 \cdot C_r)}{U} \end{bmatrix} \cdot \begin{Bmatrix} v \\ r \end{Bmatrix} + \begin{Bmatrix} -C_f \\ -a \cdot C_f \end{Bmatrix} \cdot \delta \qquad (3.66)$$

Finally, the vehicle sideslip angle can be described as the inverse tangent of the ratio of lateral velocity to longitudinal velocity. The overall vehicle model together with detailed and simple vehicle models and the yaw controllers are given in Fig. 3.7

$$\beta = \tan^{-1}(\frac{v}{u}) \cong \frac{v}{u} \qquad (3.67)$$

Fig. 3.7 Overall Vehicle Model

43
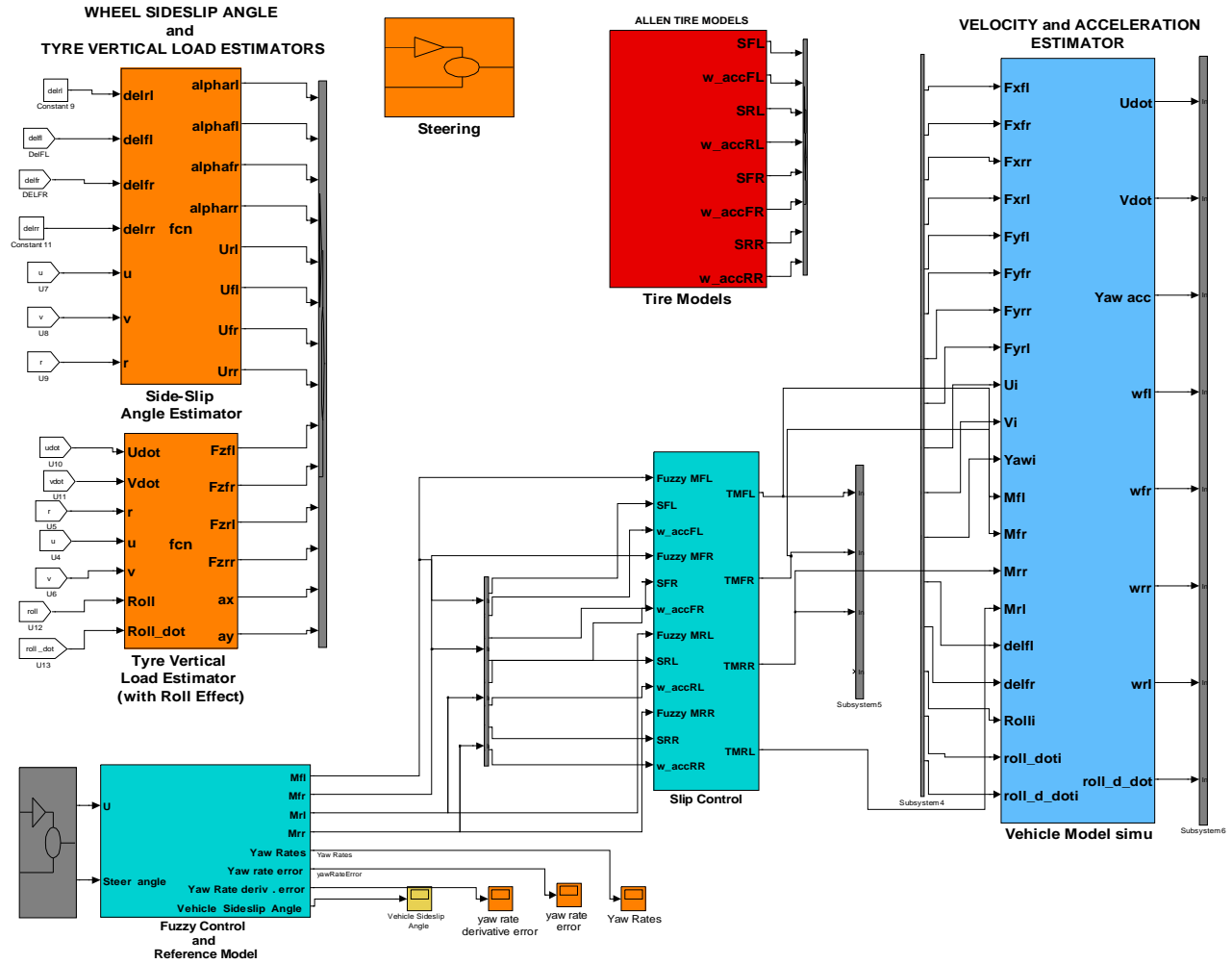
CHAPTER 4

CONTROLLER DESIGN

4.1 INTRODUCTION

The main objective of an active yaw controller is to control the yaw rate of the vehicle in case of any possible of undesired yaw behavior. Besides, during the manipulation for the control of this parameter, the designed controller should not allow the vehicle sideslip angle to surpass some predefined limits of steerability condition. This manipulation has some limits though, due to the bounded tire force generation capability defined ultimately by the coefficient of friction. The tire cornering force limits are expressed in the previous chapter in Fig. 3.5. The optimum cornering force for small longitudinal slips is obtained between 10-20 degrees. Note that, as the longitudinal slip increases the cornering force limit decreases rapidly. Therefore, for effective control, the longitudinal slip is to be controlled with a slip sub-controller. The slip sub-controller design used here is based on Şahin's work [37]. Tire slip controller will be introduced in a brief manner. In the next parts of this chapter, fuzzy based yaw controllers and tire-slip sub-controllers will be introduced and explained in detail.

4.2 FUZZY BASED YAW CONTROLLER DESIGN

The yaw controller design in this study is based on Fuzzy-control. There exist two different controller designs in this study. The first one deals only with yaw rate and the time derivative of the yaw rate. This controller continuously monitors the yaw rate and yaw acceleration and tries to estimate any undesired behavior by comparing these values with the desired values. The desired values are derived from the two degree of freedom model using driver's inputs. When any deviation from desired

behavior is detected, the yaw rate controller starts to command brake signal for the appropriate individual tires. The basic scheme for the designed yaw controller is given in Fig. 4.1.
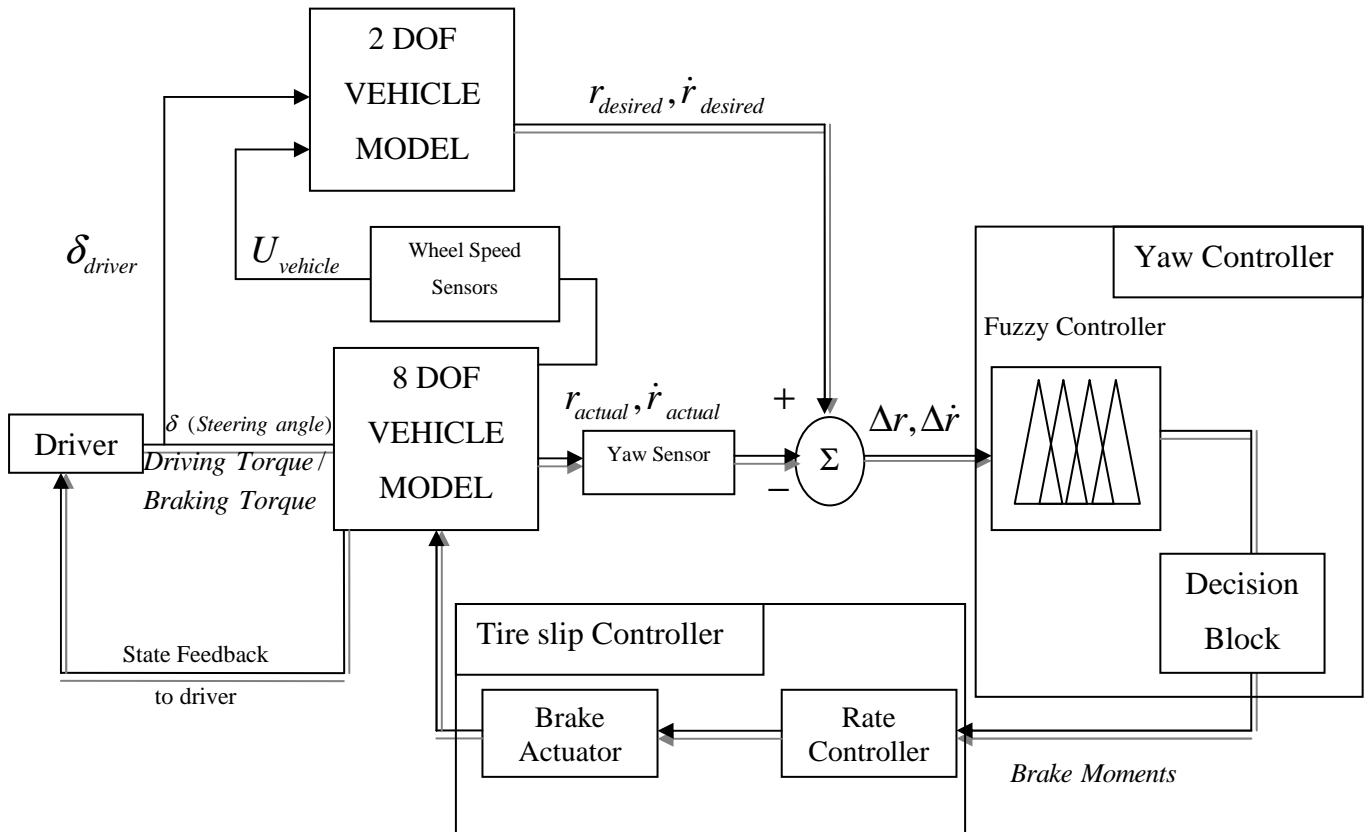

Fig. 4.1 Basic scheme of the proposed yaw controller

As it can be seen from the figure, the driver's steer and torque input (acceleration or deceleration input) are fed to both real vehicle model and simple reference model. The reference model also receives the longitudinal velocity from the real vehicle, or in our case, detailed vehicle model representing the actual vehicle. In real life applications, the longitudinal velocity is estimated via complex estimation algorithms

in especially heavy brake conditions [32][35]. The yaw rate and the derivative of the yaw rate (which is actually directly measured via a yaw acceleration sensor) are compared for the reference model and vehicle model and then the differences between reference and actual values are supplied to the fuzzy controller as error signals. A threshold mechanism exists between these error signals and the brake torque controller, so that the controller intervention is not disturbing for small deviations. The fuzzy controller then decides the brake torque necessary for counter yaw moment action. The decision block selects the appropriate tire for brake application, while the rate controller limits the brake torque change rate to applicable values so that the brake manipulation seems to be realistic considering the brake moment generation speeds. This brake torque is then applied to the detailed vehicle model. Brake torque is selected as the output for the control system. This selection is made since the available practical wheel slip controllers accept either longitudinal wheel slip or brake torque as the input. There exists a feedback signal sourcing from the 8 degree of freedom model to the driver, although this feedback is not modeled in this study. The driver in real life can receive feedback from the vehicle behavior so that s/he manipulates the control signals in a corrective manner if the vehicle is in low lateral acceleration range. The yaw controller is responsible, therefore, when the vehicle presents an uncommon behavior in case of excessive magnitude-behaviors.

The design of the fuzzy controller is based on an essentially trial and error procedure. The rule base covers the whole input domain while the output signal is unique for every input pair. The fuzzy controller mainly consists of three subsystems, namely, fuzzification, rule base, and inference mechanism and defuzzification [38]. The main scheme is shown in Fig. 4.2
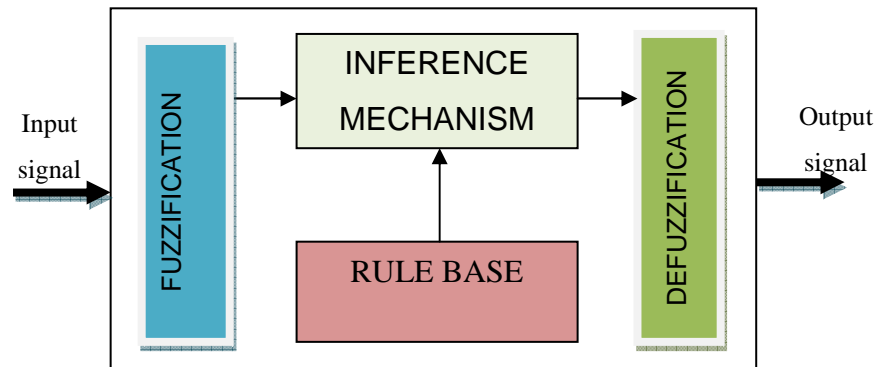
Fig. 4.2 Basic scheme of fuzzy controller

The fuzzification process is responsible for converting the control inputs into parameters which can be understood by the inference mechanism, whereas the inference mechanism is responsible for emulating the expert's decision making process, by averaging through rule based "if-then" statements. The rule base is predefined for the plant in order to guide the controller which action is to be taken in specific conditions. After this information is evaluated in inference mechanism or (inference engine), defuzzification process takes place in order to make the signal acceptable as output.

For the design and application of fuzzy control, MATLAB Fuzzy Toolbox is used. Mamdani inference method is used for implementing the inference mechanism and centroid algorithm is used for the defuzzification process. 9 different levels are defined for both the yaw rate and the yaw acceleration errors as membership functions. For different road conditions, the membership functions are defined separately as dry, wet, and icy, while the fuzzy controller scheme remains the same. The membership functions are indeed the same qualitatively, but the ranges which they cover are multiplied accordingly to comply with the need of yaw moment creation to corresponding road-tire surface friction coefficient. The membership functions of input and output parameters for the dry road condition (μ_{nom}=0.9) are shown in Fig. 4.3, Fig. 4.4 and Fig. 4.5, respectively. In these figures, the limits of different states for the inputs and outputs can be seen. For instance, the yaw rate error is expressed as negatively large (at 4th level) for the values between minus infinity to

-0.25 rad/s whereas it is also expressed as negatively large(3rd level) for the values between 0.3 rad/s and 0.1 rad/s.
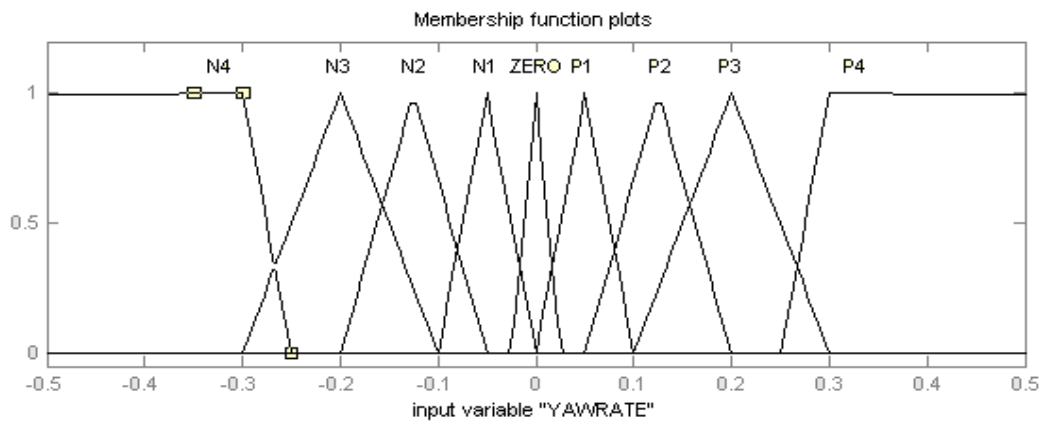

Fig. 4.3 Membership functions for yaw rate error input
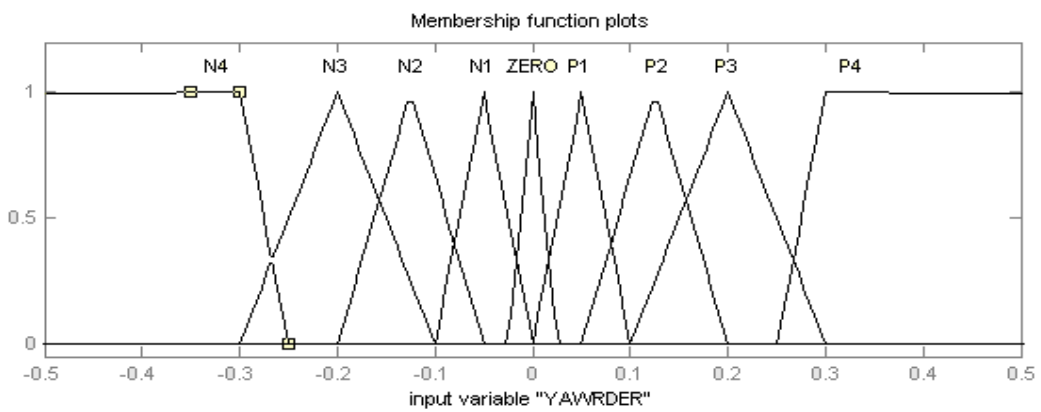
Fig. 4.4 Membership functions for yaw acceleration error input
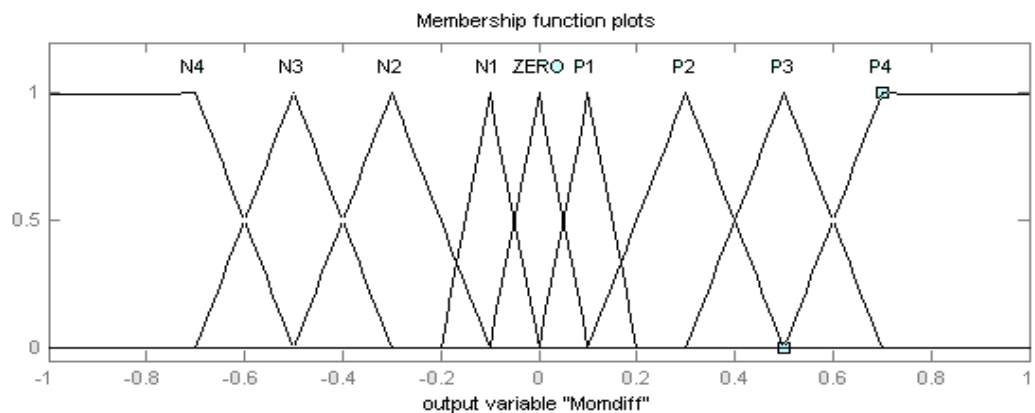
Fig. 4.5 Membership functions for brake moment difference output

The rule base is the key part of the design of fuzzy controller. The decision and trial-error processes are generally time-consuming while the tweaking of these rules is very helpful in gaining insight knowledge about vehicle lateral dynamics. The rule base has started with the following simple rules as given in the following list.

— If the yaw rate error (YAWRATE) is negative (N) and the yaw acc. error (YAWRDER) is negative (N), then brake moment difference is positively large (PL)

— If the yaw rate error (YAWRATE) is negative (N) and the yaw acc. error (YAWRDER) is zero (Z), then brake moment difference is positively medium (PM)

— If the yaw rate error (YAWRATE) is negative (N) and the yaw acc. error (YAWRDER) is positive (Z), then brake moment difference is positively small (PS)

— If the yaw rate error (YAWRATE) is zero (Z) and the yaw acc. error (YAWRDER) is negative (N), then brake moment difference is positively (PS)

— If the yaw rate error (YAWRATE) is zero (Z) and the yaw acc. error (YAWRDER) is zero (Z), then brake moment difference is zero (Z)

— If the yaw rate error (YAWRATE) is zero (Z) and the yaw acc. error (YAWRDER) is positive (P), then brake moment difference is negatively small (NS)

— If the yaw rate error (YAWRATE) is positive (Z) and the yaw acc. error (YAWRDER) is negative (N), then brake moment difference is negatively small (NS)

— If the yaw rate error (YAWRATE) is positive (Z) and the yaw acc. error (YAWRDER) is zero (Z), then brake moment difference is negatively medium (NM)

— If the yaw rate error (YAWRATE) is positive (Z) and the yaw acc. error (YAWRDER) is positive (Z), then brake moment difference is negatively large (PL)

These rules have played a guiding role as they are simple and intuitive rules for yaw control. The extended version of the rule base after extensive trial and error case is given in Table 4.1. The rows indicate the yaw rate errors while the columns indicate the yaw acceleration errors. The table remains identical for wet and ice road conditions, whereas the classification of the membership function remain identical, too. However, as the wet (μ_{nom}=0.4) and icy roads (μ_{nom}=0.1) have a narrower limit for stability, the membership functions for the yaw rate and yaw acceleration error definitions are distributed over a 3 times broader range for wet conditions and 10 times broader range for icy road conditions. This modification brings flexibility for the precise manipulation and prevents excessive intervention. Also, for these three different cases, the output is magnified with different brake torque constants. This method is also used in similar studies [35]

Table 4.1 Rule base table for active yaw controller

Yaw Rate Deriv. Error / Yaw RateError	N4	N3	N2	N1	ZERO	P1	P2	P3	P4
N4	N4	N4	N4	N4	N4	N4	N4	N4	N4
N3	N4	N4	N4	N4	N3	N3	N3	N3	N3
N2	N3	N3	N3	N3	N3	N3	N2	N2	N2
N1	N3	N3	N2	N2	N2	N2	N1	N1	N1
ZERO	N2	N2	N1	N1	ZERO	P1	P1	P2	P2
P1	P1	P1	P1	P2	P2	P2	P2	P3	P3
P2	P2	P2	P2	P3	P3	P3	P3	P3	P3
P3	P3	P3	P3	P3	P3	P4	P4	P4	P4
P4	P4	P4	P4	P4	P4	P4	P4	P4	P4

After defining the membership functions and rules to control the system, a control surface has been obtained. This 2-D plot enables the viewer to visualize the control

output (in this case, the brake torque) according to specified yaw rate error and yaw acc. error. The control surface for the designed yaw controller is given in Fig. 4.6.
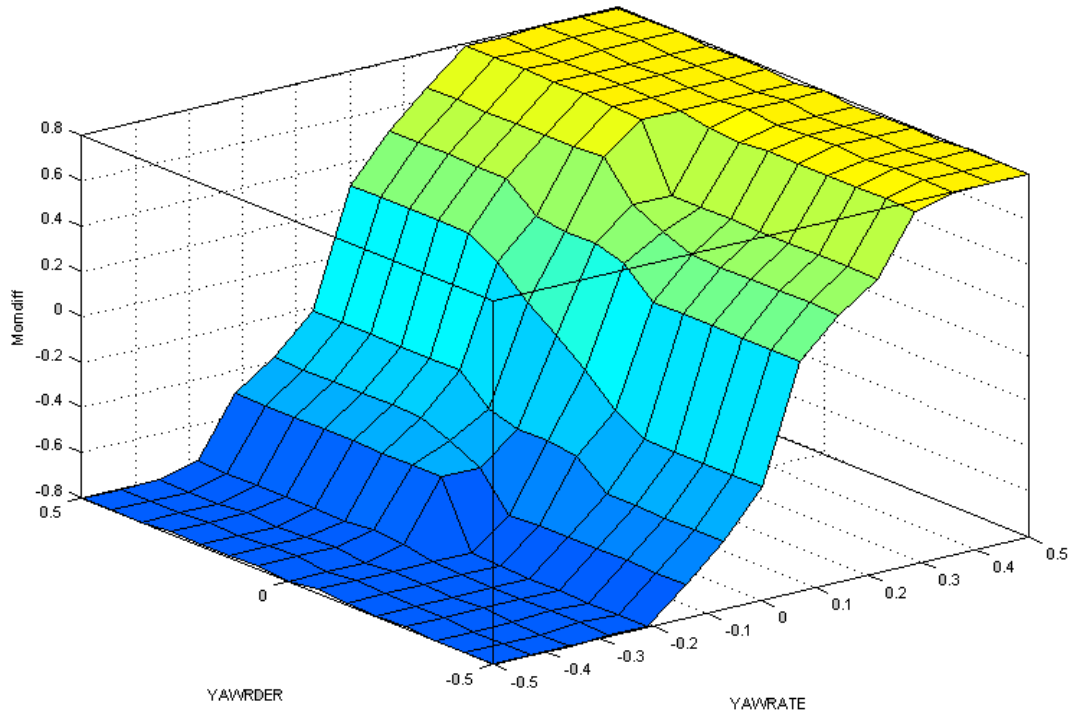

Fig. 4.6 The control surface for the designed yaw controller vs. yaw rate error and yaw acceleration error

As it can be seen from the surface, there exists one and only one output signal for every input pair. This statement is actually important for completeness and contradiction for any input pair in the rule base. There exist some formal and informal definitions and some intuitive techniques for these checks. However, neither of them has been proved to be valid for all cases and rule bases. Therefore, a logical rule base which has systematic approach will prove itself to be complete and consistent.

4.3 FUZZY BASED YAW CONTROLLER DESIGN WITH SIDESLIP LIMITATION

The fuzzy based yaw controller design given in the former section deals only with the yaw rate and yaw acceleration error of the simulated vehicle model. However, minimization of these yaw rate related errors of the vehicle at all costs does not always point to the desired motion. As it will be mentioned often later in this study, another measure of the vehicle behavior is the vehicle sideslip angle [5]. Manipulation of the yaw rate without any intention of limiting the vehicle sideslip angle generally ends with excessive sideslip angles, which means a great loss in steerability of the vehicle, in other words, controllability of the vehicle for the driver. The main reason behind this behavior is the contradictory nature of these two parameters in emergency cases. For instance, in panic maneuvers, the demanded yaw rate has a linear correlation as the steer input increases with almost constant velocity. However, limited cornering forces are generally insufficient for this demand and the desired yaw rate cannot be tracked at all costs for every time. Meantime, the vehicle sideslip angle is preferred to be zero by the driver while it tends to deviate to negative if the vehicle plows or goes unnecessarily high for vehicles with spinning tendencies. Note that, standard vehicles have a slight understeer tendency, thus, as the desired yaw rate increases, the obtained yaw rate falls below this target value. However, when this yaw rate is manipulated by generating a yaw moment in favor of tracking the desired yaw rate, the vehicle sideslip angle tends to deviate from zero excessively due to this uneven moment treatment on the vehicle. Therefore, these two parameters should be taken into account simultaneously for active yaw controlling of the dynamic behavior of the vehicle and keeping its well within the desired range.

Due to these concerns, a new fuzzy based active yaw controller design is proposed and demonstrated in this study. Here, this controller takes the yaw rate difference between simpler vehicle model yaw rate (as desired yaw rate) and detailed vehicle model (as actual yaw rate) as input. Besides, an estimator built in the eight degree of freedom model is responsible for sideslip calculation. Estimation of the lateral

velocity is a bit complicated and requires additional complexity for sensor and calculation modules, but, for the time being, these concerns are disregarded. The desired vehicle sideslip angle is taken as zero, since a novice driver expects neutral steer characteristics from the vehicle. The vehicle and the controller model together are shown in Fig. 4.7. The input and output relationships are also given. As it can be easily seen, the basic scheme is essentially the same as the former controller, except that the yaw acceleration error is replaced by the vehicle sideslip angle.
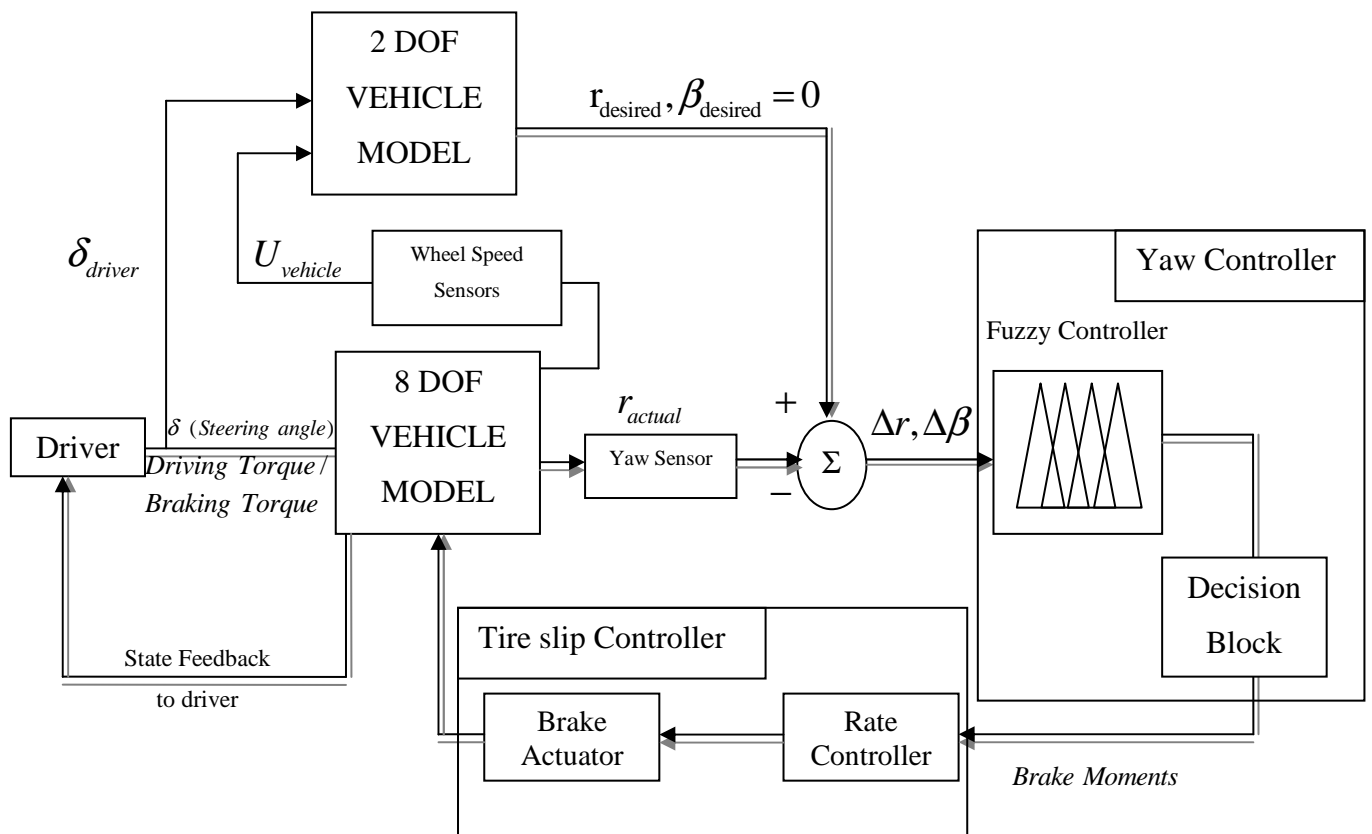
Fig. 4.7 Basic scheme of the proposed yaw controller with sideslip limitation

This yaw controller is based on some foundation rules upon which the controller rule base is established. These rules can be summarized as follows:

— The yaw rate error is of high priority when the sideslip angle is within the limits of its prespecified range.

— When the yaw rate error and the vehicle sideslip angle are high and contradicting each other, then manipulation will be done with a less braking effort than that of high yaw rate error and zero vehicle sideslip angle. This is to ensure that the vehicle is not managed to go towards extreme behavior in order to track the desired yaw rate.

— When the yaw rate error is small, the vehicle is manipulated with minute brake effort to diminish the yaw rate error unless the sideslip angle is excessively large.

After setting up some basic rules for the controller based on the above principles, the rule base is enlarged to satisfy the demand of the driver and the desired behavior. The final rule base is shown in Table 4.2. The rows indicate the yaw rate errors while the columns indicate the vehicle sideslip angle estimations.

Table 4.2 Rule Base for the designed yaw controller with sideslip angle limitation

Sideslip Angle / Yaw Rate Error	N4	N3	N2	N1	ZERO	P1	P2	P3	P4
N4	N4	N4	N4	N3	N2	N3	N3	N3	N3
N3	N4	N4	N3	N2	N2	N2	N3	N3	N3
N2	N4	N3	N2	N2	N2	N2	N3	N2	N2
N1	N3	N2	N2	N1	N1	N1	N2	N1	N1
ZERO	N2	N2	N1	N1	ZERO	P1	P1	P2	P2
P1	P3	P2	P2	P1	P1	P1	P2	P1	P1
P2	P4	P3	P2	P2	P2	P2	P3	P2	P2
P3	P4	P4	P3	P2	P2	P2	P3	P3	P3
P4	P4	P4	P4	P3	P2	P3	P3	P3	P3

For the design of this yaw controller, again, 9 different levels are defined for both the yaw rate and the vehicle sideslip angle as membership functions. For different road conditions, the membership functions are defined separately as dry, wet, and icy while the fuzzy controller scheme remains same. The membership functions are again the same qualitatively, but the ranges which they cover are multiplied accordingly to comply with the need of yaw moment creation to corresponding road-tire surface friction coefficient. The membership functions of input and output parameters for the dry road condition (μ_{nom}=0.9) are shown in Fig. 4.3, Fig. 4.4 and Fig. 4.5, respectively. The unit for the yaw rate error is rad/s whereas it is radians for the vehicle sideslip angle.
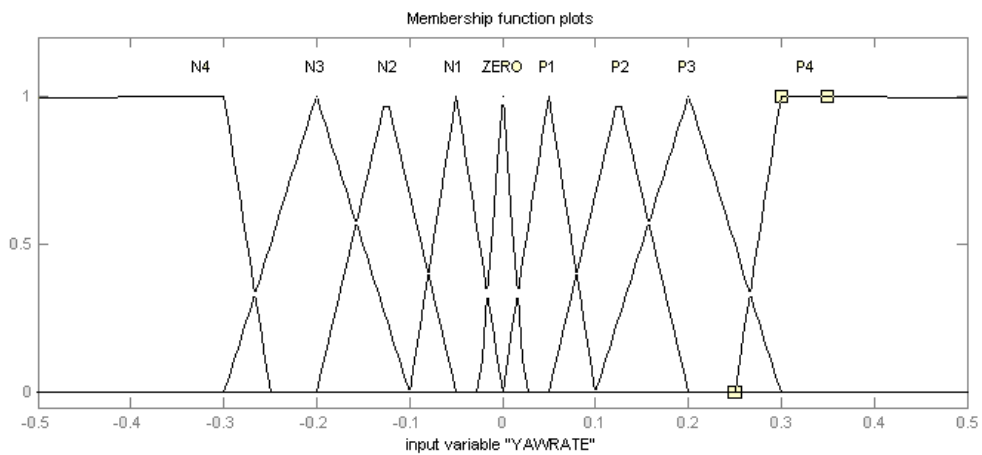
Fig. 4.8 Membership functions for yaw rate error input
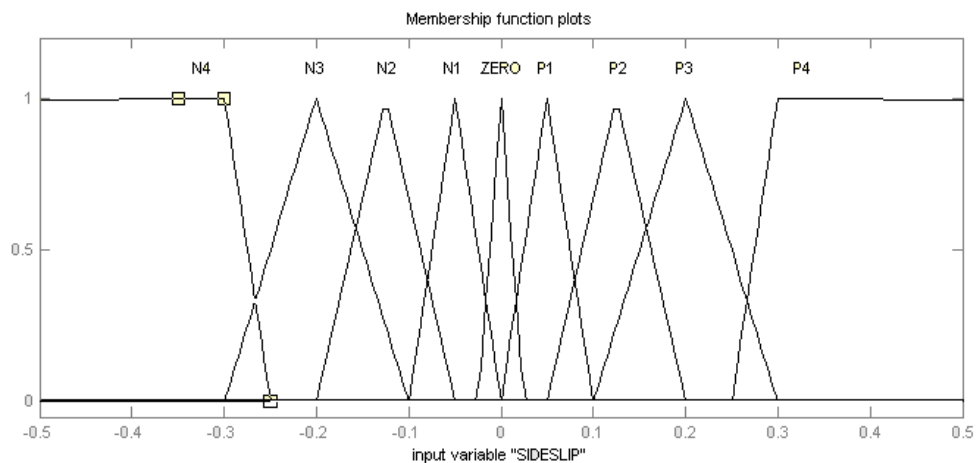
Fig. 4.9 Membership functions for vehicle sideslip angle input
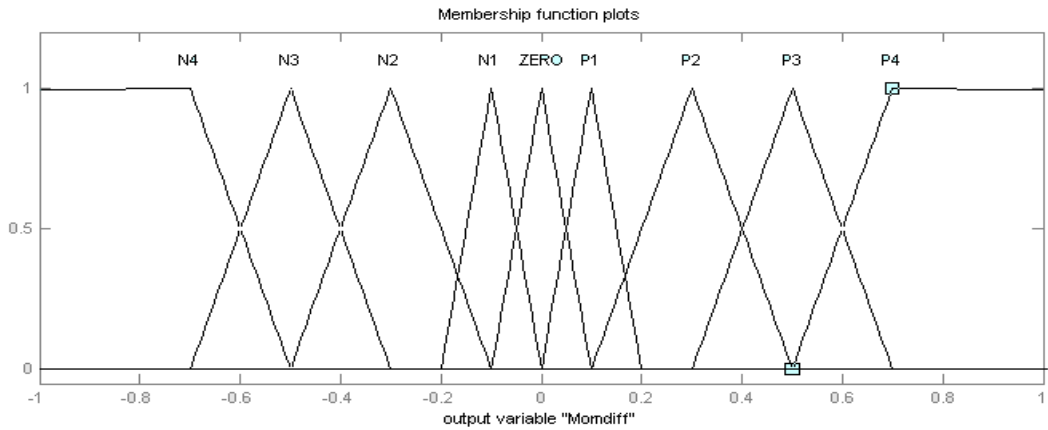
Fig. 4.10 Membership functions for brake moment difference output

The control surface obtained is given in Fig. 4.11. As it can be seen, the smoothness of the former control surface is now exchanged with a more complex surface. This is mainly due to the conflicting natures of the yaw rate demand and the vehicle sideslip angle, which tends to deviate with uneven yaw moment intervention. Note that, although the rule base table has increased its complexity, the control surface retains symmetry along sideslip angle axis, which may be a key to simplify the application of fuzzy controller in practice.
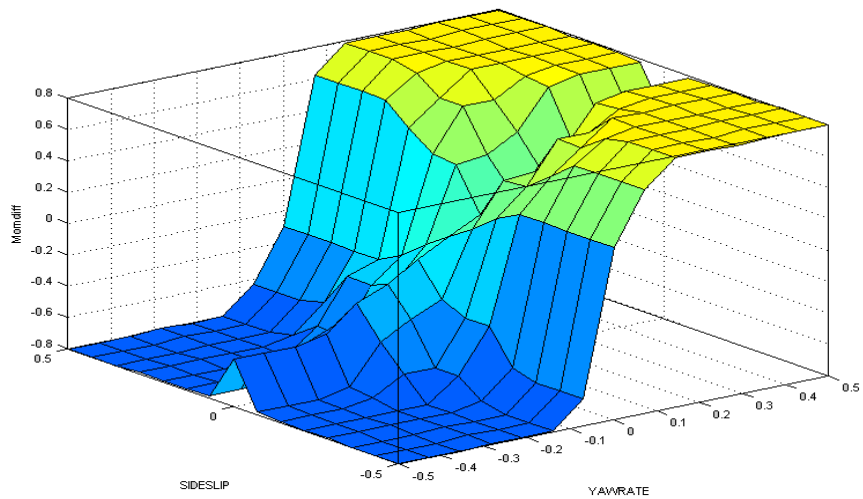
Fig. 4.11 The control surface for the designed yaw controller vs. yaw rate error and

vehicle sideslip angle

4.4 LOW LEVEL SLIP CONTROLLER DESIGN

The low level slip controller design is based on Şahin's study [37]. The main aim of this controller is to limit the slip to a reference longitudinal slip, which is defined according to road conditions. Although the optimum longitudinal slip to maximize the cornering force varies with the lateral slip angle and road-tire surface friction coefficient, this value cannot be measured online with sufficient accuracy [39]. So, a simple yet effective methodology is adopted for reference slip assignment, which is categorizing the road condition as dry wet and icy roads and assigning a single reference slip for each of these conditions. The variation of optimum slip with lateral slip angles is taken into account by selecting a compromising value for these assignments.

There exist two different control techniques for this sub controller, namely, PID and Fuzzy Logic controller. The fuzzy logic based slip controller is again developed in MATLAB/Simulink environment, using the same methods and algorithms with the former designs of fuzzy logic based controllers. The inputs are actual slip, reference slip and tire rotational acceleration. The output signal is multiplied by the given (demanded) brake torque and compared with the demanded brake torque. If the calculated brake torque is lower than the demanded torque, then it is applied to the wheel to prevent excessive longitudinal slippage. The membership functions of the inputs and the output are given in Fig. 4.12, Fig. 4.13 and Fig. 4.14, respectively. The rule base is given in Table 4.3.

The PID based controller uses nearly the same approach; but it utilizes a single input, namely the difference between reference slip and the actual tire slip. The proportional, integral, and derivative gains are not decided upon an analytical approach. Contrary, they are chosen with numerous simulations and initial guesses from the literature. The PID and fuzzy control blocks and necessary input-output relations are given in Fig. 4.15 and the overall sub controller Simulink block diagram is shown in Fig. 4. 16.
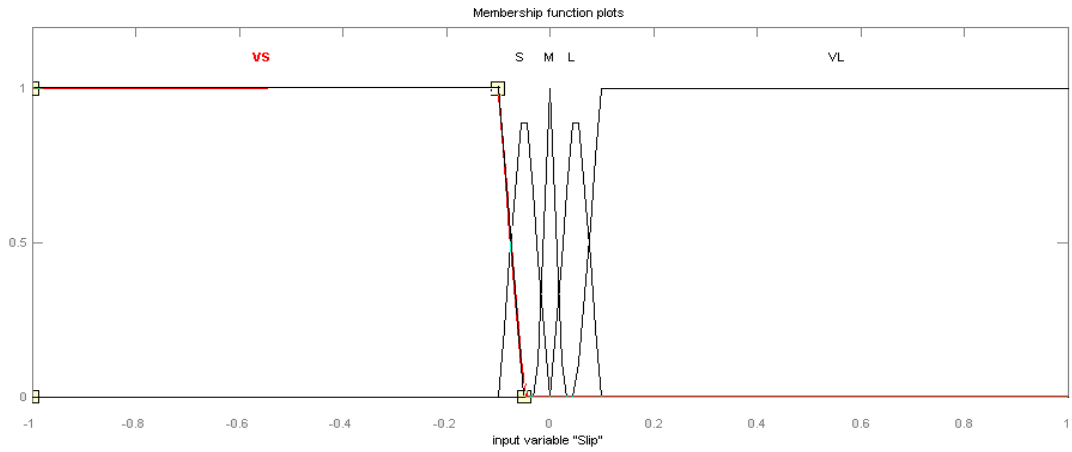
Fig. 4.12 Membership functions for longitudinal slip error input of Fuzzy slip controller
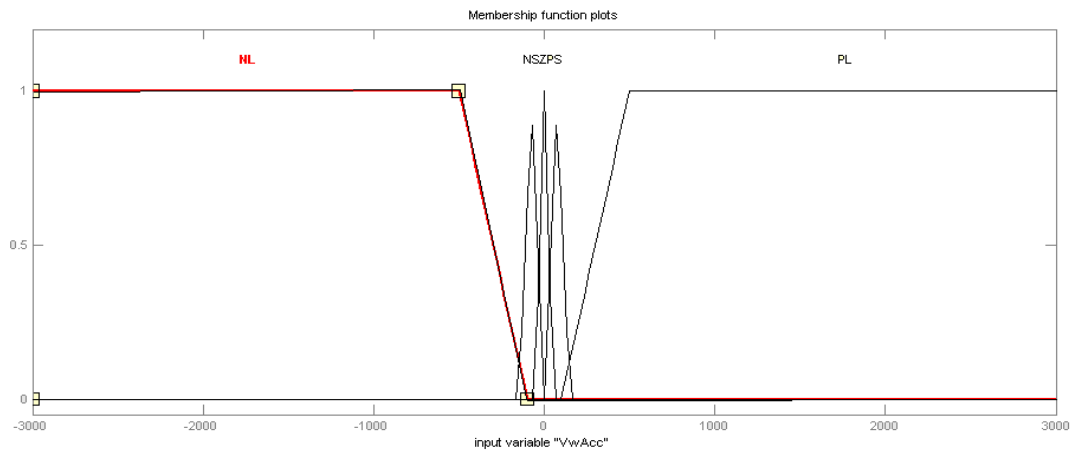
Fig. 4.13 Membership functions for wheel acceleration input of Fuzzy slip controller
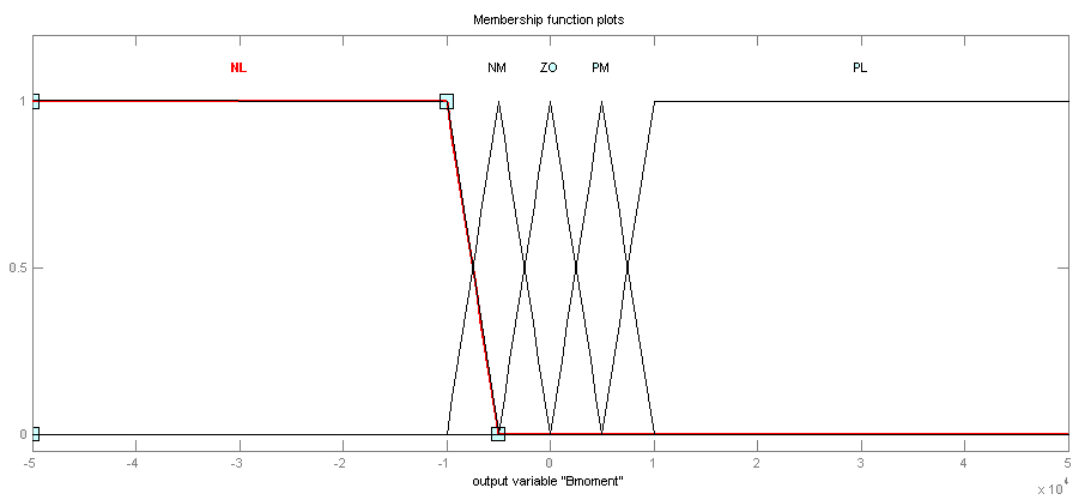
Fig. 4.14 Membership functions for brake torque output of Fuzzy slip controller

Fig. 4.15 Controller Simulink diagram
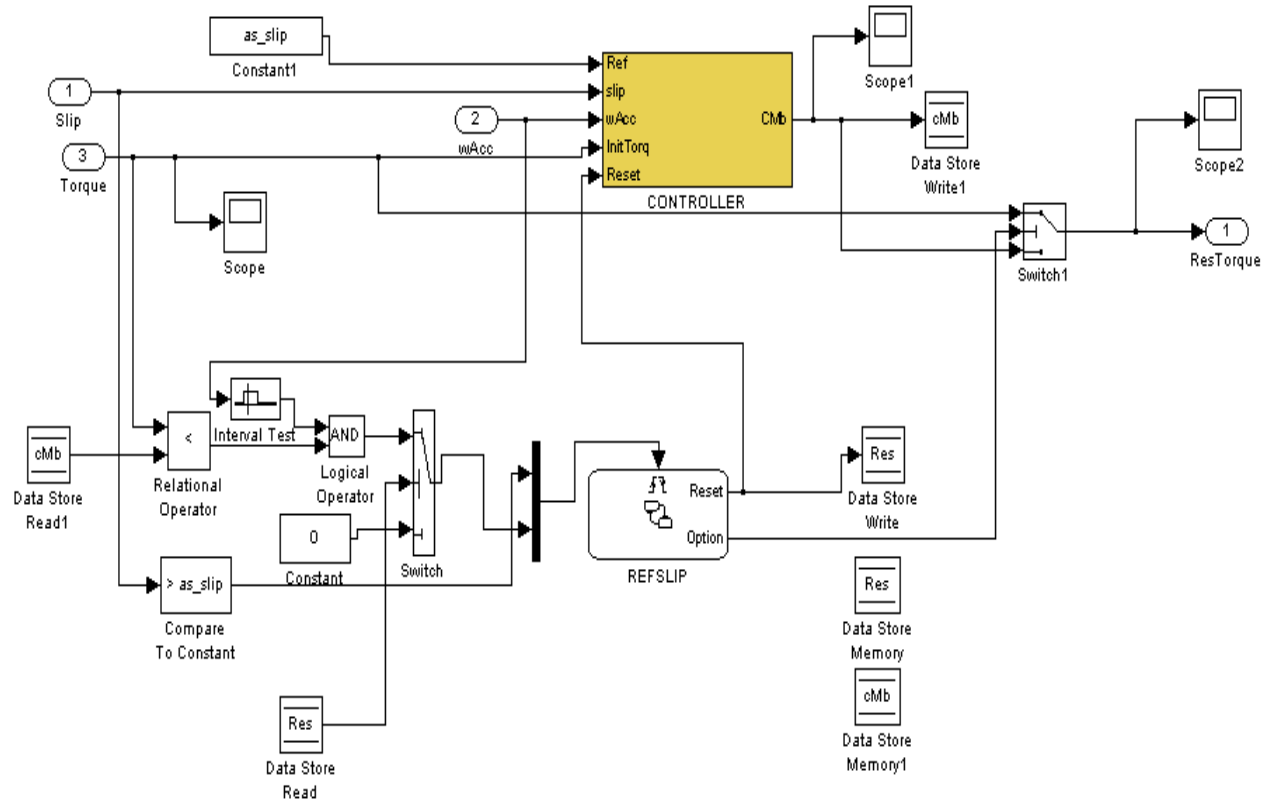
Fig. 4.16 Simulink block diagram of the slip controller
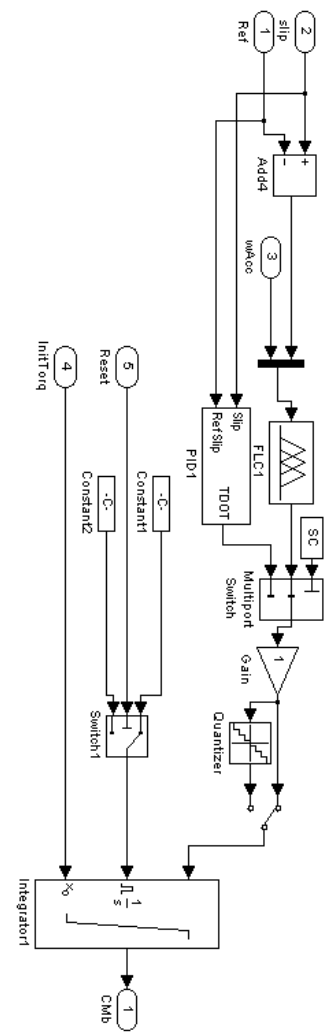
Table 4.3 Rule Base for the designed low level slip controller

Wheel Acceleration/ Tire Long. Slip error	NL	NS	ZERO	PS	PL
NL	NM	PL	PL	PL	PL
NS	NL	PL	PL	PM	PL
ZERO	NL	NM	Z	PM	PL
PS	NL	NL	NM	Z	Z
PL	NL	NL	NL	NM	Z

4.5 NECESSARY COMPONENTS FOR THE DESIGNED CONTROLLER

As mentioned in section 1.3, there exist some necessary component requirements for the functioning of the control system. The components and their functions in the general control system can be summarized as follows:

- Yaw sensor: A gyroscope or MEMS based yaw sensor in order to measure the yaw rate of the vehicle
- Lateral acceleration sensors: This sensor may be used in measuring lateral acceleration so that vehicle sideslip angle estimation will be done.
- Longitudinal acceleration: This component is generally used for vehicle speed estimation in coordination with wheel speed sensors
- Wheel speed sensors: These sensors are generally used for vehicle longitudinal speed estimation and tire slip estimation.
- Steering angle sensor: This sensor provides the steering wheel angle information to the reference model.
- Brake & Throttle Pressure Sensor: This unit provides the driver's intention to acceleration or deceleration.

All these necessary information flows are shown in Fig. 4.1 and Fig. 4.7.

CHAPTER 5

SIMULATIONS

5.1 INTRODUCTION

This chapter presents the results of the simulations performed in MATLAB/Simulink environment for a vehicle with and without the active yaw control system integrated with a sideslip angle limitation controller. To begin, the results of the simulations of the vehicle without any active control system will be discussed. This part will be helpful for gaining an in-depth knowledge of the dynamics of a vehicle under several road and maneuver conditions. Following this part, desired vehicle behavior for various road conditions and driving inputs will be given and the results will be discussed with comparing with the former findings. Then, the same vehicle will be simulated with the active yaw control system without any vehicle sideslip angle limitation. This part will demonstrate the sole yaw control system performance and its weaknesses especially for severe road conditions. Finally, the overall yaw controller integrated with the vehicle sideslip angle controller will be simulated and the results will be discussed in depth.

Since the scope of this study covers yaw-critical situations, reference maneuvers should be selected accordingly. In this study, double lane change and J-turn maneuvers will be taken to represent the yaw-critical situations. Several combined maneuvers including combined braking and steering conditions are simulated. The vehicle parameters used in the simulations can be found in Appendix A. The simulated vehicle response to these standard maneuvers will be given in the following section.

5.2 VEHICLE SIMULATION RESULTS WITHOUT THE ACTIVE YAW CONTROL SYSTEM

Before starting to design and evaluate the active yaw controller, an appropriate vehicle model should be presented in order to demonstrate the dynamics and the physical situations that may occur if the designed controller should be applied on a real vehicle. Furthermore, the uncontrolled behavior of the vehicle model will be used as a reference in order to compare different control algorithms. The input maneuvers used in the simulations are selected from standard maneuvers, which can exhibit emergency situations. In this part, two different conditions will be examined: namely, J-turn maneuver and double lane change maneuver. These selected maneuvers are used to simulate most common maneuvers in everyday situations [41]. The road conditions applied in the simulation will be in three categories: dry, wet, and ice. The dry road condition implies a nominal friction coefficient of 0.9 which is distributed evenly throughout the road tire interaction. For the simulations, this dry road condition will be taken into account and the velocity of the vehicle is taken as 90 km/h.

5.2.1 CASE 1: J-TURN MANEUVER

In this part of the simulation, response of the vehicle to a steer input donated as J-turn maneuver. Figure 5.1 represents the steering wheel angle input change with respect to time. The steering wheel ratio is 1/18, which means that the steer angle for the wheels is reduced to 1/18th of the steering wheel angle. The longitudinal velocity of the vehicle in this maneuver is depicted in Fig. 5.2.
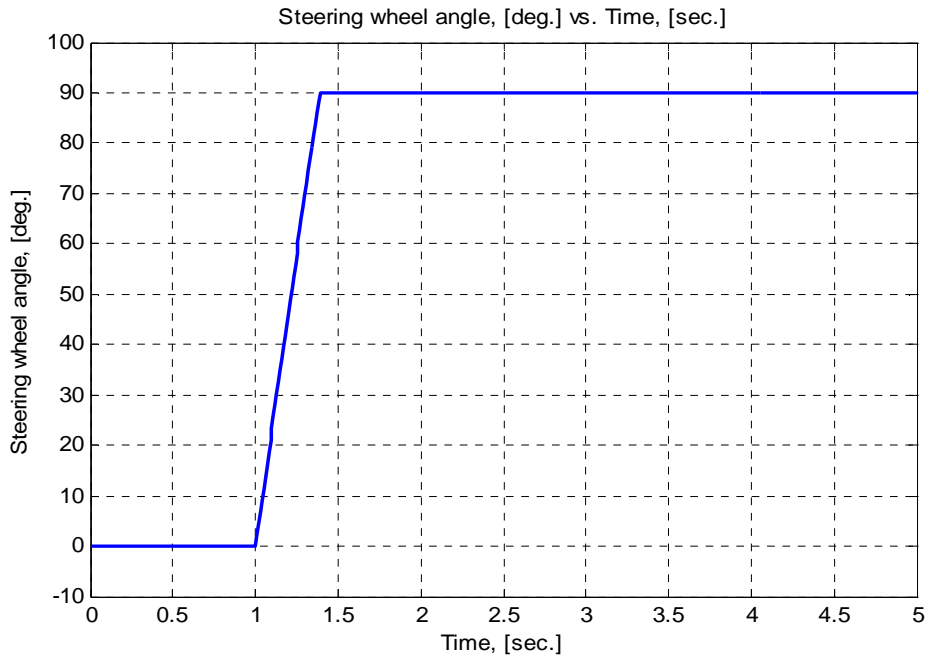
Fig. 5.1 Steering wheel angle vs. time for J-Turn maneuver of the uncontrolled
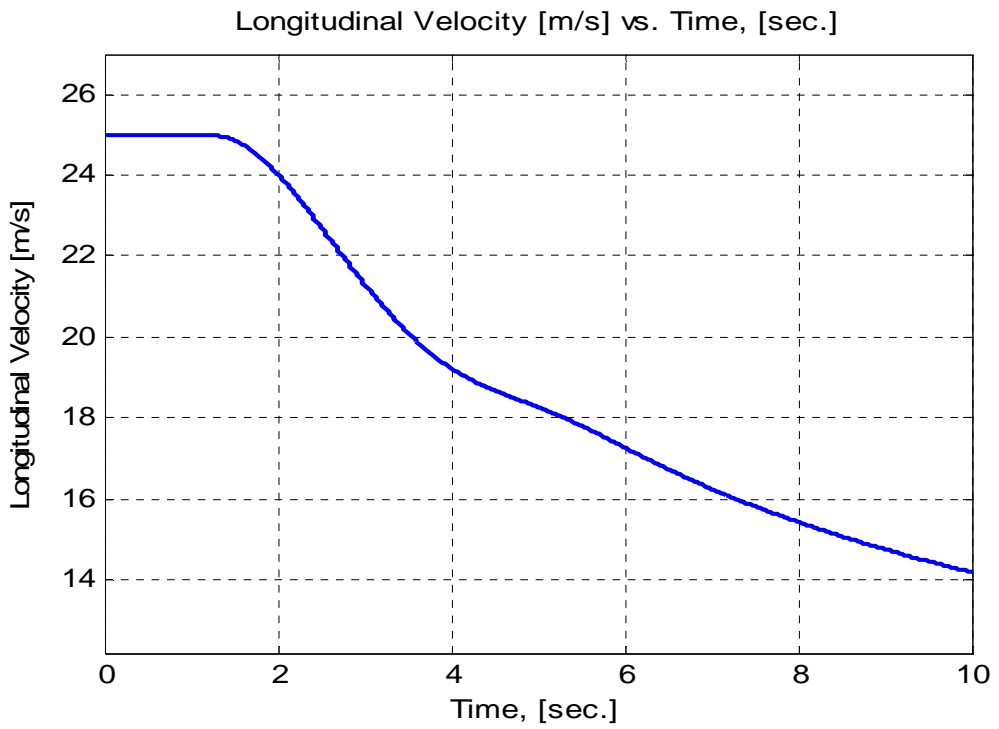
vehicle

Fig. 5.2 Longitudinal velocity vs. time for J-Turn maneuver of the uncontrolled

vehicle

The following figures represent the vehicle response to the J-turn maneuver. Figure 5.3 depicts the yaw rate of the vehicle versus time. As it can be seen from the figure, the yaw rate initially increases as it is expected from the steer input. However, after a certain position, the yaw rate represents a contradictory behavior by decreasing drastically. This is generally due to the heavy understeer characteristic of the vehicle, which results in an oscillatory performance. This oscillatory behavior is damped with increasing time. The peak value of the yaw rate is about 0.56 rad/s, which is rather high for average driving conditions at high speeds.
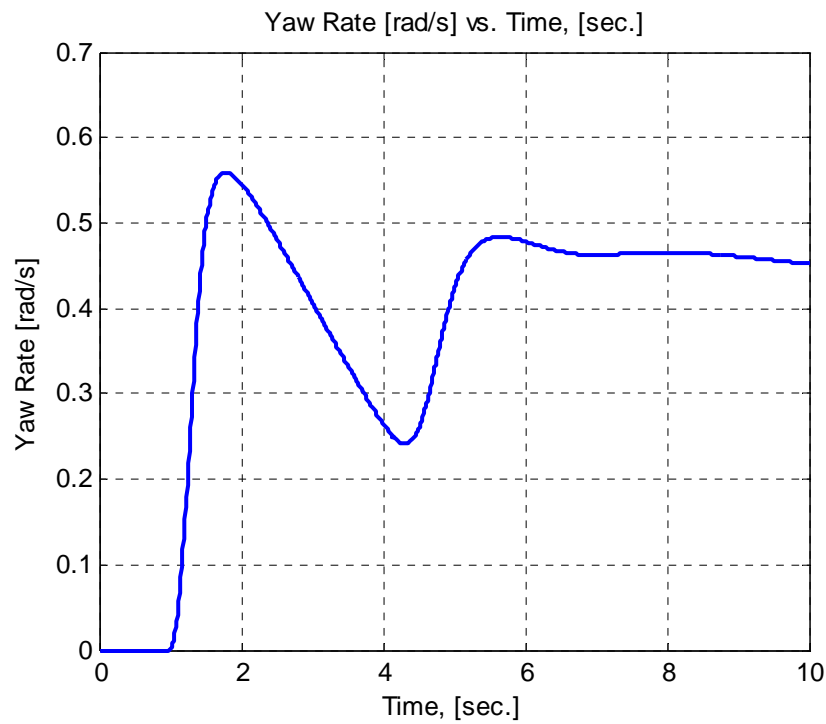
Fig. 5.3 Yaw rate versus time for J-Turn maneuver of the uncontrolled vehicle

64
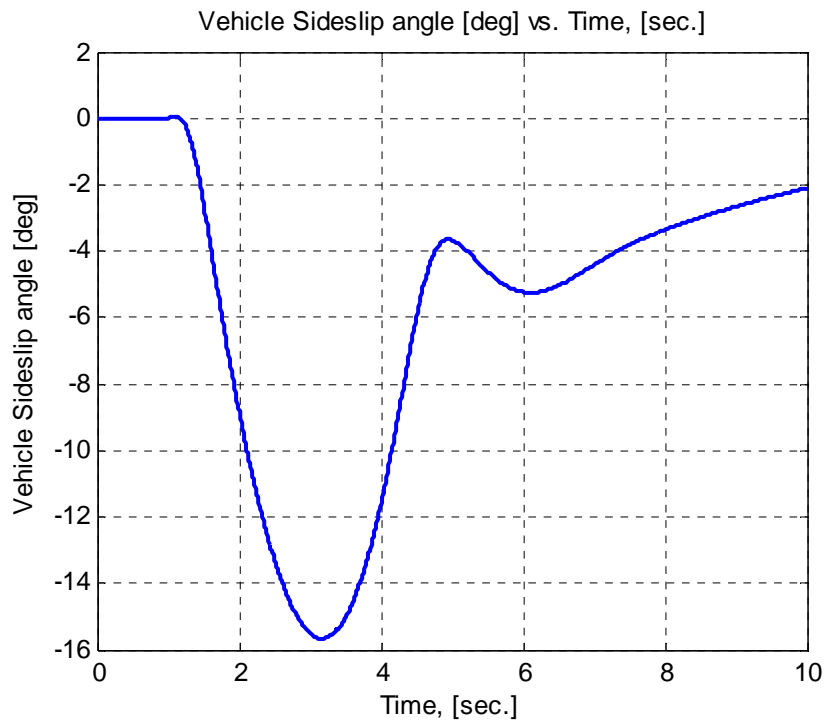
Fig. 5.4 Vehicle sideslip angle versus time for J-Turn maneuver of the uncontrolled vehicle

Figure 5.4 shows the vehicle sideslip angle change with respect to time under specified conditions. The peak value of the slip angle is above 16º, which exceeds acceptable region for dry asphalt road, limited by a maximum of 12 degrees. This result shows that the controllability (in other words, steerability) of the vehicle is degraded.
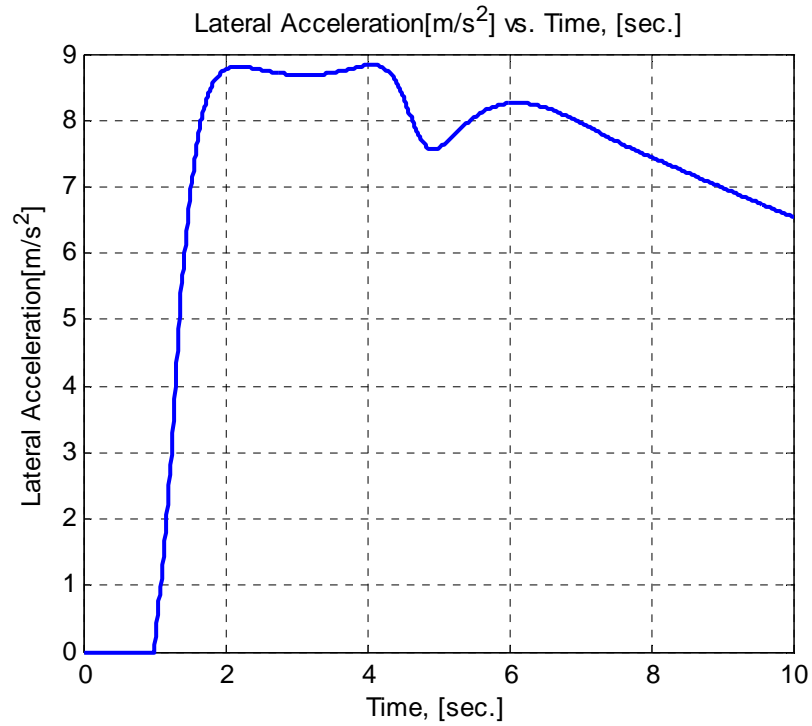
Fig. 5.5 Lateral acceleration versus time for J-Turn maneuver of the uncontrolled vehicle

Figure 5.5 displays the lateral acceleration of the vehicle. As it can be seen clearly, the lateral acceleration reaches its maximum rapidly and holds its value nearly constant for the whole maneuver. The sudden drop about 4th second is related with the yaw rate change and longitudinal velocity decrease, which sources from the longitudinal tire force generation. Fig. 5.6 displays the trajectory of the vehicle and Fig. 5.7 displays the normal tire load change on the wheels with respect to time. Fig. 5.8 shows generated cornering force of the tires vs. time.

66
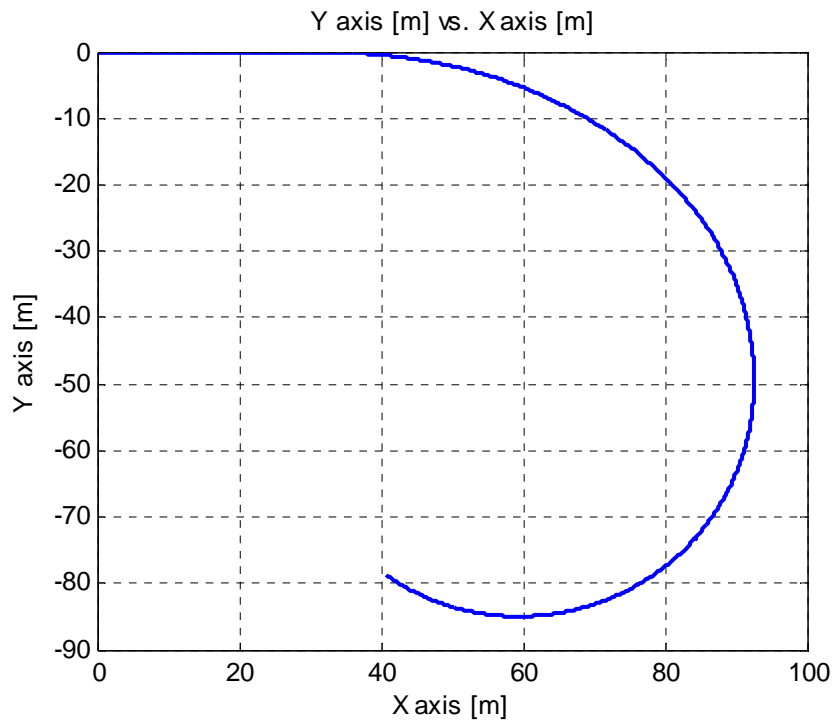
Fig. 5.6 Trajectory for J-Turn maneuver of the uncontrolled vehicle
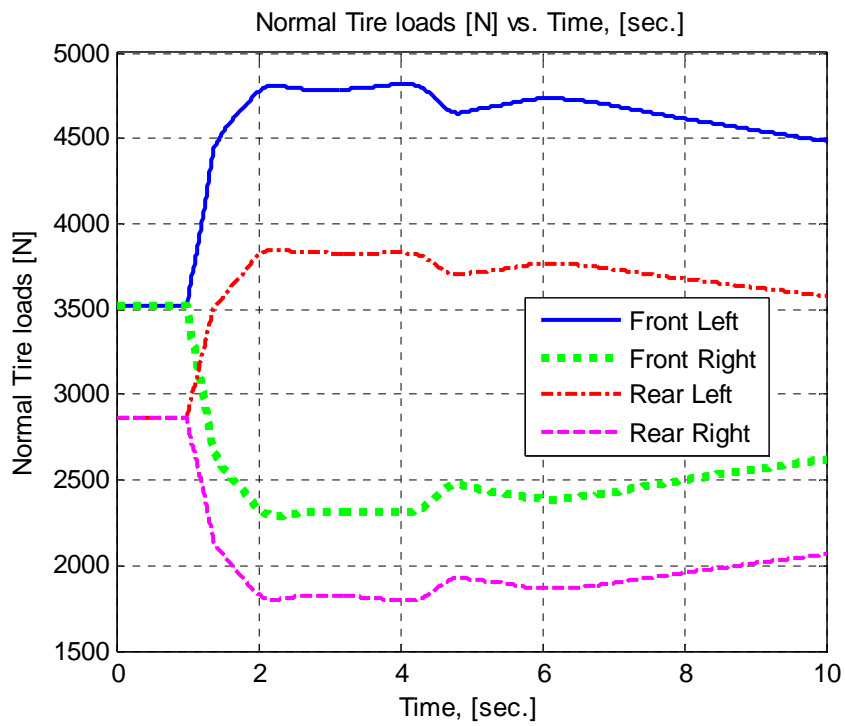
Fig.5.7 Normal Tire loads versus time for J-Turn maneuver of the uncontrolled vehicle
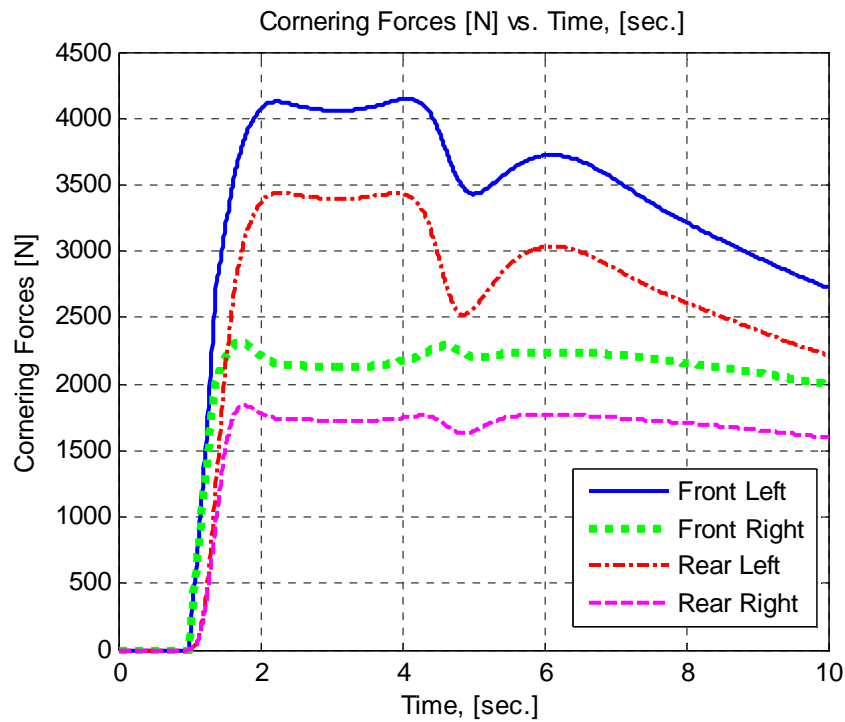
Fig. 5.8 Cornering forces versus time for J-Turn maneuver of the uncontrolled vehicle

Up to this point, only dry asphalt road conditions are considered. For other conditions, simulations have also been performed. For wet asphalt road conditions, 50º steer angle J-turn maneuver is applied with an initial vehicle speed of 90 km/h and with a road tire surface friction coefficient of 0.4. Fig. 5.9 presents the yaw rate of the uncontrolled vehicle behavior under wet road conditions. Fig. 5.10 displays the vehicle sideslip angle and Fig. 5.11 presents the lateral acceleration of the simulated uncontrolled behavior under wet road conditions. The yaw rate reaches a maximum of 0.28 rad/s, which is by far lower than that of dry road conditions. The maximum vehicle sideslip angle is about 11 degrees, which can be interpreted as a total degradation of steerability for wet road conditions. The lateral acceleration is lowered to half of its original value on dry asphalt, which is a result of lower friction coefficient, thus lower cornering forces.
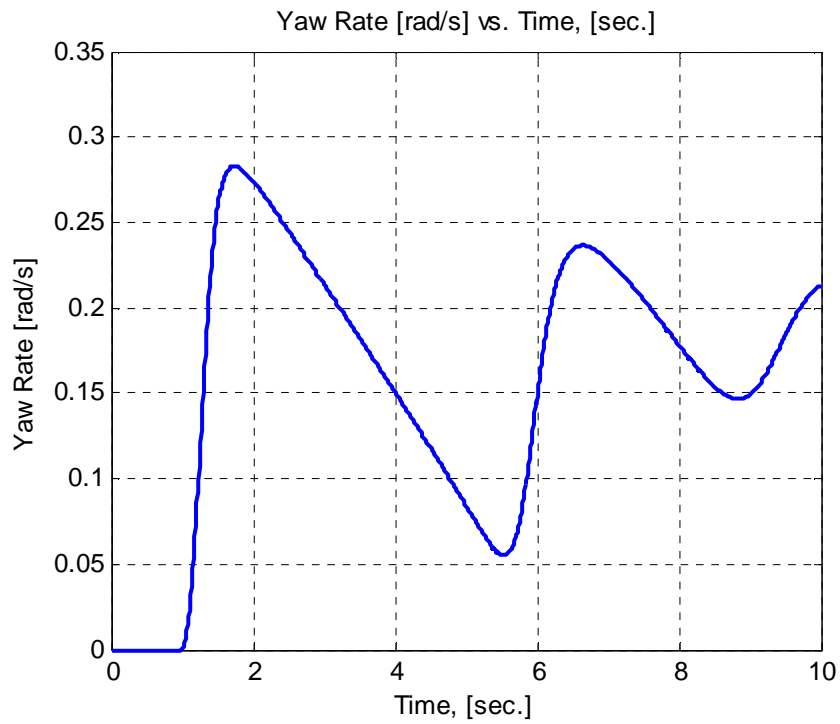
Fig. 5.9 Yaw rate versus time for wet conditions and J-Turn maneuver of the uncontrolled vehicle
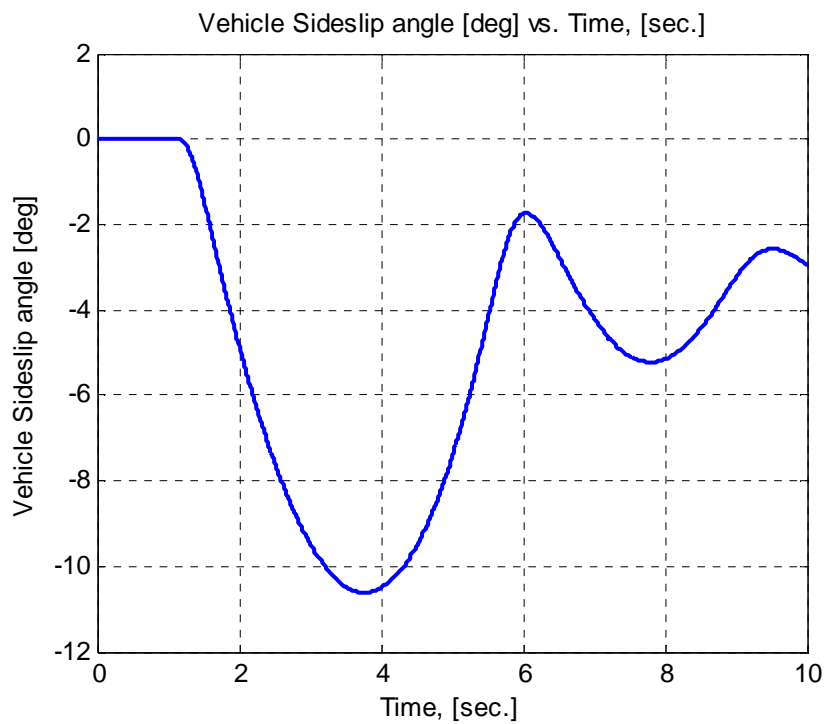

Fig. 5.10 Vehicle sideslip angle versus time for wet conditions and J-Turn maneuver of the uncontrolled vehicle
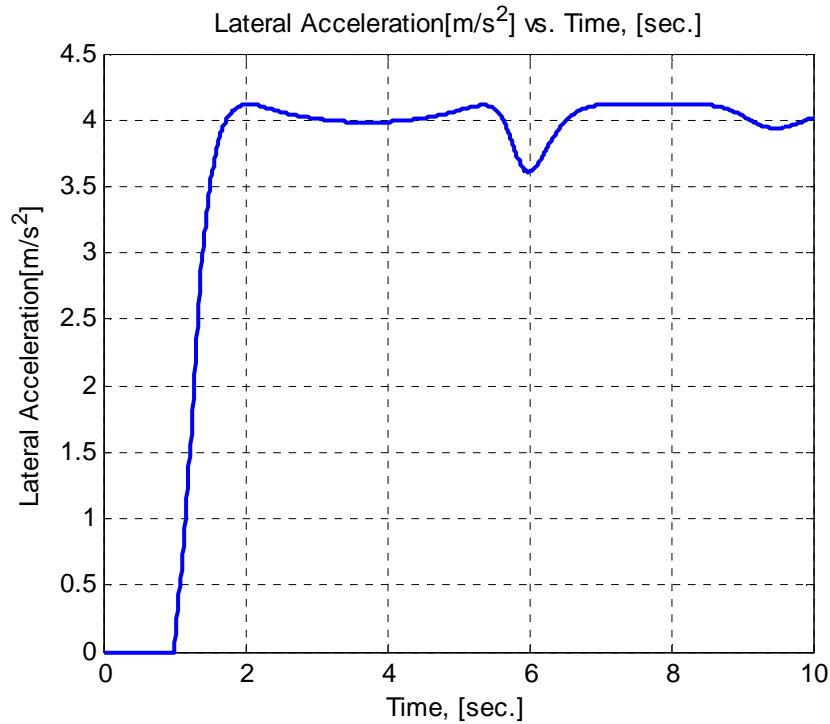
Fig. 5.11 Vehicle lateral acceleration versus time for wet conditions and J-Turn maneuver of the uncontrolled vehicle

For icy asphalt road conditions, 40º steer angle J-turn maneuver is applied with an initial vehicle speed of 40 km/h and a road tire surface friction coefficient of 0.1. Fig. 5.12 presents the yaw rate of the uncontrolled vehicle behavior under wet road conditions. Fig. 5.13 displays the vehicle sideslip angle and Fig. 5.14 presents the lateral acceleration of the simulated uncontrolled behavior under icy road conditions. As can be seen, the yaw rate and lateral acceleration are pretty low compared to those of the former road conditions, which results in a small vehicle sideslip angle deviation. The upcoming simulations will show, however, that the desired yaw rate will be much higher than this obtained value.
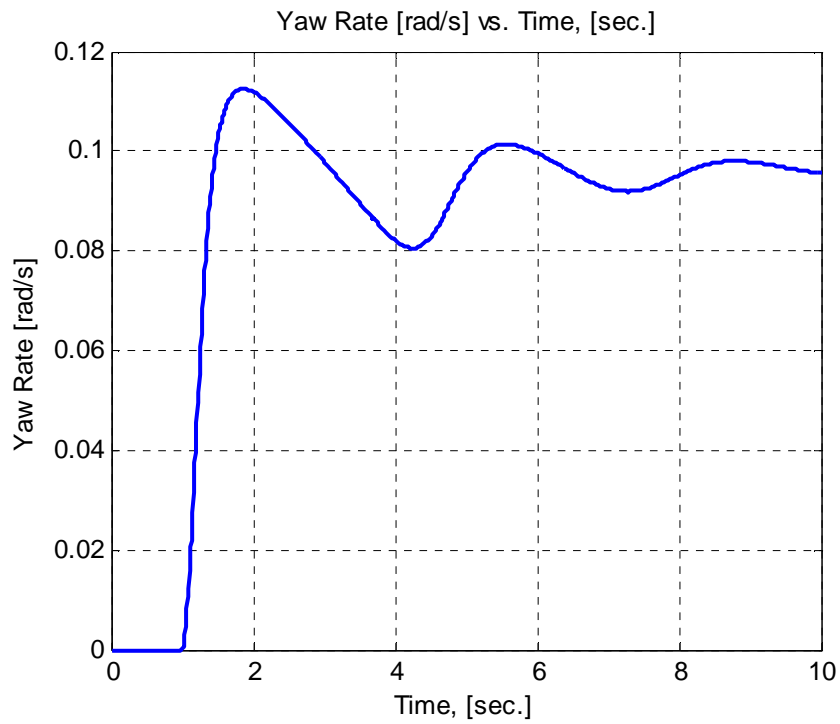
Fig. 5.12 Yaw rate versus time for icy conditions and J-Turn maneuver of the uncontrolled vehicle
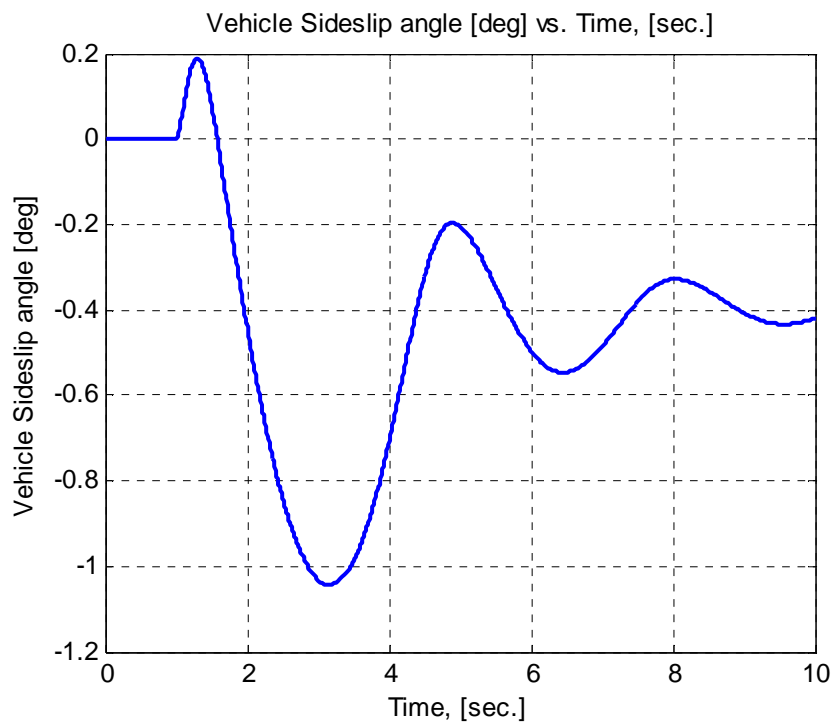
Fig. 5.13 Vehicle sideslip angle versus time for icy conditions and J-Turn maneuver of the uncontrolled vehicle
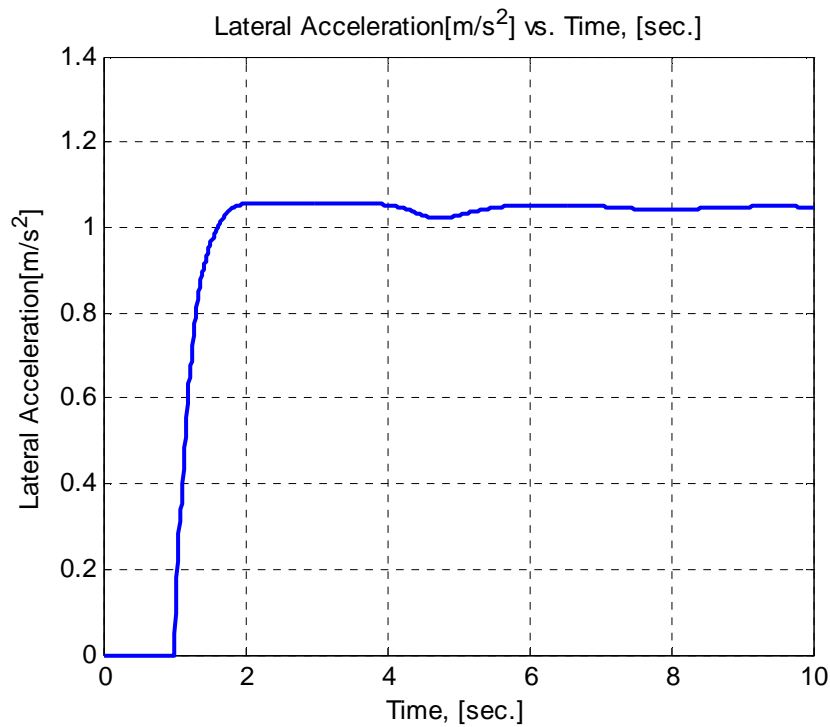
Fig. 5.14 Vehicle lateral acceleration versus time for icy conditions and J-Turn maneuver of the uncontrolled vehicle

5.2.2   CASE 2: DOUBLE LANE CHANGE MANEUVER

In this part of the simulation results section, the vehicle response to the double lane change maneuver will be analyzed. The double lane change maneuver test, also known as "Moose Test", includes a sharp evasive maneuver to avoid a sudden obstacle show-up or to follow a sharp curvature followed by the reverse of this initial movement [41]. The steering wheel angle change of the double lane change is shown in Fig. 5.15. Steering angle function consists of a single sine wave with amplitude of 90 degrees and a frequency of 0.25Hz. The initial velocity of the vehicle is 90 km/h and the steering wheel gear reduction ratio is 1/18, so that the front wheels turn with a maximum angle of 5 degrees.

72
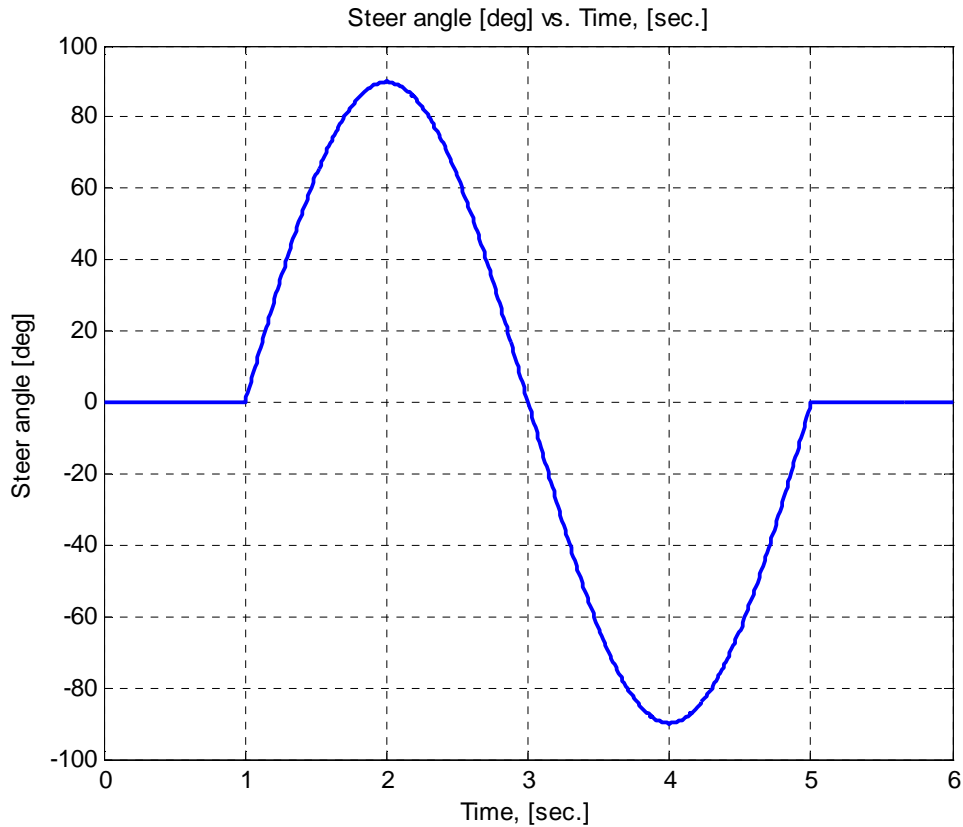
Fig. 5.15 Steering wheel angle versus time for double lane change maneuver of the
uncontrolled vehicle

Fig. 5.16 displays the yaw rate change of the uncontrolled vehicle in a double lane
change maneuver. It can be easily seen that the yaw rate of the simulated vehicle
resembles the steer command in qualitative form. However, especially the second
part of the oscillation by far exceeds the limitations, which is mostly caused by the
sudden sideslip change of the vehicle. Fig. 5.17 shows the vehicle sideslip change of
the vehicle. The maximum value of the vehicle sideslip angle surpasses the
maximum allowable range slightly, which is about 12º for dry asphalt conditions.
Fig. 5.18 shows the lateral acceleration of the uncontrolled vehicle. As can be
noticed, there exists a lag between the steer input and the contours of the responses.
This is generally caused by the longitudinal dynamics of the vehicle and the time to
build up necessary forces on the wheels.
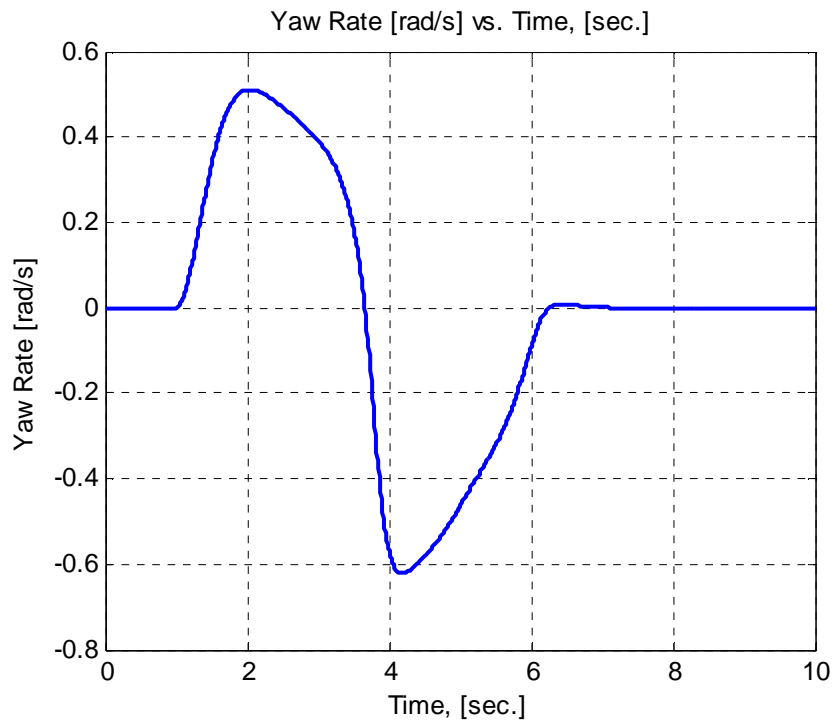
Fig. 5.16 Yaw rate versus time for double lane change maneuver of the uncontrolled
vehicle
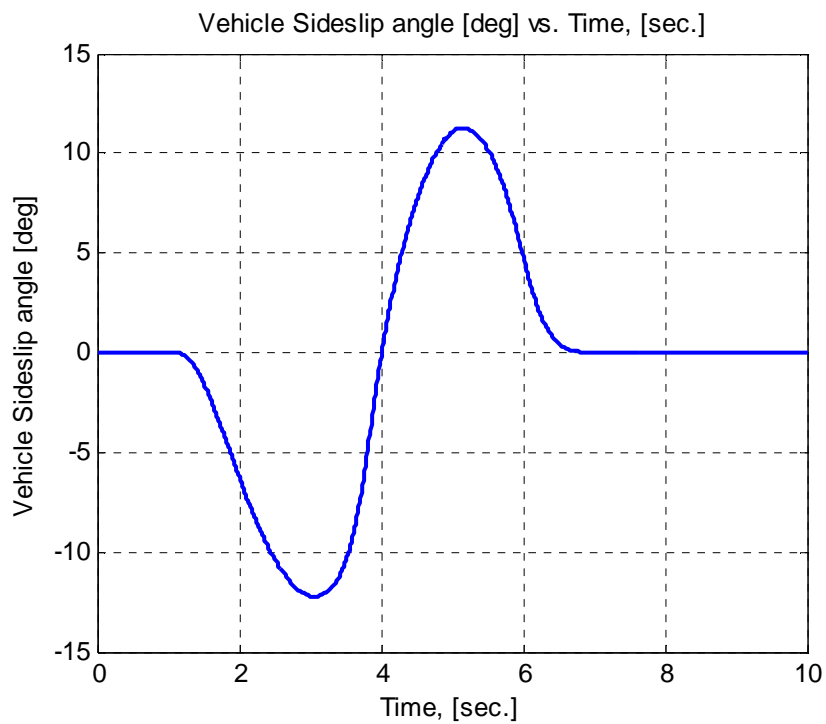
Fig. 5.17 Vehicle sideslip angle versus time for double lane change maneuver of the
uncontrolled vehicle
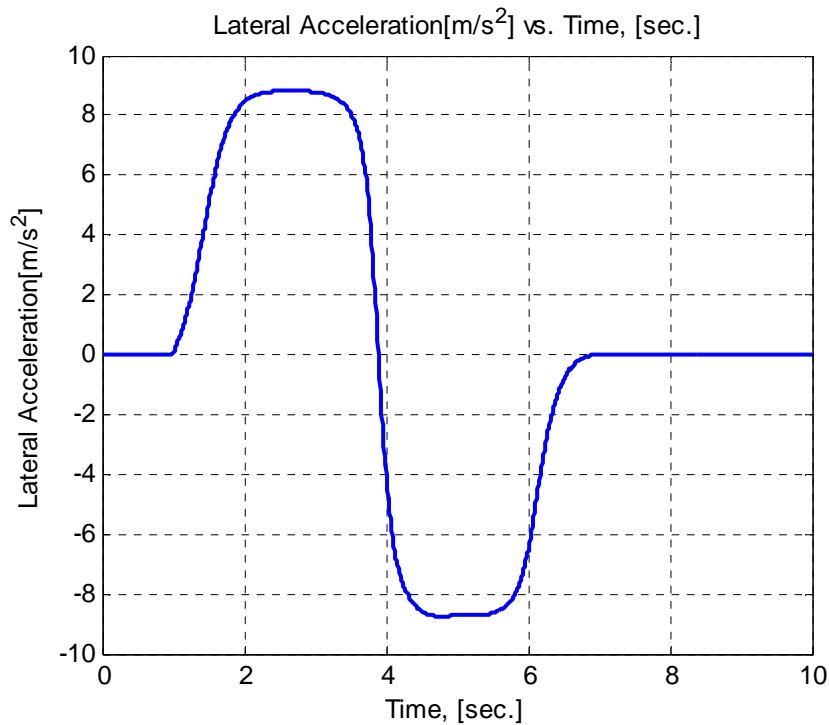
Fig. 5.18 Lateral acceleration versus time for double lane change maneuver of the uncontrolled vehicle

Fig. 5.19 shows the trajectory of the vehicle. As can be seen clearly, the lateral displacement of the vehicle is undoubtedly high, which can be accepted as a result of high lateral acceleration and vehicle sideslip angle. Fig. 5.20 represents the normal loads change carried by the wheels. The wheel loads decrease drastically as the maneuver takes place. As for other responses, the wheel loads follow the steer input contour with a slight lag. Finally, Fig. 5.21 presents the cornering forces generated by the wheels. As the vehicle turns right, in the first part of the evasive maneuver, the front left tire generates the maximum cornering force, due to the normal force distribution. By passing to the second part of the sine wave maneuver, the normal load on the front right tire increases with respect to front left tire, thus generating the leading cornering force. Since the steer input is given by front wheels, high slip angles on front tire are produced, thus having high cornering forces on these wheels with respect to rear tires.
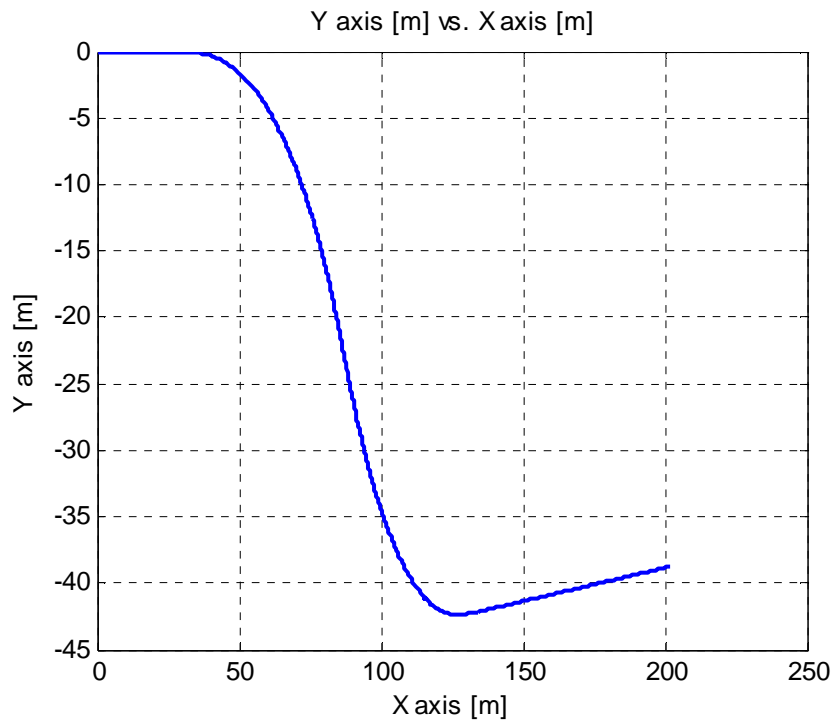
Fig. 5.19 Trajectory for double lane change maneuver of the uncontrolled vehicle
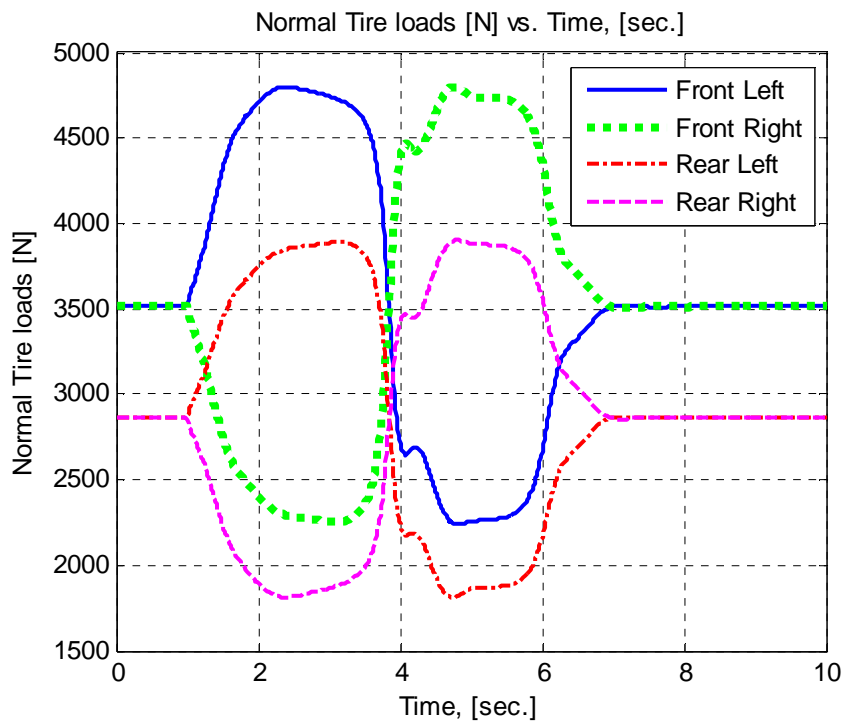

Fig.5.20 Normal Tire loads versus time for double lane change maneuver of the
uncontrolled vehicle
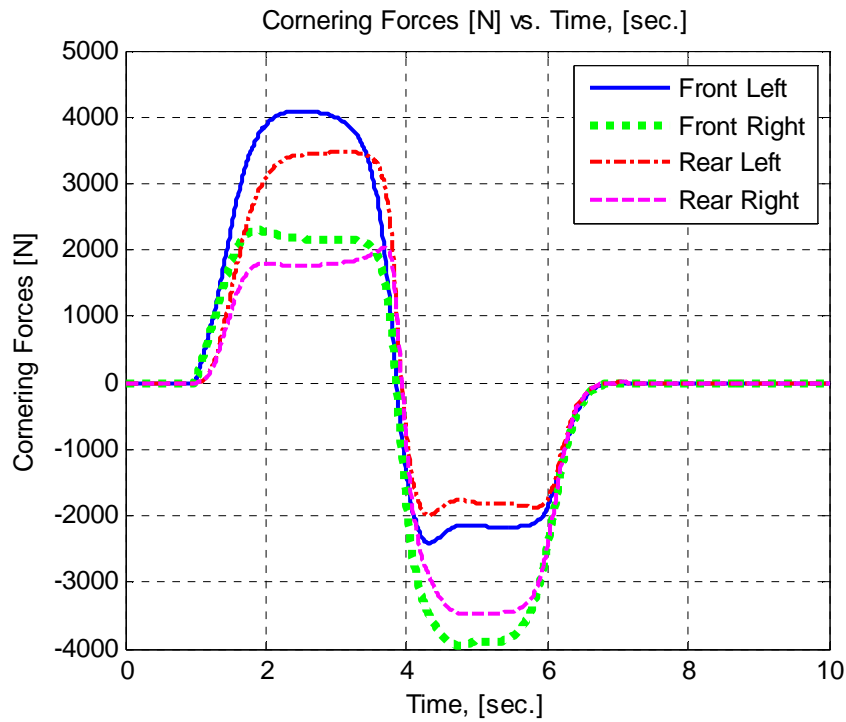
Fig. 5.21 Cornering forces versus time for double lane change maneuver of the uncontrolled vehicle

For wet asphalt road conditions, 50º steer angle double lane change is applied with an initial vehicle speed of 90 km/h and 0.4 road tire surface friction coefficient. Fig. 5.22 presents the yaw rate of the uncontrolled vehicle behavior under wet road conditions. Fig. 5.23 displays the vehicle sideslip angle and Fig. 5.24 presents lateral acceleration of the simulated uncontrolled behavior under wet road conditions. The yaw rate of the uncontrolled vehicle exhibits a totally different performance in this case. Contrary to oscillatory steering demand, the yaw velocity does not follow the steering input and the vehicle performs excessive yaw rate values. The reason behind this situation can be observed in vehicle sideslip angle attaining a maximum value of about 9º, which exceeds the maximum allowable range for wet road conditions. This behavior results in degraded steerability [40].
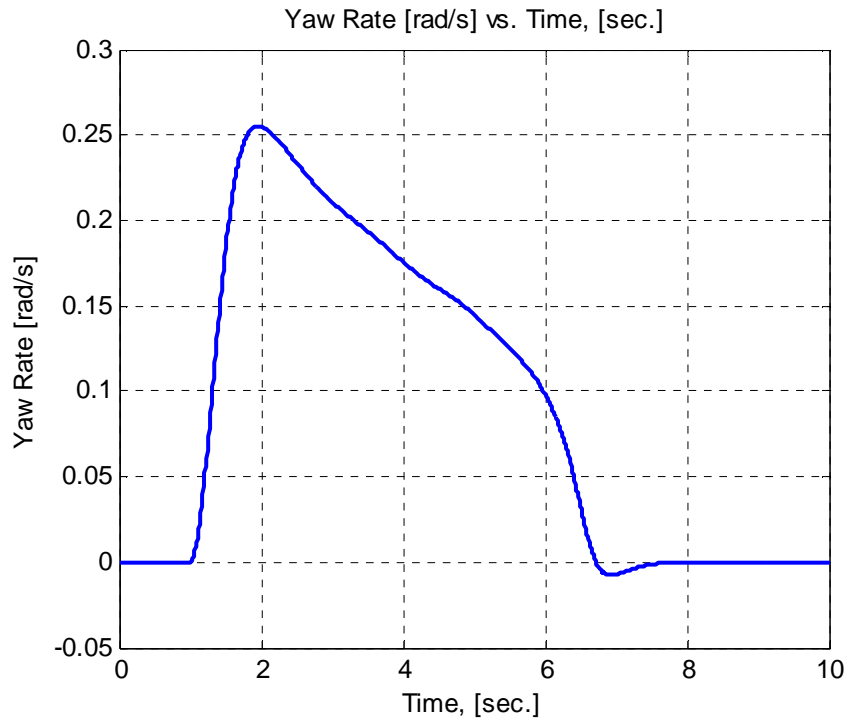
Fig. 5.22 Yaw rate versus time for wet road conditions and for double lane change
maneuver of the uncontrolled vehicle
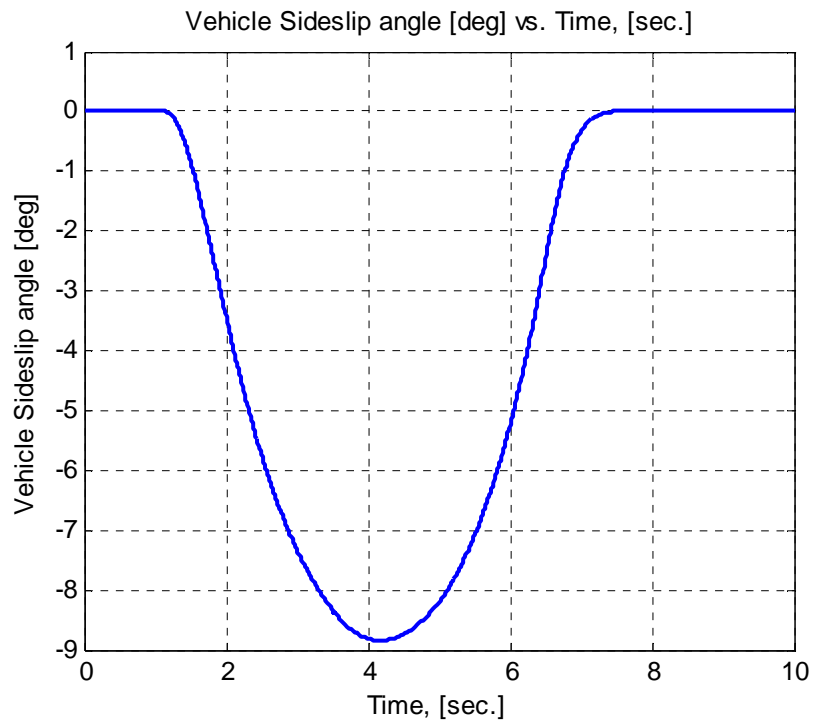
Fig. 5.23 Vehicle sideslip angle versus time for wet road conditions and for double
lane change maneuver of the uncontrolled vehicle
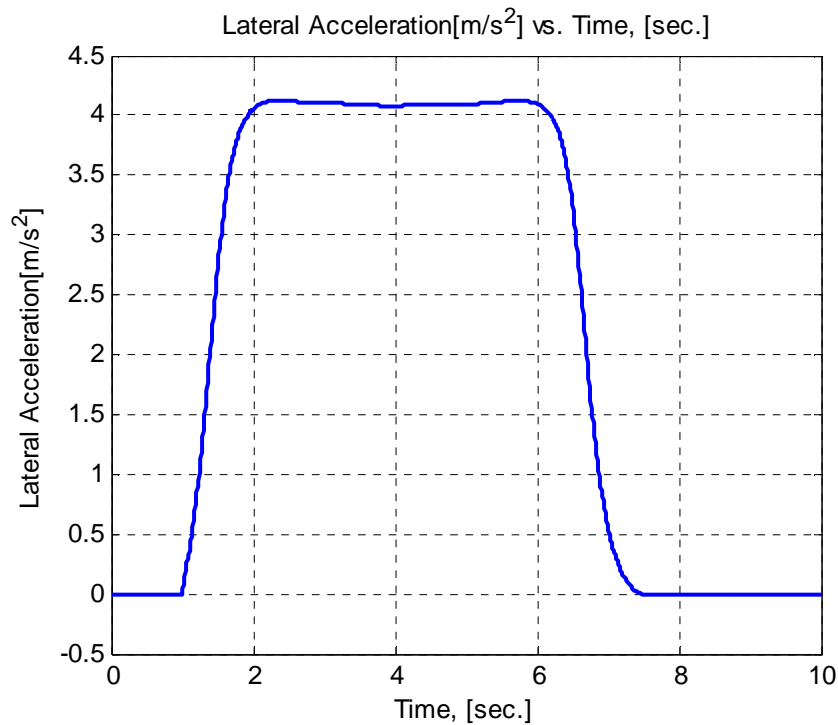
Fig. 5.24 Vehicle lateral acceleration versus time for wet road conditions and for double lane change maneuver of the uncontrolled vehicle

For icy asphalt road conditions, 50º steer angle double lane change maneuver is applied with an initial vehicle speed of 50 km/h and 0.1 road tire surface friction coefficient. Fig. 5.25 presents the yaw rate of the uncontrolled vehicle behavior under wet road conditions. Fig. 5.26 displays the vehicle sideslip angle and Fig. 5.27 presents lateral acceleration of the simulated uncontrolled behavior under icy road conditions. In this case, the vehicle is able to follow the steering command in a qualitative manner, but of course there exist some deformation on the sine shape of the desired maneuver. Attained vehicle sideslip value rising to 5 degrees or higher indicates a possibility of loss of steerability. Unlike J-turn maneuver, in which vehicle sideslip angle is somehow stabilized to a moderate value on icy road, double lane change causes a loss of control, which can be associated with the decline in lateral tire force generation.
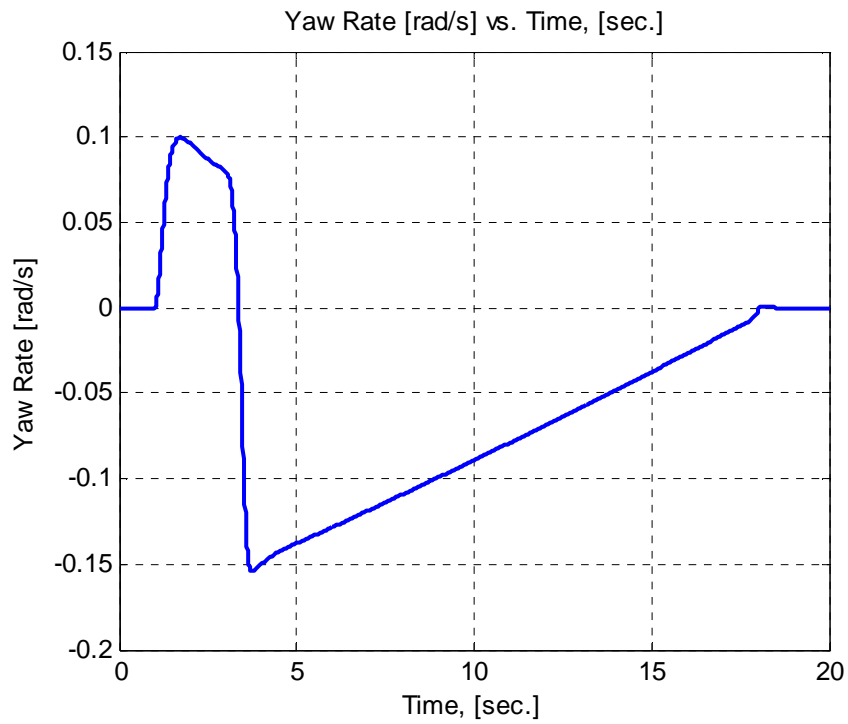
Fig. 5.25 Yaw rate versus time for icy road conditions and for double lane change
maneuver of the uncontrolled vehicle
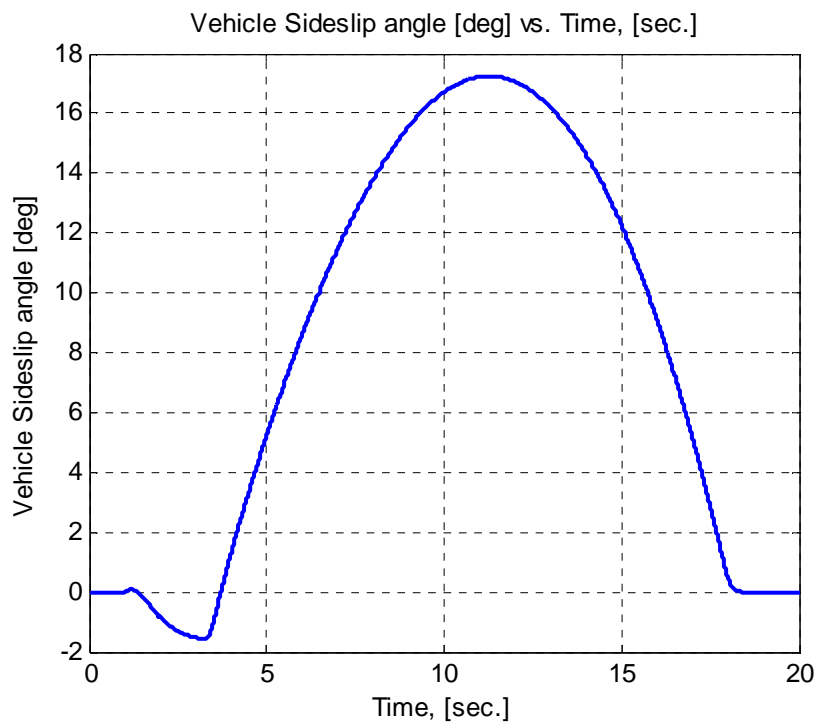
Fig. 5.26 Vehicle sideslip angle versus time for icy road conditions and for double
lane change maneuver of the uncontrolled vehicle
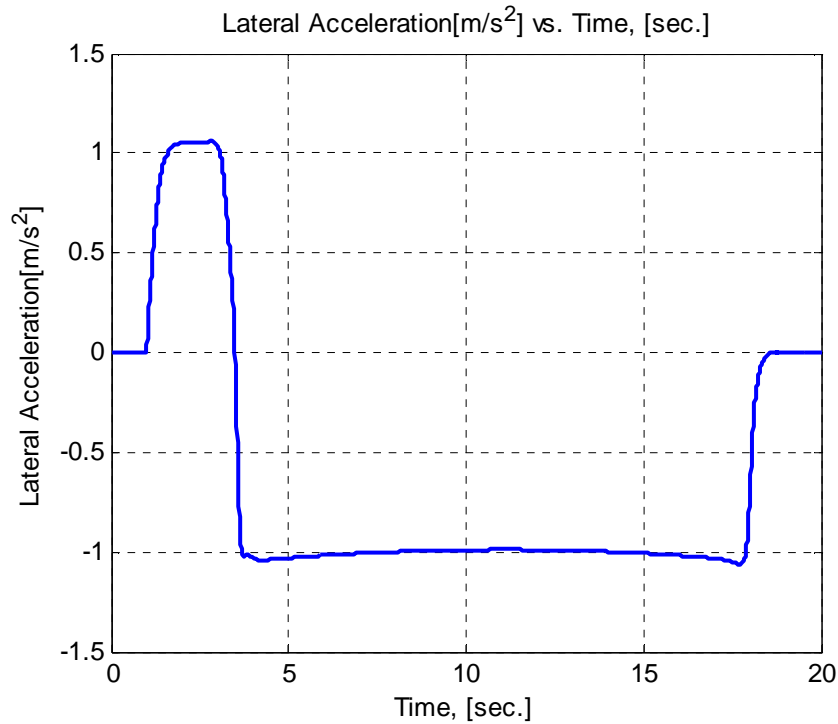
Fig. 5.27 Vehicle lateral acceleration [m/s^2] vs. time [sec.] for icy road conditions and for double lane change maneuver of the uncontrolled vehicle

5.2.3 DESIRED VEHICLE BEHAVIOR CALCULATIONS DERIVED FROM TWO DEGREES OF FREEDOM VEHICLE MODEL

The uncontrolled vehicle model is shown with several aspects of its general motion. However, to evaluate clearly, the desired vehicle behavior of the vehicle implied by the control demands of the driver should be also discussed. The model used here to represent the desired motion is a two degree of freedom vehicle model (also referred as bicycle model). This model is selected arbitrarily, since the desired behavior for a particular behavior is not unique. Due to the subjective nature of the desired behavior prediction, the design of the desired vehicle model is realized by utilizing experience-based characteristics. As mentioned in section 3.4, the determination of this vehicle tendency is a key point here. In this study, applied vehicle's general tendency (slight understeer) is taken as a base to construct the reference model. In

81

this part of chapter, the calculated desired vehicle behavior based on 2 degrees of freedom model will be demonstrated and compared with uncontrolled behavior of the vehicle. The simulations will include dry, wet and icy road conditions. The desired vehicle sideslip angle is not given as figure, since the main aim is to confine the vehicle sideslip to small values possible, in other words, restrict it to values close to zero.

5.2.3.1 CASE 1: J-TURN MANEUVER

Fig. 5.28 presents the desired yaw rate behavior of the vehicle under dry road conditions. The initial parameters and steer command is same as in part 5.2.1. Desired yaw rate behavior has a maximum of 0.57 rad/s, which is similar to uncontrolled behavior of the vehicle. However, the desire yaw rate is then nearly stabilized to a steady state value. In fact, it decreases gradually due to the slow velocity decrease. This is unlikely for the uncontrolled behavior of the vehicle, which suffers a sharp decrease in the latter part of the maneuver, namely between 2-4 seconds of the simulation. The uncontrolled vehicle surpasses the desired yaw rate initially by 0.125 rad/s, then, after the mentioned sharp decrease, is passed by about 0.13 rad/s.
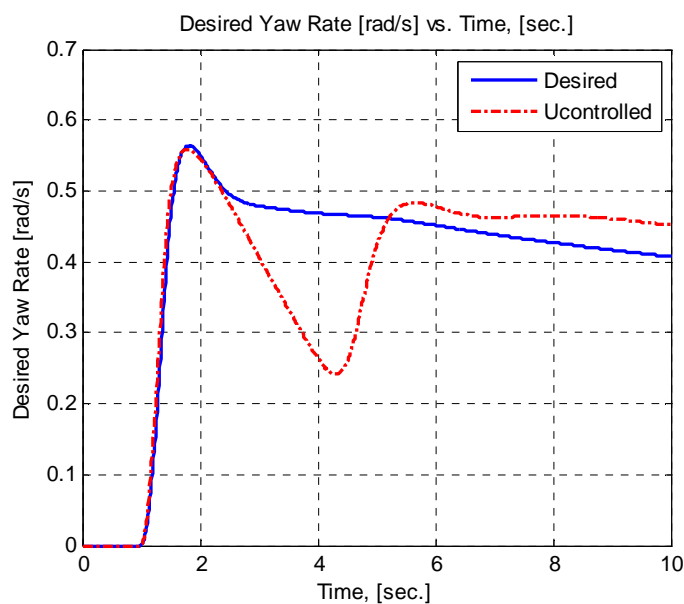

Fig. 5.28 Desired yaw rate versus time for J-Turn maneuver of the simulated vehicle

Fig. 5.29 demonstrates the corresponding desired lateral acceleration of the vehicle. The desired lateral acceleration reaches a maximum of 12.4 m/s^2, which is about 1.26 g-force. Note that the desired lateral acceleration overwhelms the uncontrolled lateral acceleration by an amount 3 m/s^2. The difference is the result of the limited road tire interaction forces, namely lateral tire forces. The desired trajectory is shown in Fig. 5.30, which differs from that of uncontrolled vehicle. The curvature requires a high rate of turning, which can be nearly interpreted as oversteer behavior. However, this small curvature radius is the result of uncommon high steer angle command.
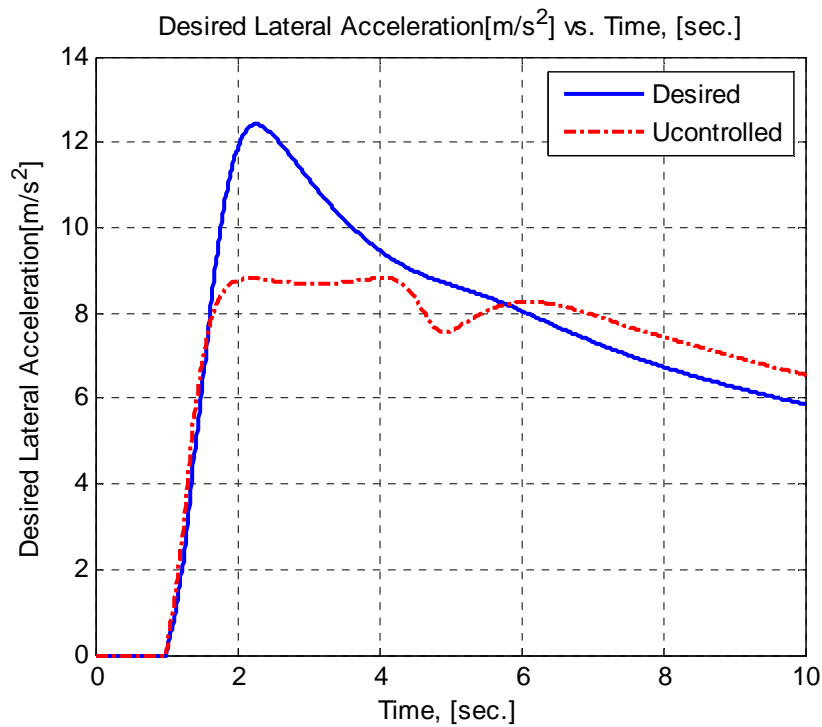
Fig. 5.29 Desired lateral acceleration for J-Turn maneuver of the simulated vehicle
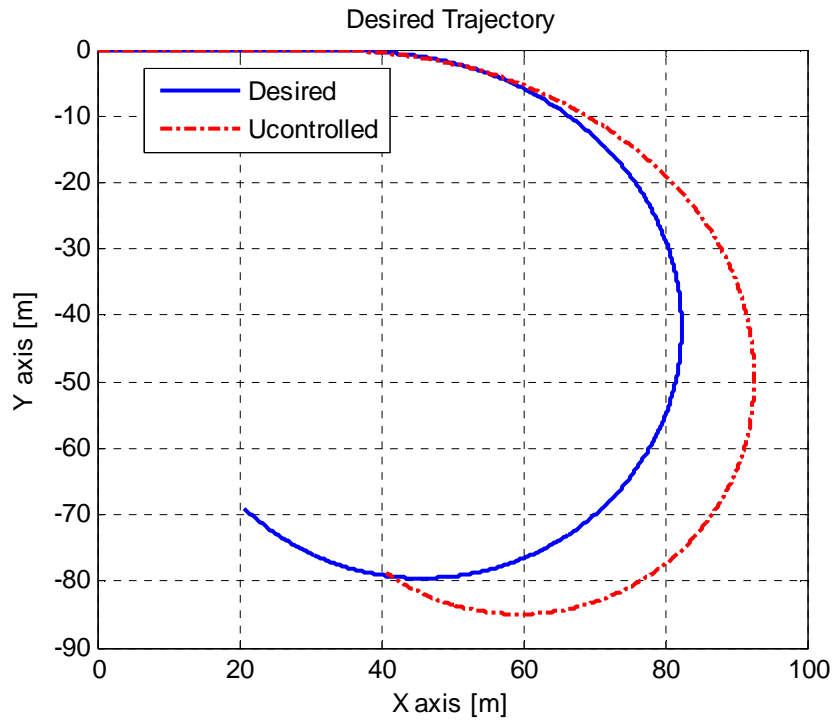
Fig. 5.30 Desired trajectory for J-Turn man. of the simulated vehicle

For wet asphalt road conditions, 50º steer angle J-turn maneuver is applied with an initial vehicle speed of 90 km/h and 0.4 road tire surface friction coefficient. Fig. 5.31 displays the desired yaw rate versus time for wet road conditions. Here, the continuous decline of the uncontrolled vehicle yaw rate is not observed. On the contrary, the yaw rate is stabilized after a single oscillation. This can be explained by the inherent stability of the two degree of freedom model, in which the effect of the vehicle sideslip angle is not taken into account. Fig. 5.32 displays the corresponding desired lateral acceleration and Fig. 5.33 shows the desired trajectory of the vehicle under wet-road conditions.
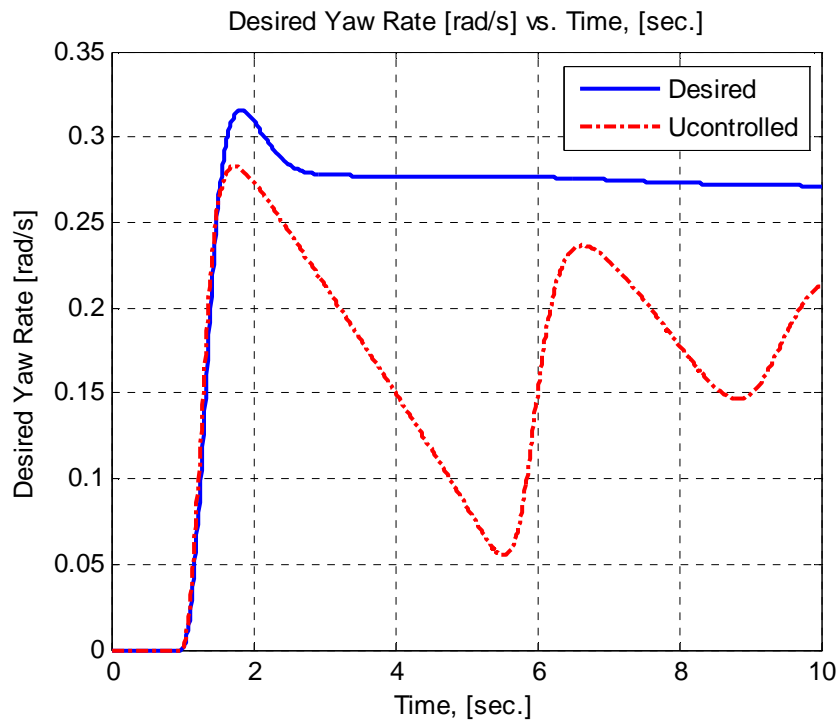
Fig. 5.31 Desired yaw rate versus time for wet road conditions and for J-Turn maneuver of the simulated vehicle
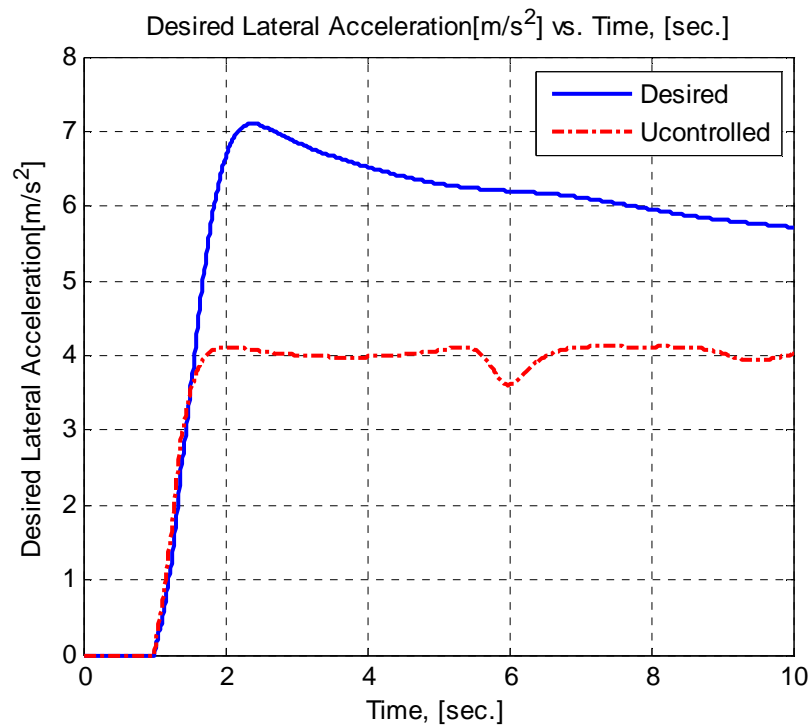

Fig. 5.32 Desired lateral acceleration versus time for wet road conditions and for J-Turn maneuver of the simulated vehicle
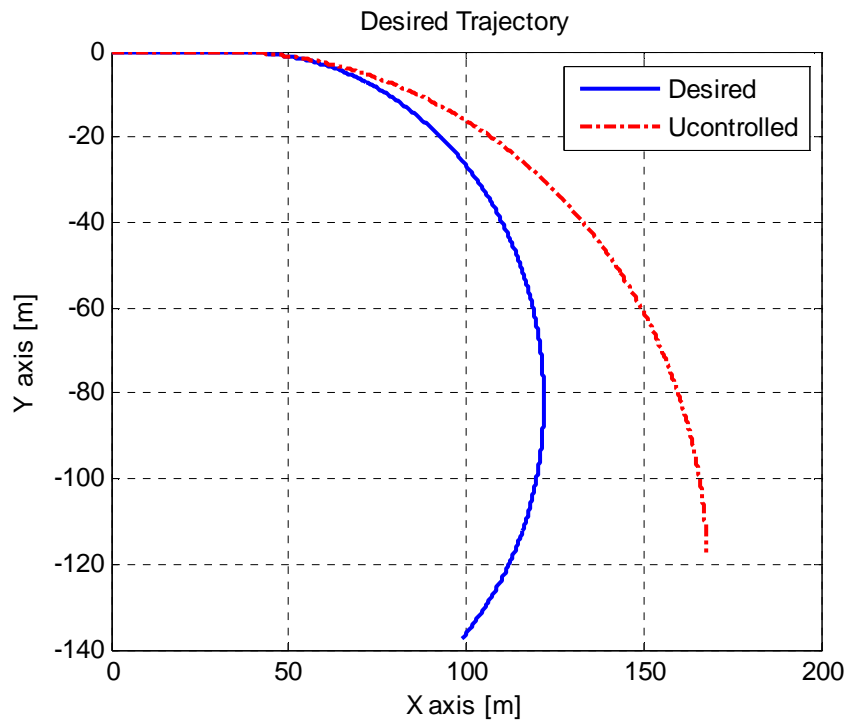
Fig. 5.33 Desired trajectory for the simulated vehicle for wet road conditions and for J-Turn maneuver of the simulated vehicle

For icy asphalt road conditions, 40º steer angle double lane change maneuver is applied with an initial vehicle speed of 40 km/h and 0.1 road tire surface friction coefficient. Fig. 5.34 shows the desired yaw rate of the vehicle according to the specified steer input for icy road conditions. The maximum of the desired yaw rate is 0.18 rad/s, which is high compared to obtained 0.1 rad/s for the uncontrolled behavior. The reason is the same as that mentioned for wet road conditions; the vehicle sideslip angle affects the yaw rate capability together with the limited cornering force. For icy road conditions, the vehicle sideslip angle should be about 1º at most. Figure 5.35 displays the desired lateral acceleration of the vehicle and Fig. 5.36 shows the desired vehicle trajectory.
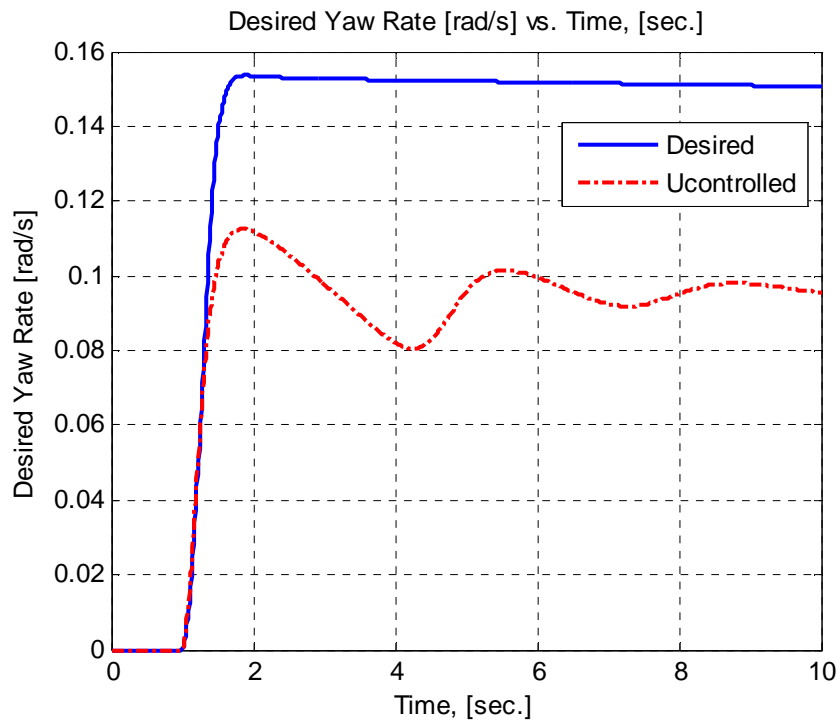
Fig. 5.34 Desired yaw rate versus time for icy road conditions and for J-Turn maneuver of the simulated vehicle
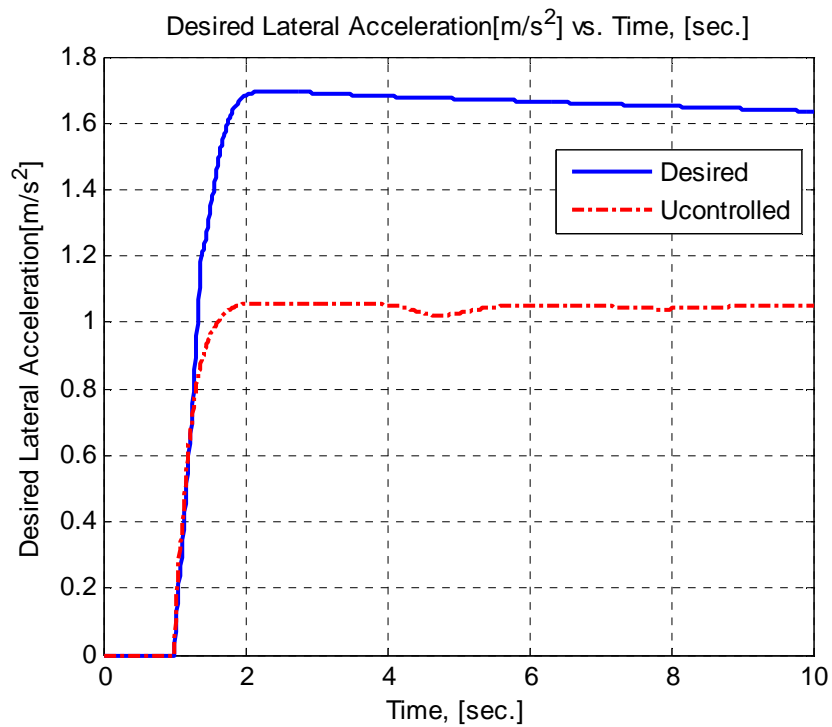

Fig. 5.35 Desired lateral acceleration versus time for icy road conditions and for J-Turn maneuver of the simulated vehicle
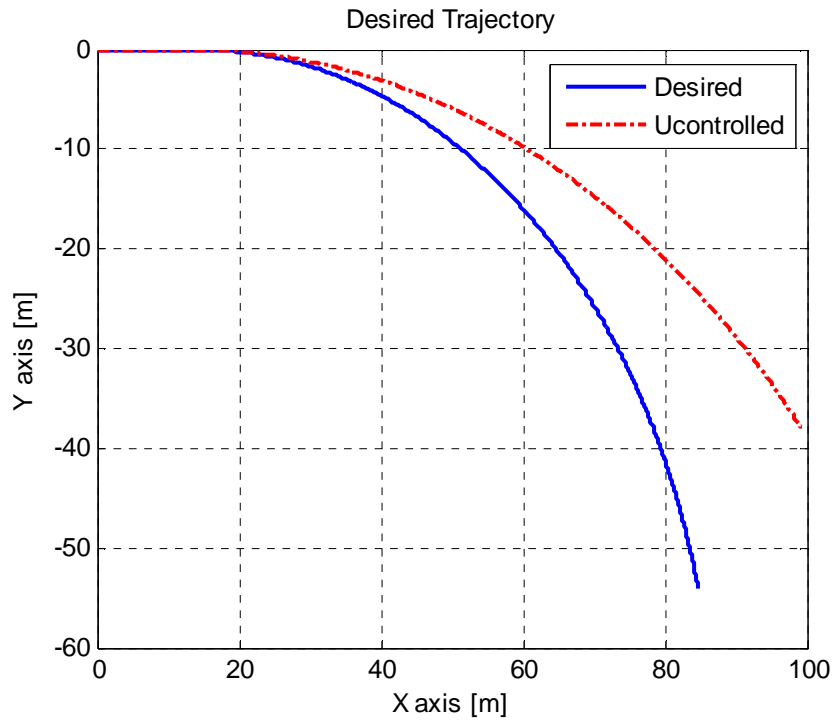
Fig. 5.36 Desired trajectory for the simulated vehicle for icy road conditions and for J-Turn maneuver of the simulated vehicle

5.2.3.2 CASE 2: DOUBLE LANE CHANGE MANEUVER

As mentioned before, the double lane change maneuver is used to simulate the evasive maneuver or series cornering situations. The desired behavior of the vehicle is shown in the following parts. First, the dry road conditions are considered for simulation. The initial conditions remain the same, so that the steering angle function consists of a single sine wave with amplitude of 90 degrees and a frequency of 0.25Hz, the initial velocity of the vehicle is 90 km/h and the steering wheel gear reduction ratio is 1/18, so that the front wheels turn with a maximum angle of 5 degrees.
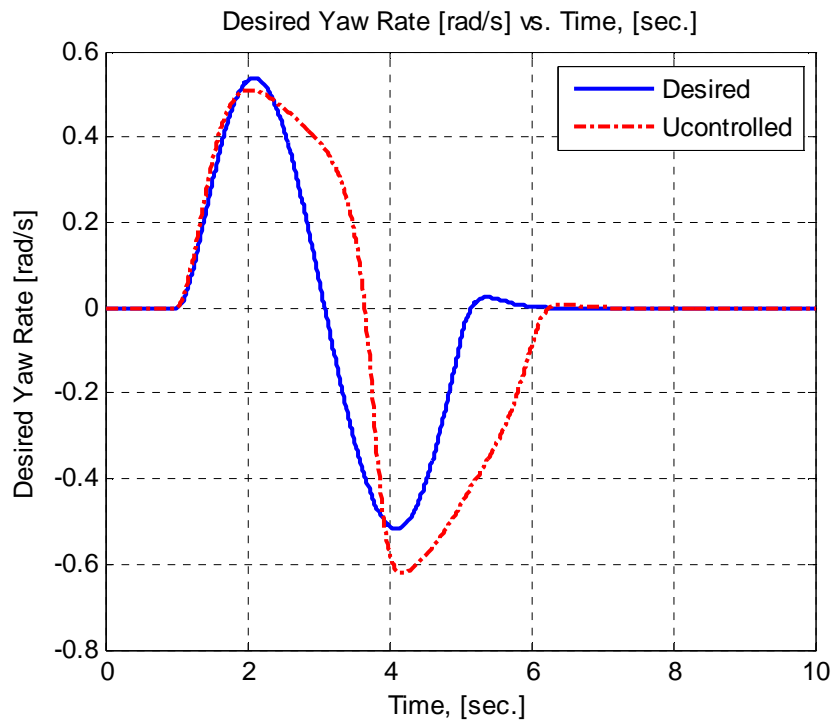
Fig. 5.37 Desired yaw rate versus time for double lane change maneuver of the simulated vehicle

Fig. 5.37 demonstrates the desired yaw rate of the vehicle for double lane change simulated for 10 seconds. This figure shows that the desired yaw rate has the same form with a small lag. When compared to uncontrolled behavior, the initial peak of the yaw rate is nearly same but the second peak is roughly $5/6^{th}$ of the uncontrolled behavior. Carefully investigated, the peak points of two oscillations do not have the same value. This is due to the velocity decline, forcing the yaw rate to decrease. Fig. 5.38 shows the desired lateral acceleration versus time and Fig. 5.39 shows the desired trajectory for the simulated vehicle. Note that, the last figure displaying the trajectory is also held for 10 seconds. As one can notice, the final course is not level, instead have a small angle with the horizontal axis. This is due to yaw rate variation, which results in a nonzero yaw angle at the end of the maneuver.
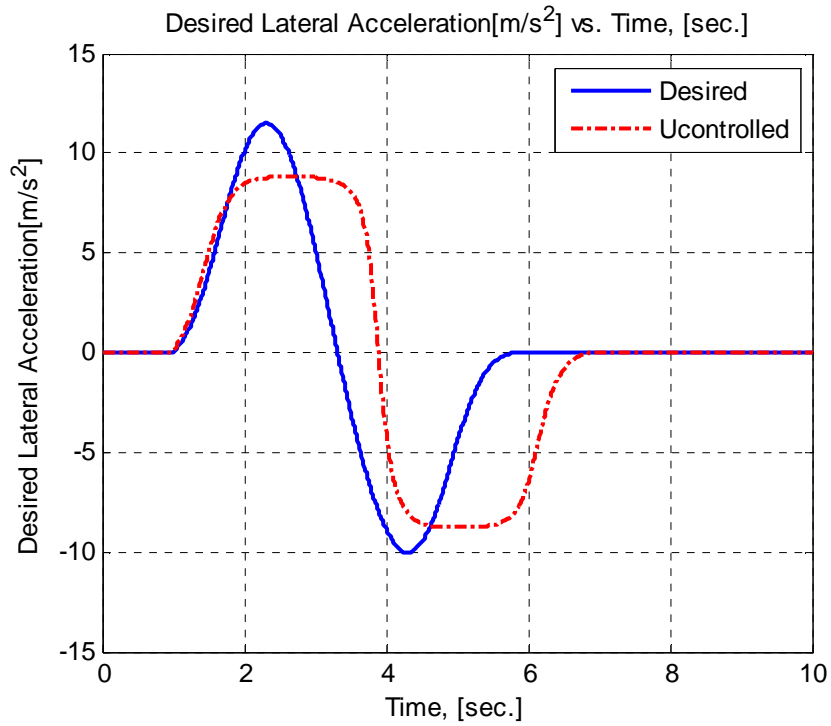
Fig. 5.38 Desired lateral acceleration versus time for double lane change maneuver
of the simulated vehicle (simulated for 10 seconds for clarity)
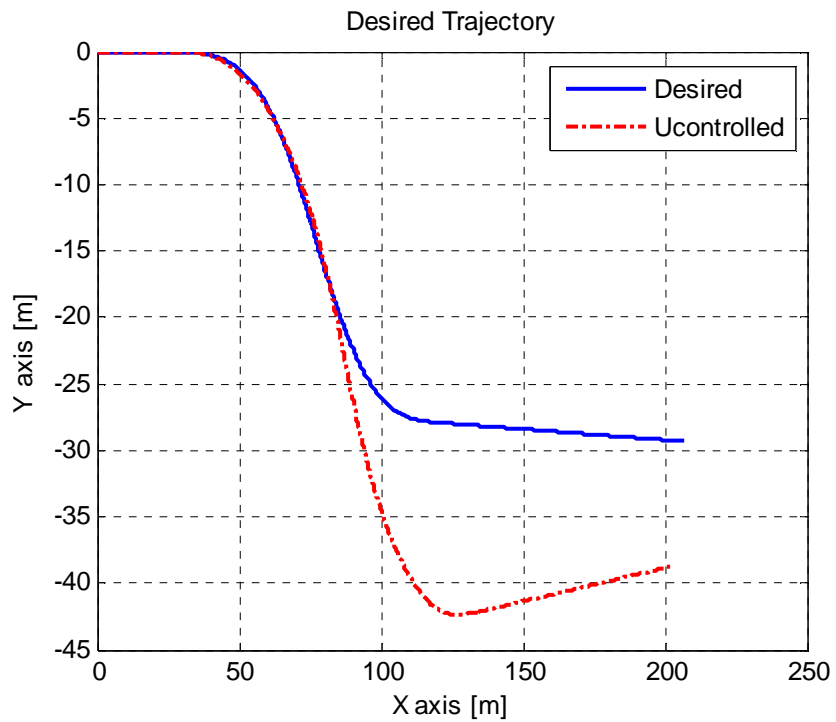
Fig. 5.39 Desired trajectory for double lane change maneuver of the simulated
vehicle (simulated for 10 seconds for clarity)

90

For wet asphalt road conditions, 50º steer angle J-turn maneuver is applied again with an initial vehicle speed of 90 km/h and 0.4 road tire surface friction coefficient. Fig. 5.40 displays the desired yaw rate vs. time for wet road conditions. The general manner is the same as that with the dry road conditions; that is, the peak value of the first oscillation is slightly larger than the peak of second oscillation. The reason behind this situation is the same; reduction in velocity. Fig. 5.41 shows the corresponding desired lateral acceleration and Fig. 5.42 shows the resulting desired trajectory of the vehicle. Note that, in order to give a better insight, the simulation time is elongated to 10 seconds.
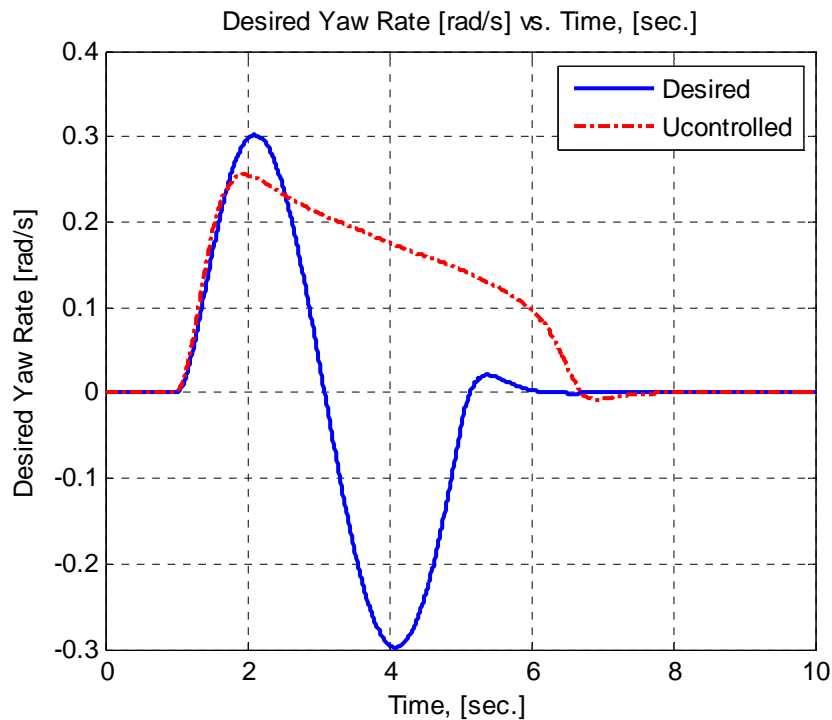

Fig. 5.40 Desired yaw rate of the vehicle versus time for wet road conditions and for double lane change maneuver of the simulated vehicle
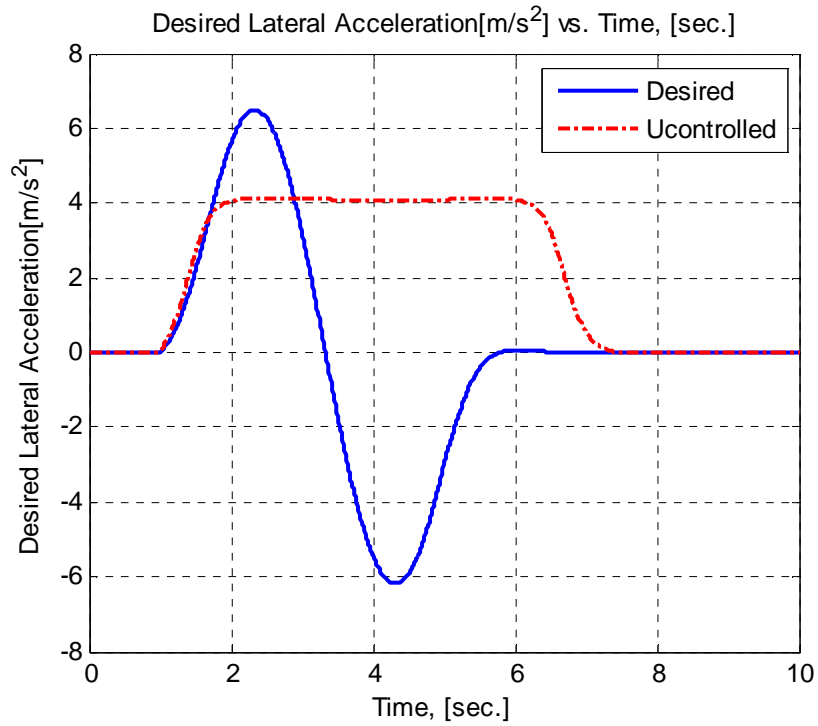
Fig. 5.41 Desired lateral acceleration versus time for wet road conditions and for double lane change maneuver of the simulated vehicle
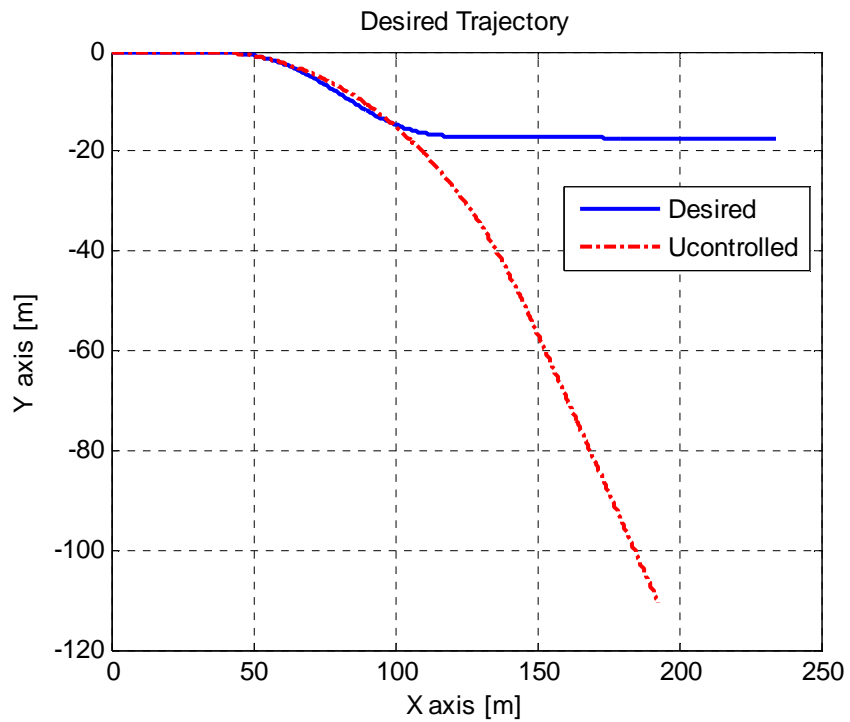

Fig. 5.42 Desired trajectory for wet road conditions and for double lane change maneuver of the simulated vehicle

92

For icy asphalt road conditions, 50º steer angle double lane change maneuver is applied with an initial vehicle speed of 50 km/h and 0.1 road tire surface friction coefficient. Fig. 5.43 shows the desired yaw rate of the vehicle according to the specified steer input for icy road conditions. In this situation, the difference between the peak values is nearly zero, since the velocity decrease has nearly vanished. This has led to a final course nearly parallel to horizontal axis. The results for lateral acceleration and desired trajectory can be seen of Fig. 5.44 and Fig. 5.45, respectively.
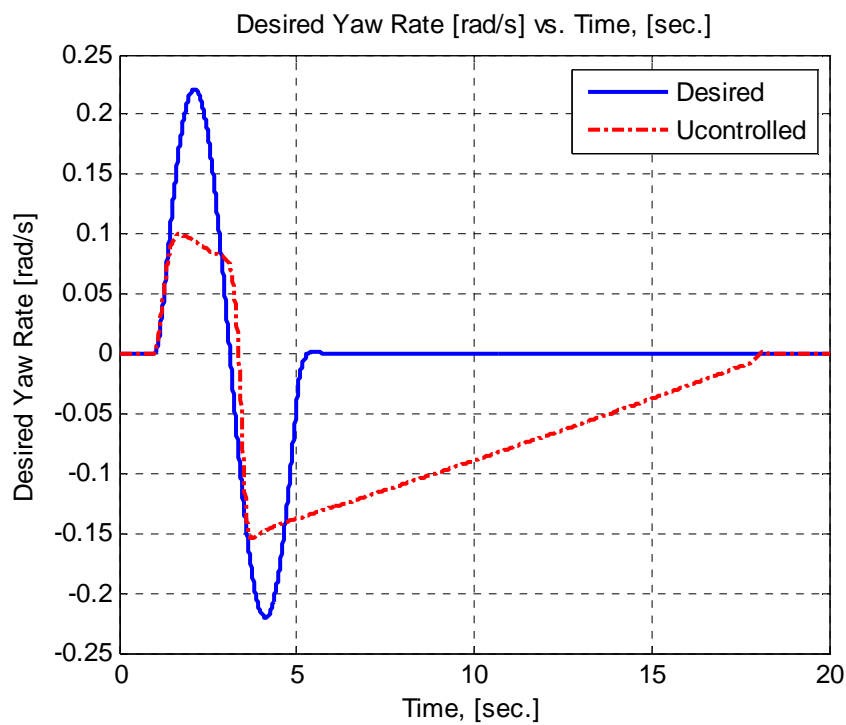

Fig. 5.43 Desired yaw rate of the vehicle versus time for wet road conditions and for double lane change maneuver of the simulated vehicle
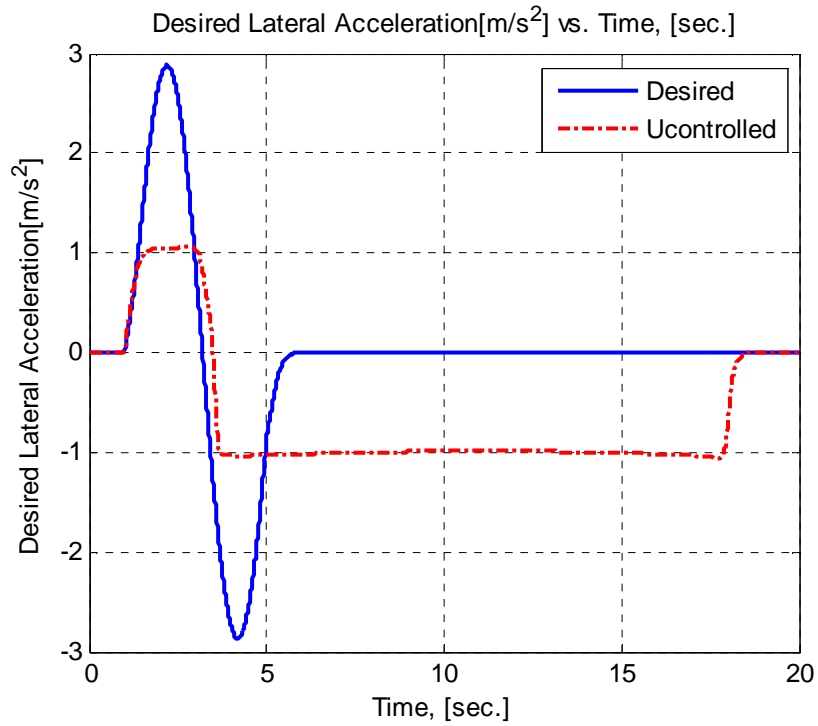
Fig.5.44 Desired lateral acceleration versus time for icy road conditions and for double lane change maneuver of the simulated vehicle
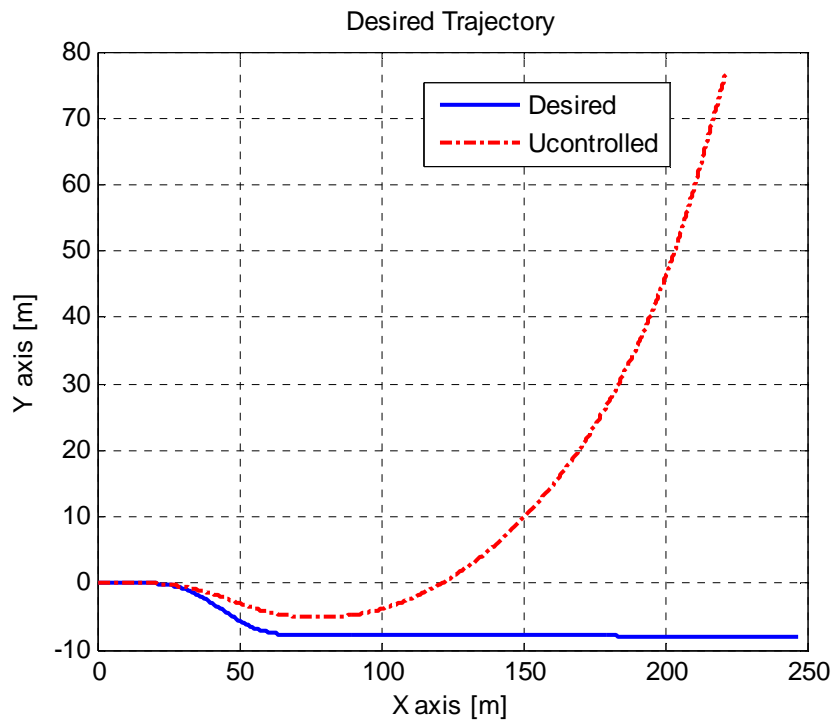

Fig. 5.45 Desired trajectory for wet road conditions and for double lane change maneuver of the simulated vehicle

5.3 VEHICLE SIMULATION RESULTS WITH ACTIVE YAW CONTROL SYSTEM

Up to this point, the uncontrolled and desired vehicle behavior has been simulated and compared for different road conditions and driver inputs. In this section, various aspects of vehicle behavior under control of an active yaw control system based on independent wheel braking will be introduced. The input maneuvers taken into account for this section will be the same as the former simulation maneuvers. After obtaining result for each particular maneuver and road condition, a comparison will be made to evaluate the performance of the designed controller.

Simulations will consist of two main parts: J-turn maneuver and double lane change maneuver tests. The simulation results will include not only motion, but also control input characteristics, such as brake moment variations. The overall performance evaluation will be done for all effective characteristics.

One critical point is the simulation is done with a fixed step time interval basis of 0.01 seconds. The selection of this simulation step time interval is based on two main reasons:

- For the practical applications, the general controller cycle time is about 0.04 to 0.01 seconds. In other words, in-use active yaw controllers do check for any undesired behavior or change their manipulative effort within these intervals.
- Computational accuracy for the detailed vehicle model used to simulate the real vehicle decreases rapidly as the time intervals of the simulation increases. After several trials, 0.01 second is selected for this purpose.

5.3.1 CASE 1: J-TURN MANEUVER

A J-turn maneuver has been examined in this part of the study. The main aim of this maneuver is to maintain a constant turning radius during a sharp turn. The input parameters are kept same as in section 5.2.1. Initial vehicle velocity is taken as 90 km/h while the road surface friction coefficient is taken as 0.9 and the maximum level of the steer input is taken as 90 degrees. The steering wheel ratio is 1/18; therefore the front wheels are turned by 5 degrees. Fig. 5.46 shows the resulting steer angle variation and Fig. 5.47 demonstrates the uncontrolled, desired and the controlled vehicle yaw rates versus time graph.
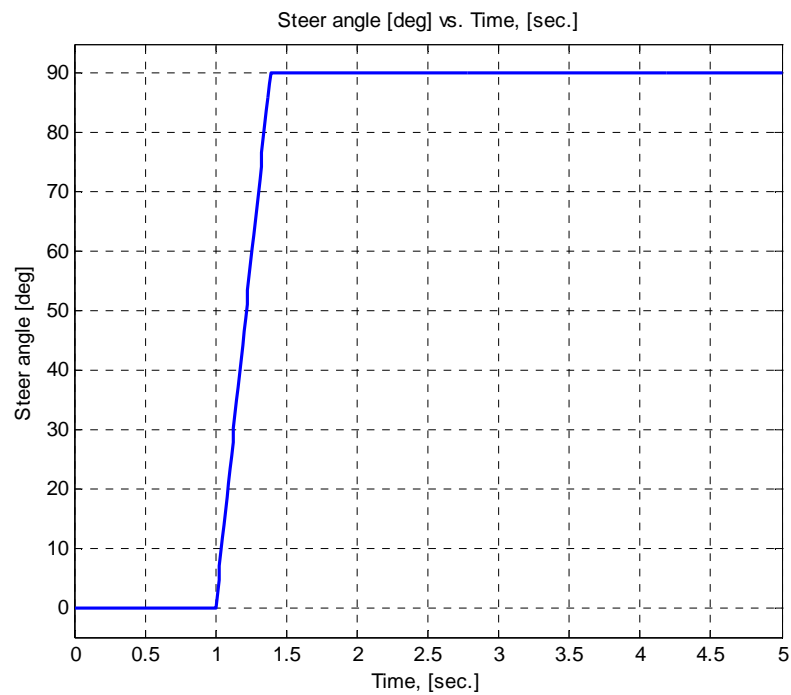

Fig. 5.46 Steer angle variation versus time for yaw controlled vehicle in a J-Turn maneuver
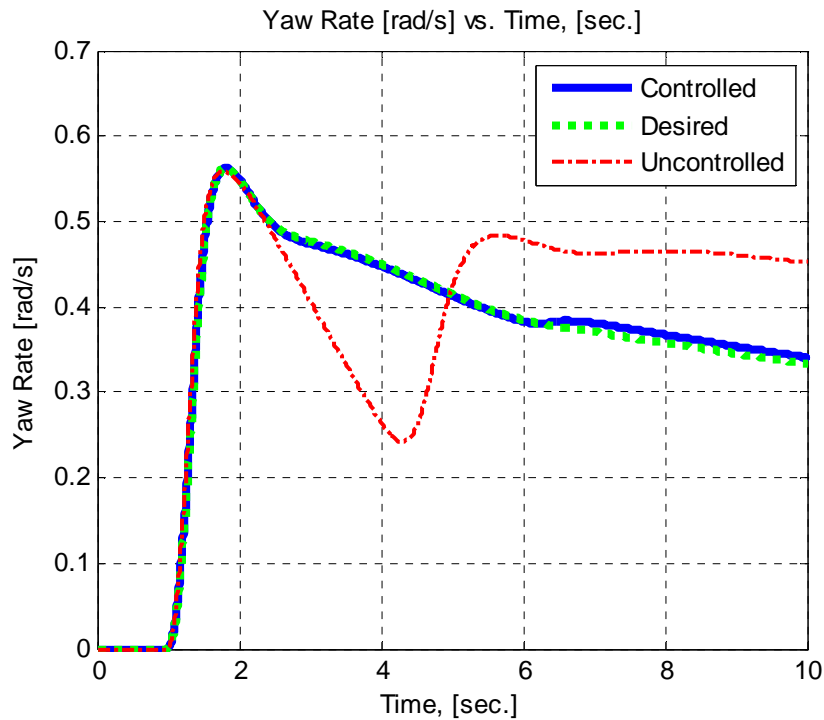
Fig. 5.47 Uncontrolled, desired and controlled vehicle yaw rate versus timein a J-Turn maneuver

As can be seen from the above figure, the controller can track the dictated demand by following the calculated desired vehicle yaw rate. This case seems to be flawless, since the demanded yaw rate is successfully followed. However, when the corresponding vehicle sideslip angles, shown in Fig. 5.48, are examined, it is seen that this successful behavior has been obtained at the cost of an excessive sideslip angle even higher than that of the uncontrolled vehicle. This situation brings a contradiction, since the yaw rate controller should; ideally, preserve the sideslip stability as well as tracking the demanded yaw rate. Since the sideslip limit for steerability on dry road condition is about 12º, the overall control seems to have failed [40]. Fig. 5.49 illustrates the lateral accelerations of the uncontrolled, desired and controlled vehicle simulations. This figure also illustrates that the sideslip limitation performance is insufficient. The lateral acceleration has reached the limits for the uncontrolled and controlled vehicles, which is by far lower than the desired value. Although the redistribution of tire forces by activating individual brakes has

97

opened the way to achieve the tracking of desired yaw rate, it is inadequate for maintaining the required vehicle sideslip angle. Fig. 5.48 shows the brake torques applied to the wheels.
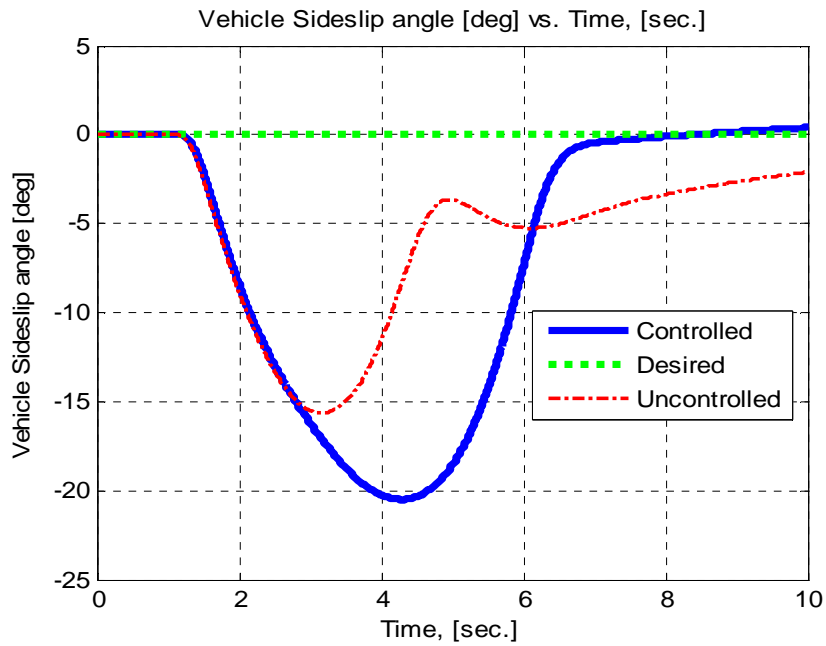

Fig. 5.48 Uncontrolled, desired and controlled vehicle sideslip angles versus time in a J-Turn maneuver
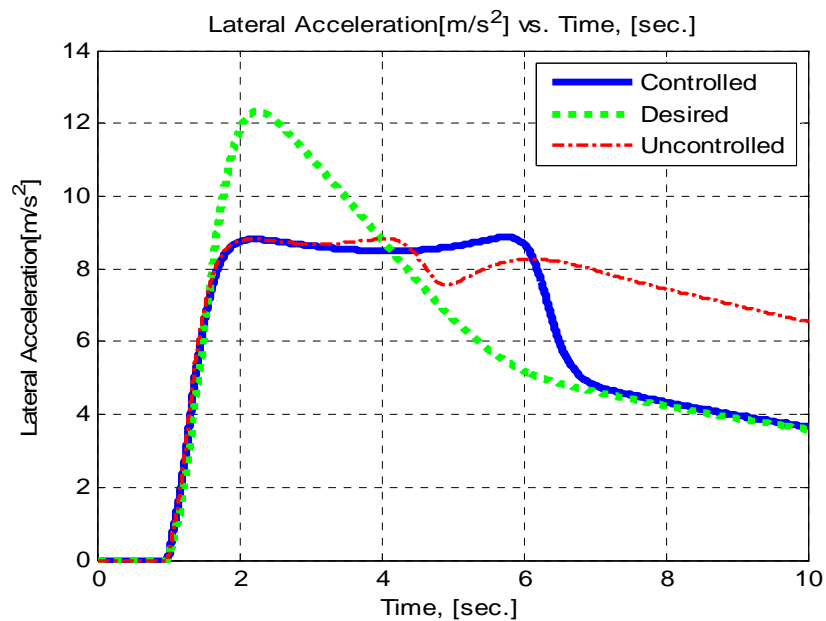

Fig. 5.49 Uncontrolled, desired and controlled vehicle lateral acceleration versus time in a J-Turn maneuver
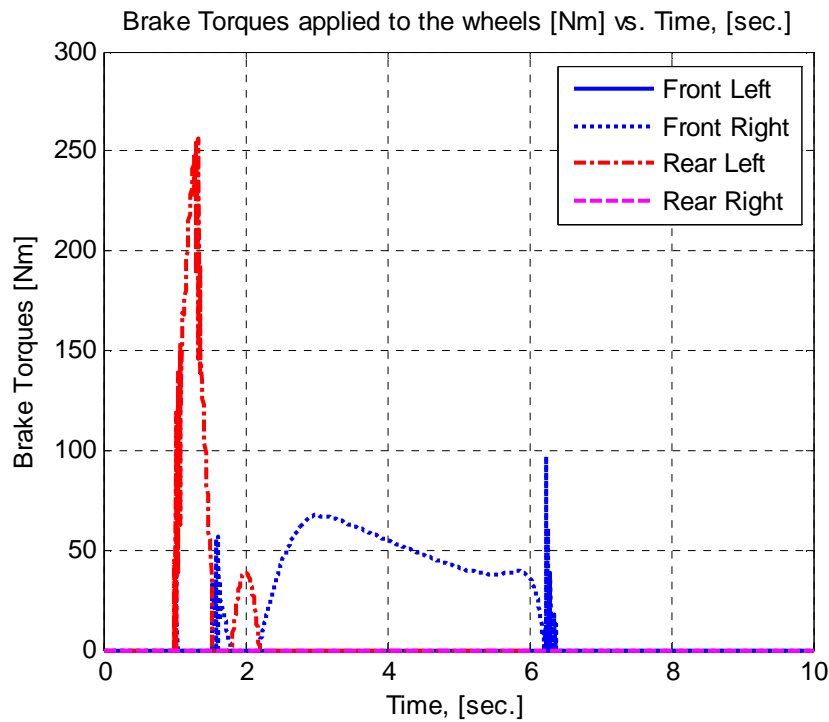
Fig. 5.50 Brake torques applied to the wheels in a J-Turn maneuver for yaw controlled vehicle

Fig. 5.50 shows the brake torques applied to the wheels to track the desired yaw rate. As can be seen, front left and rear right tires have not been manipulated by the controller. Instead, the rear left tire brake has been applied so that the desired yaw rate can be followed. After a while, due to the fishtail effect of the manipulation, cross tire (rear right) has been brake applied. The trajectories for uncontrolled, desired and controlled vehicles have been presented in Fig. 5.51. Although the yaw rate controller seems to track the desired yaw rate, there exist almost no difference between yaw rate controlled vehicle and uncontrolled vehicle. In this situation, it can be thought that the velocity reduction as a possible solution in the first glance. Considering the increasing yaw rate demand tendency with increasing velocity, this kind of manipulation may be favorable. However, the speed reduction has the disadvantage of needing longitudinal brake forces, which in turn decreases the overall cornering force capacity. When compared, the velocity decrease by even braking (that is, braking with cross tires which are not manipulated in order to

prevent any extra yaw moments) works generally worse than single yaw control brake manipulation.
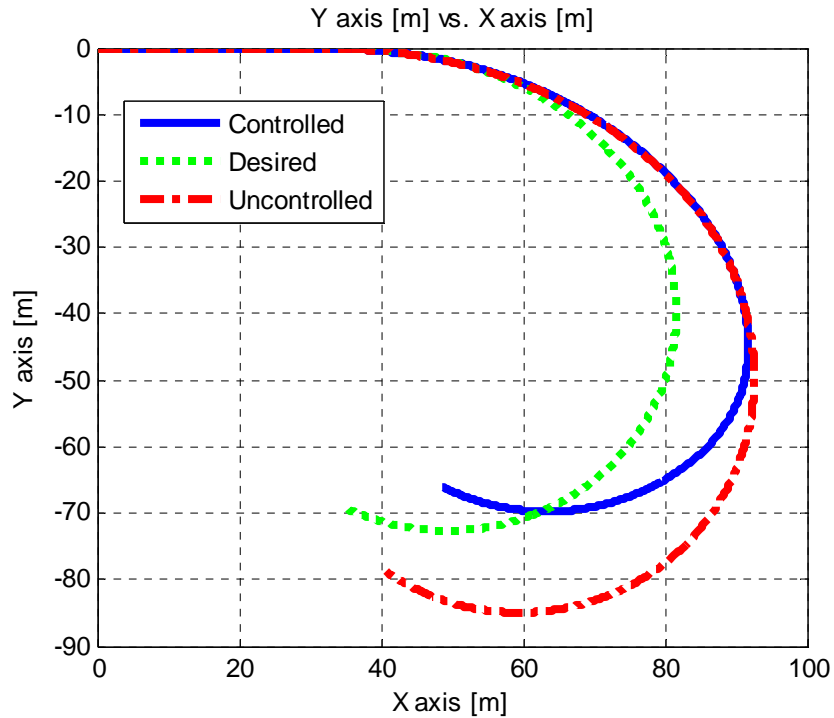

Fig. 5.51 Uncontrolled, desired and controlled vehicle trajectories versus time in a J-Turn maneuver

The next simulation is for wet asphalt road conditions, where 50º steer angle J-turn maneuver is applied again with an initial vehicle speed of 90 km/h and 0.4 road tire surface friction coefficient. Fig. 5.52 shows the uncontrolled, desired and the controlled vehicle yaw rates vs. time graph. Again, the yaw controller has satisfied its responsibility to track the desired yaw rate. However, as can be observed on Fig. 5.53, the vehicle sideslip angle has gone beyond stability limits by reaching almost 25º, in which the steerability limit for the sideslip angle limit is about 4º [40]. Fig. 5.54 demonstrates the uncontrolled, desired and the controlled vehicle lateral accelerations vs. time and Fig. 5.55 shows the brake torques applied to control the vehicle. Fig. 5.56 presents the resulting trajectories.
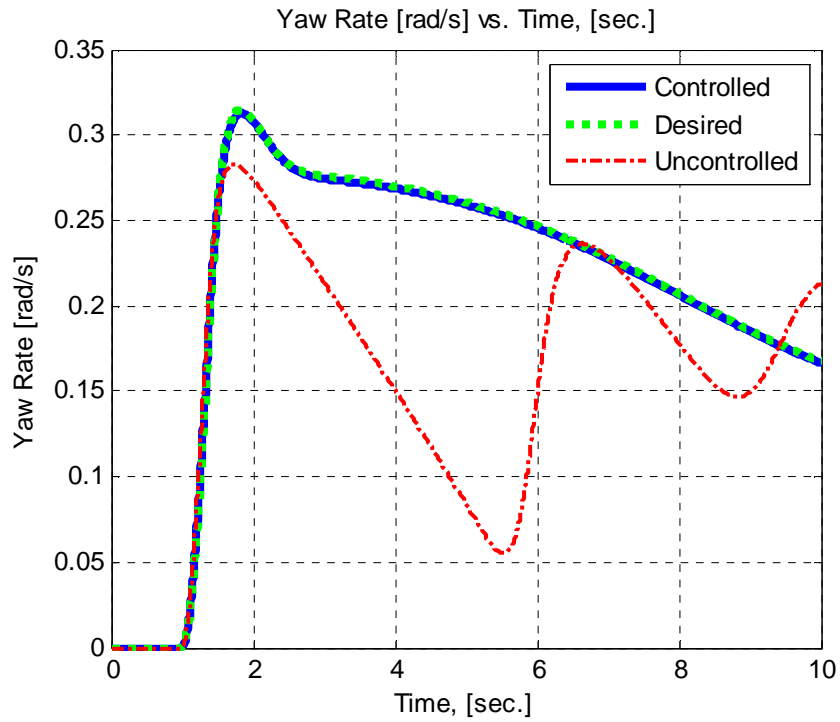
Fig. 5.52 Uncontrolled, desired and controlled vehicle yaw rates versus time for wet conditions in a J-Turn maneuver
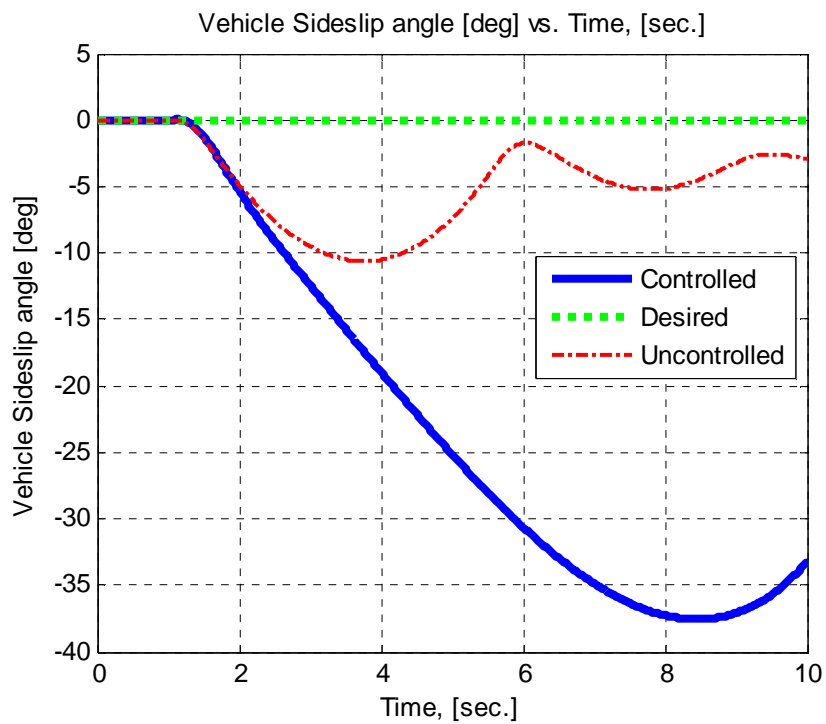

Fig. 5.53 Uncontrolled, desired and controlled vehicle sideslip angles versus time for wet conditions in a J-Turn maneuver
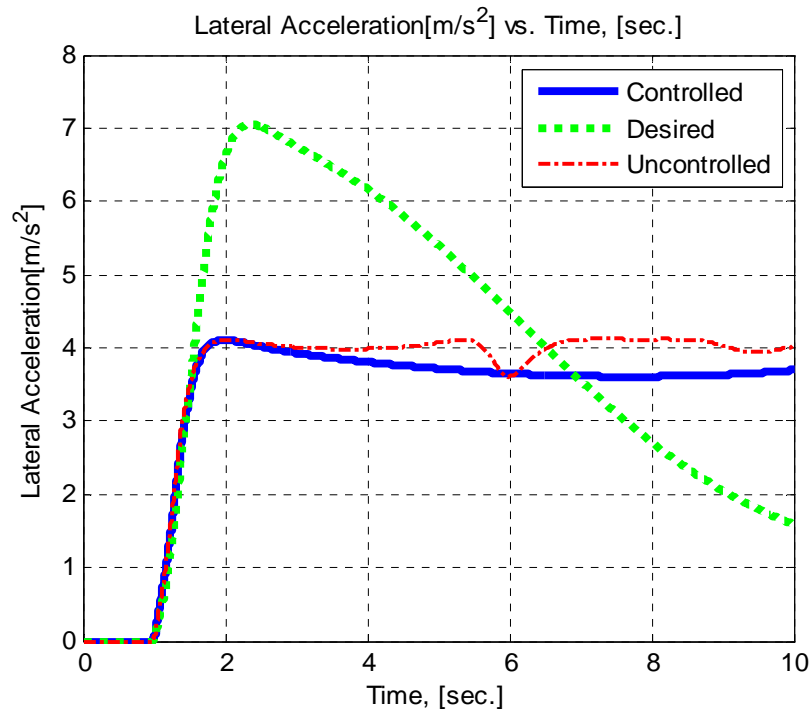
Fig. 5.54 Uncontrolled, desired and controlled vehicle lateral acceleration versus
time for wet conditions in a J-Turn maneuver
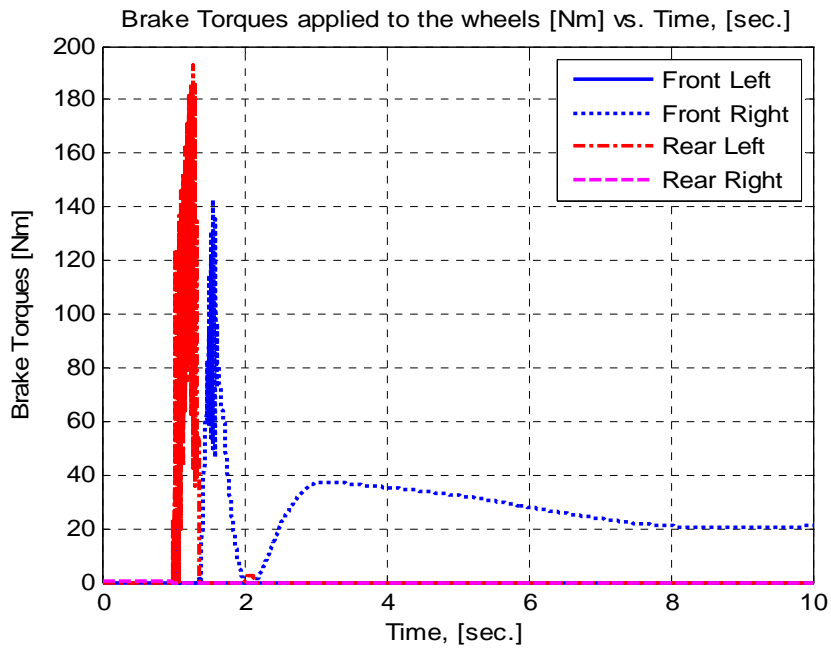
Fig. 5.55 Brake Torques applied to the wheels for the yaw controlled vehicle and for
wet conditions in a J-Turn maneuver

102
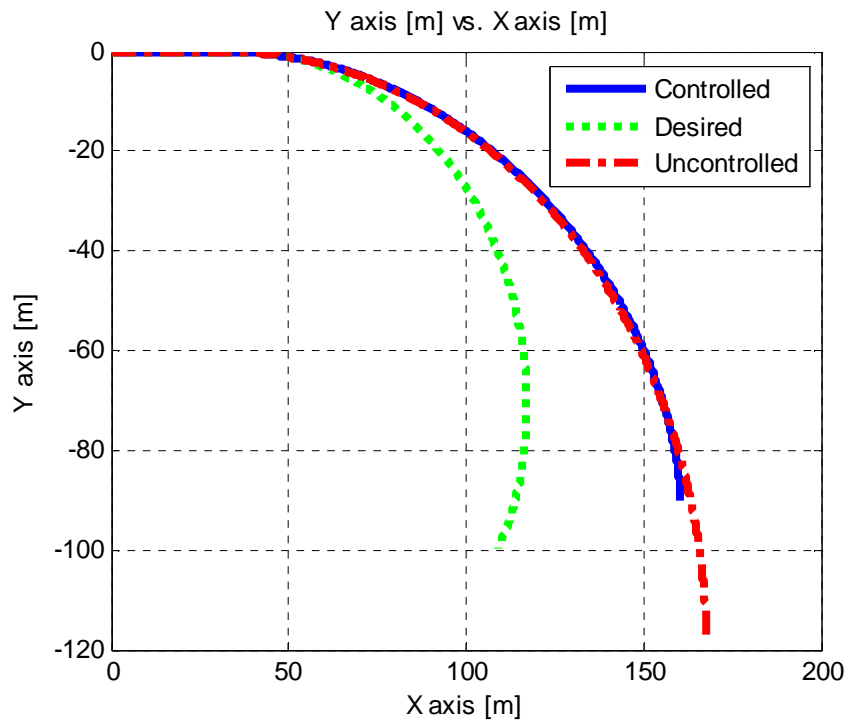
Fig. 5.56 Uncontrolled, desired and controlled vehicle trajectories versus time for wet conditions in a J-Turn maneuver

For the last simulation of yaw controlled vehicle in a J-turn maneuver, icy road conditions with 40º steer angle J-turn maneuver is applied with an initial vehicle speed of 40 km/h and 0.1 road tire surface friction coefficient. Fig. 5.57 presents the uncontrolled, desired and the controlled vehicle yaw rates vs. time graph. Once more, however, as shown on Fig. 5.58, the vehicle sideslip angle has gone beyond stability limits by reaching almost 8º, in which the steerability limit for the sideslip angle limit is about 1º [40]. Fig. 5.59 demonstrates the uncontrolled, desired and the controlled vehicle lateral accelerations versus time and Fig. 5.60 shows the brake torques applied to control the vehicle. The lateral acceleration obtained by yaw controller is about same with the uncontrolled vehicle behavior. This can prove that the controller actually can obtain little changes for manipulating the vehicle since the physical adhesion limits have been reached already. Fig. 5.61 presents the resulting trajectories. The trajectories do not differ crucially, so the most important parameter in this situation is the yaw rate and vehicle sideslip angles.
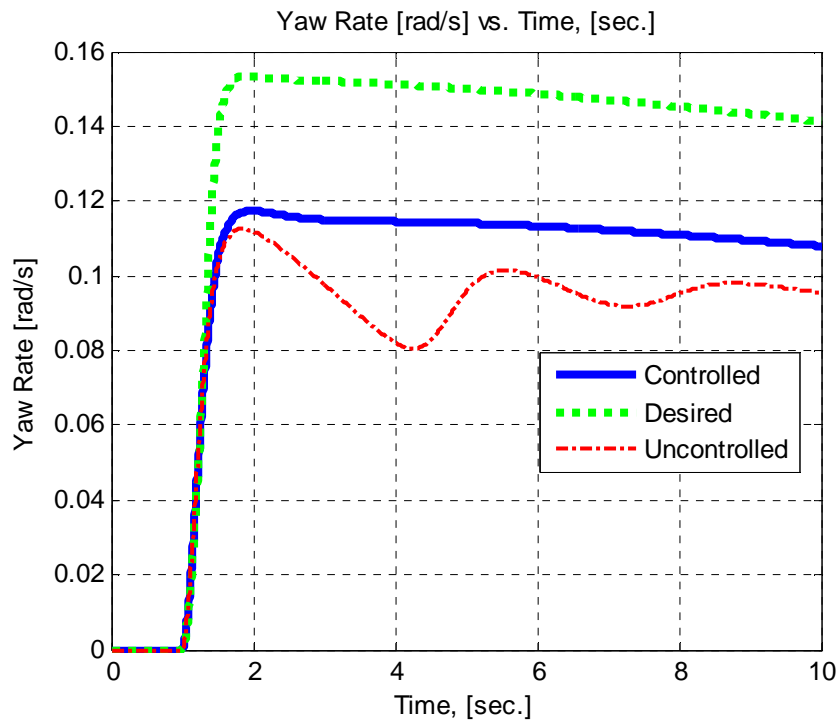
Fig. 5.57 Uncontrolled, desired and controlled vehicle yaw rates versus time in a J-Turn maneuver
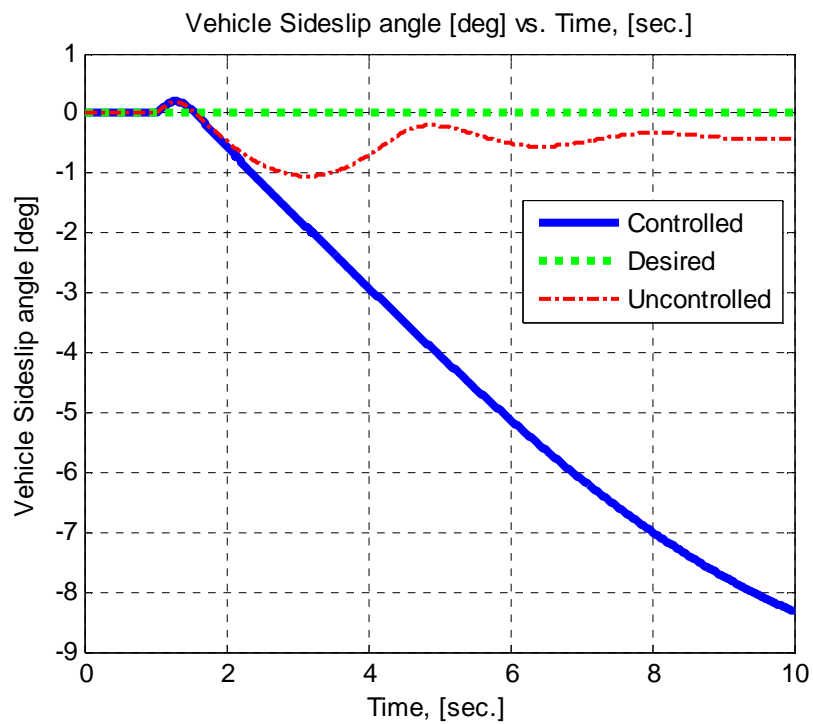

Fig. 5.58 Uncontrolled, desired and controlled vehicle sideslip angles versus time in a J-Turn maneuver

104
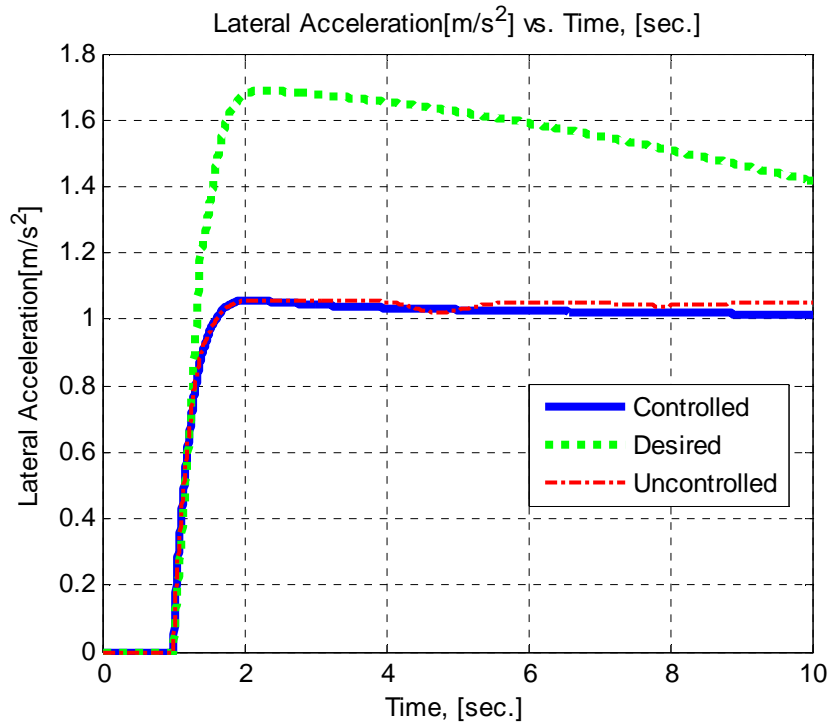
Fig. 5.59 Uncontrolled, desired and controlled vehicle lateral acceleration versus time in a J-Turn maneuver
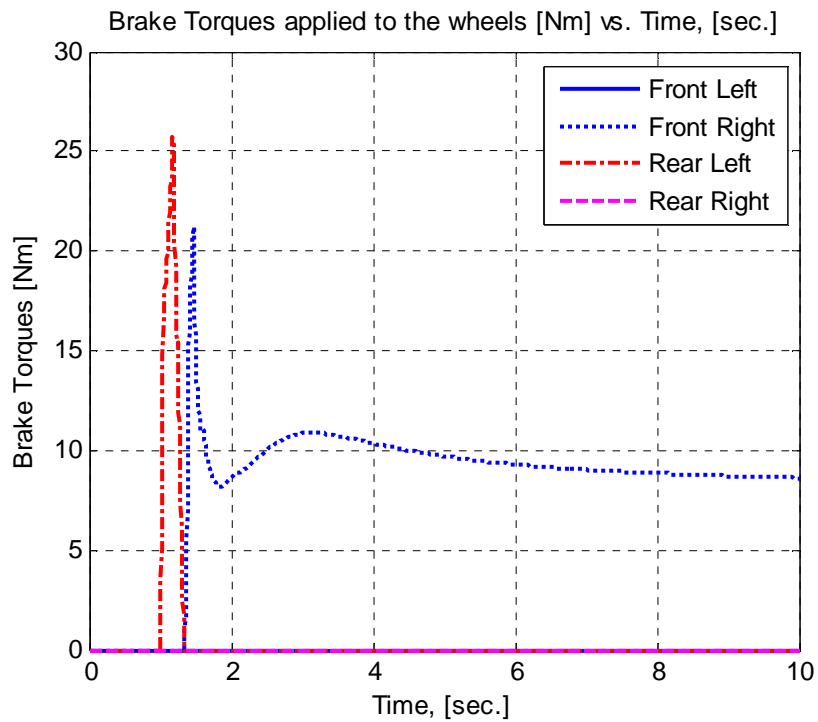

Fig. 5.60 Brake Torques applied to the wheels in a J-Turn maneuver for yaw controlled vehicle

105
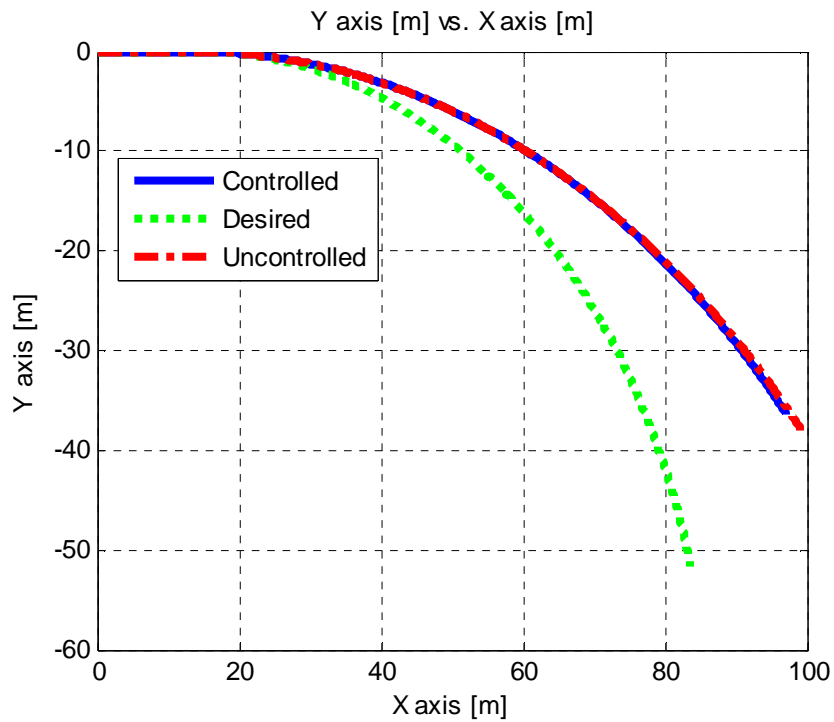
Fig. 5.61 Uncontrolled, desired and controlled vehicle trajectories versus time in a J-Turn maneuver

Up to this point, the yaw rate controller did not perform with enough accomplishment since it does not take the vehicle sideslip angle variation into account. This is a crucial deficiency, since vehicle sideslip angle is an important vehicle steerability parameter. However, if the desired yaw rate is manipulated by replacing the two degree of freedom model with another custom model [21][42], the desired yaw rate may be calculated in a less demanding way, which can lead this yaw controller perform better.

5.3.2   CASE 2: DOUBLE LANE CHANGE MANEUVER

A double lane change maneuver has been examined in this part of the study. The main aim of this maneuver is to demonstrate the vehicle handling performance in case of

    — Series rapid steering and counter steering while traveling too fast, or
    — A sudden obstacle has been faced and needed to be avoided[41]

The input parameters are kept same as in section 5.2.2. Initial vehicle velocity is taken as 90 km/h while the road surface friction coefficient is taken as 0.9 and the maximum level of the steer input is taken as 90 degrees. The steering wheel ratio is 1/18; therefore the front wheels are turned by 5 degrees. Fig. 5.60 shows the resulting steer angle variation and Fig. 5.64 demonstrates the uncontrolled, desired and the controlled vehicle yaw rates vs. time graph.
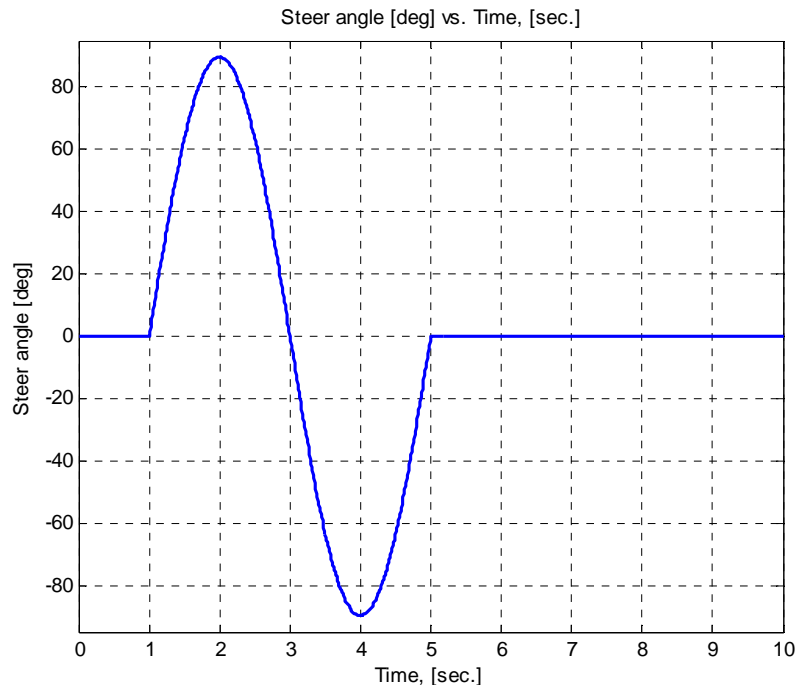
Fig. 5.63 Steer angle variation versus time for yaw controlled vehicle in a double lane change maneuver
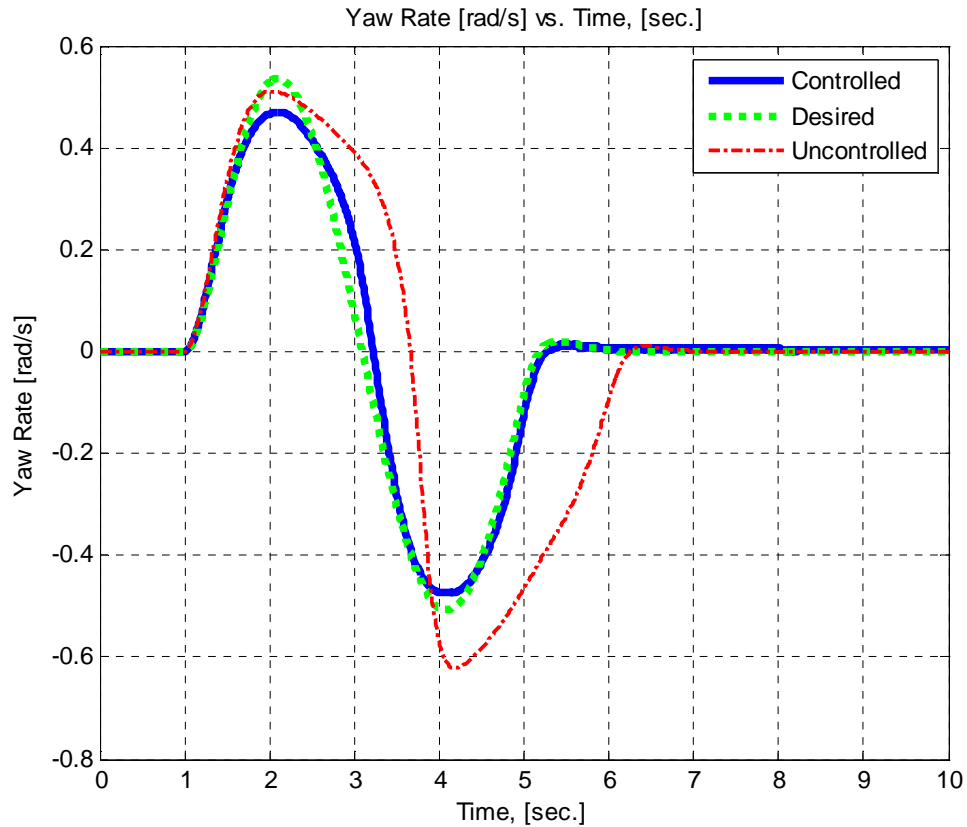
Fig. 5.64 Uncontrolled, desired and controlled vehicle yaw rates versus time in a double lane change maneuver

As can be observed from the yaw rate graph, the controller has decreased the overall yaw rate error and been able to follow the desired yaw rate successfully. If Fig. 5.65, which demonstrates uncontrolled, desired and the controlled vehicle sideslip angle versus time, is also examined the controlled vehicle sideslip angle can be seen to have decreased and brought to the steerability limits. This parameter has –as mentioned- an essential task in evaluating vehicle handling performance, and the yaw controller seems to be correcting the sideslip angle as required. Fig. 5.66 shows the uncontrolled, desired and controlled vehicle lateral accelerations versus time. The lateral accelerations obtained here are also limited by the road tire interaction limits, which is the same as those in uncontrolled case. However, the redistribution of the tire forces has helped the vehicle to track the desired behavior in a good manner.
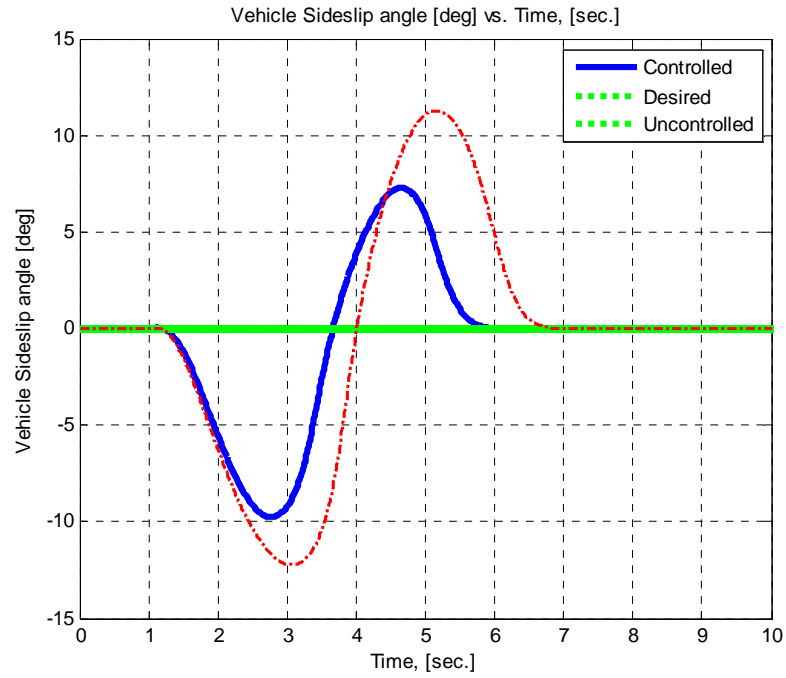
Fig. 5.65 Uncontrolled, desired, and controlled vehicle sideslip angles versus time in a double lane change maneuver
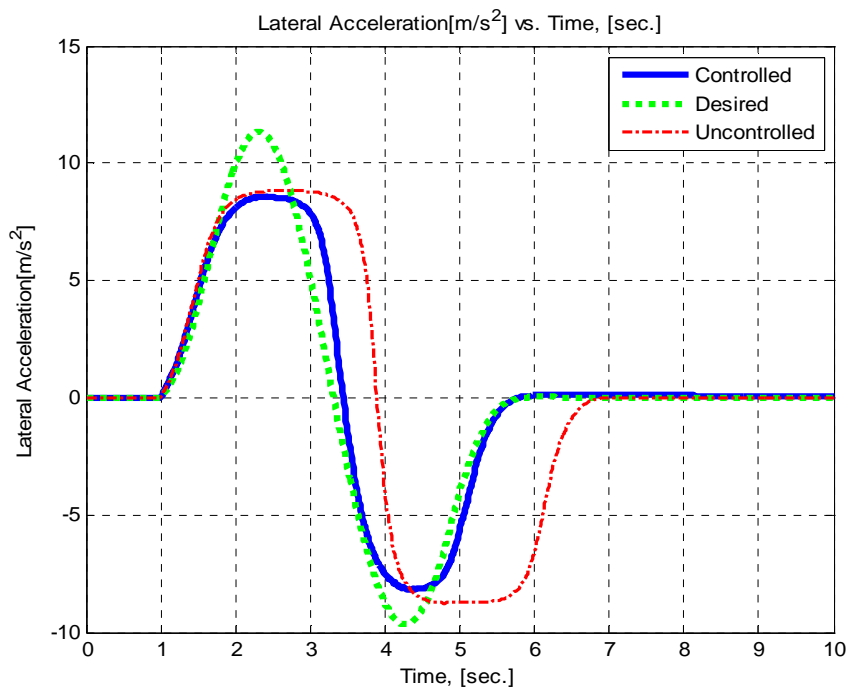

Fig. 5.66 Uncontrolled, desired and controlled vehicle lateral acceleration versus timein a double lane change maneuver

Fig. 5.67 presents the brake torques applied during the control of the vehicle. The trajectories for the uncontrolled, desired, and controlled vehicles have been presented in Fig. 5.68. The trajectory followed by the driver has become closer to the desired track of the vehicle. There still exists a small deviation in the final course. It should be noted, however, that these maneuvers are assumed to be definite before the undesired actions of the vehicle are observed. On the other hand, the driver is also capable of correcting these minor errors such as going out of track while steering with small angles. Therefore, the minor errors can be neglected by taking the driver's manipulation into effect.[11]
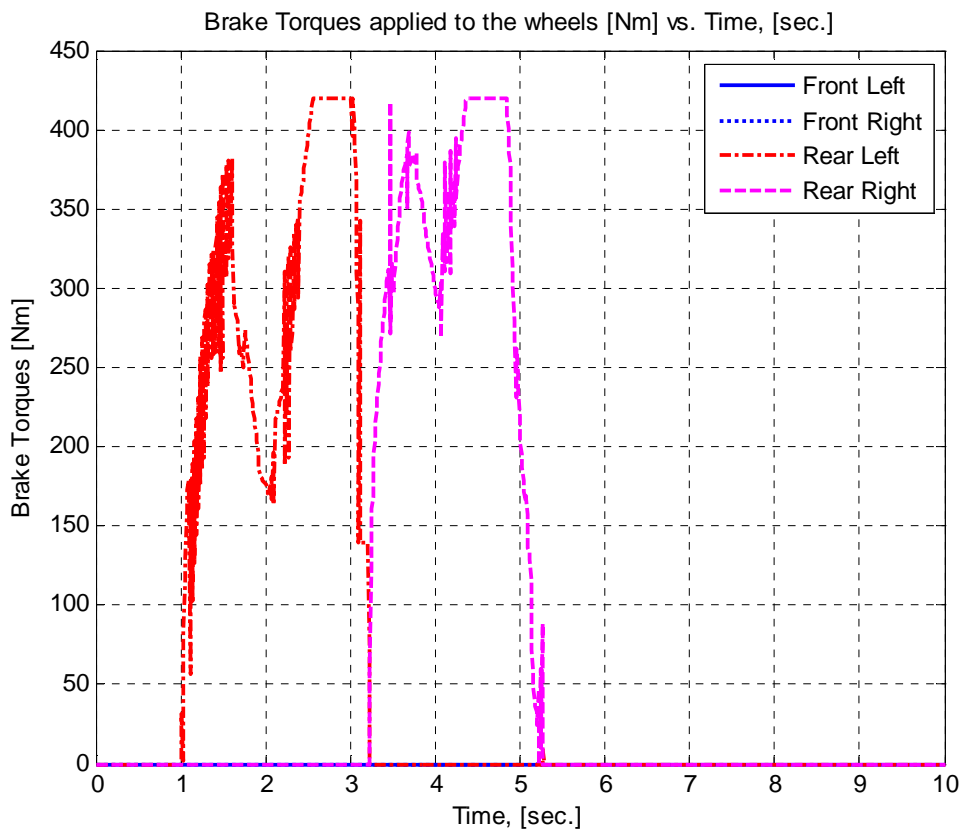

Fig. 5. 67 Brake torques applied to the wheels in a double lane change maneuver for the yaw controlled vehicle
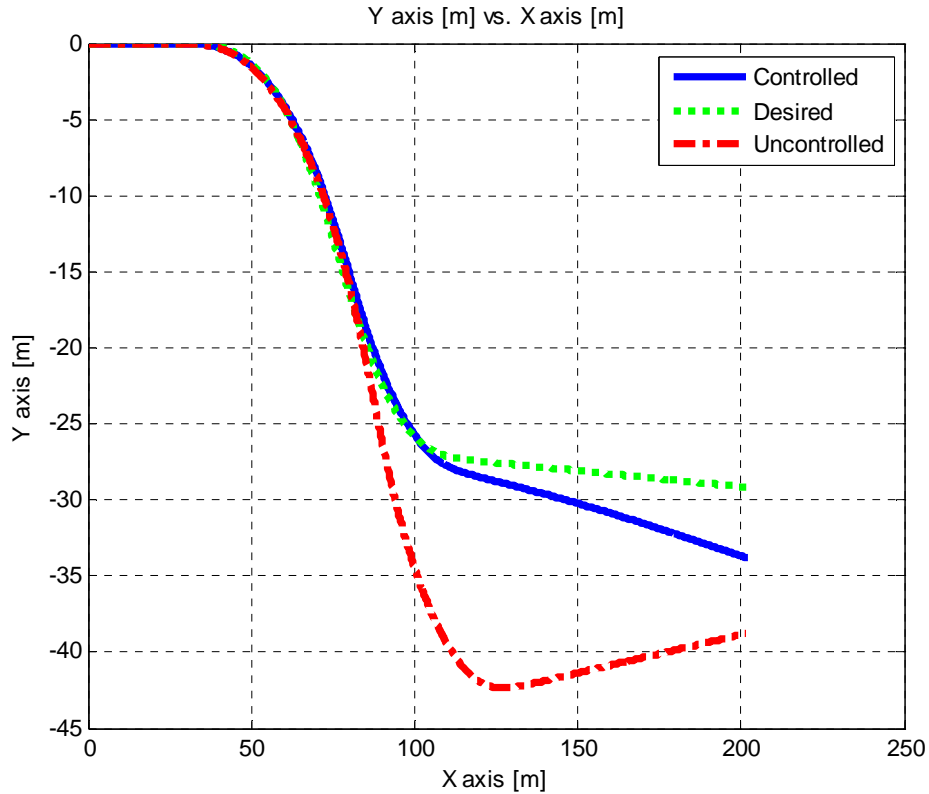
Fig. 5.68 Uncontrolled, desired, and controlled vehicle trajectories versus time in a double lane change maneuver

The next simulation is for wet asphalt road conditions, where a 50º steer angle double lane change maneuver is applied again with an initial vehicle speed of 90 km/h and 0.4 road tire surface friction coefficient. Fig. 5.69 shows the uncontrolled, desired, and the controlled vehicle yaw rates versus time graph. As before, the yaw controller has satisfied its responsibility to track the desired yaw rate. Also, as shown on Fig. 5.70, the vehicle sideslip angle is limited to acceptable values and oriented such that the sideslip angle has the same form as the steer angle input. Fig. 5.71 demonstrates the uncontrolled, desired, and controlled vehicle lateral accelerations versus time. Again, due to the limited tire cornering force capabilities, the required forces in order to generate enough lateral acceleration necessary for desired yaw rate is not obtained. On the other hand, the redistribution of these forces has led the vehicle to be able to follow the desired yaw behavior. Fig. 5.72 shows the brake torques applied to control the vehicle. As it can be seen, the brake pressures have

saturated for short terms, which indicates that the tire slip controller have encountered a tire slip surpassing the defined limits.
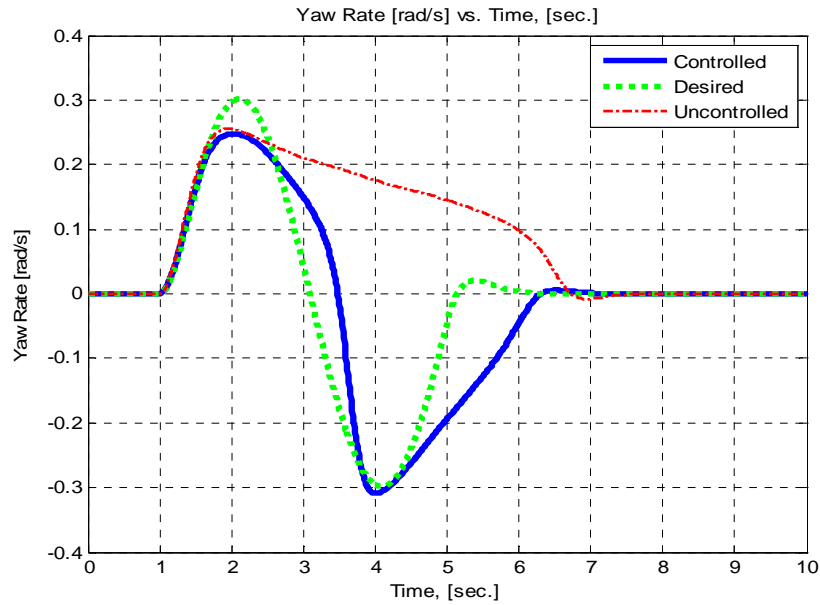
Fig. 5.69 Uncontrolled, desired, and controlled vehicle yaw rates versus time for wet road conditions in a double lane change maneuver
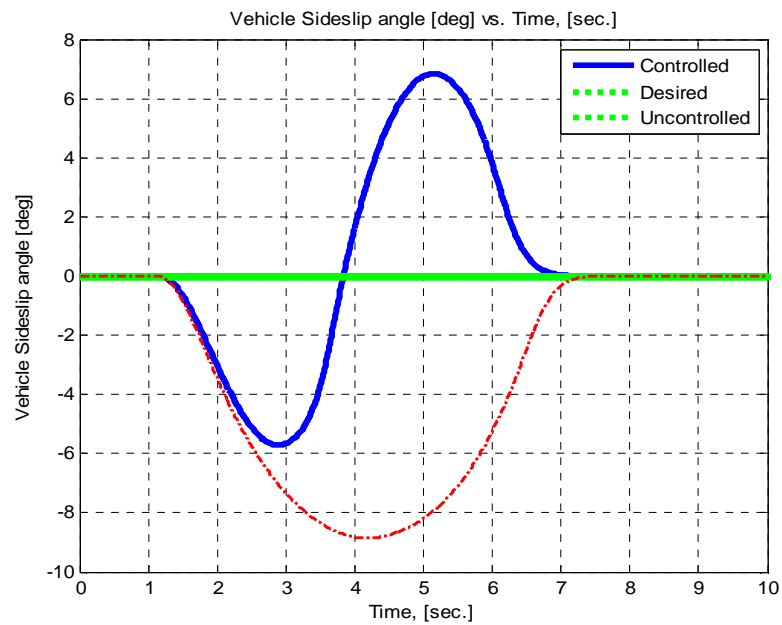
Fig. 5.70 Uncontrolled, des. and controlled vehicle sideslip angles [deg] vs. time[sec] for wet road conditions in a double lane change maneuver
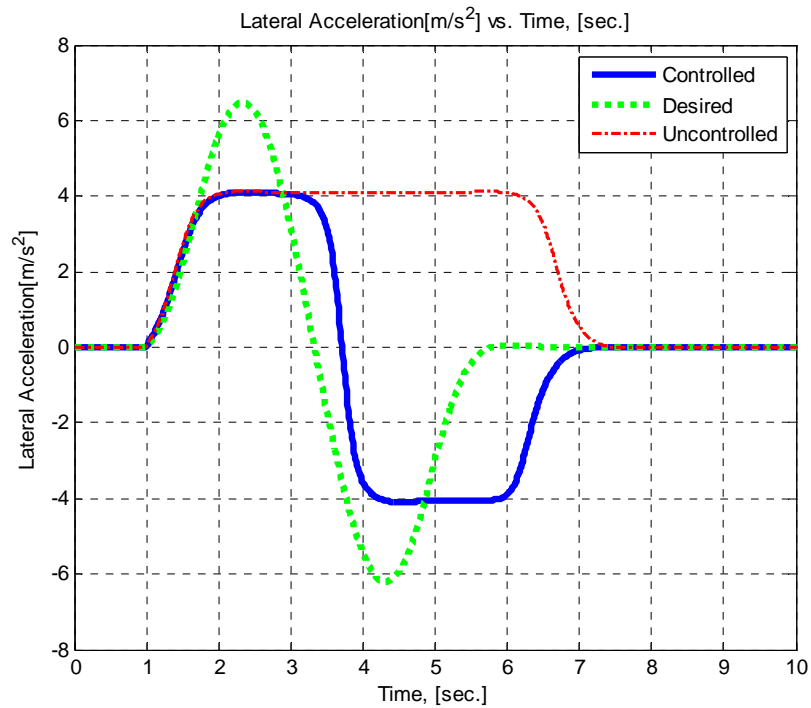
Fig. 5.71 Uncontrolled, desired, and controlled vehical lateral acceleration versus time for wet road conditions in a double lane change maneuver
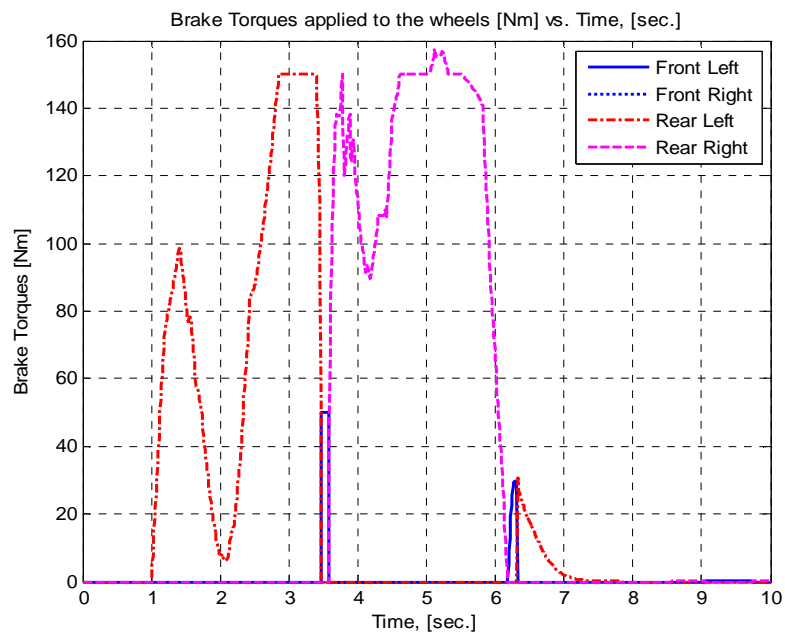
Fig. 5.72 Brake torques applied to the wheels for wet road conditions in a double lane change maneuver
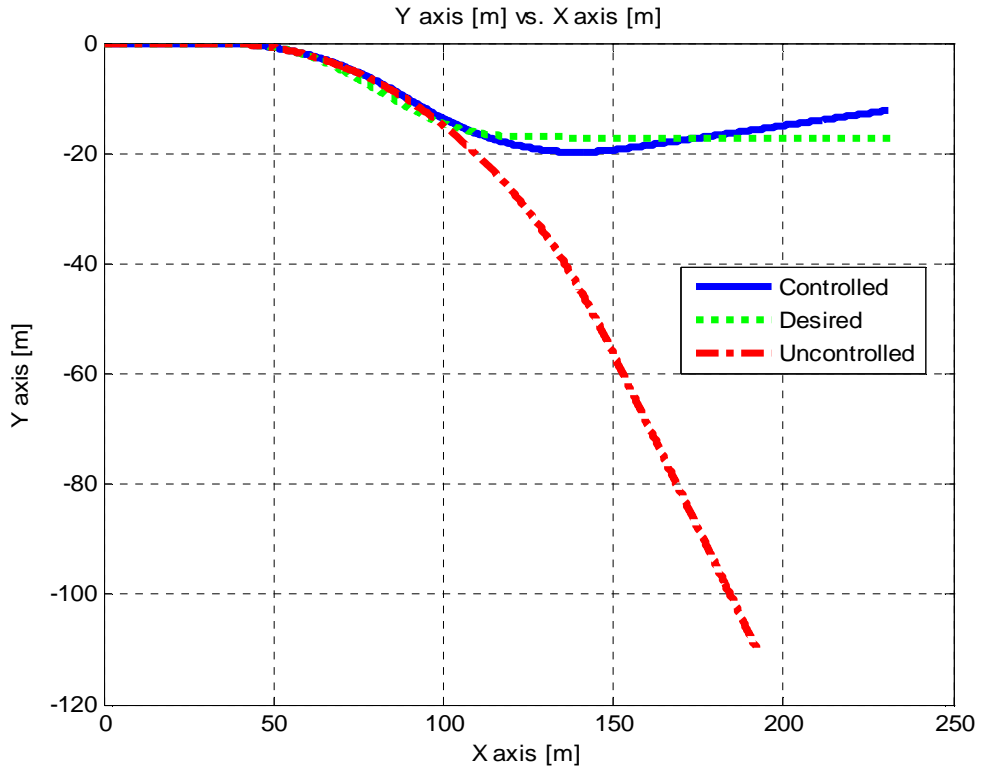
Fig. 5.73 Uncontrolled, desired, and controlled vehicle trajectories versus time] for wet road conditions in a double lane change maneuver

Fig. 5.73 presents the resulting trajectories. Easily observed, the vehicle is able to tag along with the desired course, with minor differences, which can be eliminated by small steering angle modifications.

For the last simulation of yaw controlled vehicle in a double lane change maneuver, icy road conditions with 50º steer angle J-turn maneuver is applied with an initial vehicle speed of 50 km/h and 0.1 road tire surface friction coefficient. Fig. 5.74 presents the uncontrolled, desired, and the controlled vehicle yaw rates versus time graph and Fig. 5.75 presents the sideslip angles versus time. The yaw rate tracking capacity has been lowered while the overall vehicle sideslip limits have been preserved. The yaw rate tracking is slightly better than that of the uncontrolled vehicle.
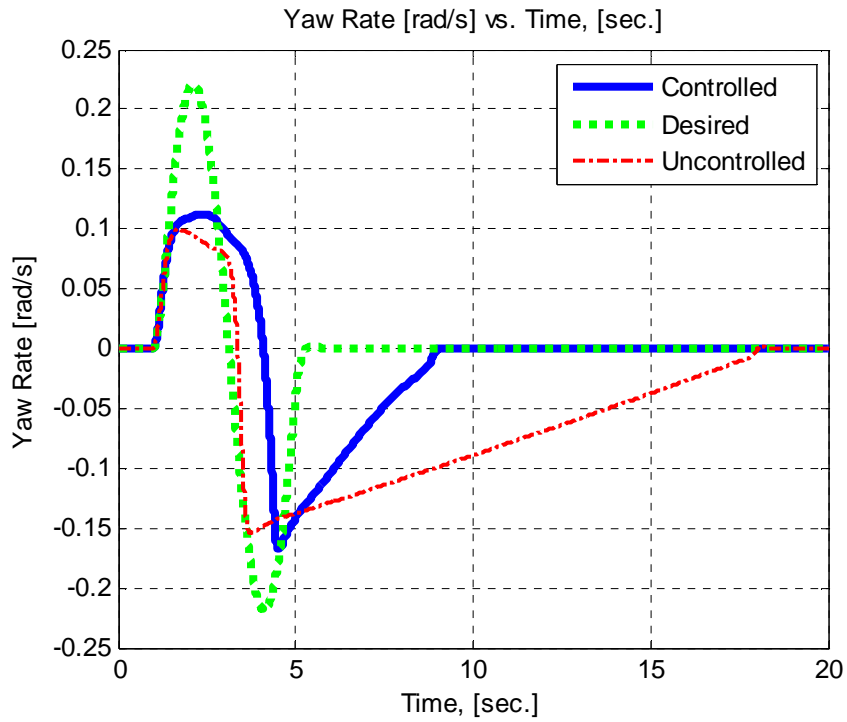
Fig. 5.74 Uncontrolled, desired, and controlled vehicle yaw rates versus time for icy road conditions in a double lane change maneuver
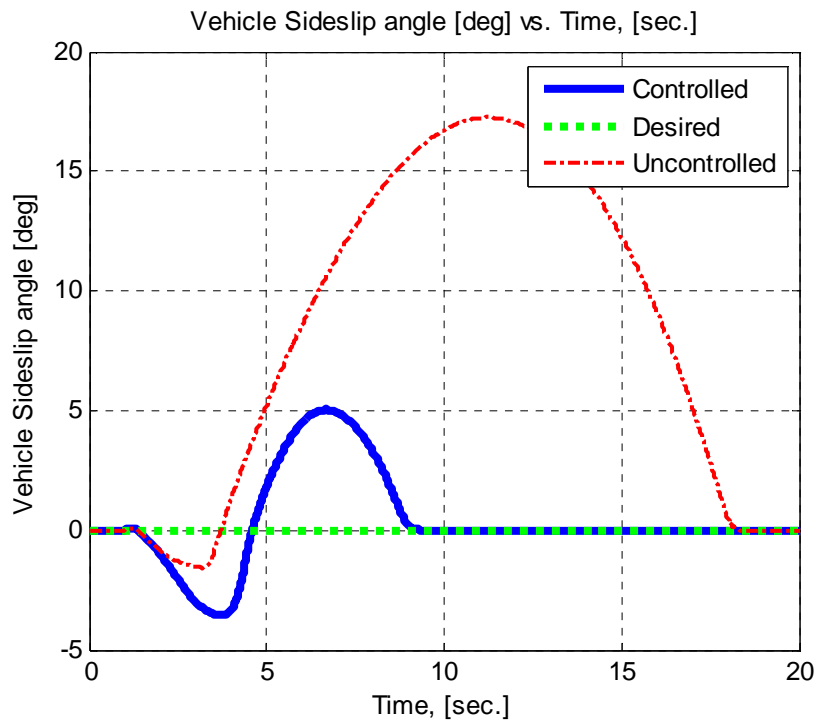
Fig. 5.75 Uncontrolled, desired, and controlled vehicle sideslip angles versus timefor icy road conditions in a double lane change maneuver
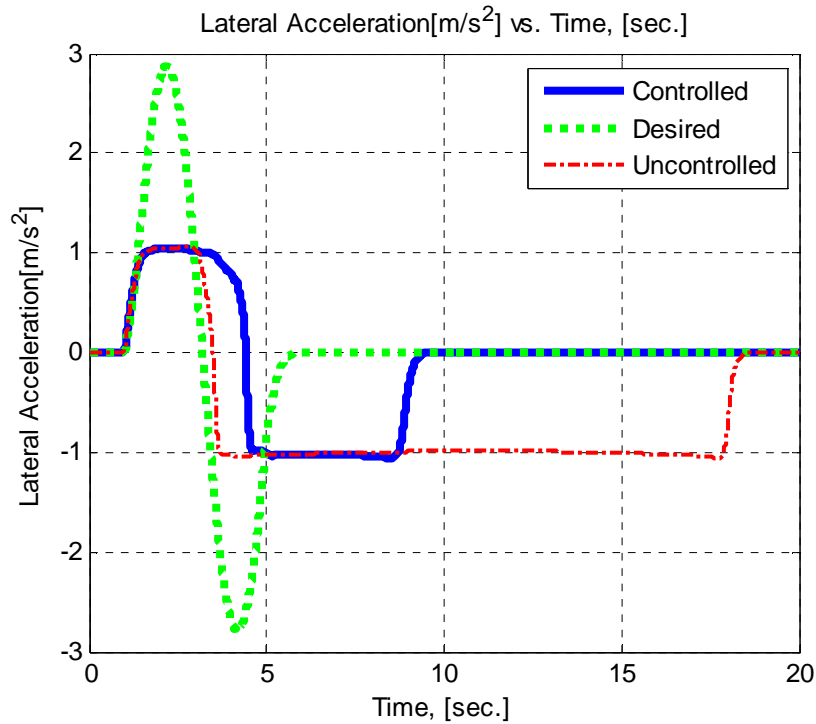
Fig. 5.76 Uncontrolled, desired, and controlled vehical lateral accelerations versus time or icy road conditions in a double lane change maneuver

Fig. 5.76 demonstrates the lateral accelerations of the vehicle. The limits of the traction have been reached by both the controlled and uncontrolled vehicle. However, the redistribution of the tire forces, that is manipulating them in order to rearrange the lateral acceleration have led the vehicle to pursue the yaw rate and (although not controlled) vehicle sideslip angle in a more efficient way. Fig. 5.77 shows the manipulated brake torques and Fig. 5.78 presents the resulting trajectories. The trajectory manner, which is the subsequent curvatures of the trajectories, of the controlled vehicle resembles that of the desired vehicle trajectory. The yaw angle difference between desired and obtained at the end of the road is a result of uneven yaw rate change of the obtained vehicle behavior. However, as mentioned before, this problem can actually be eliminated by replacing the pre-defined steer input with real life minor interruption of an average driver [11].
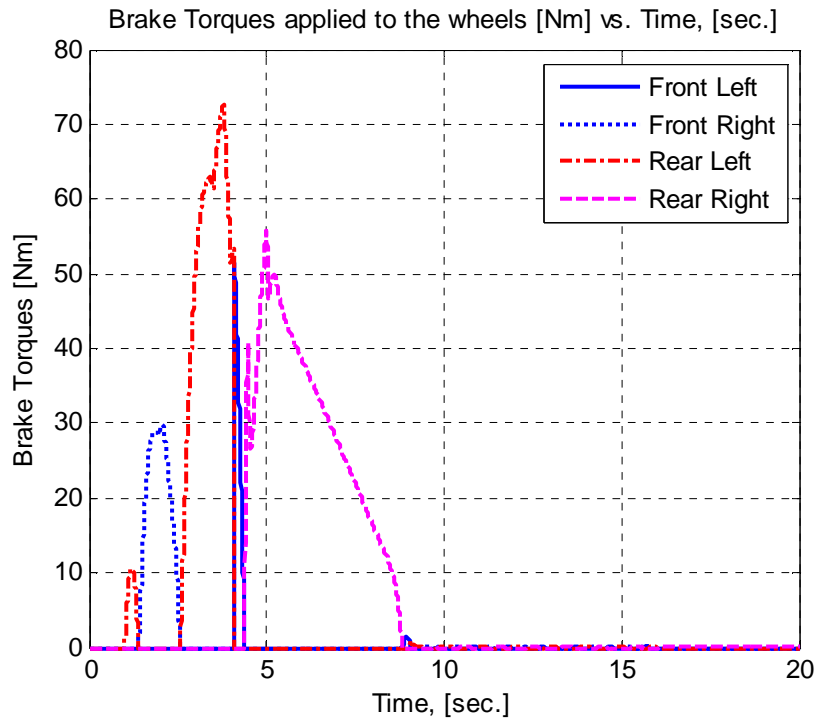
Fig. 5.77 Brake Torques applied to the wheels for icy road conditions in a double
lane change maneuver
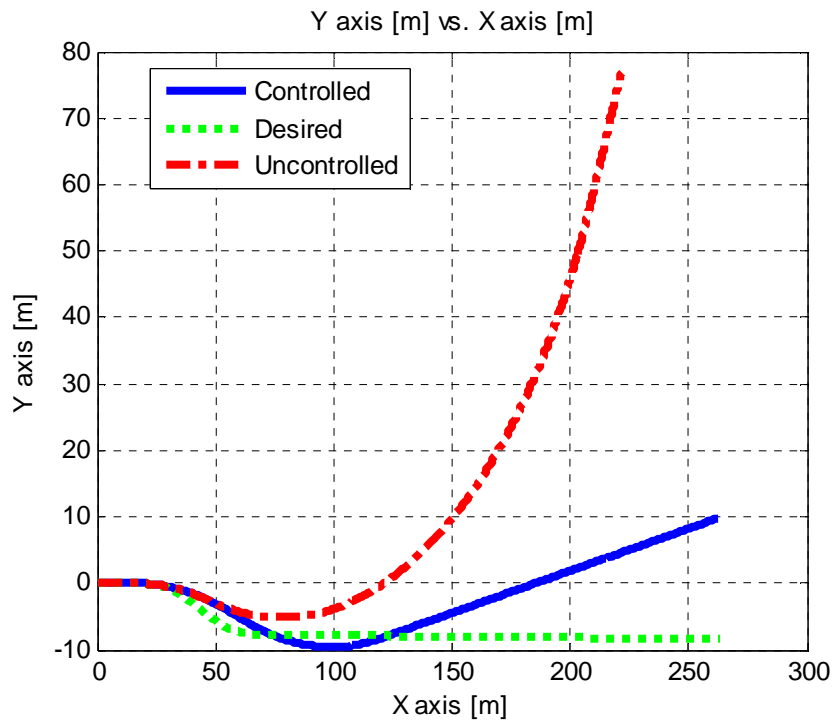
Fig. 5.78 Uncontrolled, desired, and controlled vehicle trajectories versus time for
icy road conditions in a double lane change maneuver

117

5.4 VEHICLE SIMULATION RESULTS WITH ACTIVE YAW CONTROL SYSTEM TOGETHER WITH SIDESLIP ANGLE LIMITATION

Up to this point, yaw controlled behavior of the simulated vehicle has been presented and discussed. In this section, the yaw controlled vehicle with sideslip angle limitation will be presented. The sideslip angle estimation for this purpose has been presented earlier in the "Estimated States" section in Chapter 3. This estimation scheme will be used in this section. The yaw controller with sideslip angle limitation takes the estimated sideslip angle into account and tries to limit it within some specified boundaries, which differs for different road types. The main reason behind this modification of the original yaw controller is the need for controlling sideslip angle while keeping the yaw rate error in acceptable values.

The input maneuvers taken into account for this section will be the same as the former simulation maneuvers. After obtaining the results for a particular maneuver and road condition, a comparison will be conducted to evaluate the designed and modified controller performance. The comparison with figures will include desired, uncontrolled, only-yaw controlled, and yaw controlled with sideslip limitation behaviors. After each simulation, the results will be discussed in detail.

5.4.1   CASE 1: J-TURN MANEUVER

A J-turn maneuver has been examined in this part of the study. The main aim of this maneuver is to maintain a constant turning radius during a sharp turn. The input parameters are kept same as in section 5.2.1. Initial vehicle velocity is taken as 90 km/h while the road surface friction coefficient is taken as 0.9 and the maximum level of the steer input is taken as 90 degrees. The steering wheel ratio is 1/18; therefore the front wheels are turned by 5 degrees. Fig. 5.79 demonstrates the uncontrolled, desired, and the controlled vehicle yaw rates versus time graph. Fig. 5.80 presents the corresponding vehicle sideslip angles versus time graph.

As can be seen from the graphs, the overall yaw rate tracking capability is reduced for the yaw rate controller with sideslip limitation. The desired yaw rate reaches its

maximum at about the 2nd second by 0.6 rad/s. The yaw controlled vehicle without any sideslip limitation follows this desired yaw rate pattern successfully as mentioned before. However, the yaw rate controlled vehicle with sideslip limitation can only achieve 0.5 rad/s and remains at about %70 value of the desired yaw rate. On the other hand, the sideslip angle goes to about 20 degrees for only-yaw controlled vehicle. This value surpasses acceptable limits of the vehicle sideslip angle for steerability. Although, the desired yaw rate is not obtained with a negligible error, the steerability of the vehicle is assured and this situation can be regarded as a successful compromise. A similar J-Turn maneuver with a vehicle model showing more understeer characteristics, similar yaw rate tracking and vehicle sideslip angle limitation performance have been observed in the study of Boada [13]. The desired yaw rate has been very low, to be more precisely speaking about 0.3 rad/s of peak value for that study. The vehicle sideslip angle has reached to about 6 degrees with this yaw rate demand, which is comparable with the high yaw rate obtained in this study and corresponding sideslip angle.

Fig. 5.81 demonstrates the corresponding lateral accelerations of the simulated vehicles versus time. When examined, this graph shows that the lateral acceleration is narrowly limited to obtain the desired vehicle behavior. On the contrary, lateral acceleration can be adjusted and tire forces can be redistributed in order to assure vehicle steerability and yaw rate tracking in an acceptable manner. Here, the uncontrolled, only-yaw controlled, and yaw controlled with sideslip limitation vehicles all experience nearly the same lateral acceleration. However, the yaw rate and sideslip angles obtained for these controllers are totally different.

Fig. 5.82 presents the corresponding individual brake torques and Fig. 5.83 presents the resulting trajectory. Here, the trajectories for controlled and uncontrolled vehicle remain nearly the same. The main reason behind this outcome is again the lateral accelerations, which, in all three cases, reached its limits during the motion of the vehicle.

119
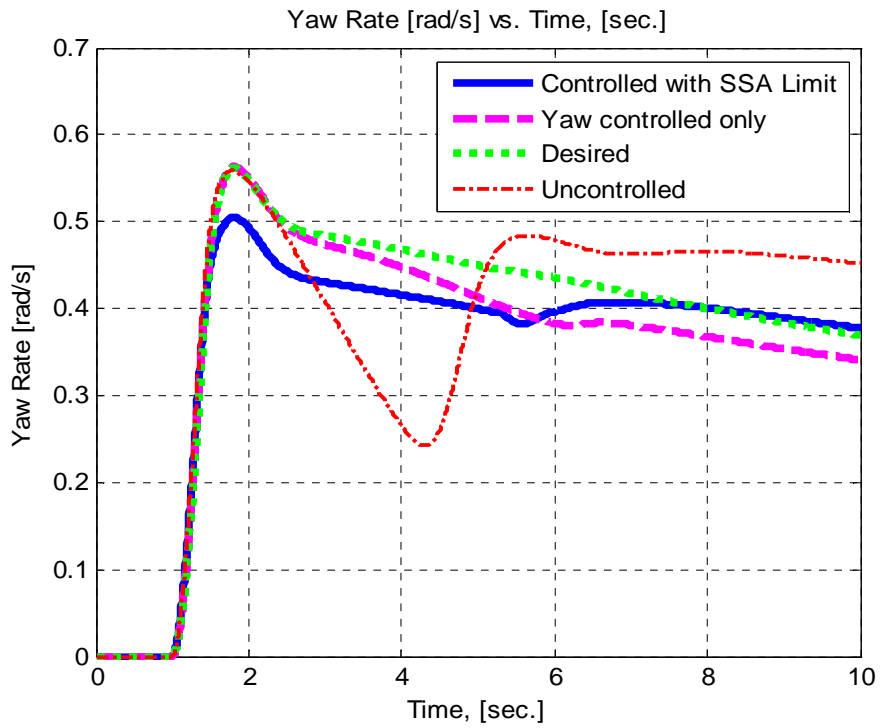
Fig. 5.79 Uncontrolled, desired and controlled vehicle yaw rates [rad/s] vs. time[sec]
in a J-Turn maneuver
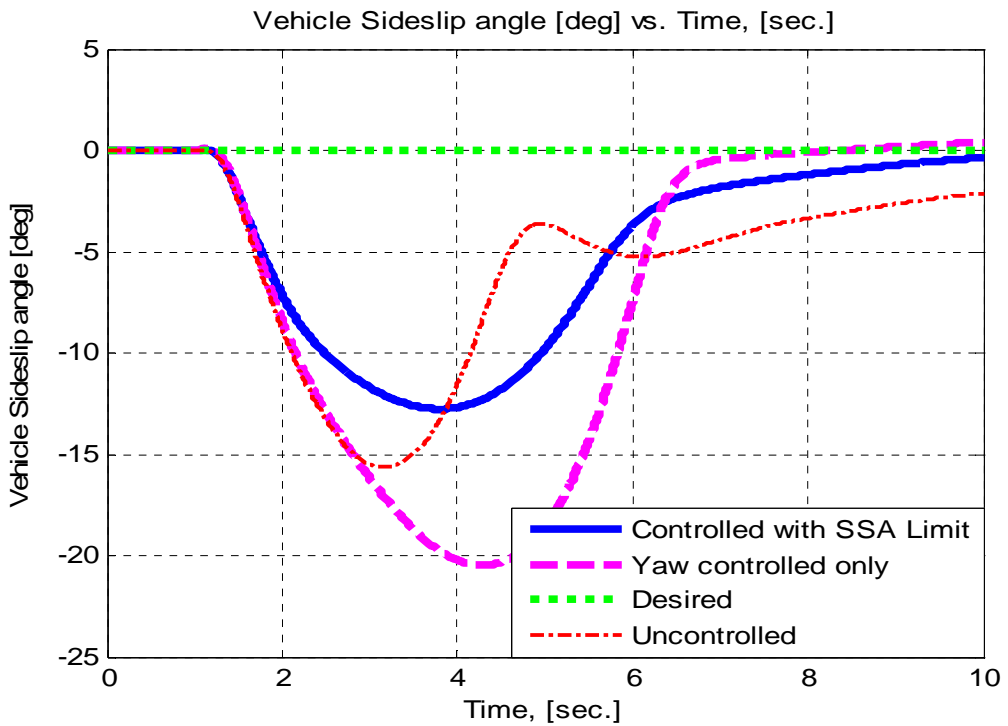
Fig. 5.80 Uncontrolled, desired and controlled vehicle sideslip angles versus time in

a J-Turn maneuver

120
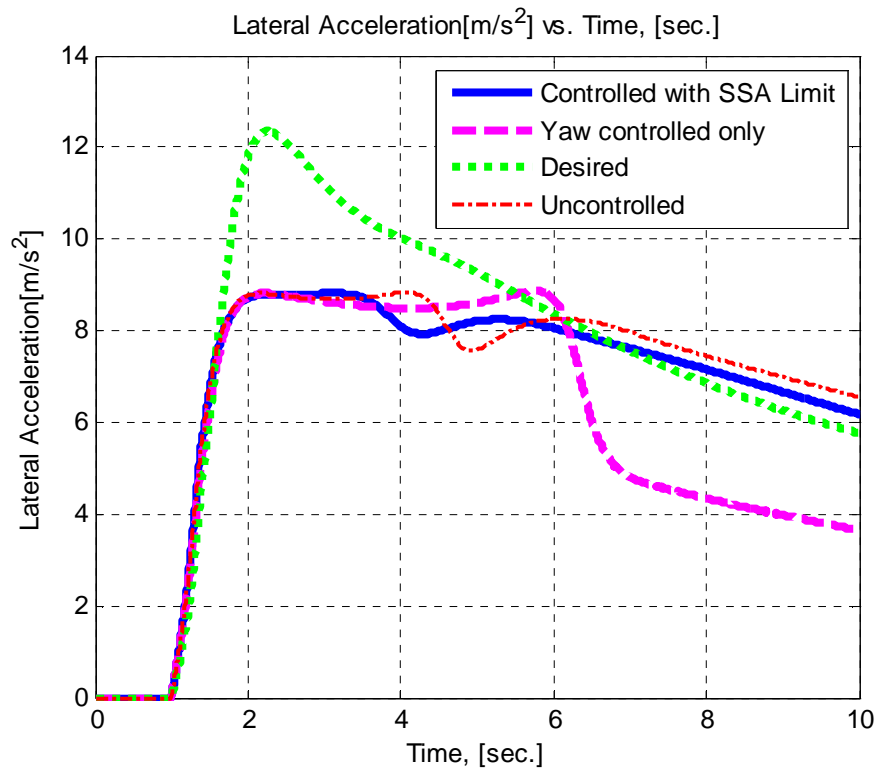
Fig. 5.81 Uncontrolled, desired and controlled vehicle lateral accelerations versus
time in a J-Turn maneuver
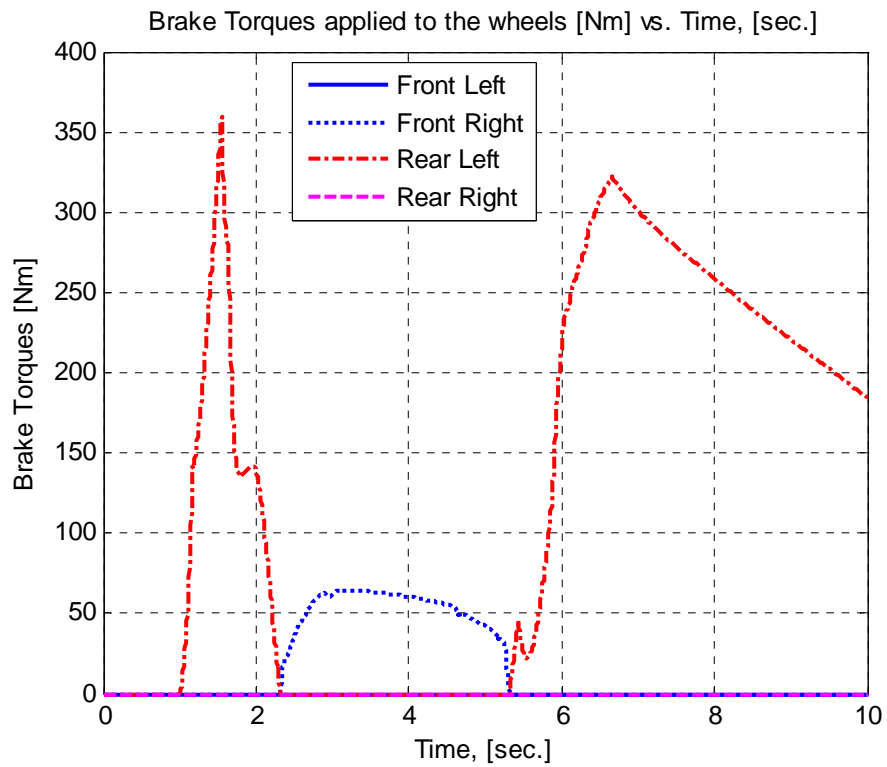
Fig. 5.82 Brake Torques applied to the wheels in a J-Turn maneuver

121
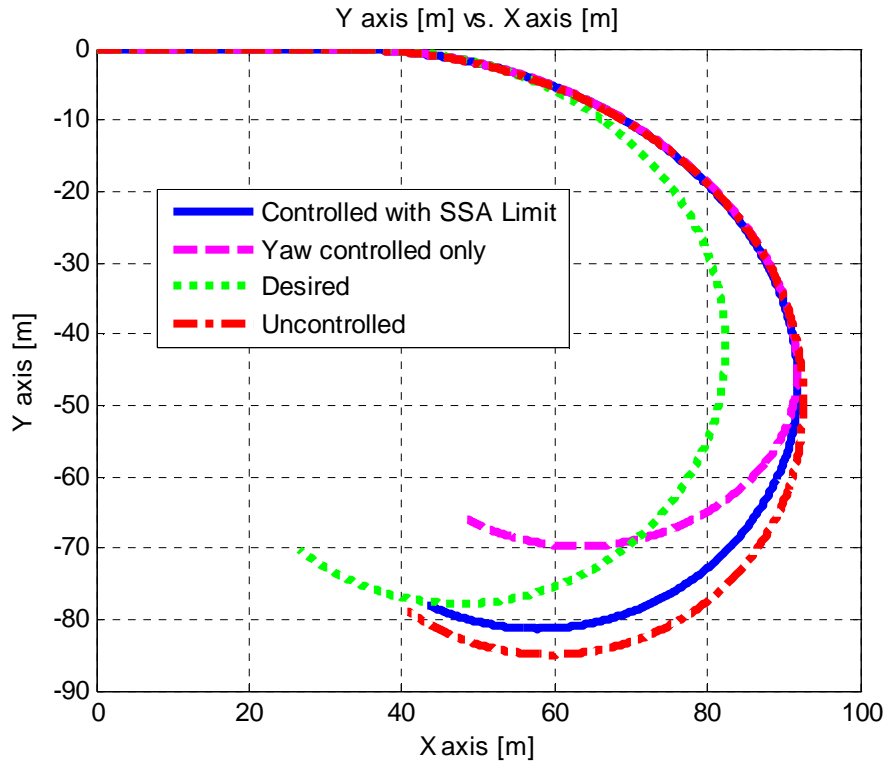
Fig. 5.83 Uncontrolled, desired and controlled vehicle trajectories in a J-Turn maneuver

The next simulation is for wet asphalt road conditions, where 50º steer angle J-turn maneuver is applied again with an initial vehicle speed of 90 km/h and 0.4 road tire surface friction coefficient. Fig. 5.84 shows the uncontrolled, desired, and the controlled vehicle yaw rates versus time graph and Fig. 5.85 presents the corresponding vehicle sideslip angles versus time graph. As in the former case, the yaw rate controller without any sideslip angle limitation performed almost flawless considering the desired yaw rate. However, the vehicle sideslip angle increases then almost linearly passing the steerability limit of the vehicle defined for wet road conditions, which is about 4 degrees, as mentioned before. The second controller with sideslip angle limitation has performed poorly considering the desired yaw rate. However, the vehicle sideslip angle is limited in steerability range, allowing the driver to stabilize the vehicle correspondingly. Although the yaw rate obtained is not very satisfactory, reached value is also challenging considering real life application with this road conditions.

Fig. 5.86 demonstrates the corresponding lateral accelerations of the simulated vehicles versus time. Yet again, the lateral acceleration is limited to a certain value, which is far below the requested lateral acceleration for desired vehicle behavior. However, with the obtainable tire forces, the stabilization of the vehicle is achieved while responsiveness to steering input is conserved.

Fig. 5.87 presents the corresponding individual brake torques and Fig. 5.88 presents the resulting trajectory. Here, the trajectories for controlled and uncontrolled vehicle remain again nearly the same. The main reason behind this outcome is as before, the lateral accelerations, which, in all three cases, reached its limits during the motion of the vehicle.
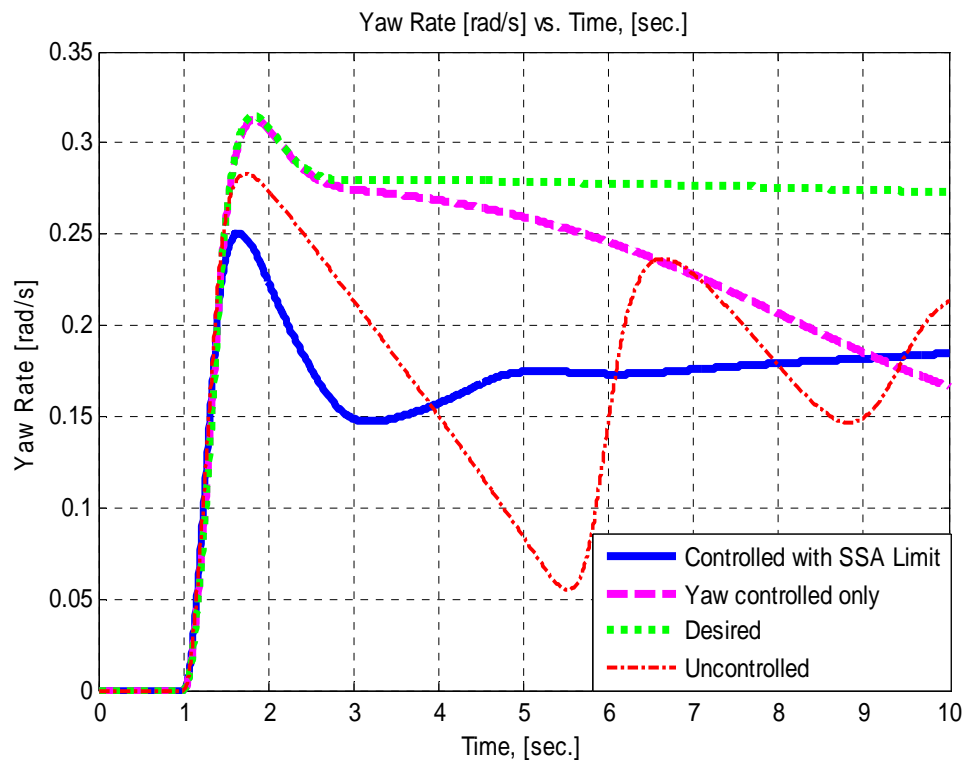
Fig. 5.84 Uncontrolled, desired and controlled vehicle yaw rates versus time for wet conditions in a J-Turn maneuver
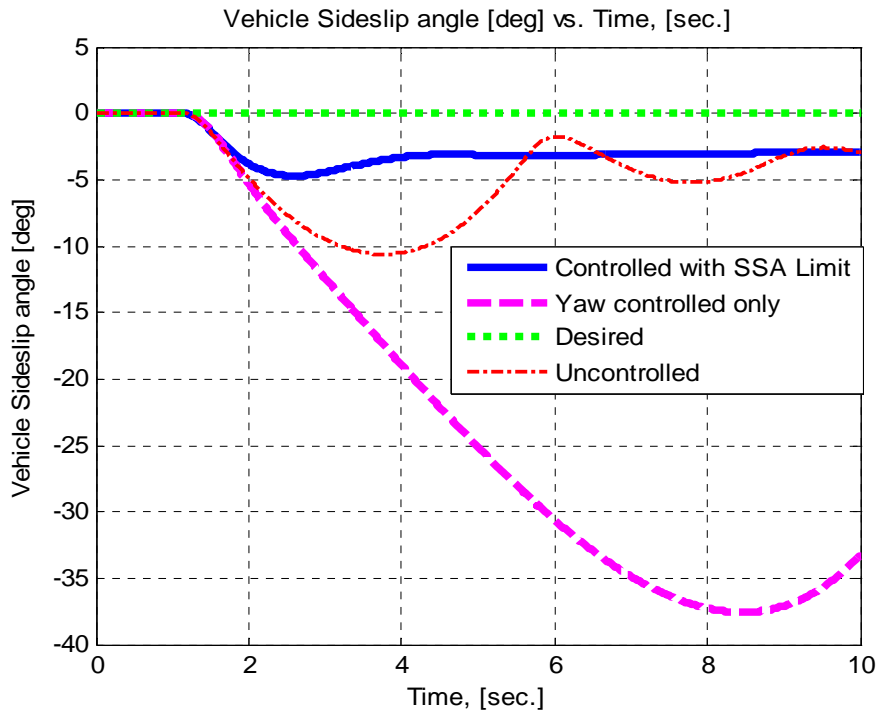
Fig. 5.85 Uncontrolled, desired and controlled vehicle sideslip angles versus time for wet conditions in a J-Turn maneuver
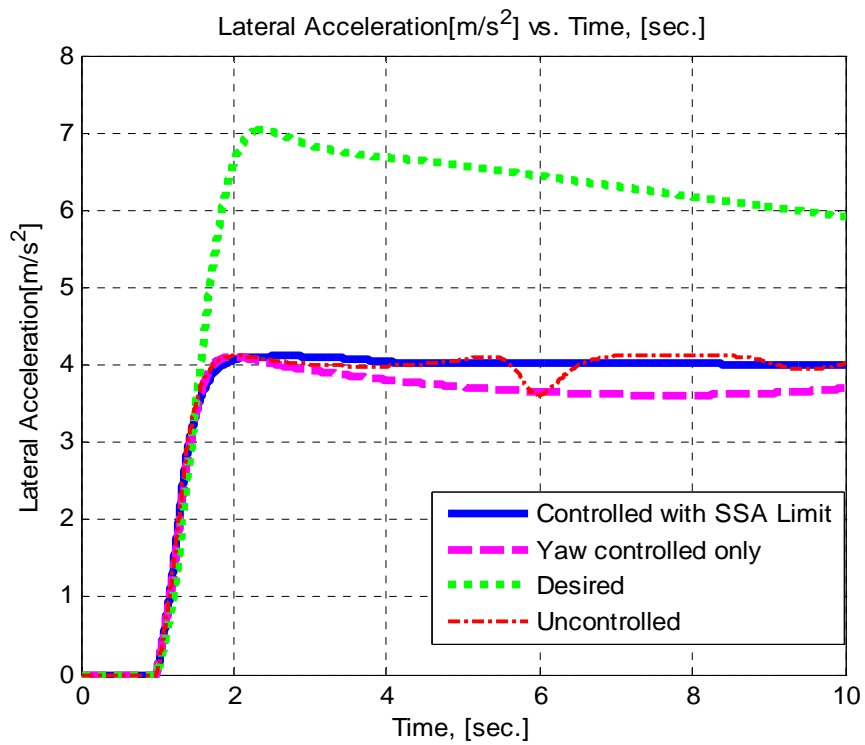
Fig. 5.86 Uncontrolled, desired and controlled vehicle lateral accelerations [rad/s] vs. time [sec] for wet conditions in a J-Turn maneuver

124
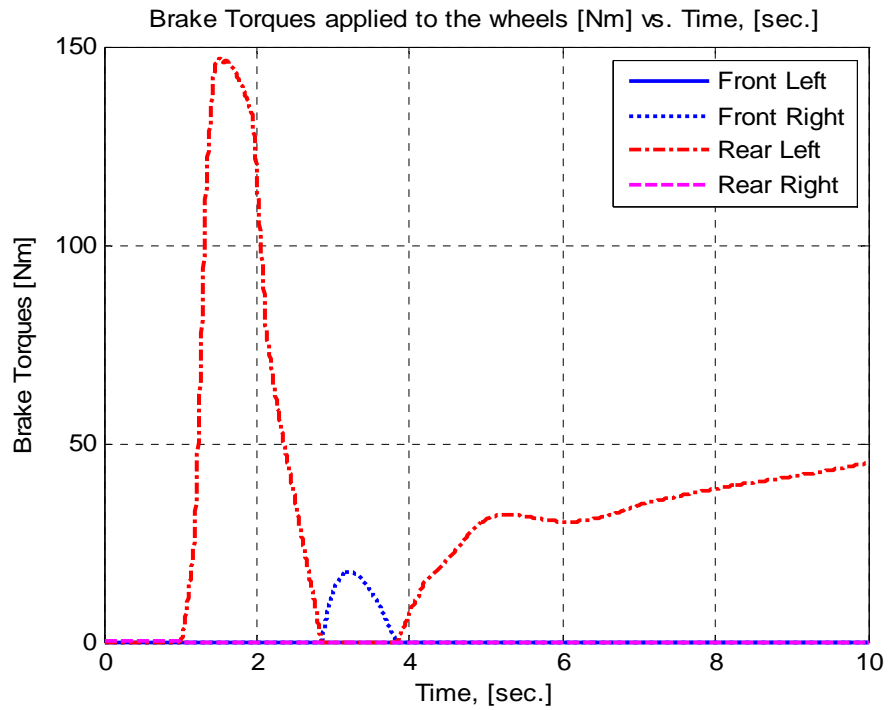
Fig. 5.87 Brake torques applied to the wheels for wet conditions in a J-Turn
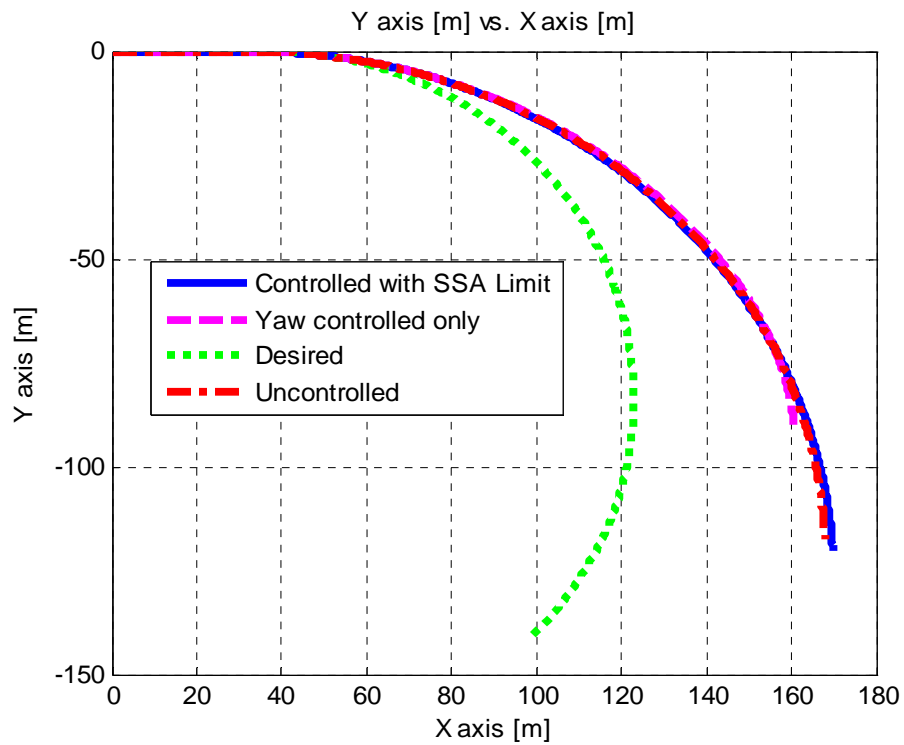
maneuver

Fig. 5.88 Uncontrolled, desired and controlled vehicle trajectories for wet conditions

in a J-Turn maneuver

125

For the last simulation of yaw controlled vehicle with sideslip angle limitation, icy road conditions with 40º steer angle J-turn maneuver is applied with an initial vehicle speed of 40 km/h and 0.1 road tire surface friction coefficient. Fig. 5.89 presents the uncontrolled, desired, and the controlled vehicle yaw rates versus time graph and Fig. 5.90 presents the corresponding vehicle sideslip angles versus time graph. Differing from the former cases, the only-yaw controlled vehicle performs relatively substandard comparing with dry and wet road conditions. However, it is still better than uncontrolled and yaw controlled vehicle with sideslip limitation. On the contrary, the sideslip angle of the only-yaw controlled vehicle increases rapidly exceeding the corresponding icy road vehicle sideslip angle limit for steerability. To compare, the yaw controlled vehicle with sideslip limitation could preserve its steerability limit by remaining in ± 1degrees. Note that, the uncontrolled and controlled vehicle with sideslip limitation has a similar behavior considering yaw rate and sideslip angle. However, the sideslip angle of the uncontrolled vehicle is about 1 degree which is at the limit while the controlled vehicle reaches only 0.5 degrees, which is half way to the limit. Therefore, the proposed controller has succeeded to hold the vehicle in desired conditions.
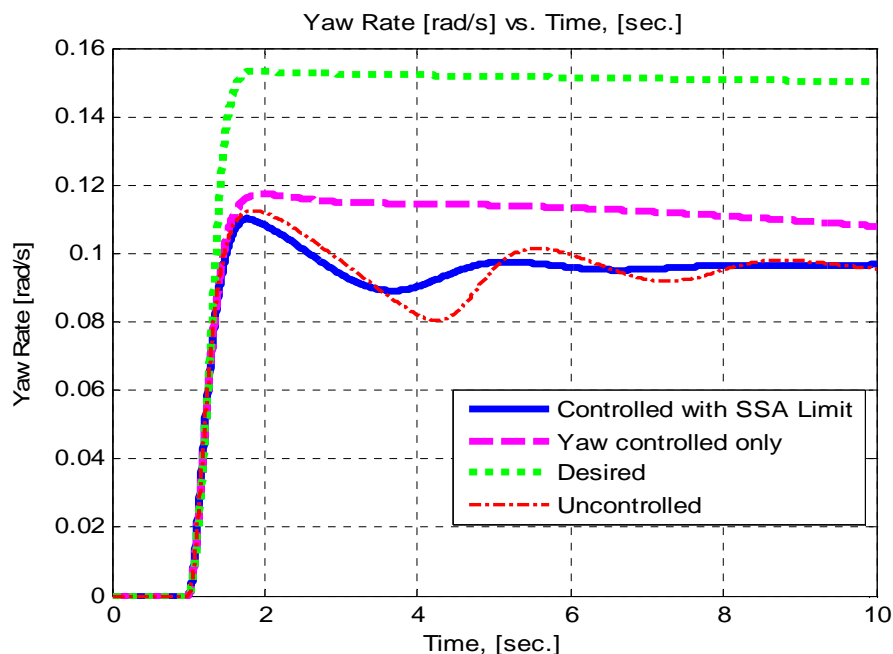

Fig. 5.89 Uncontrolled, desired and controlled vehicle yaw rates versus time for icy conditions in a J-Turn maneuver

126
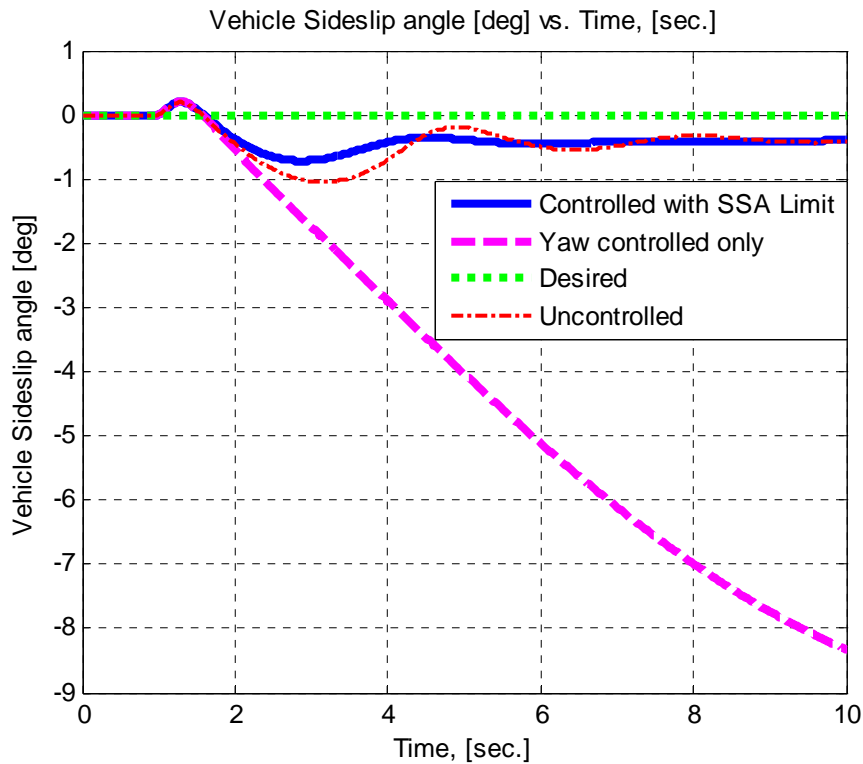
Fig. 5.90 Uncontrolled, desired and controlled vehicle sideslip angles [rad/s] vs. time [sec] for icy conditions in a J-Turn maneuver

The obtained yaw rate and sideslip angles are comparable with those which Esmailzadeh et. al. [19] has obtained in their study. On a snow covered road with similar configuration and vehicle parameters, the achieved peak yaw rate is about 0.1 rad/s while the obtained maximum sideslip angle is about 1 degree. The design presented in this presented study seems to perform better while compared with Esmailzadeh et. al.'s results when these two parameters are compared, but extensive simulations should be held in order to compare with enough accuracy.

Fig. 5.91 demonstrates the corresponding lateral accelerations of the simulated vehicles vs. time. Yet again, the lateral acceleration is limited with about 1 m/s^2, which is the physical limit for the specified icy road case. This value is far below the requested lateral acceleration for desired vehicle behavior. Still, the sideslip angle limitation can be achieved with this limited lateral force affecting the vehicle.
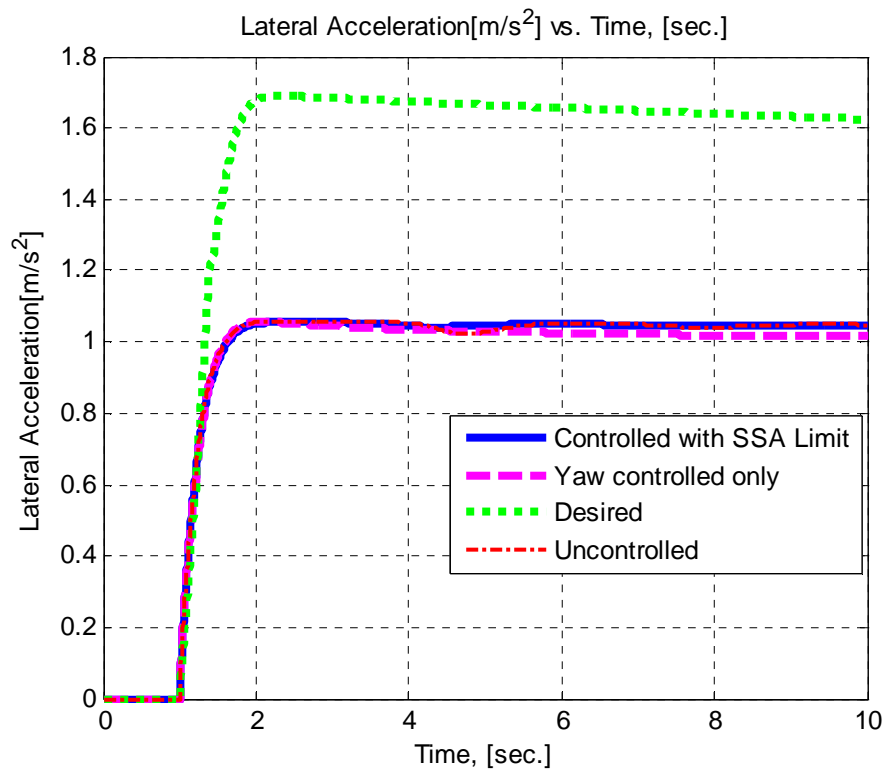
Fig. 5.91 Uncontrolled, desired and controlled vehicle lateral accelerations [rad/s] vs. time [sec] for icy conditions in a J-Turn maneuver

Fig. 5.92 presents the corresponding individual brake torques and Fig. 5.93 presents the resulting trajectory. Note that, the brake torque is only applied to rear left tire, which is enough to create necessary yaw moment to stabilize the vehicle. Here, the trajectory for controlled and uncontrolled vehicle remains again nearly the same. The main reason behind this outcome is as before, the lateral accelerations, which, in all three cases, reached its limits during the motion of the vehicle.
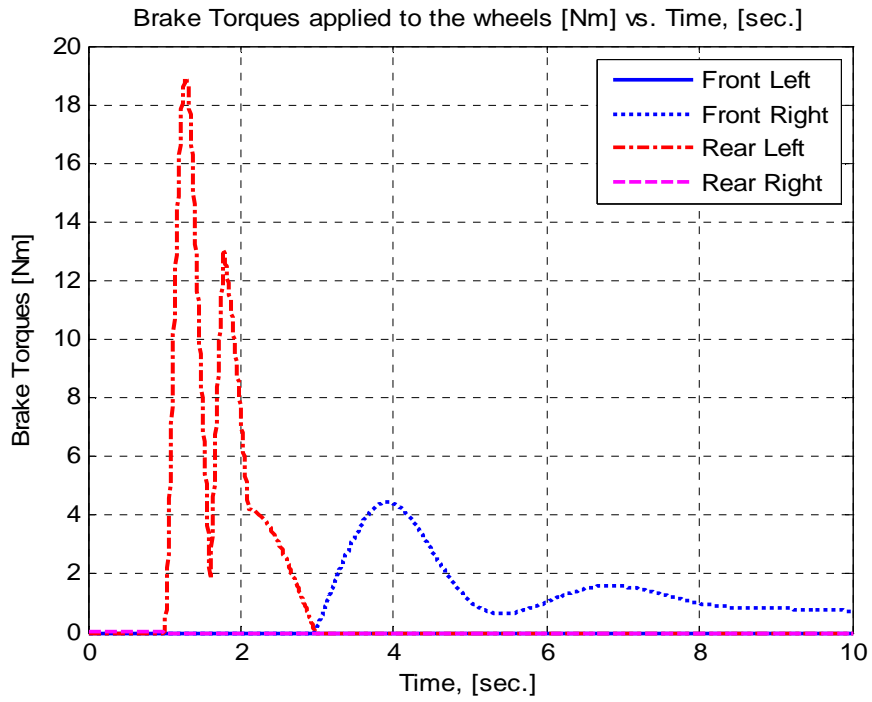
Fig. 5.92 Brake Torques applied to the wheels [Nm] for icy conditions in a J-Turn
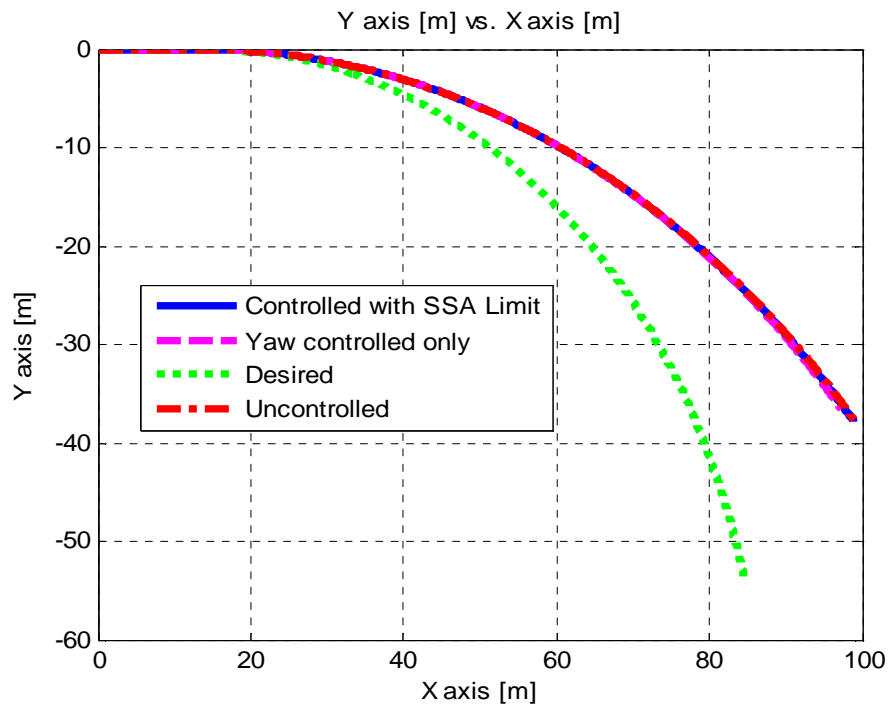
maneuver

Fig. 5.93 Uncontrolled, desired and controlled vehicle trajectories for icy conditions

in a J-Turn maneuver

5.4.2   CASE 2: DOUBLE LANE CHANGE MANEUVER

A double lane change maneuver has been examined in this part of the simulation. The input parameters are kept same as in section 5.2.2. Initial vehicle velocity is taken as 90 km/h while the road surface friction coefficient is taken as 0.9 and the maximum level of the steer input is taken as 90 degrees. The steering wheel ratio is 1/18; therefore the front wheels are turned by 5 degrees. The simulation time is taken as 10 seconds for clarity and conformity with the previous double lane simulations. Fig. 5.94 demonstrates the uncontrolled, desired and the controlled vehicle yaw rates vs. time graph and Fig. 5.95 presents the consequent vehicle sideslip angle variation vs. time graph. The desired yaw rate reaches a value of about 0.55 rad/s whereas the desired sideslip angle is set to zero.
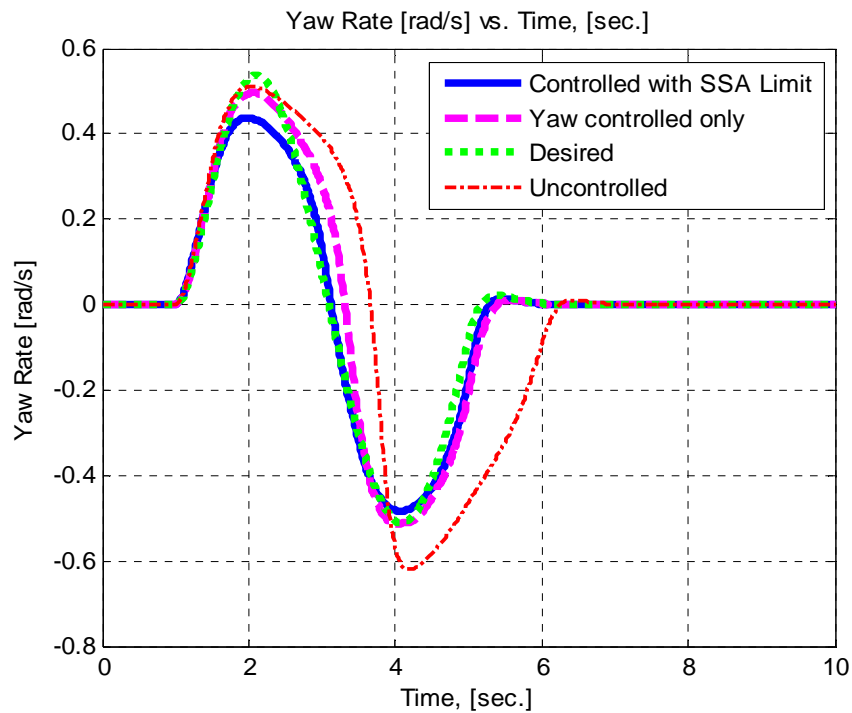
Fig. 5.94 Uncontrolled, desired and controlled vehicle yaw rates [rad/s] vs. time[sec] in double lane change man.
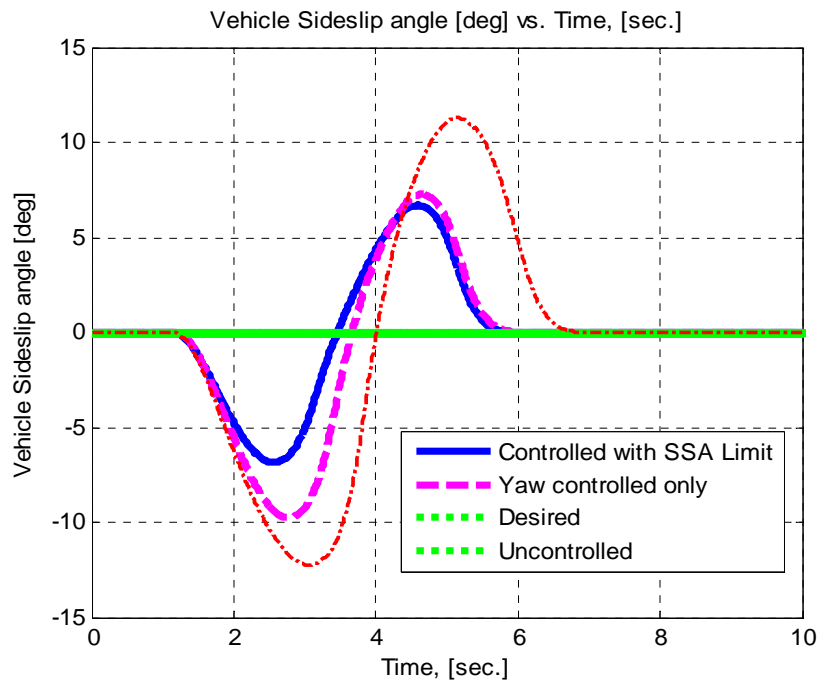
Fig. 5.95 Uncontrolled, desired and controlled vehicle sideslip angles [rad/s] vs. time [sec] in double lane change man.

When the graphs are inspected, the controlled yaw rates have a major compliance with the desired yaw rate variation. The controlled yaw rate without sideslip angle limitation has a slightly better fit with desired yaw rate. On the other hand, controlled sideslip angles have more difference than that in the yaw rates section. The yaw controlled vehicle with sideslip limitation has better sideslip angle characteristics. To clarify, obtained results may be compared with those of Boada et. al [13] and Mokhiamar et. al. [21], which are simulated under similar simulation parameters and conditions. The former paper has utilized the same concept for control, namely fuzzy logic independent brake control while the latter study utilizes both direct yaw control and active steering to achieve these tracking and stability objectives. The former study uses the most understeer characterized vehicle data and obtained 0.2 rad/s with about 3 degrees of sideslip angle. The latter study presents the same maneuver with 50 degrees steering wheel angle variation, obtaining 0.35 rad/s with 5 degrees sideslip angle. Thus, the proposed controller has shown a comparable performance with these studies.

131

Fig. 5.96 demonstrates the corresponding lateral accelerations of the simulated vehicles vs. time. When examined, this graph shows that the lateral acceleration is narrowly limited for the uncontrolled and controlled vehicles to obtain the desired vehicle behavior. Here, the uncontrolled, only-yaw controlled and yaw controlled with sideslip limitation vehicle all experience nearly the same lateral acceleration with some minor variations. On the other hand, the obtained sideslip angles, which are especially sensitive for vehicle stability, differ with significant differences. On the other hand, the obtained sideslip angles, which are especially sensitive for vehicle stability, differ with significant differences. To clarify, obtained results may be compared with those of Boada et. al [13] and Mokhiamar et. al. [21]. The former paper has utilized the same concept for control, namely fuzzy logic independent brake control while the latter study utilizes both direct yaw control and active steering to achieve these tracking and stability objectives. The former study uses the most understeer characterized vehicle data and obtained
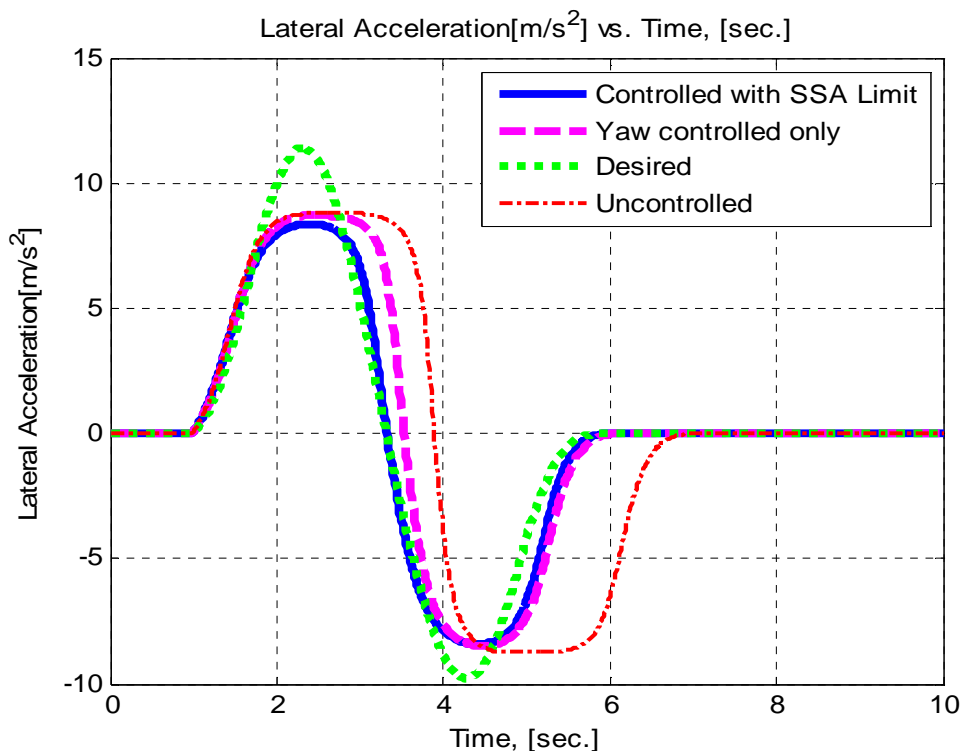

Fig. 5.96 Uncontrolled, desired and controlled vehicle lateral accelerations [rad/s] vs. time[sec] in double lane change man.

Fig. 5.97 presents the brake torques applied during the control of the vehicle and Fig. 5.98 illustrates the resulting trajectories for uncontrolled, desired and controlled vehicles. The trajectory followed by the driver with the yaw controller with sideslip limitation has a slight oversteer behavior compared to only-yaw controlled and desired vehicle trajectory. Since the vehicle has been limited to a shorter course, the driver may modify his/her steering input by decreasing the steering angle wheel in magnitude so that the controlled vehicle behavior can conform to the desired behavior. On the other hand, the only-yaw controlled vehicle has passed the desired trajectory in the y axis, meaning that the driver has to command larger steering wheel angles, so that the desired vehicle track can e obtained. On the other hand, when the steering angle is increased in magnitude, there may occur some stability problems like oversteering or unacceptable sideslip angle values. Therefore, the trajectory obtained with the yaw controller with sideslip angle limitation is superior to that of the only-yaw controlled vehicle.
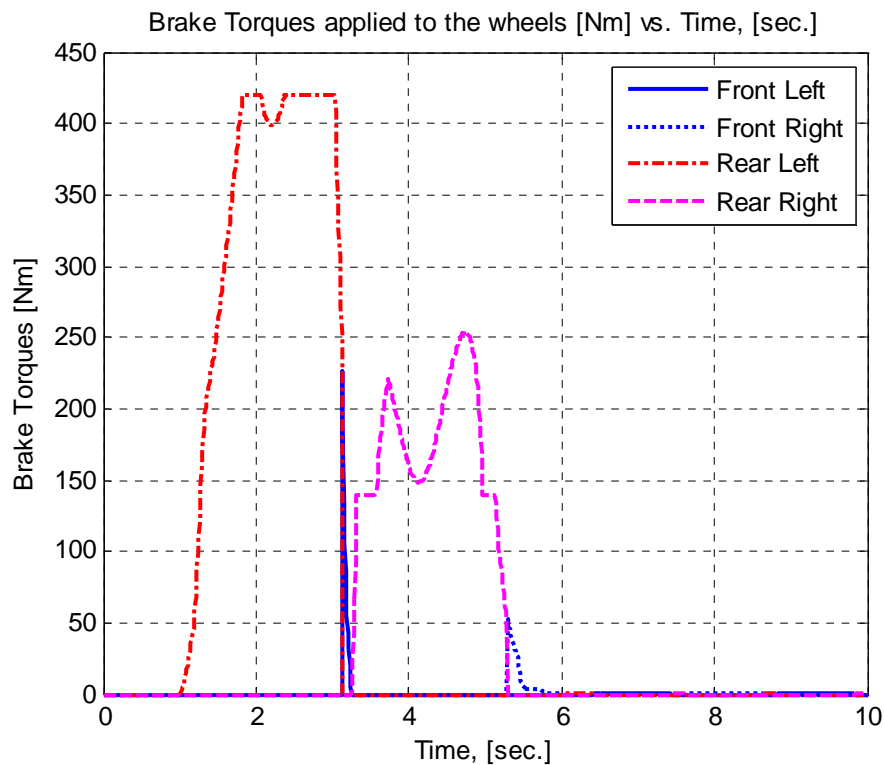
Fig. 5.97 Brake Torques applied to the wheels [Nm] in double lane change man.
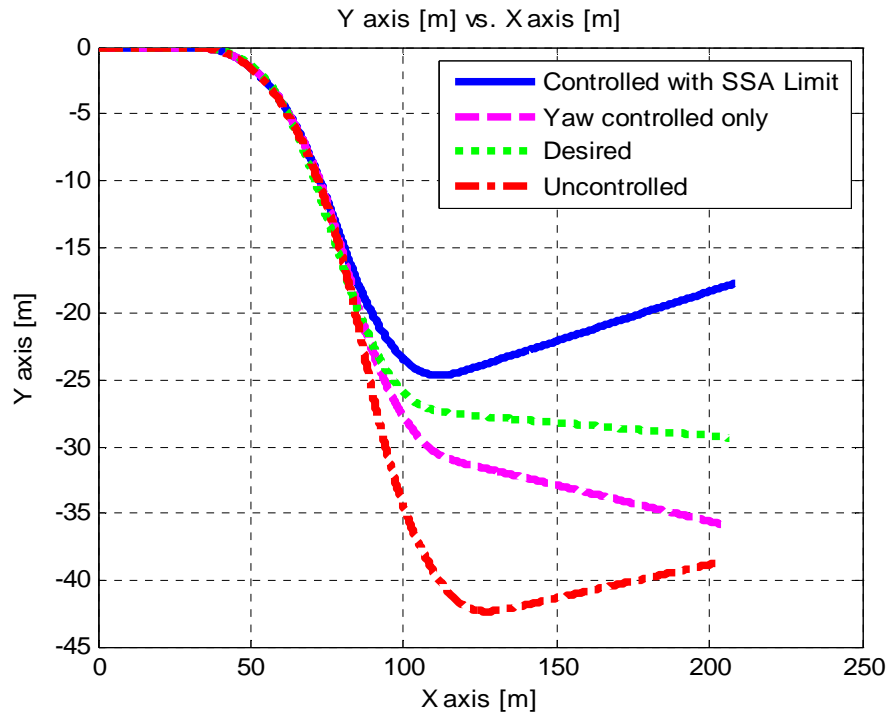
Fig. 5.98 Uncontrolled, desired and controlled vehicle trajectories in double lane change man.

The next simulation is for wet asphalt road conditions, where 50° steer angle double lane change maneuver is applied again with an initial vehicle speed of 90 km/h and 0.4 road tire surface friction coefficient. Fig. 5.99 shows the uncontrolled, desired and the controlled vehicle yaw rates vs. time graph and Fig. 5.100 presents the corresponding vehicle sideslip angles [deg] vs. time graph. As seen from the yaw rate graph, the desired yaw rate conformity is achieved for both only-yaw controlled and yaw controlled with sideslip limitation vehicles. The deviations from the desired yaw rate is about 0.1 rad/s for the latter controller, which is not crucially important since this can be eliminated by proper braking and steering manipulation that can be done by a novice driver. on the other hand, the sideslip angle is limited to about 5 degrees for the specified controller whereas this limit is pushed to 7 degrees for the only-yaw controlled vehicle. However, after all, both controlled vehicles could have tracked the steer angle variation qualitatively while the uncontrolled vehicle has failed to track.
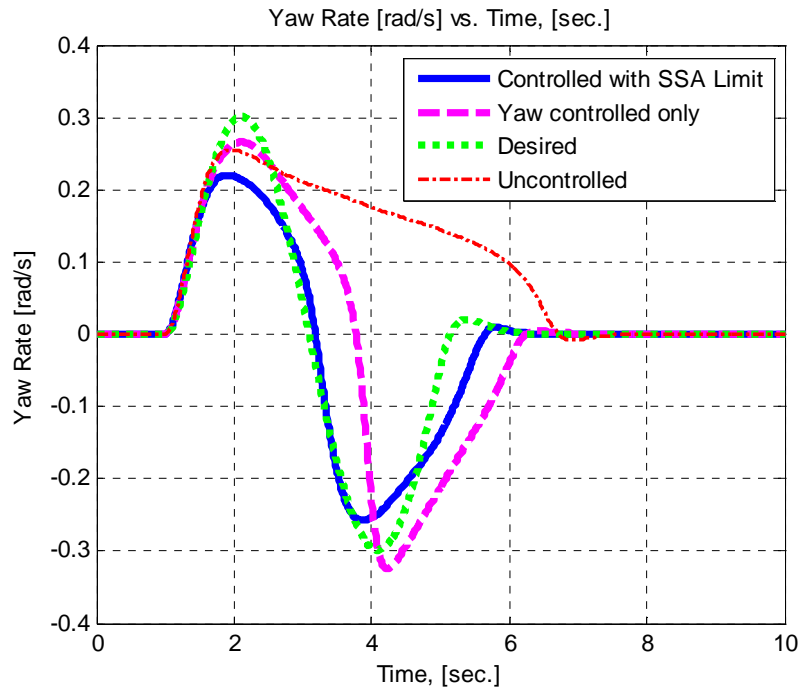
Fig. 5.99 Uncontrolled, desired and controlled vehicle yaw rates [rad/s] vs. time[sec] for wet conditions in double lane change man.
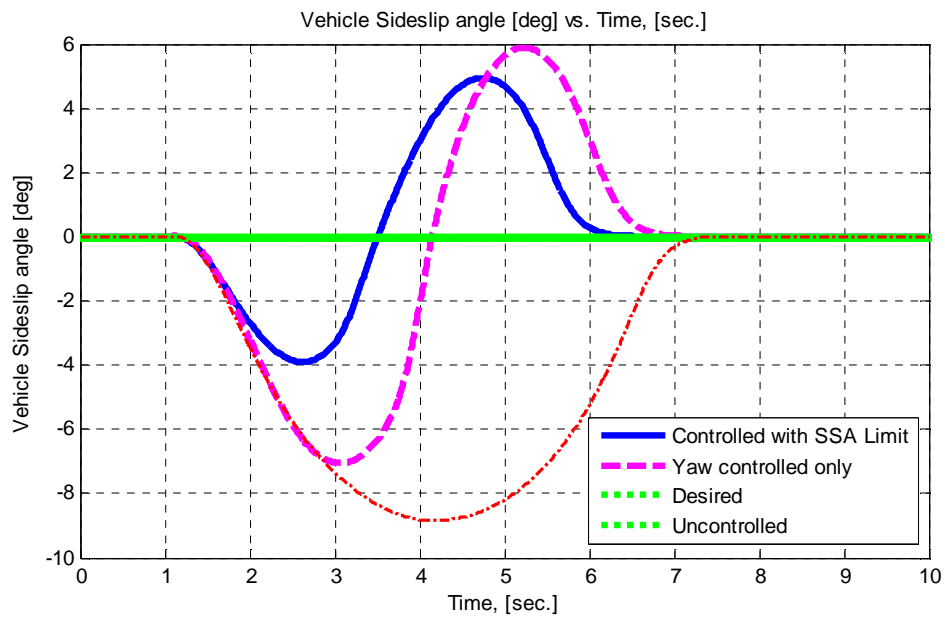
Fig. 5.100 Uncontrolled, desired and controlled vehicle sideslip angles [rad/s] vs. time[sec] for wet conditions in double lane change man.

Fig. 5.101 demonstrates the corresponding lateral accelerations of the simulated vehicles vs. time. When inspected, it can be seen that the lateral acceleration limit has been reached by all three simulated vehicles, uncontrolled and two different controlled cases. However, the capabilities of achieving different lateral accelerations for different instantaneous conditions have led the controlled vehicle behaviors to pursue the desired vehicle behavior changes. Minor modifications between only-yaw controlled vehicle and yaw controlled with sideslip angle limitation has appeared as yaw rate and sideslip angle differences, thus trajectory difference.

Fig. 5.102 presents the brake torques applied during the control of the vehicle and Fig. 5.103 illustrates the resulting trajectories for uncontrolled, desired and controlled vehicles. The rear left tire has been braked first to create the necessary contra yaw moment. After that, a sudden intervention of the cross tire, which is front right has been observed. At that time, the controller detects that the steer input has been reversed, thus applies counter brake to rear right and stabilizes the vehicle. If the trajectories obtained are compared, there can be concluded that minor difference is observed. On the other hand, the latter controller, that is the controller with the sideslip limitation, has a narrower trajectory. This case resembles the same situation with dry road condition case, where the only-yaw controlled vehicle has passed the desired vehicle behavior in y axis direction. One can conclude that the yaw controlled vehicle with sideslip angle limitation may be modified easily by the driver so that the desired track is obtained, by decreasing the steer input in magnitude. However, for the only-yaw controlled vehicle, the driver has to either increase the steer command or slow down, both of which may lead to stability problems. One interesting point is, the uncontrolled vehicle has turned to an acceptable steady state value considering the trajectory for the dry road case, while having gone to instability for the wet road condition.
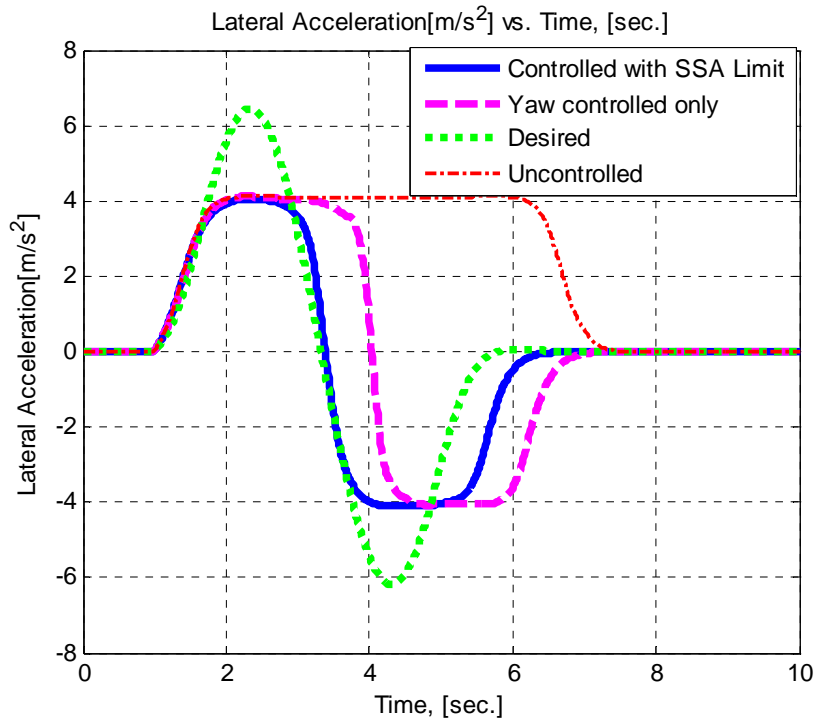
Fig. 5.101 Uncontrolled, desired and controlled vehicle lateral accelerations [rad/s] vs. time[sec] for wet conditions in double lane change man.
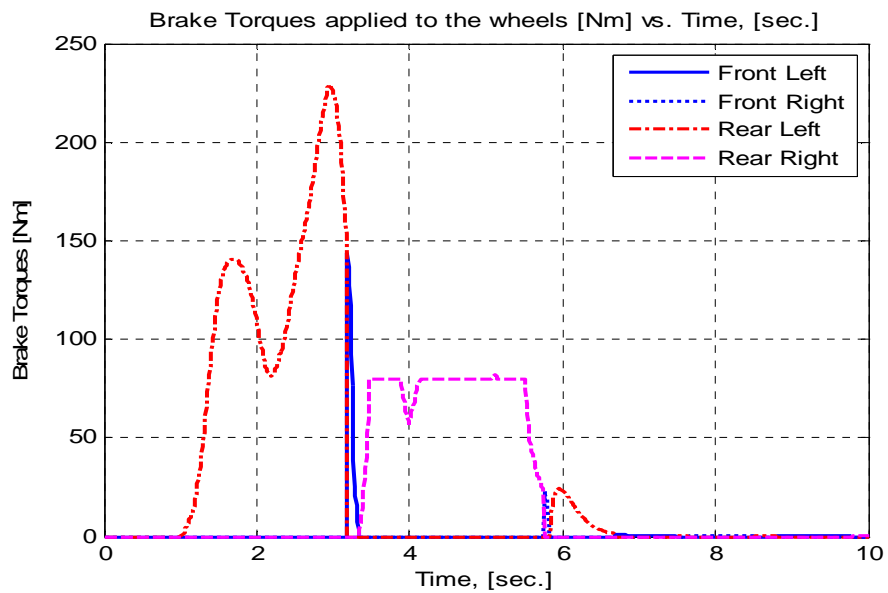
Fig. 5.102 Brake Torques applied to the wheels [Nm] for wet conditions in double lane change man.
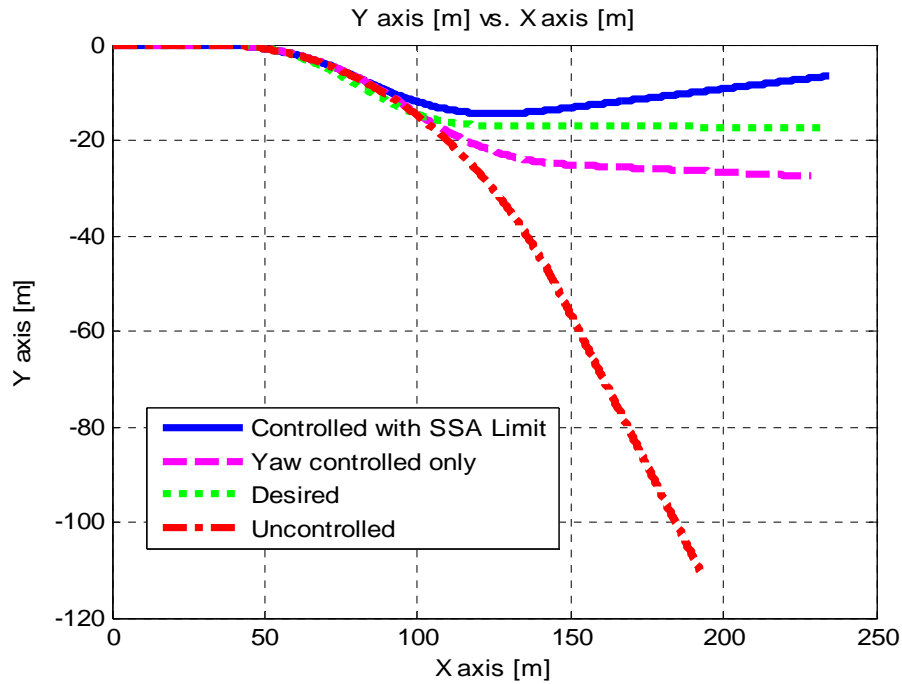
Fig. 5.103 Uncontrolled, desired and controlled vehicle trajectories for wet conditions in double lane change man.

For the last simulation of yaw controlled vehicle in a double lane change maneuver, icy road conditions with 50º steer angle J-turn maneuver is applied with an initial vehicle speed of 50 km/h and 0.1 road tire surface friction coefficient. Fig. 5.104 presents the uncontrolled, desired and the controlled vehicle yaw rates vs. time graph and Fig. 5.105 presents the vehicle sideslip angles vs. time. As it can be seen from the yaw rate graph, the desired yaw rate is far beyond the obtained yaw rates. The reason behind this situation is the low achievable tire forces due to the low coefficient of friction. However, these low tire forces may still be used for stabilizing the vehicle by redistributing the brake amounts among tires. The obtained vehicle sideslip angles have shown that the latter controller has achieved a much narrower sideslip angle limitation than the only-yaw controlled vehicle's sideslip angle. The uncontrolled vehicle has gone unstable with these conditions.
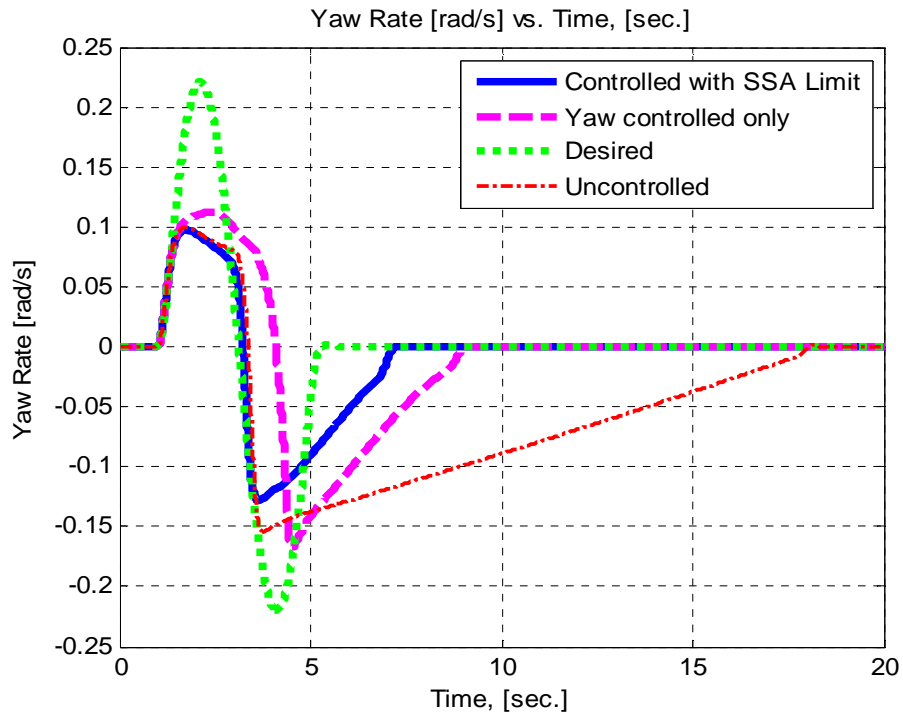
Fig. 5.104 Uncontrolled, desired and controlled vehicle yaw rates [rad/s] vs.

time[sec] for icy conditions in double lane change man.
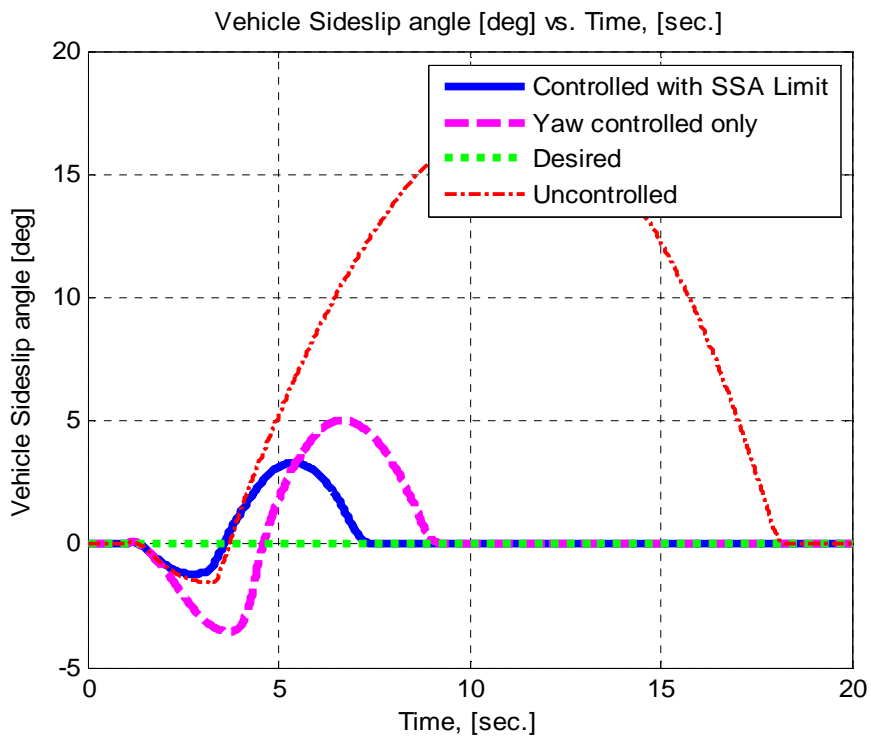
Fig. 5.105 Uncontrolled, desired and controlled vehicle sideslip angles [rad/s] vs.

time[sec] for icy conditions in double lane change man.

139

Fig. 5.106 demonstrates the corresponding lateral accelerations of the simulated vehicles vs. time. The attainable lateral acceleration for this road condition is achieved by all three vehicles, which is about 1 m/s^2. However, for the desired motion of the vehicle according to the driver's inputs, the necessary lateral acceleration is about 3 m/s^2, which is three times that of the attainable lateral acceleration limit.

Fig. 5.107 presents the brake torques applied during the control of the vehicle and Fig. 5.108 illustrates the resulting trajectories for uncontrolled, desired and controlled vehicles. The manipulation is done in this system in a little bit complex scheme. For the first part of the maneuver, the rear left tire has been braked and necessary contra yaw moment has been created. After that, the front left tire is used to create stabilizing yaw moment which follows the first handling. After the steer input has changed its sign, the rear right tire together with the rear left tire has been used to stabilize the vehicle. Comparing the trajectories, the controlled and uncontrolled vehicles follow the tracks resembling each other. However, since the steerability is conserved for only the latter controller with sideslip angle limitation, it can be concluded that the driver may intervene the course by decreasing the second steer oscillation part and thus obtaining the necessary speed and direction to follow the desired track.

The overall icy road performance of the yaw controller with sideslip limitation is satisfactory, since the yaw rate obtained is realized near the physical limits and the steerability is conserved by limiting the sideslip angle to predefined values for this kind of road condition.
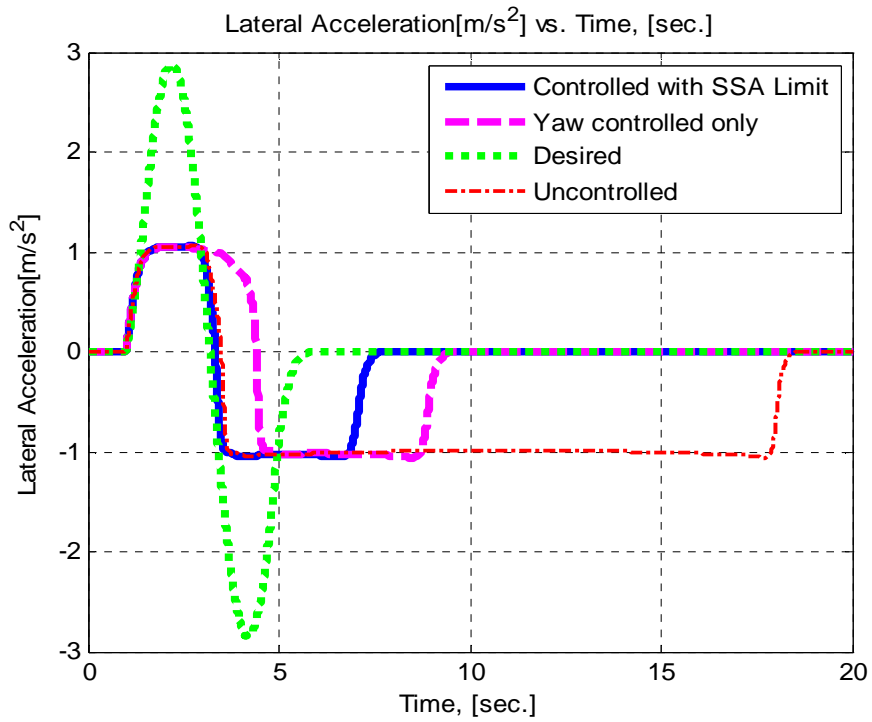
Fig. 5.106 Uncontrolled, desired and controlled vehicle lateral accelerations [rad/s] vs. time[sec] for icy conditions in double lane change man.
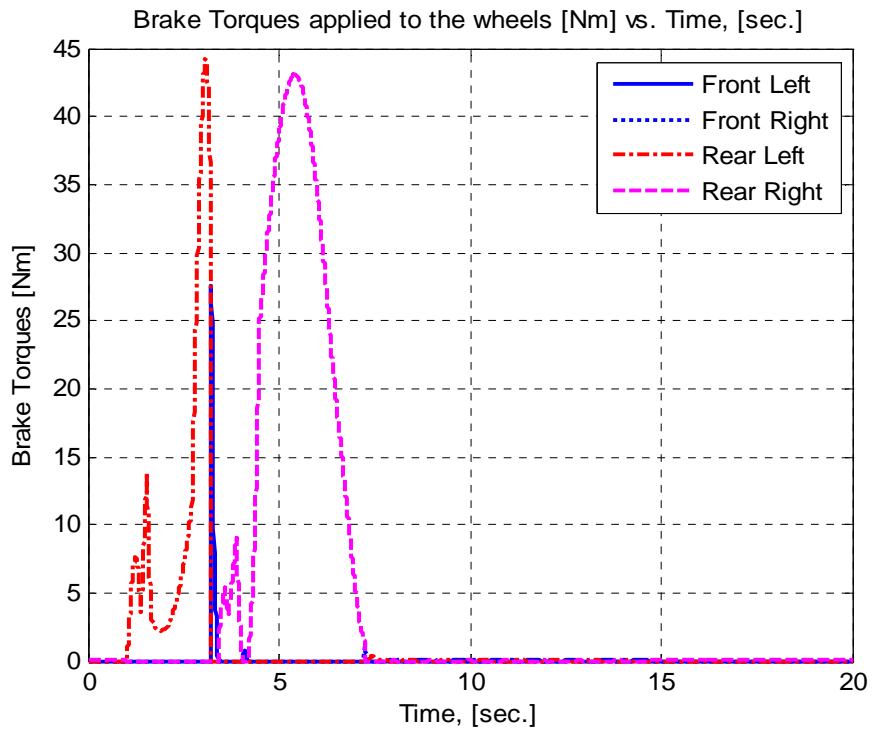
Fig. 5.107 Brake Torques applied to the wheels [Nm] for icy conditions in double lane change man.

141
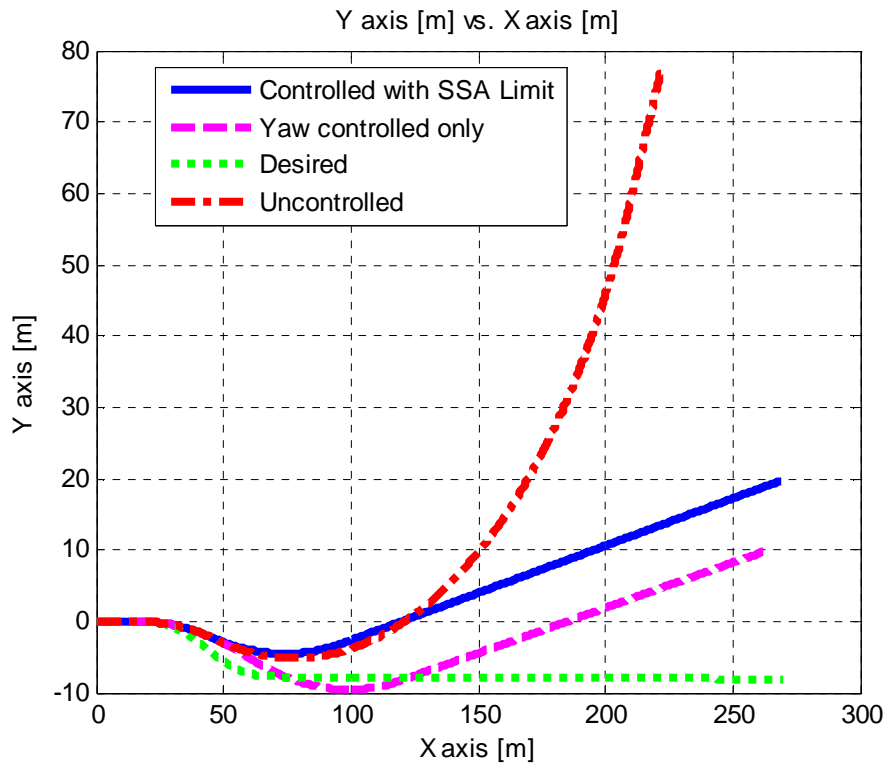
Fig. 5.108 Uncontrolled, desired and controlled vehicle trajectories for icy conditions in double lane change man.

CHAPTER 6

DISCUSSION AND CONCLUSIONS

The main aim of this study was to design a Fuzzy-Logic based controller in order to control the yaw rate of the vehicle while limiting the vehicle sideslip angle in order to conform to the driver's demand without losing the vehicle stability. Second aim of the study was to integrate the designed yaw controller with the tire slip sub-controller, thus obtaining a more complex active safety system covering a broader range of problems. After the design stage presented in chapter 4 and the through simulations presented in chapter 5, these two aims can be concluded as satisfied.

The simulation is carried out on MATLAB/Simulink environment using an 8 degree of freedom model, which can imitate the real life vehicle successfully considering the handling behaviors of the vehicle. The vehicle dynamics behind this model is presented in chapter 3, modeling part. While choosing the degree of freedoms to be included in the vehicle model, direct vehicle handling parameters and parameters which have indirect yet important effects on the handling behavior of the model are tried to be utilized. The direct parameters can be exampled as the yaw freedom while roll may be exampled as a parameter affecting the load transfer, thus indirect. The overall degrees of freedoms are longitudinal, lateral, yaw, roll and wheel rotational freedoms. A simpler 2 degree of freedom model is also constructed with the intention of predicting the driver's intention for the vehicle motion. After this, Allen tire model has been introduced, which is used to estimate the tire forces resulting from the vehicle motion as well as steer and brake actions.

As it can be seen in the simulations, uncontrolled vehicle may perform hazardously, especially in yaw-based maneuvers with slippery road conditions. The vehicle is generally behaves in a linear mode which, for example, can be defined as the yaw rate obtained increases linearly with steer angle input. However, this case is not valid in emergency situations, which forces the vehicle to limits of linear operation. At this point, the vehicle starts to behave in a totally different manner since the saturation of tire forces has been achieved quickly. After reaching the limits of the tire force capabilities, general driver is unconscious about what to do in order to manipulate the vehicle to the stability environment. The designed controller(s) are responsible at this point, since yaw manipulation cannot be done unless the driver has extensive experience in steer manipulation of nonlinear vehicle behavior.

Two different yaw controllers have been presented and compared throughout the simulation chapter. The first design deals with the yaw rate correction of the simulated vehicle, which is the first objective of this study. As the design of the controller has matured and this design has been tested numerously, the capabilities of the yaw-rate-only based approach have seem to be reached. However, there was still a bunch of problems with the controlled vehicle behavior, such as losing stability with reaching high vehicle sideslip angles. The results of the uncontrolled, desired and controlled behaviors of the simulated vehicle have been presented in chapter 5. As it can be seen in the discussion parts of this simulation results sections, the yaw controller have been proved as unsatisfactory for specific cases. This dissatisfaction case can be related into two main parameters:

— The sideslip angle has increased to unacceptable values so that the steerability of the vehicle can be assumed as lost.
— The trajectory is far from that of desired vehicle behavior

For both of these cases, the reasons vary as the case studies are carefully examined. However, the most important reason is the unreachable demand derived from the driver's commands. If carefully investigated, in specific cases, the lateral accelerations needed to obtain the desired behavior (yaw rate, trajectory etc.) cannot

144

be obtained from the current road-tire interactions. There exist a physical limitation for a vehicle to realize driver's command, which can be observed as cornering force limitations and inadequate lateral acceleration. For these reasons, the original yaw rate controller has been modified so that it also takes the vehicle sideslip angle into account. In this design, only the yaw rate error and the vehicle sideslip angle has been taken as inputs while the manipulation is again realized by individual braking. This novel design has been also tested with several maneuvers, vehicle data and road conditions. The overall controller system has been extended in various aspects so that the stability of system is assured if possible. The results of the new controller with sideslip angle limitation have proven itself to be superior against the actual yaw rate controller.

Second aspect of this study was the integration of sub-slip controller with the designed high level yaw rate controller. For this purpose, the general literature has been reviewed extensively and a detailed study has been completed with Şahin, who has completed a M.Sc. thesis which also includes tire slip controllers. After these efforts, a tire slip sub-controller has been designed and tested as it is effective or not. This brake manipulation has turned out to be successful in especially icy road conditions.

For the brake manipulation, a brake torque change rate is applied to the controller model in order to comply with the real life application. This torque change rate limitation was actually effective in the vehicle handling performance, since this limit is actually causes excessive slippage during icy road operation. However, the manipulation of the yaw controller with sideslip angle limitation is yet enough to stabilize the vehicle and track the proposed yaw rate.

The active yaw control system is considered as a part of the integrated active safety system. Thus, it can benefit from the general vehicle data share and operate synchronously via CAN bus or a similar vehicle network system. For instance, the wheel slip manipulation may be operated by the low level ABS controller by just assigning the necessary reference slip. The sensor network will be common for all

independent safety systems while more complex calculations will be available by running the dynamic models in the hardware of the vehicle in real time.

6.1 FUTURE WORK

The main scope of the active safety systems can be extended in various aspects. However, in this study, the design of an active yaw control mechanism with sideslip angle limitation together integrated to a sub-level slip controller is considered as the objective. Future work will include the following items, which, in turn, will be of importance for the realization and development of the study presented below.

— The detailed model will be extended with additional degree of freedoms and the brake component dynamics, which will result in more realistic outcomes

— Together with the brake manipulation, engine torque management will be designed and utilized for faster responses and better handling characteristics in acceleration demand with hard maneuvers.

— The control techniques may be developed and tweaked with Hardware-in-the-Loop (HIL) simulations.

— The overall control system may be broadened with addition active steering, hence the tracking of the desired behavior as well as tire force managing.

REFERENCES

[1]   "Driving Safety Systems", Bosch GmbH, 2nd edition, 1999

[2]   Ünlüsoy, S., Balkan, T., Tekin, G., Şahin, M., Oktay, G., "Integrated active safety systems for road vehicles", TRODSA 2006 vol.2

[3]   Fukada, Y., "Slip-Angle Estimation for Vehicle Stability Control", Vehicle System Dynamics, 32 (1999), pp. 375-388

[4]   Hac, A., Simpson, M. D., "Estimation of Vehicle Sideslip Angle and Yaw Rate", SAE Paper 200-01-0696

[5]   Kin, K., Yano, O., Urabe, H., "Enhancements in vehicle stability and steerability with slip control" , JSAE Review 24 (2003) pg. 71-79

[6]   Hewson, P., "Method for estimating tyre cornering stiffness from basic tyre information", Proceeding of IMechE Vol. 219, Part D: J. Automobile Engineering

[7]   Takano, S., Nagai, M., Taniguchi, T., Hatano, T., "Study on a vehicle dynamics model for improving roll stability", JSAE Review 24 (2003) pp. 149-156

[8]   Nguyen, V., "Vehicle handling, stability and bifurcation analysis for nonlinear vehicle models", M.Sc. Thesis, University of Maryland, 2005

[9]   Babala, M., Kempen G., Zatyko, P., "Trade-Offs For Vehicle Stability Control Sensor Sets", SAE Paper 2002-01-1587

[10]   Noomwongs, N., Yoshida, H., Nagai, M., Kobayashi, K., Yokoi, T., "Study on handling and stability using tire hard ware-in-the-loop simulator" JSAE Review 24 (2003) pg. 457-464

[11]   Tseng, H. E., Ashrafi, B., Madau, B., Brown, T.A., Recker, D., "The Development of Vehicle Stability Control at Ford", IEEE/ASME Transactions on Mechatronics, Vol. 4 No. 3 September 1999

[12]   Hahn, J., Hur, J., Yi, K., Kang, S., Lee, K., "Nonlinear Vehicle Stability Control Using Disturbance Observer", Proceedings of the 2002 IEEE International,

[13]   Boada, B. L., Boada, M. J. L., Díaz, V., "Fuzzy-logic applied to yaw moment control for vehicle stability", Vehicle System Dynamics, Vol. 43 No. 10,October 2005, pp. 753-770

[14]   Park, J. H., Kim C.H., "Wheel Slip Control in Traction Control System for Vehicle Stability", Vehicle System Dynamics, 31 (1999) pp.263-278

[15]   Drakunov, S., Ashrafi, B., Rosiglioni, A., "Yaw Control Algorithm via Sliding Mode Control", Proceedings of the American Control Conference, June 2000

[16]   Güvenç, B.A., Acarman, T., Güvenç L., "Coordination of Steering and Individual Wheel Braking Actuated Vehicle Yaw Stability Control", 2003 IEEE

[17]   Güvenç, B.A., Güvenç L., Öztürk, E. S., Yiğit, T., "Model Regulator Based Individual Wheel Braking Control", 2003 IEEE

[18]   Zhou, Q., Wang, F., "Driver Assisted Fuzzy Control of Yaw Dynamics for 4WD Vehicles", 2004 IEEE Intelligent Vehicles Symposium, June 2004

[19]   Esmailzadeh, E., Goodarzi, A., Vossoughi, G.R., "Optimal yaw moment control law for improved vehicle handling", Mechatronics 13 (2003), pp. 653-675

[20]   Kuang, M. L., Fodor, M., Hrovat, D., "Hydraulic Brake System Modeling and Control for Active Control of Vehicle Dynamics", Proceedings of the American Control Conference, June1999

[21]   Mokhiamar, O., Abe, M., "Effects of model response on model following type of combined lateral force and yaw moment control performance for active vehicle handling safety", JSAE Review 23 (2002), pp. 473-480

[22]   Youa, S., Hahnb, J., Choa, Y. M., Leea, K. I.., "Modeling and control of a hydraulic unit for direct yaw moment control in an automobile", Control Engineering Practice 14 (2006), pp. 1011-1022

[23]   Mokhiamar, O., Abe, M., "How the four wheels should share forces in an optimum cooperative chassis control", Control Engineering Practice 14 (2006), pp. 295-304

[24]   Shim,   T., Margolis, D., "Using µ Feedforward for Vehicle Stability Enhancement", Vehicle System Dynamics 2001, Vol. 35, No. 2, pp. 103-119

[25] Choi, S., Cho, D., "Design of Nonlinear Sliding Mode Controller with Pulse Width Modulation for Vehicular Slip Ratio Control", Vehicle System Dynamics 2001, Vol. 35, No. 1, pp. 53-72

[26] BuckHoltz, K. R., "Use of Fuzzy logic in wheel Slip Estimate- Part II: Yaw Rate Control with Sideslip angle limitation", SAE Paper 2002-01-1220

[27] Sorniotti, A., Velardocchia, M., "Hardware-in-the-Loop (HIL) Testing of ESP (Electronic Stability Program) Commercial Hydraulic Units and Implementation of New Control Strategies", SAE Paper 2004-01-2770

[28] Mitsubishi-Motors website, http://www.mitsubishi-cars.co.uk/ Last visited on 17.10.2007

[29] Osborn, R.P., Shim, T., "Independent control of all-wheel-drive torque distribution", Vehicle System Dynamics, July 2006, Vol. 44 No. 7 pp. 529-546

[30] Gordon, T., Howell, M., Brandao, F., "Integrated Control Methodologies for Road Vehicles", Vehicle System Dynamics 2003, Vol. 40 Nos. 1-3, pp 157-190

[31] Burgio, G., Zegelaar, P., "Integrated vehicle control using steering and brakes", International Journal of Control, May 2006, Vol. 79, No. 5, pp. 534-541

[32] "Tahami, F., Farhangi, S., Kazemi, R., "A Fuzzy Logic Direct Yaw-Moment Control System for All-Wheel-Drive Electric Vehicles", Vehicle System Dynamics 2004, Vol.41, No. 3, pp. 203-221

[33] Zheng, S., Tang, H., Han, Z., Zhang, Y., "Controller design for vehicle stability enhancement", Control Engineering Practice 14 (2006) 1413-1421

[34] Allen, R.W., Rosenthal, T.J., et al, "Steady State and Transient Analysis of Ground Vehicle Handling", SAE Paper 870495, 1987.

[35] Ghelardoni, M., "Feasibility Study of Yaw Control by active 4-Wheel Drive", B.Sc Thesis, Universit`a degli Studi di Pisa & Technische Universiteit Delft, 2004

[36] Nishio, A., Tozu, K., Yamaguchi, H., Asano, K., Amano, Y., "Development of Vehicle Stability Control System based on Sideslip Angle Estimation", SAE Paper 2001-01-0137

[37] Şahin, M. "Design And Simulation Of An Abs For An Integrated Active Safety System For Road Vehicles", M.Sc. Thesis, METU, September 2007,

[38] Passino, K.M., Yurkovich, S. "Fuzzy control", Addison-Wesley- 1998

[39] Alvarez, L., Yi, J., Horowitz, R., Olmos, L., "Dynamic Friction Model based Tire Road Friction Estimation and Emergency Braking Control", Vol.127, Journal of Dynamic Systems, Meas. and Control, March 2005

[40] Chung, T., Yi, K., "Design and Evaluation of Sideslip Angle-Based Vehicle Stability Control Scheme on a Virtual Test Track", IEEE Transact. On Control Systems Technology, Vol. 14, No. 2, March 2006

[41] "Safety, comfort and convenience systems" Bosch GmbH, June 2006

[42] Morgando, A., "Linear Approach to ESP Control Logic Design", SAE Paper 2006-01-1017

APPENDIX A

VEHICLE DATA

Table A.1 8 degree of freedom and 2 degree of freedom vehicle data (originated from the study of Zheng [33] and Esmailzadeh [19]

PARAMETER NAME	VALUE
M	1300 kg
Ms	1160 kg
t_f	1,45 m
t_r	1,45 m
a	1,1 m
b	1,35 m
R	0,33 m
I_w	2,03 kg m2
I_{zz}	1620 kg m2
I_{xx}	750 kg m2
$k_{\Phi f}$	20250 Nm/rad
$k_{\Phi r}$	24750 Nm/rad
$C_{\Phi f}$	2600 Nms/rad
$C_{\Phi r}$	2600 Nms/rad
C_f (for 2 dof model)	45312 kN/rad
C_r (for 2 dof model)	45312 kN/rad
SWR	01:18

Table A.2. Allen tire model parameters based on the work of Allen [34]

P185/70R13 -

PARAMETER NAME	VALUE
Tw	7,3 inches
Tp	24 psi
Fzt	980 lbs
C1	1
C2	0,34
C3	0,57
C4	0,32
A0	1068
A1	11,30
A2	2442,73
A3	0,31
A4	-1877
ka	0,05
Cs/Fz	17,91
B1	-0,000169
B3	1,04
B4	1,69*e-8

APPENDIX B

CASE STUDY: SIMULATION FOR A J-TURN MANEUVER AND DOUBLE LANE CHANGE WHILE DECELERATING THE VEHICLE

This simulation case study is actually the continuing part of the chapter 5. In this simulation, a vehicle is studied on a J-turn maneuver and double lane change while decelerating with an acceleration of about 2 m/s^2. The initial velocity is 90 km/h (25 m/s) and the nominal road surface friction coefficient is 0.9. Figures B.1 through B.12 demonstrates the vehicle behavior under these conditions.
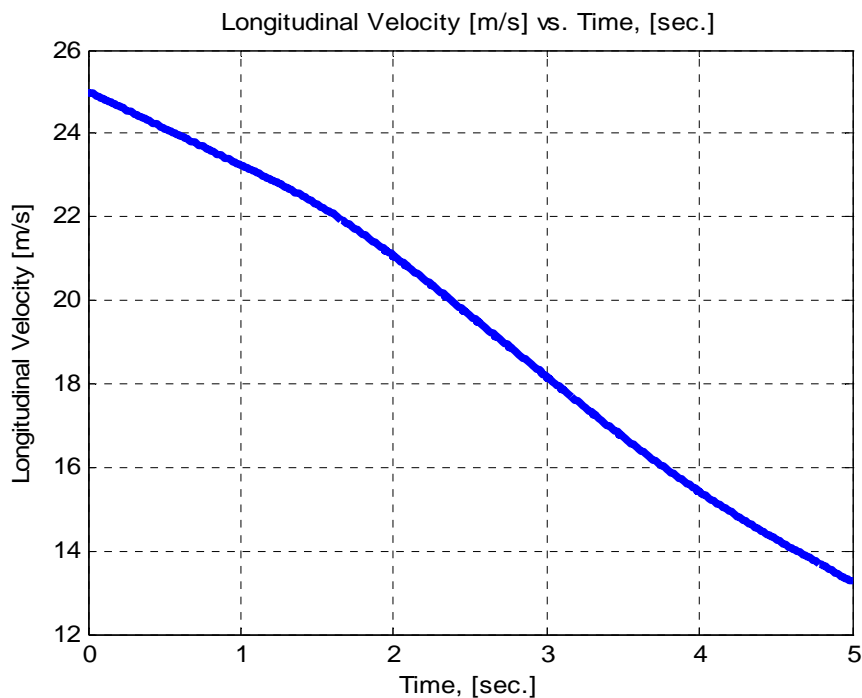
Fig. B.1 Longitudinal Velocity change [m/s] vs. time [s] for a decelerating vehicle in a J-Turn maneuver
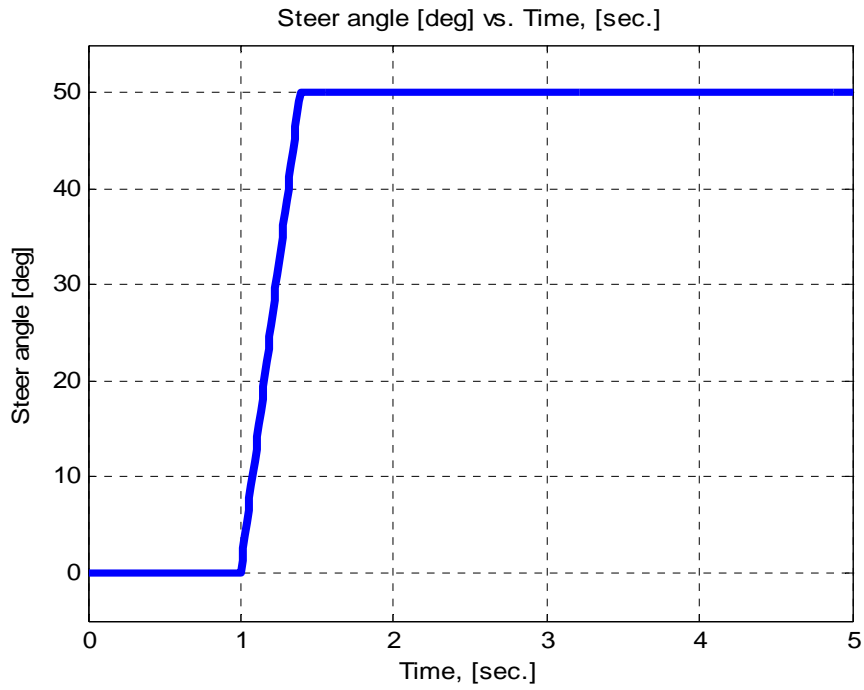
Fig. B.2 Steering wheel angle change [deg/s] vs. time [s] for a decelerating vehicle in
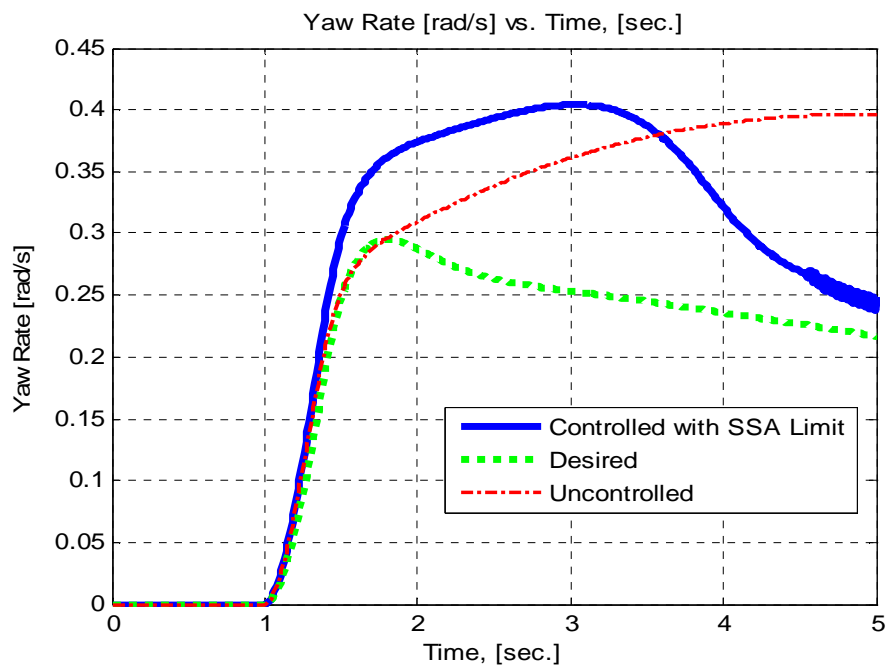
a J-Turn maneuver

Fig. B.3 Yaw rate change [rad/s] vs. time [s] for a decelerating vehicle in a J-Turn

maneuver

154
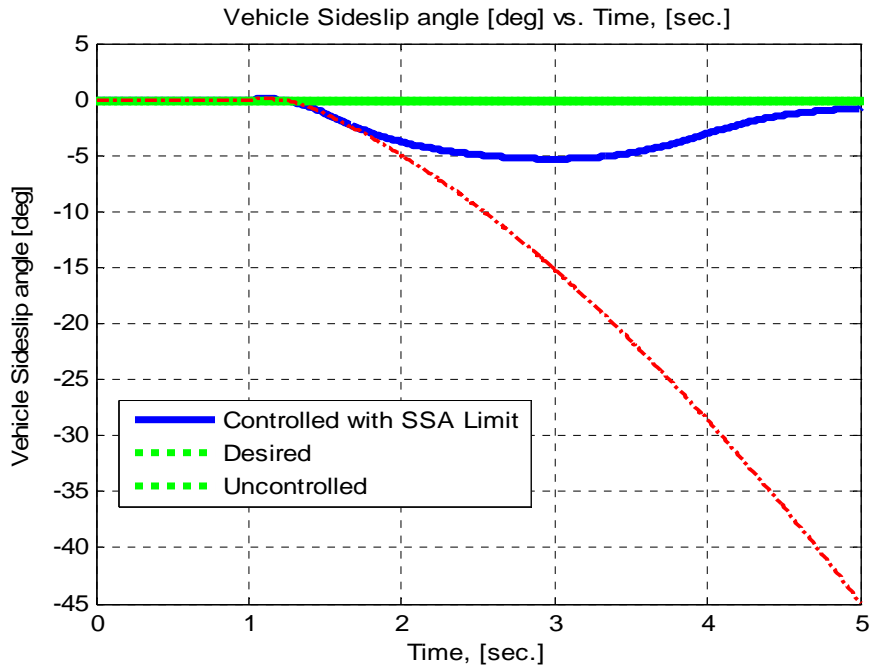
Fig. B.4 Vehicle Sideslip angle change [deg] vs. time [s] for a decelerating vehicle in
a J-Turn maneuver
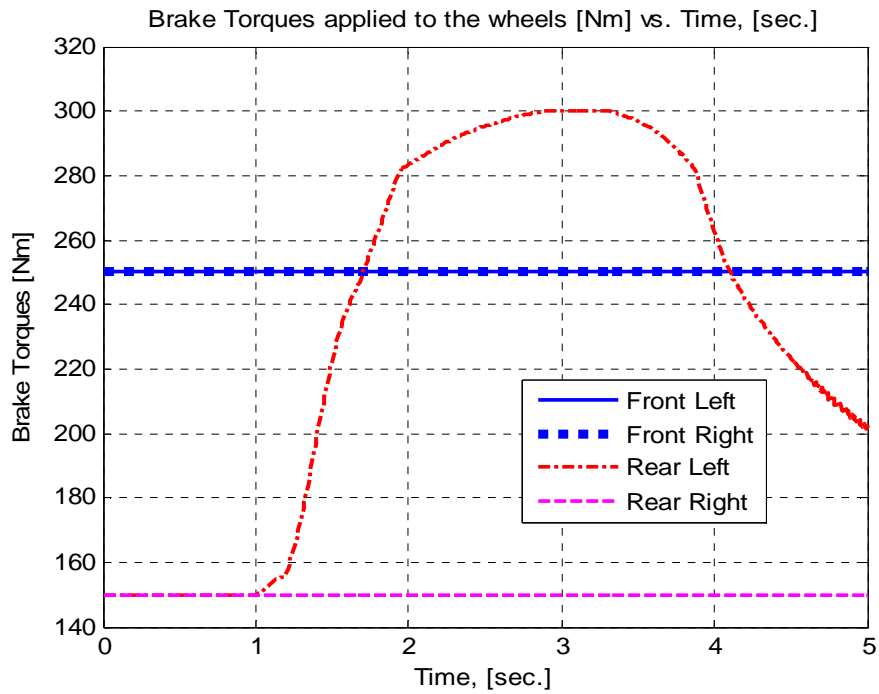
Fig. B.5 Brake Torques applied to wheels [Nm] vs. time [s] for a decelerating vehicle
in a J-Turn maneuver

155
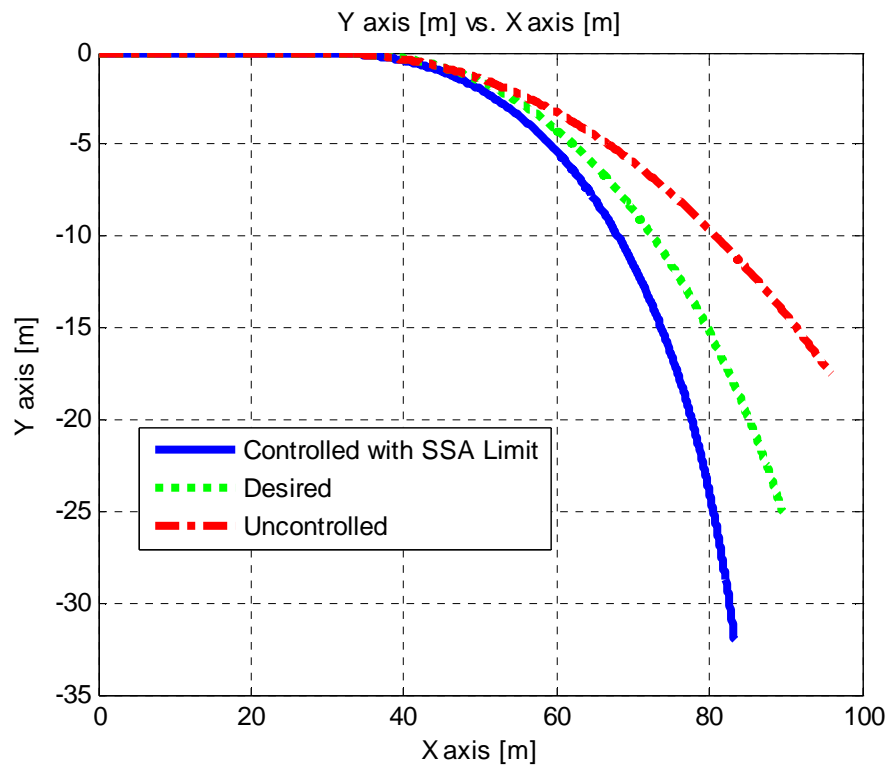
Fig. B.6 Trajectory of a decelerating vehicle in a J-Turn maneuver

The same simulation will be repeated with replacing the J-turn maneuver with double lane change maneuver. All other parameters remain same. This maneuver also includes a deceleration of about 2 m/s^2 (roughly 0.2g), which is a normal deceleration value for controlling the vehicle while in a sharp evasive maneuver in the elevated speeds.
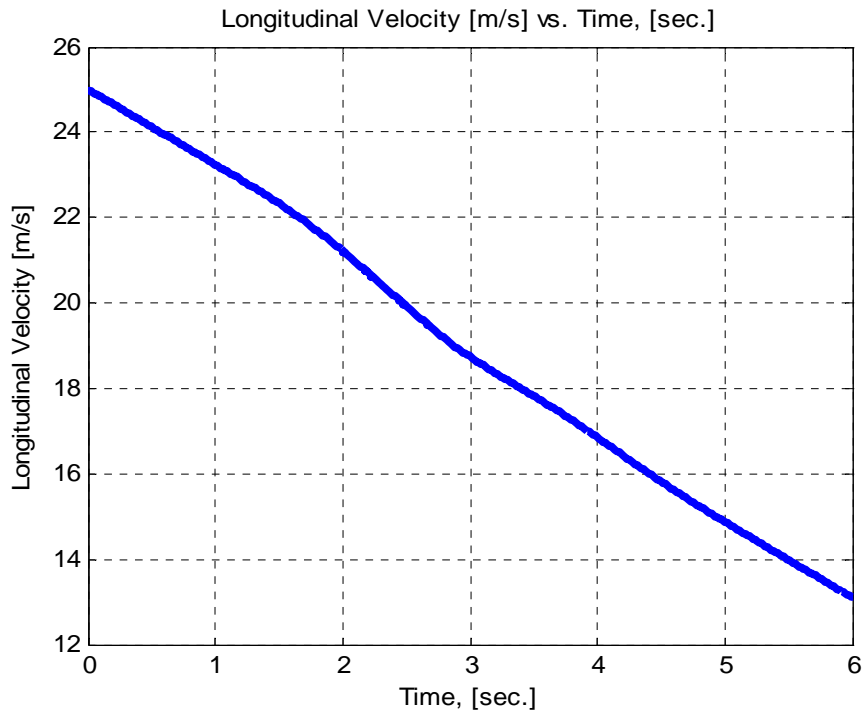
Fig. B.7 Longitudinal Velocity change [m/s] vs. time [s] for a decelerating vehicle in
a double lane change maneuver
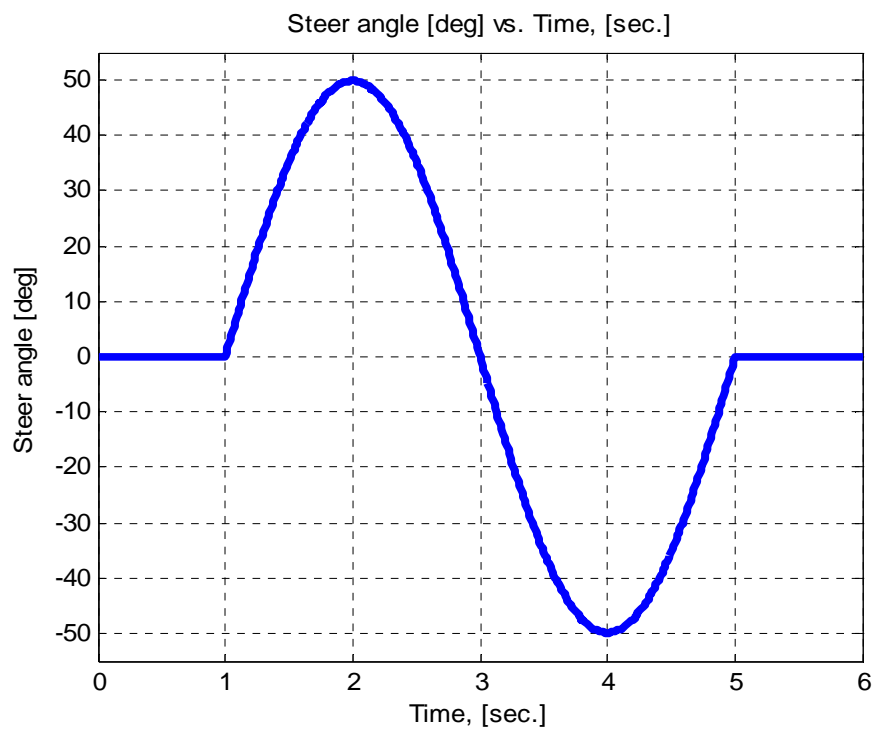
Fig. B.8 Steering wheel angle change [deg/s] vs. time [s] for a decelerating vehicle in
a double lane change maneuver

157
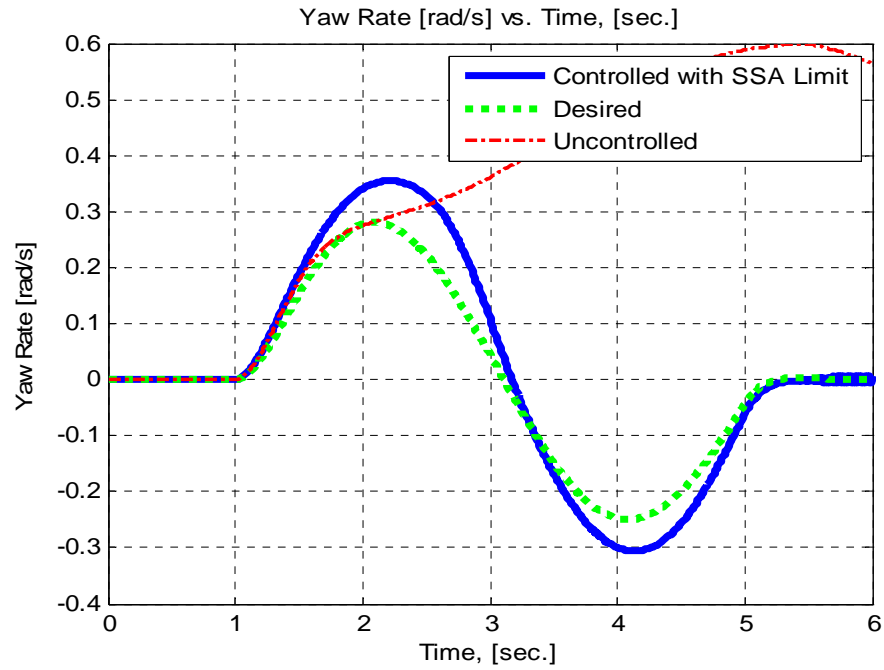
Fig. B.9 Yaw rate change [rad/s] vs. time [s] for a decelerating vehicle in a double lane change maneuver
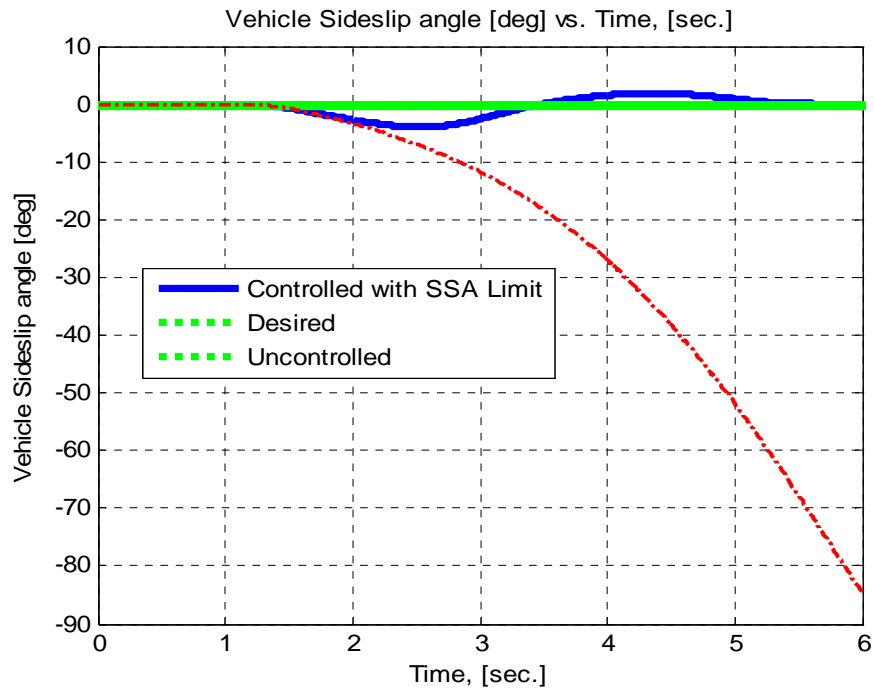

Fig. B.10 Vehicle Sideslip angle change [deg] vs. time [s] for a decelerating vehicle in a double lane change maneuver
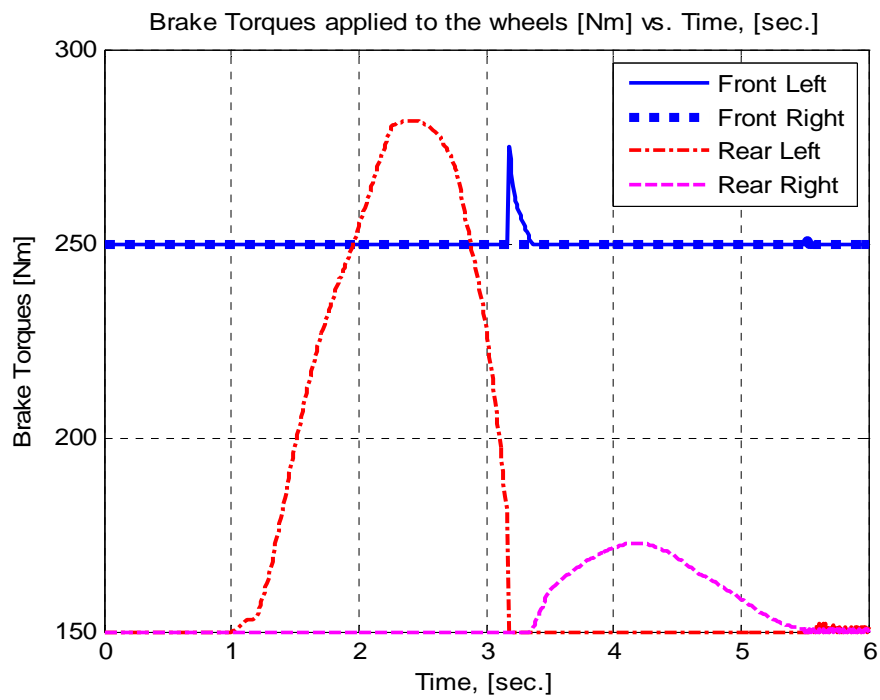
Fig. B.11 Brake Torques applied to wheels [Nm] vs. time [s] for a decelerating

vehicle in a double lane change maneuver
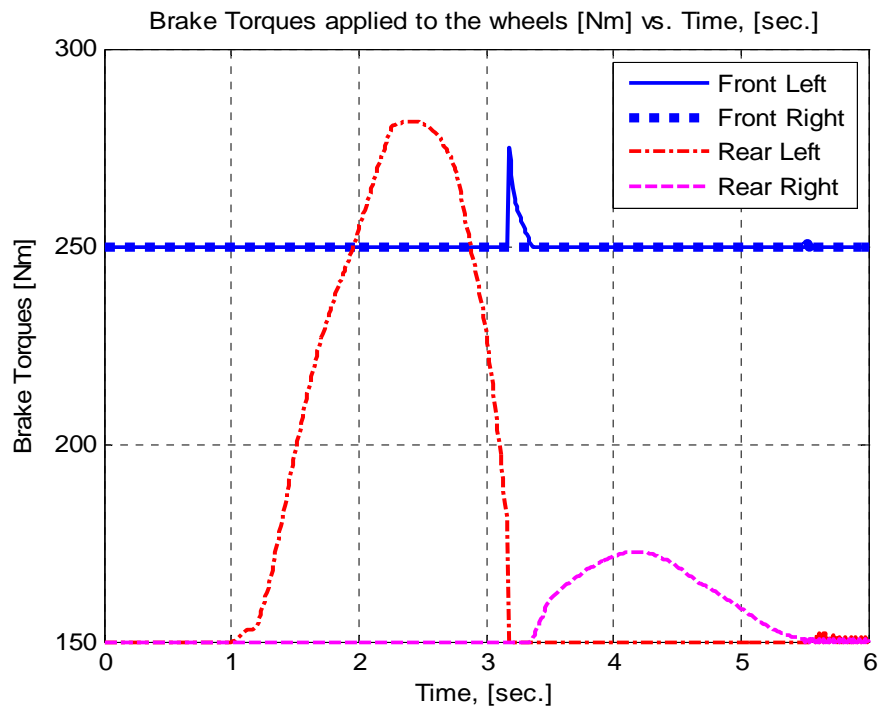
Fig. B.12 Trajectory of a decelerating vehicle in a double lane change maneuver

159